DESIGN AND BEHAVIOR OF COPED BEAM

by

J. J. Cheng, J. A. Yura, and C. P. Johnson

Sponsored by

American Institute of Steel Construction

Phil M. Ferguson Structural Engineering Laboratory
Department of Civil Engineering
The University of Texas at Austin
Austin, Texas 78758

July 1984

ACKNOWLEDGEMENTS

This research project, Design of Coped Beam Connections, whose results are reported herein, was sponsored by the American Institute of Steel Construction. The guidance of the project Task Committee members, L. Kloiber (Chairman), R. Tide, J. Wooton, N. Young, and N. Iwankiw, is greatly appreciated. Many thanks to Paxton & Vierling Steel Co. for providing some of the test beams.

The tests were conducted at the Phil M. Ferguson Structural Engineering Laboratory, Department of Civil Engineering, The University of Texas at Austin. The computer analysis was done using the computer system at The University of Texas at Austin. The help of the laboratory staff is greatly appreciated. Special thanks are extended to Dr. Eric B. Becker for his help and suggestions.

ABSTRACT

The behavior of coped beams with various coping details was examined by conducting a theoretical parametric study using the elastic and inelastic finite element programs BASP and ABAQUS. The design models and recommendations for different types of coped connections (top, bottom and double coped) are made according to the behavior and results of the analytical studies. In addition to yielding, coped beams can fail in two distinct instability modes, lateral-torsional buckling over the span and local web buckling at the cope region. Cope length, cope depth and span length were found to have a significant influence on the buckling capacity.

Simple interaction equations, which utilize the individual lateral buckling capacities of the coped region and the uncoped length, were developed for design of lateral buckling of top (compression) flange coped beams and double coped beams. Copes on the bottom (tension) flange reduced the lateral buckling capacity 10 percent of the uncoped case. A plate buckling model was developed to check for web buckling in compression flange coped beams and a lateral buckling model was adopted for web buckling in double flange coped beams.

A series of sixteen full scale tests, 14 rolled sections and two plate girders, was used to check the reliability of the design recommendations. Six of the tests considered lateral-torsional buckling. The remainder were for local web buckling. The test

results indicate that the proposed design recommendations for both lateral-torsional buckling and local web buckling give conservative and reasonable results.

Various types of reinforcement at the cope region were studied to determine their effectiveness in improving the strength of coped beams.

TABLE OF CONTENTS

TABLE OF CONTENTS (continued)

TABLE OF CONTENTS (continued)

TABLE OF CONTENTS (continued)

CHAPTER 1

INTRODUCTION

1.1 General

In steel construction beam flanges must often be coped to provide enough clearance for the supports when the framing beams are at the same elevation as the main girders or when the bottom flanges of intersecting beams are held to the same elevation for architectural purposes. The framing beams must be notched out at the top or bottom as shown in Fig. 1.1 to prevent interference with the flanges of the main girders. Generally, the notches will extend into the web of the framing beams. Such a cutout is called a cope, block or cut. Throughout this study, it is referred to as the cope. The copes can be at the top (compression), the bottom (tension), or both flanges in combination with the various types of simple shear connections as shown in Fig. 1.1. Simply supported end conditions are usually assumed in the design of the coped beam connections.

The generalized behavior of a simple supported uncoped steel beam can be expressed by the moment-deflection relationship shown in Fig. 1.2. Experimentally, the beam ultimately fails by some types of instability, namely lateral-torsional buckling, local plate buckling of the compression flange, or web buckling. If the laterally unbraced length and the width-thickness ratios of the plate elements of the cross section are sufficiently small, buckling can be

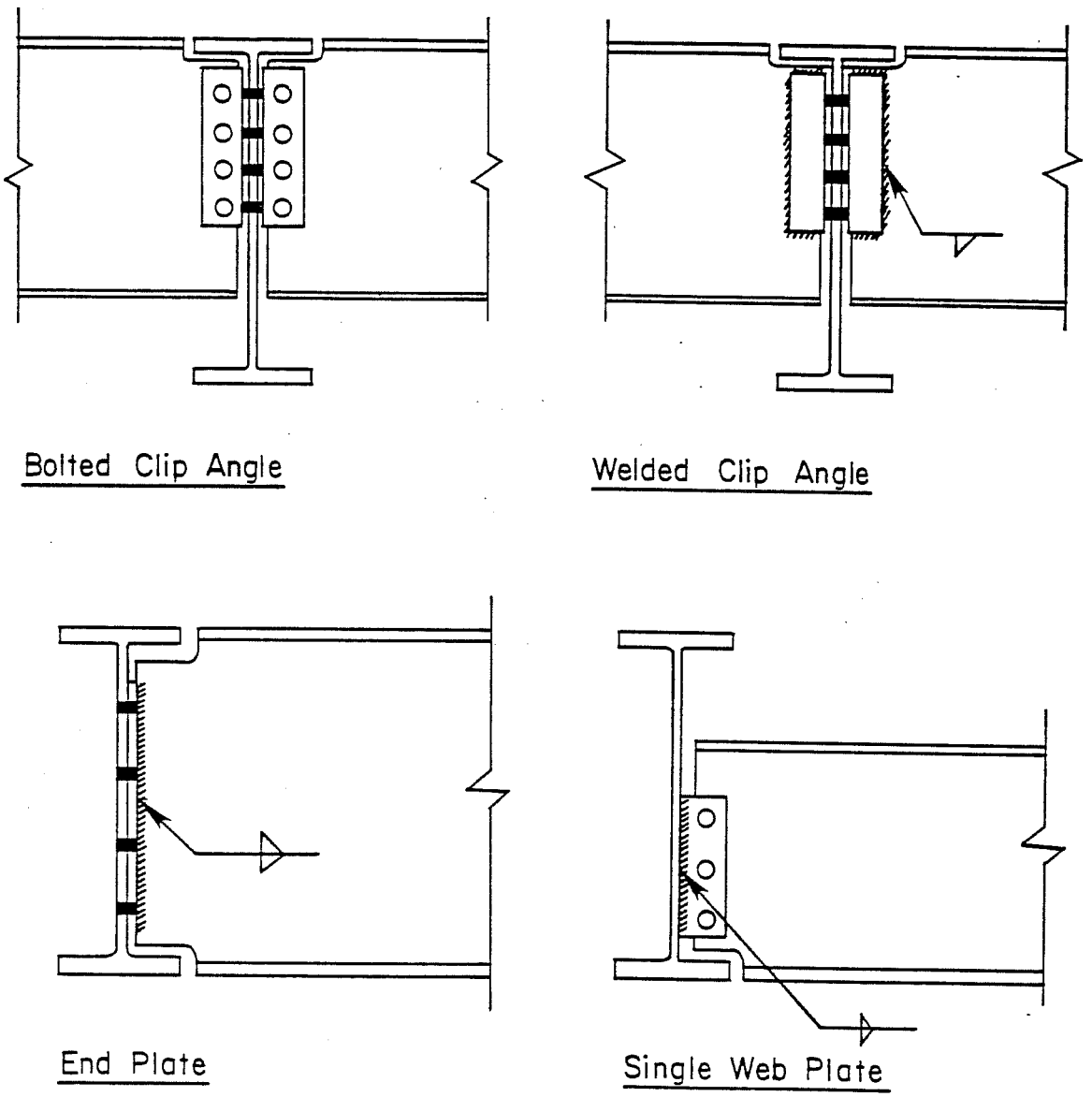

Fig. 1.1 Types of Coped Beam Connection

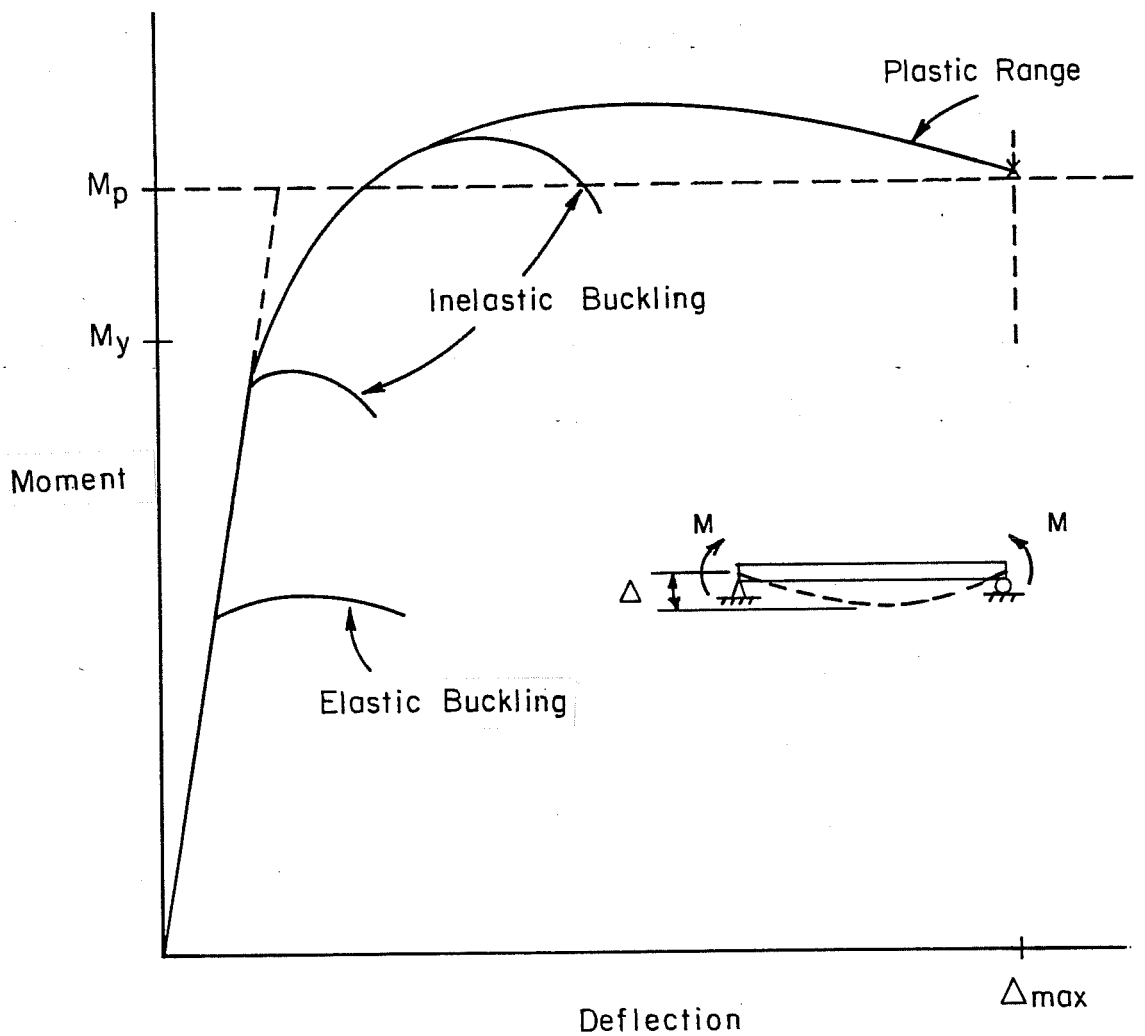

Fig. 1.2 Generalized Load-Deflection Curves for Beams

curtailed until maximum stress at the extreme fiber reaches the yield strength at the yield moment, M_y, (neglecting residual stresses) and possibly the fully plastic moment, M_p [1]. In such cases, yielding controls the design of the beams. The design of most laterally supported uncoped rolled beams is controlled by yielding at the point of maximum moment.

In the beams with copes, special attention must be given to the coped region. The strength and torsional stiffness at the coped section are reduced so that buckling, both local and lateral, as well as yielding can be affected as discussed by Milek [2]. Due to the discontinuity of the flange and web at the coped corner, high stress concentration could occur at this location depending upon the cope profile at the corner. Thus, the conventional Mc/I and VQ/It calculations for bending and shear stresses respectively may not give the actual stress distributions at the coped region. High stress concentration could cause localized yield at the coped corner which might cause the beam to fail in inelastic local web buckling. For thin webs in laterally supported beams, failure could occur by elastic local web buckling at the coped region since the coped region is not stiffened by the flanges. Theoretically, the buckling load can be much lower than the yielding stress. Copes can also affect the lateral-torsional buckling strength. The basic theoretical formulas for lateral-torsional buckling of pinned end beams derived by Timoshenko [3] upon which current design specifications are based assume that the flanges at the ends of the beam are restrained

against lateral movement. However, when a laterally unsupported beam has copes at the connections, the lateral end restraint would be decreased since movement at the end of the flange is not positively prevented. The effectiveness of the restraint depends upon the torsional strength and stiffness of the coped section. The lateral-torsional buckling strength of the coped beams would be less than that predicted by current theoretical formulas. In addition to the above considerations, special attention must also be focused on failure by tensile rupture at the corner of the coped region. Most grades of steel possess sufficient ductility; a fracture failure generally does not occur prior to a buckling type failure for a beam. However, it is possible for tension zone fracture failure to occur due to high stress concentration at the corner of the coped region.

There is one published study on the effect of copes in lateral torsional buckling. Du Plessis [3] tested four laterally unsupported beams which failed in lateral-torsional buckling. All beams had a W10x21 section with a 158-in. span length. Beam 1 had no copes in the flange, beams 2 and 4 had copes in the top flange only, and beam 3 had double-flange copes. A cope length of 6-in. and a cope depth of 1-3/8 in. were adopted for all three coped beams. The test beams framed into girders at each end using single end plate shear connections. The 3/8-in. connection plates were welded to the web of the test beam in beams 3 and 4. In beams 1 and 2, the end plate extended below the bottom flange and was fillet-welded to the

flange also. In all cases, the end plates were bolted to the support girders. Two series of tests were done on these four test beams, one with midspan loading and the other loading at 13.75 in. from the end of the beam (hereinafter called notch loading). The results of the tests showed that the buckling capacities were reduced up to 34 percent for midspan loading and 77 percent for notch loading compared to the uncoped beam. The critical loads of beam 2 were more than 30 percent higher than beam 4 due to the difference in connection detail. The double coped beam (beam 3) had lower buckling load, 6 percent in midspan loading and 23 percent in notch loading, compared to the top flange coped beam (beam 4). The results show the importance of the coping details, connection restraints and loading conditions on the buckling capacities of a coped beam. However, his study is not general enough to develop design recommendations.

There is also some recent research which has focused on the connection behavior at copes [4,5,6] but relatively little data was developed concerning the structural behavior at the cope itself. These studies focused on fracture at the minimum section at the bolt locations and all beams were laterally supported. In some of the connection tests, however, failure initiated in the web at the end of the cope rather than at the connection. Figure 1.3 shows that local web buckling occurred in the coped region. Some unpublished beam failures have also occurred in practice with three distinct failure modes observed as discussed above, lateral-torsional buckling of the

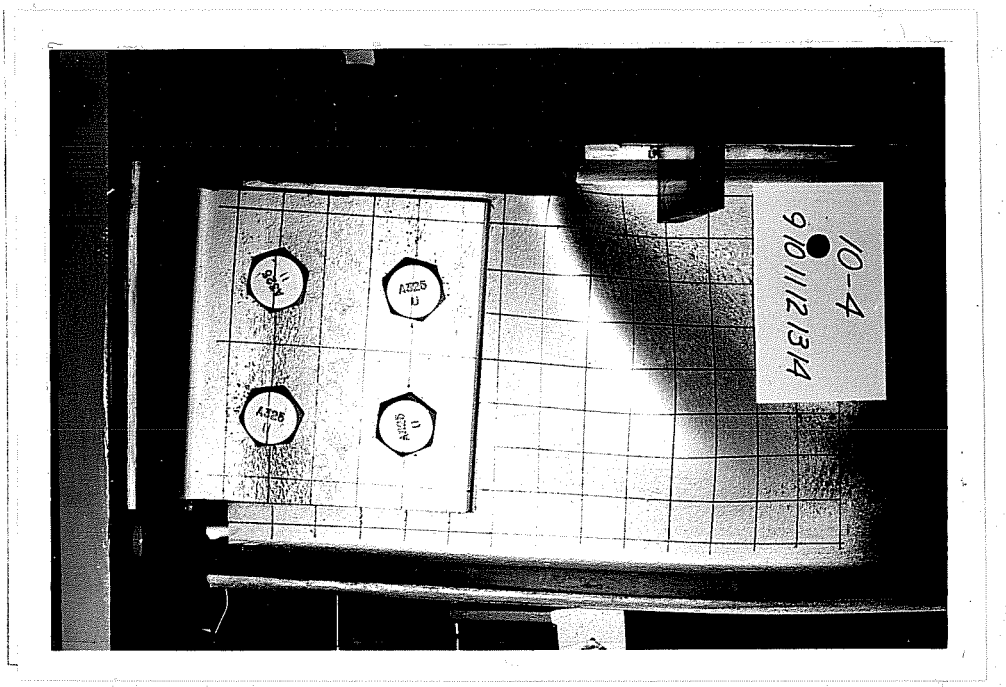

Fig. 1.3 Local Web Buckling

beam, local web buckling in the compression zone, and crack initiation at the cope in the tension region [8].

In order to provide more information about the behavior of coped beams, an elastic analysis was performed on a W10x22 section by the finite element program BASP [13]. The sample elastic shear and bending stress distribution given in Fig. 1.4 shows very significant deviations from the simple design assumptions, Mc/I and $V/h_o t_w$, close to the cope. Both bending stresses and shear stresses are high at the cope even for the coarse 1-in. mesh size used in this example. The local bending stress concentration factor (SCF) is 1.7 in this case with a 90^o cope profile. A few inches away from the end of the cope, simple bending and shear theory was quite satisfactory.

The general influence of the copes on the three failure modes is summarized below.

a. Lateral-torsional buckling: The compression flange of a laterally unsupported beam without copes takes the shape of a half sine curve when buckling occurs as shown by the dashed line in Fig. 1.5. When the top flange is coped, cross section distortion causes increased lateral displacements near the ends of the beams, thus reducing the lateral buckling capacity. The reduction of the buckling loads can be as high as 77 percent of the uncoped beam lateral buckling capacities, according to du Plessis's [3] test results.

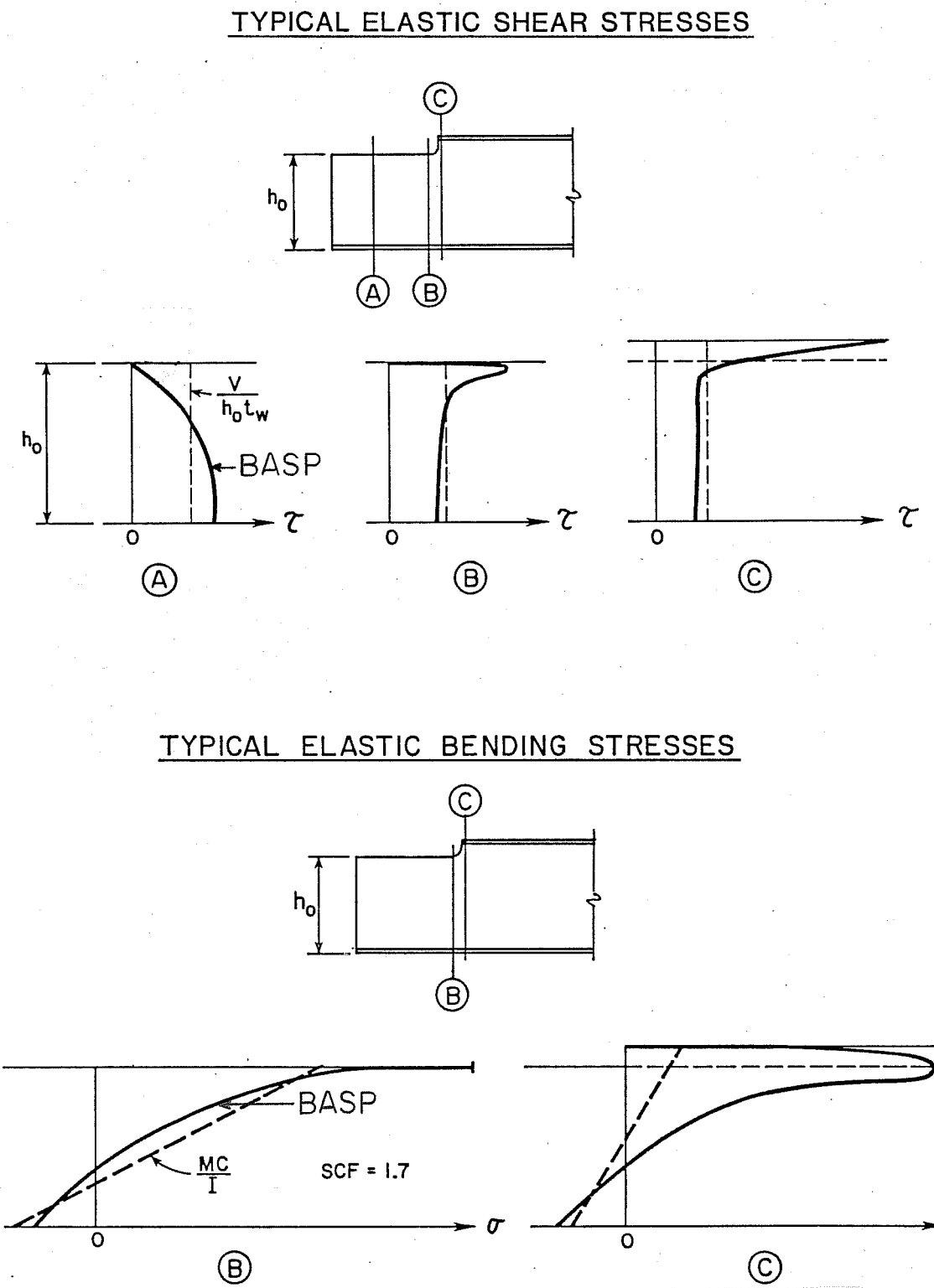

Fig. 1.4 Typical Elastic Stress Distributions at Coped Region

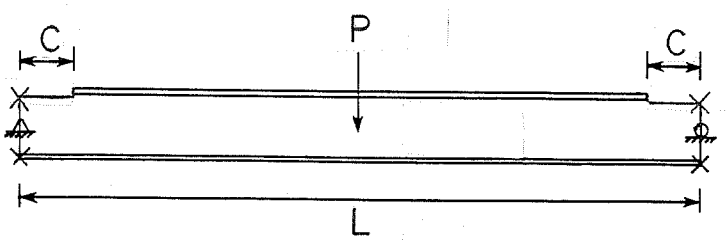

X — LATERAL BRACING

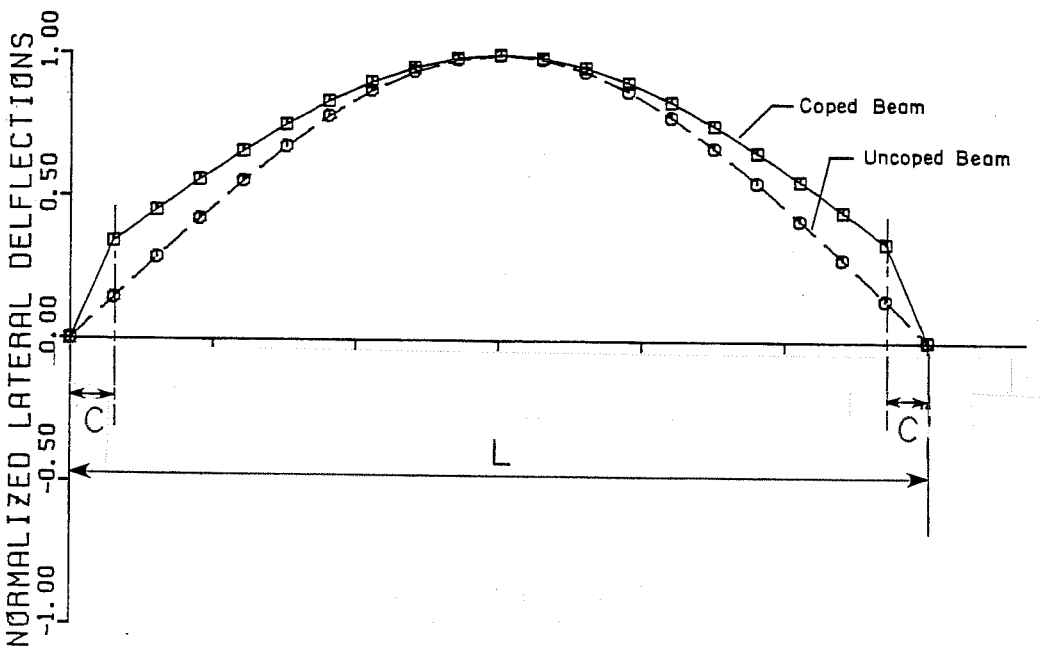

Fig. 1.5 Top Flange Buckling Shapes of Lateral-Torsional Buckling

b. Local web buckling: When the top flange is laterally supported, the coped beam can "fail" at the reduced section due to yielding from shear and bending stresses or from elastic local web buckling. First yielding is generally localized so deformations might not be large enough to curtail the usefulness of the beam. As yielding spreads, however, failure due to inelastic web buckling occurs since the yielding will reduce the stiffness of the web in the coped region. In the case of long copes or thin web plate girders, a beam could fail by elastic local web buckling at the coped portion. Therefore, the maximum shear and bending capacity of a coped section is controlled by elastic or inelastic local web buckling which is a function of the cope length, cope depth and the beam depth to web thickness ratio of the beam.

c) Fracture: The discontinuity of the cross section at the cope causes a stress concentration at this location; an SCF = 1.7 was calculated in the example shown in Fig. 1.4b. However, the very local stress concentration factor at the reentrant corner can be much higher depending on the cope profile at the corner. The American Institute of Steel Construction (AISC) suggests a minimum radius of 1/2 in. [9]. High SCF can cause problems of fatigue due to cyclic stresses and/or brittle fracture if tensile stresses are present at the cope, as shown in Fig. 1.6.

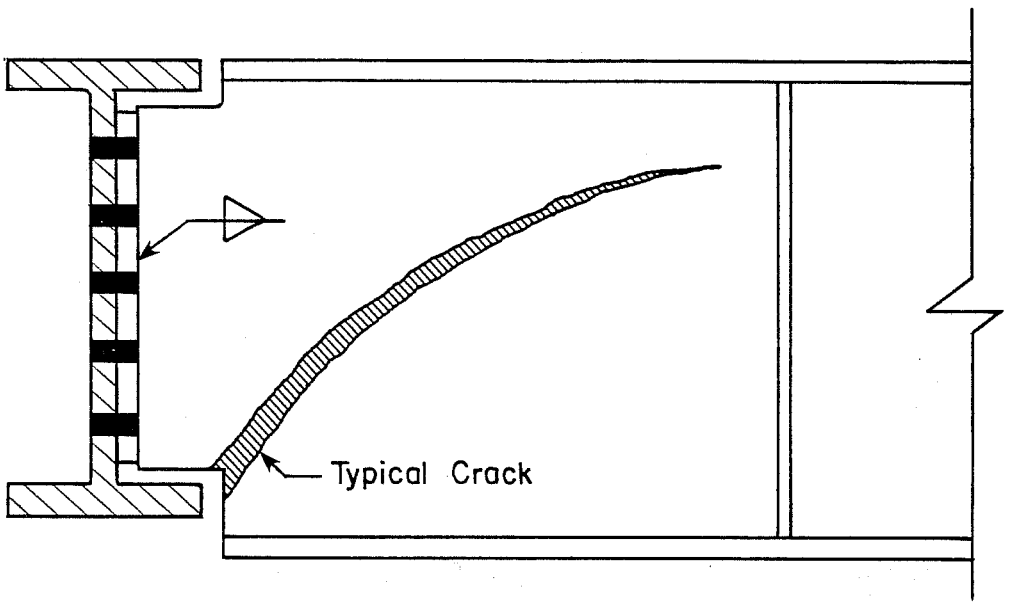

Fig. 1.6 Typical Crack Configuration for Coped Beams

The fracture and fatigue problems can usually be controlled by properly detailing to the cope profile in tensile regions, so this behavior will not be considered herein. Only problems related to compressive stresses will be studied.

1.2 Present Practice

Both the 1978 AISC Specification [10] and the Structural Stability Research Council (SSRC) Guide [11] contain provisions for designers to calculate the lateral-torsional buckling moment for I-beams. The design recommendations in various specifications have basically come from the following elastic solution:

$$M_{LTB} = (C_b \pi / L_b)\sqrt{EI_yGJ + E^2 I_y C_w \pi^2 / L_b^2} \qquad (1.1)$$

where

$$C_b = 1.75 + 1.05\, M_{sm}/M_{lg} + 0.3\, (M_{sm}/M_{lg})^2 \leq 2.3 \qquad (1.1a)$$

and L_b is the unbraced length. C_b is a modification factor for different loading conditions. $C_b = 1.0$ for uniform moment. C_b in Eq. (1.1a) is for a linear moment diagram where the moments are maximum at the ends of the unbraced length. C_b for other cases are found elsewhere [11]. The other terms are defined in the nomenclature. No reduction is made in any of the specifications to account for the presence of the coping. As mentioned in section 1.1 and as will be seen later, the effect of coping could be very

significant depending upon the cross section of beams, the coping detail and the span length.

For local web buckling, the 8th Edition of the AISC Manual of Steel Construction [9] states on p. 4-167,

> Unusually long and deep copes and blocks, or blocks in beams with thin webs, may materially affect the capacity of the beam. Such beams must be investigated for both shear and moment at lines A and C [Fig. 1.4] and, when necessary, adequate reinforcement provided.

In the AISC manual Structural Steel Detailing [12] examples of coped beam connections are provided. According to the design recommendations in Chapter 9 of the Detailing Manual, yielding due to bending moment at the coped section is checked using the reduced cross-sectional properties at the cope and neglecting stress concentrations. The shear capacity is determined by the standard AISC procedure, area of remaining web times the allowable shear stress: $V_{allow} = h_o t_w (0.4F_y)$, where h_o is the reduced beam depth in the coped region (Fig. 1.7). This procedure would only be valid for stocky webs where buckling would not be important. For thin webs where buckling is a consideration, some engineers have developed design procedures for coped beams which closely follow the buckling recommendation for tees given in Appendix C of the AISC Specification.

The elastic plate buckling formula upon which Appendix C is based has been derived as

$$F_{cr} = k \frac{\pi^2 E}{12(1-\nu^2)(b/t)^2} \qquad (1.2)$$

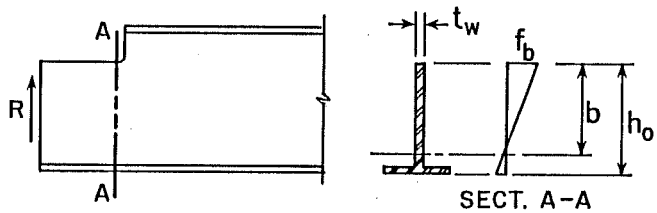

AISC DETAILING MANUAL

$f_b \leq 0.6 F_y$

$f_v = \frac{R}{h_o t_w} \leq 0.4 F_y$

(a)

BUCKLING OF TEES
APPENDIX C, AISC SPEC.

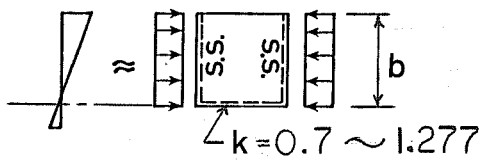

$f_b \leq 0.6 F_y \, Q_s$

(b)

Fig. 1.7 Current Design Methods

where k is a plate buckling coefficient which depends on the types of loading, edge conditions and length to width ratio, and b/t is the width to thickness ratio [3]. The k values in Appendix C assume a long rectangular plate (length $\geq$ width) with uniform compression along the length of the plate with two simply supported edges at both sides of the length and one free edge parallel to loading as shown in Fig. 1.7(b). For the fourth edge pinned, the plate buckling coefficient k is 0.425 and for a fixed condition, k = 1.277.

In Appendix C, the allowable bending stress, $F_b = 0.6\ F_y\ Q_s$, where Q_s is a reduction factor adopted to consider the different edge conditions so that yielding, inelastic buckling and elastic buckling are handled by one factor. k = 1.277 (fixed) was used to obtain the limiting b/t ratio for stems of tees in Appendix C where Q_s = 1.0 (yielding) and for elastic plate buckling, k = 0.7 (between simple support and fixed) is used to calculate the Q_s. Linear interpretation is applied to obtain Q_s for the inelastic range. No post-buckling strength is considered in the provisions for stems of tees. To apply the Appendix C design approach to the coped beams, the distance from the neutral axis of the coped section to the top fiber of the cope is taken as the width of the plate, b, as shown in Fig. 1.7, and Q_s for stems of tees in Appendix C is applied accordingly to determine the strength of the coped region.

These two design procedures, based on the AISC Detailing Manual and on Appendix C of the AISC Specification, are summarized in Fig. 1.7 for top coped beams. Hereinafter, these two approaches are

identified simply by Detailing Manual and Appendix C; design examples using them are given in Appendix A of this report.

Comparing the stress distribution of the coped beam as given in Fig. 1.4 with those used in the two design methods in Fig. 1.7 show a number of inconsistencies. First of all, in Fig. 1.4, both bending and shear stresses produce high stress concentration at the corner of copes which are not considered in design. It is necessary to investigate the effect of the stress concentration factor and the interaction of bending and shear stresses at the coped region. In addition, the high stress concentration probably will cause localized yielding at the corner of copes which can reduce the lateral stiffness of the web. Furthermore, the AISC Appendix C approach which neglects the bending stress gradient and stress variation from the beam end to the cope can produce a very conservative solution. Besides, if the cope length c is smaller than beam depth, the plate buckling coefficient k (based on an infinitely long plate) could be increased significantly depending on the length to width ratio which will also give conservative results. However, both design methods neglect the cope depth effects which will decrease the lateral restraint at the corner of the cope and probably will produce unconservative results, especially when the copes are deep.

1.3 Purpose and Scope

It can be seen from the above discussion that there is little research, both theoretical and experimental, on the topic of

coped beam design. Therefore, a research project sponsored by AISC was initiated to investigate the behavior of coped beams and to provide practical design recommendations for both lateral-torsional buckling and local web buckling. The research program developed to fulfill this purpose is primarily theoretical with some experiments conducted to verify the design recommendations. Parametric studies were conducted to establish the effect of cope length, cope depth and web thickness on elastic and inelastic local web buckling and elastic lateral buckling. Cope lengths up to two times the beam depth and cope depths up to one-half the beam depth were considered. The span-depth ratio was also evaluated for lateral buckling. Pinned end conditions, both in-plane and out-of-plane, were used to develop conservative design recommendations. Various stiffener arrangements at the cope were studied to determine their effectiveness in improving buckling strength.

Sixteen full size beams, 14 rolled sections and 2 plate girders, were tested for comparison with the theoretical results. Experiments by others were also used. Six of the tests considered lateral buckling; the remainder were for local web buckling at the cope.

Because two distinct problems were addressed for coped beams, namely lateral buckling and local web buckling, the results for both of these phenomena are presented separately. Chapters 2 through 7 deal with lateral-torsional buckling while web buckling at

the cope is treated in Chapters 8 through 12. The theoretical solution to both problems made extensive use of two computer programs: BASP, originally written by H. U. Akay and C. P. Johnson at The University of Texas [13] for buckling analysis, and ABAQUS, written by Hibbit and Karlsson, Inc. [14] for in-plane inelastic analysis. More details about the analysis techniques are given in Chapters 2 and 8, respectively.

Part I

LATERAL-TORSIONAL BUCKLING

CHAPTER 2

TOP FLANGE COPED BEAMS

In this chapter the design models for top (compression) flange coped beams are developed based on the behavior and results from a preliminary computer analysis. Further investigations and developments of the theories are given in Sec. 2.5 and final design recommendations are summarized.

2.1 Analysis Program

The computer program BASP, originally written by H. U. Akay and C. P. Johnson at The University of Texas, was used, which provides a general solution for the buckling analysis of plates having stiffener elements placed symmetrically about the plates. In the analysis, the web of an I-shaped section represents the plate while flanges are treated as stiffener elements. The web is idealized by two-dimensional finite elements while the flanges are idealized by conventional one-dimensional elements (Fig. 2.1).

The problems solved by this program are treated as a linear-elastic buckling problem. The yield strength of the material was assumed to be the upper limit for the material. The solution considers cross-section distortion as well as local buckling of the plates and torsional buckling of the stiffeners. The typical buckled shape of a 20-ft uncoped W16x26 section with lateral supports only at

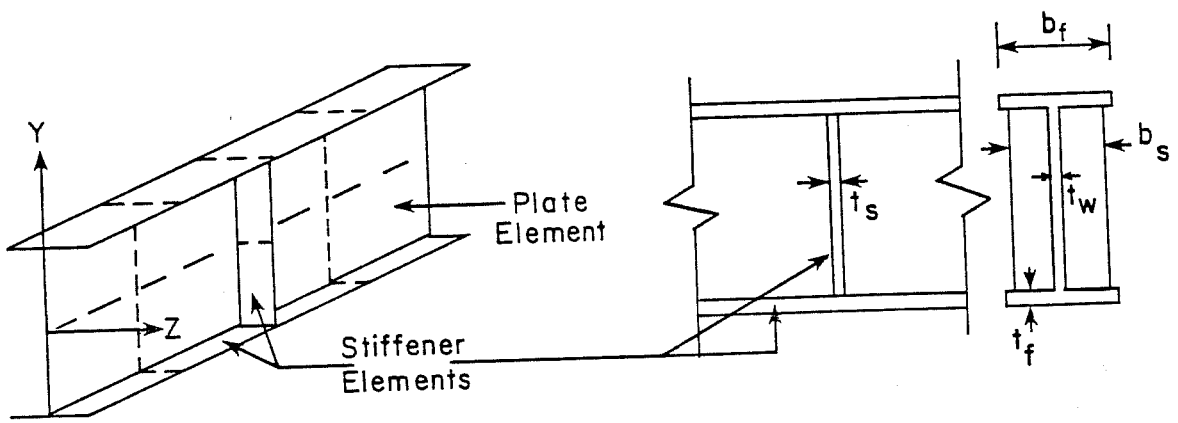

Fig. 2.1 Finite Element Model

the ends is shown in Fig. 2.2 where the horizontal axis is the length of the beam. Inverse iteration is used in this program to solve the resulting eigenvalue problem for the smallest load causing buckling. More details about the computer program BASP are given in Ref. 13.

A W16x26 section which has a $d/t_w = 62.8$ was used in this study. This rolled section has one of the most slender webs, so it was felt the results would be conservative for other rolled sections. The loading arrangement is shown in Fig. 2.2. Vertical web stiffeners were placed at the load position to prevent local buckling or eliminate the effects of cross-section distortion due to the concentrated load. Similar cope details were used at both ends so the beam would be symmetrical about midspan. This simplified the number of cases that needed to be studied and the results will be conservative if the two end details are different.

2.2 Scope and Limitation

The lateral-torsional buckling formula, Eq. (1.1), is based on elastic behavior. This assumption allows simple mathematical solutions, but excludes the consideration of inelastic buckling of beams. However, as discussed in Ref. 1, when yielding is confined to a zone close to a lateral support, the theoretical inelastic solution deviates very little from the elastic solution almost up to a maximum moment equal to M_p, the plastic bending moment. A typical situation would be a simple beam with a concentrated load at midspan where the load point, which is the point of maximum moment is also a brace

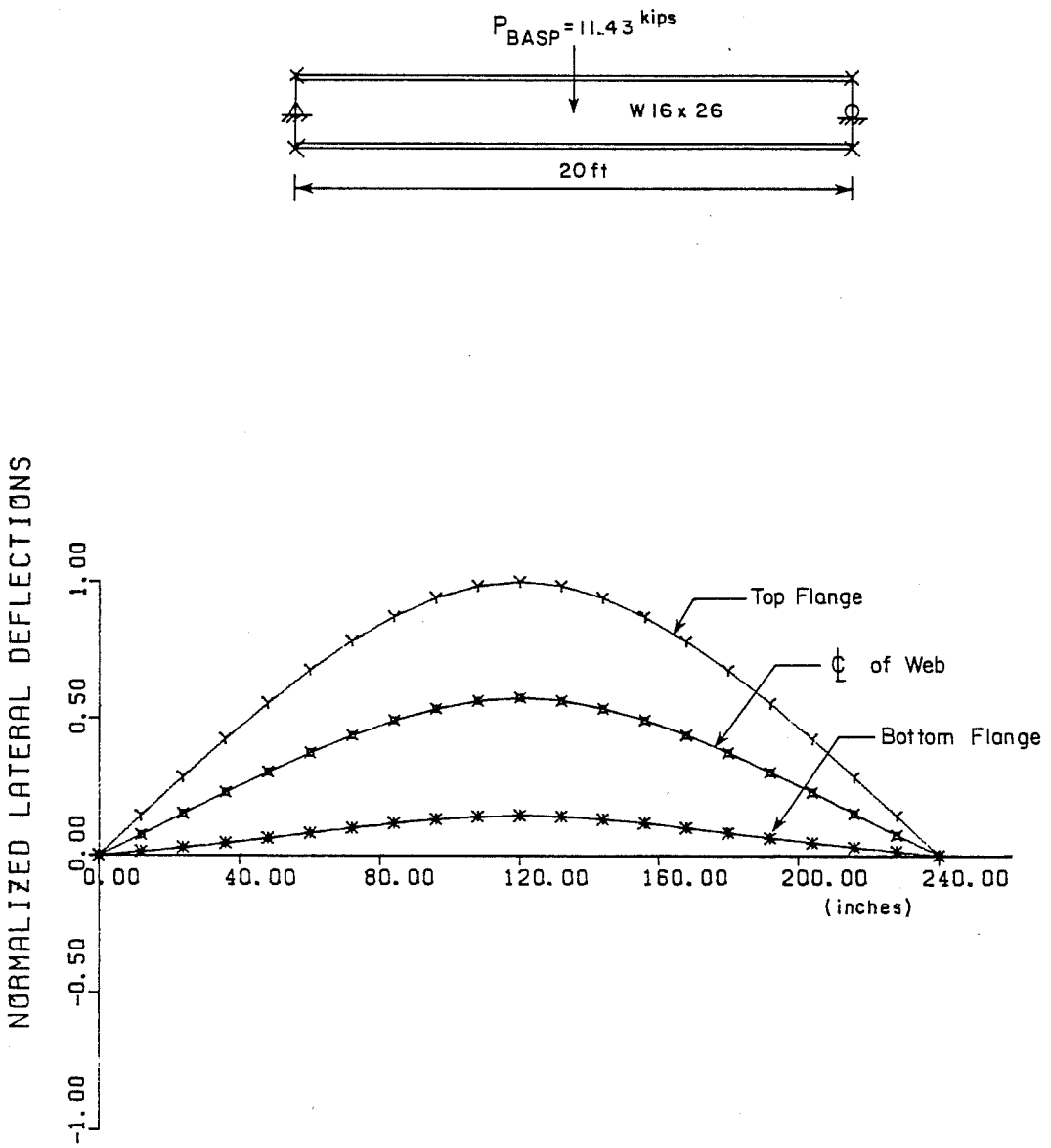

Fig. 2.2 Typical Buckled Shape of Uncoped Beams

point. Since load points usually act as brace points, yielding at the load point will not significantly affect lateral buckling. Therefore, in this study inelastic effects on lateral torsional buckling of coped beams were not considered.

The end restraints, both in-plane and out-of-plane, caused by the connection material such as web clip angles were not considered in developing design models in order to obtain conservative design recommendations. However, the effects of end restraint are discussed briefly in the Chapter 6. In addition, the effects of local flange and web buckling were eliminated by the use of stiffeners at the positions where local buckling might occur.

As mentioned in Chapter 1, only coped beams with a cope length less than twice the beam depth ($C \leq 2d$) and with a cope depth less than one-half the beam depth ($d_c \leq d/2$) will be considered in this study.

2.3 Preliminary Studies

Two beams as shown in Figs. 2.3 and 2.4 were analyzed. In each case the cope details were identical, 8 in. long and 1.5 in. deep, but two span lengths, 5 ft and 30 ft, were used. The main differences between the two cases is the ratio of coped length to span length (26 percent and 3 percent for L = 5 ft and 30 ft, respectively) and the ratio of warping term to the torsion term in Eq.(1.1), $EC_w\pi^2/GJL_b^2$, of the W16x26 section which is 14.9 and 0.41

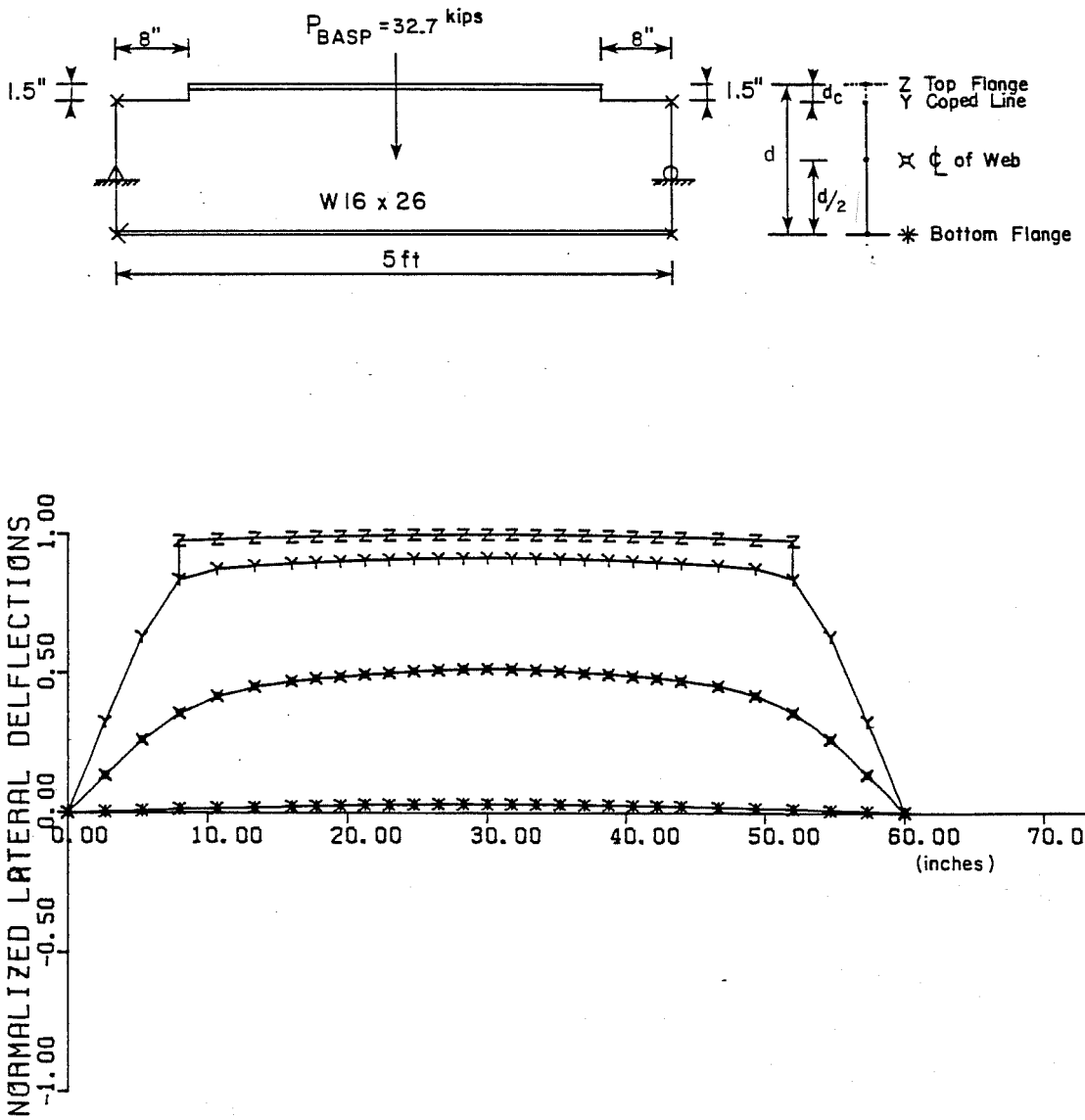

Fig. 2.3 Buckled Shape of 5ft Top Flange Coped Beam

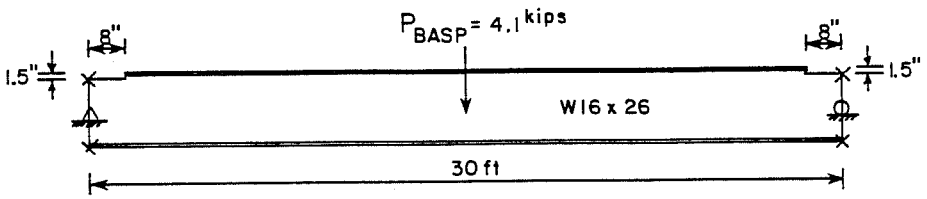

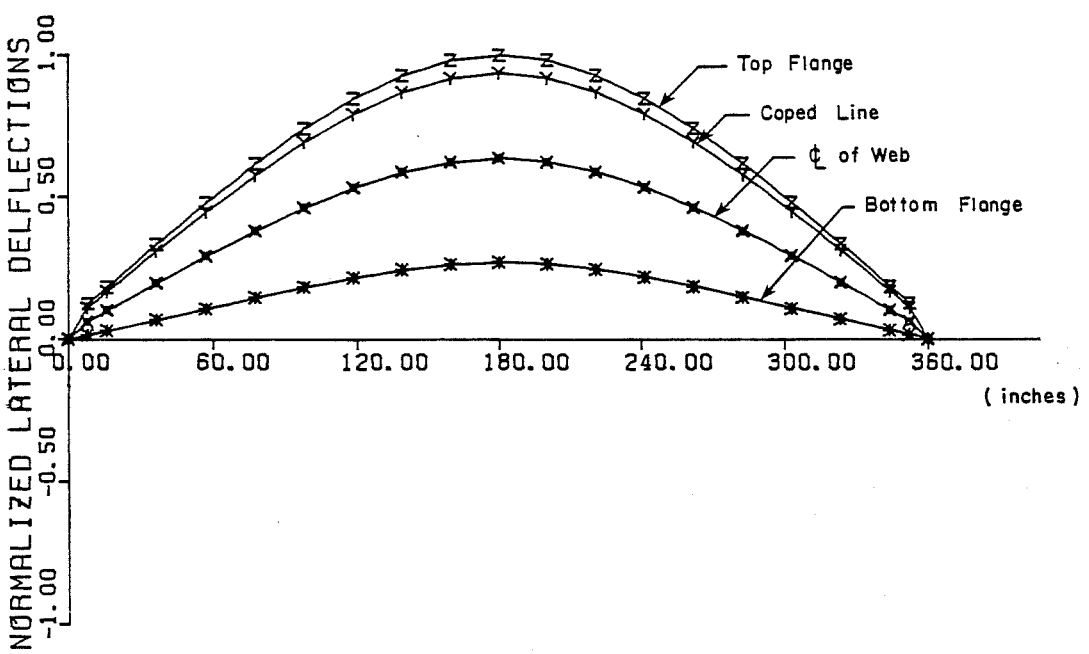

Fig. 2.4 Buckled Shape of 30ft Top Flange Coped Beam

for the 5 ft and 30 ft spans, respectively. These ranges cover most design conditions.

The buckled shape and buckling load for the two cases, which are shown in Figs. 2.3 and 2.4, provide many important characteristics of top-flange coped beams. The buckled shape of the 20-ft long uncoped beam shown in Fig. 2.2 should be used for comparison.

For the short beam it is obvious that the buckling capacity is controlled by the coped (tee) section. The uncoped (I) section simply deflects by rigid body motion. Severe cross-section distortion occurs in the coped region. The elastic buckling load, P_{BASP} = 32.7 kips, is much less than the theoretical elastic buckling load, P_{LTB} = 544 kips, for the uncoped beam, calculated by Eq. (1.1). Also, the theoretical load at first yielding at the edge of the cope using F_y = 50 ksi is 102 kips which indicates that lateral buckling will occur before yielding in this short beam.

The beam with a span L = 30 ft shown in Fig. 2.4 behaves like the uncoped beam shown in Fig. 2.2 and the buckling load P_{BASP} reaches 90 percent of P_{LTB} given by Eq. (1.1). In other words, the buckling capacity of Beam 2 is controlled mainly by the uncoped section although coping does decrease the buckling load.

2.4 Proposed Design Model

As discussed above, the buckling capacity of the short beam is controlled mainly by the capacity of the coped (tee) section since

the full section remains relatively straight in the buckled position. For long span beams, the buckling capacity of the uncoped region is smaller than that for the coped portion, if the two regions are treated as separate buckling problems. Based on these observations and some trials, a preliminary design model for top flange coped beams was developed assuming the buckling capacity of coped beams is the interaction of the lateral buckling capacity of the coped region (tee section) with span 2c and the uncoped region (I-section) with span L as shown in Fig. 2.5. For simplicity, the span of the "uncoped" region is chosen as L rather than (L - 2c). In accordance with this design model, the interactive design formula is proposed as follows:

$$1/P_{Tee} + 1/P_{LTB} = 1/P_{cr} \tag{2.1}$$

where P_{Tee} is the buckling load of the coped region and can be calculated by using the following equations from Ref. 15.

$$M_{Tee} = \frac{\pi}{2c} \sqrt{EI_y GJ} \left[\sqrt{1 + \left(\frac{\pi \gamma_m}{2}\right)^2} + \frac{\pi \gamma_m}{2}\right] \tag{2.2}$$

where

$$\gamma_m = \frac{\beta_x}{2c} \sqrt{\frac{EI_y}{GJ}} \tag{2.2a}$$

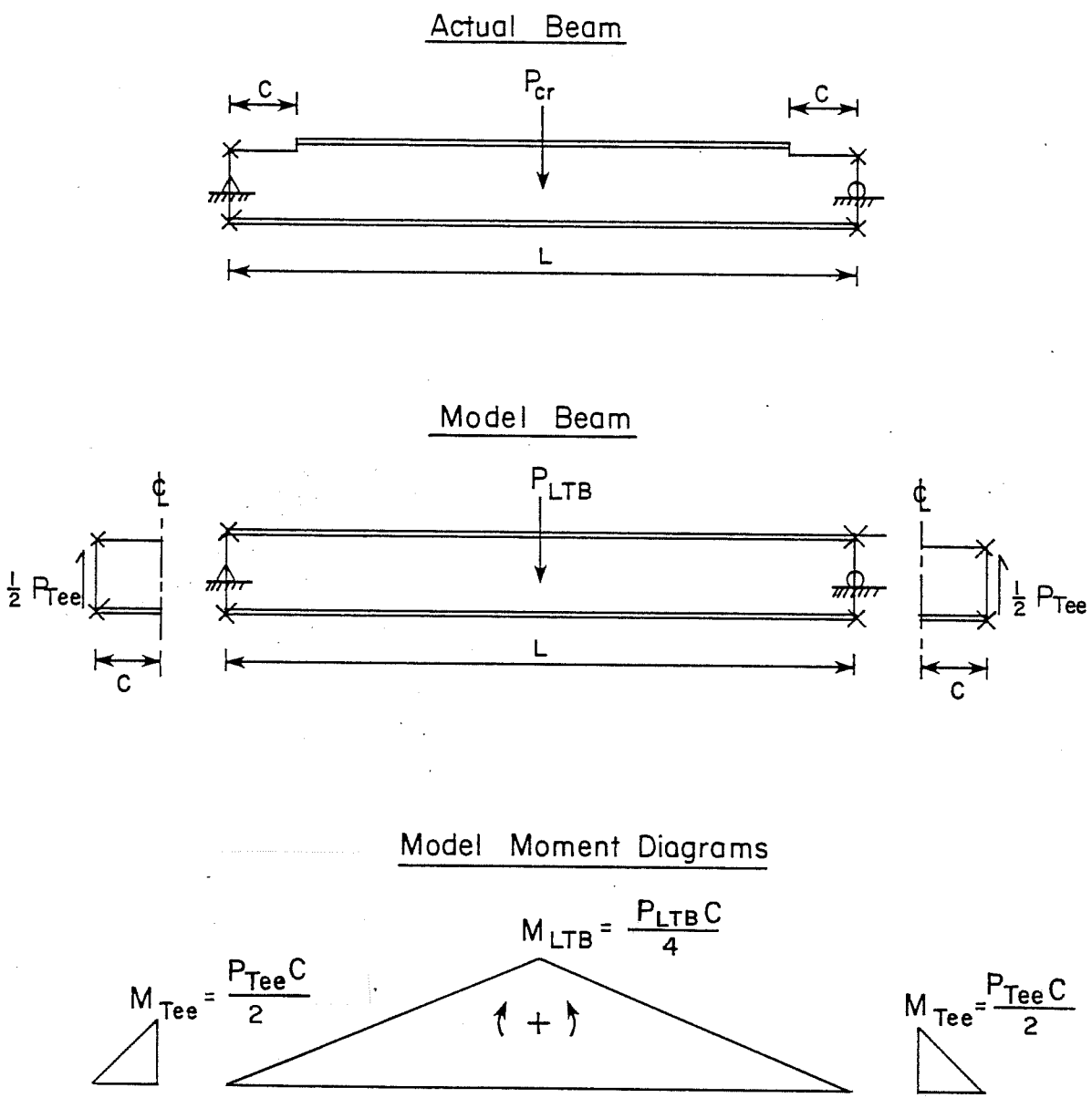

Fig. 2.5 Priliminary Design Model for Top Flange Coped Beams

$$\beta_x = - \left[\frac{1}{I_x} \left[\frac{t_w}{4} \left[(h_o - \bar{y})^4 - (\bar{y} - t_f)^4 \right] \right. \right.$$

$$\left. \left. - (\bar{y} - \frac{t_f}{2}) \left[\frac{b_f^3 t_f}{12} + b_f t_f (\bar{y} - \frac{t_f}{2})^2 \right] \right] + 2\bar{y} - t_f \right] \qquad (2.2b)$$

where y is the distance between the neutral axis and the extreme fiber of the flange. For the P_{LTB} calculation, Eq. (1.1) is used and L_b and C_b are defined in Eq. (1.1). For Case 1, the span length is 5 ft. Equation (2.1) yields P_{cr} = 34.8 kips, which is about 6 percent higher than the BASP prediction. For Case 2, the span length is 30 ft. Equation (2.1) gives P_{cr} = 4.0 kips, which is 3 percent lower than the BASP prediction. There is good correlation between the BASP solutions and the design interaction equation (Eq. (2.1)) for the two cases above. Further parametric studies with different cope details, loads and braces will be investigated in order to apply the model to more general design conditions.

2.5 Parametric Studies

The proposed design model in Sec. 2.4 was developed by a beam with single load at centroid of mid-span, laterally unsupported along the entire span, and coped with a single detail at both ends of the unbraced span. While it was expected that this case would probably cover the most important variables, there are other

practical bracing conditions and cope details that need to be considered before the design recommendations can be used with confidence.

Three parameters, span length, cope length and cope depth, were studied to check and modify the design recommendations proposed in Sec. 2.4. Two bracing conditions, with (Fig. 2.6) and without (Fig. 2.2) brace at the load positions were studied with each of the three parameters to cover most of the practical design conditions. Figure 2.6 shows the typical buckled shape for a 20 ft uncoped W16x26 section with a brace at the load position.

2.5.1 Variation of Span Length. The span length was varied from 5 ft to 30 ft in which the ratio of the warping term to the torsion term in Eq. (1.1) ranges between 0.41 to 59.6. A single coping detail (C = 8 in. and d_c = 1.5 in.) was adopted for this study. The BASP results for the two bracing conditions are compared with the proposed design equation (Eq. (2.1)) in Figs. 2.7 and 2.8, respectively. The loads at yielding of the coped and uncoped regions with Gr. 50 material are also shown in the figures for comparison. The load to cause yielding at the cope, P_y at cope = 102 kips, is constant for the two cases since the cope length is not varied. The top flange buckled shapes in which the span lengths and deflection shapes have been normalized are shown in Fig. 2.9.

Figure 2.7 shows that Eq. (2.1) gives results very close to the theoretical buckling solutions generated by BASP. It confirmed that the buckling capacity of coped beams can be treated as a

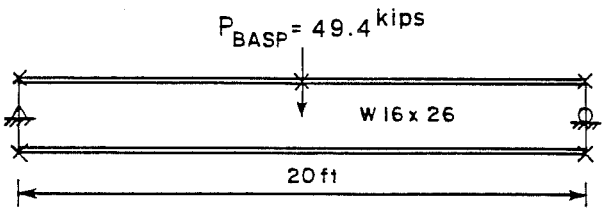

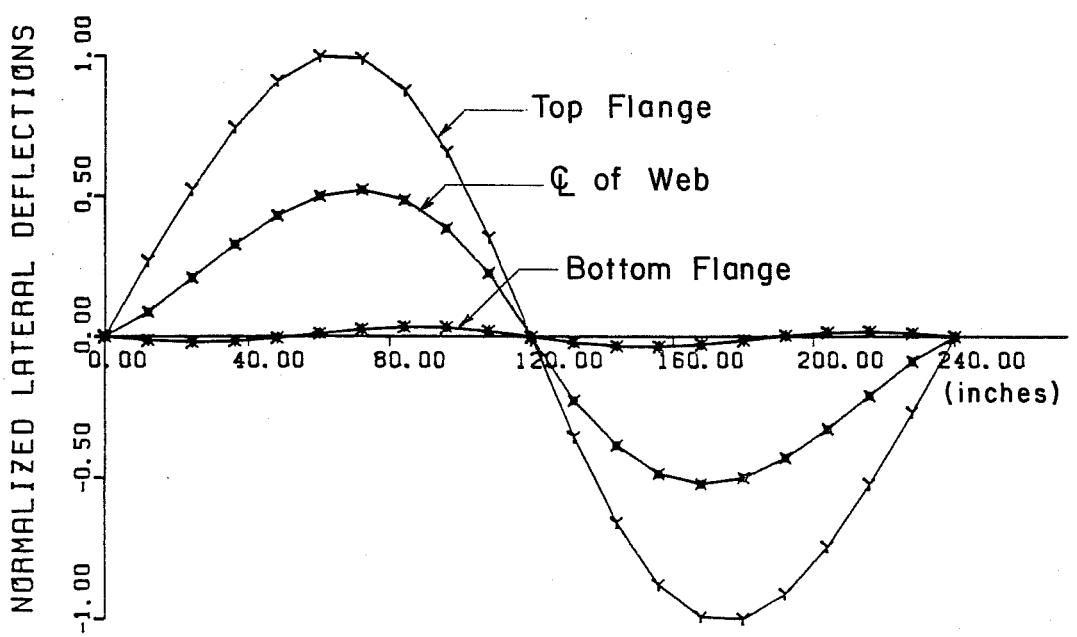

Fig. 2.6 Buckled Shape of Uncoped Beam with Brace at the Load Position

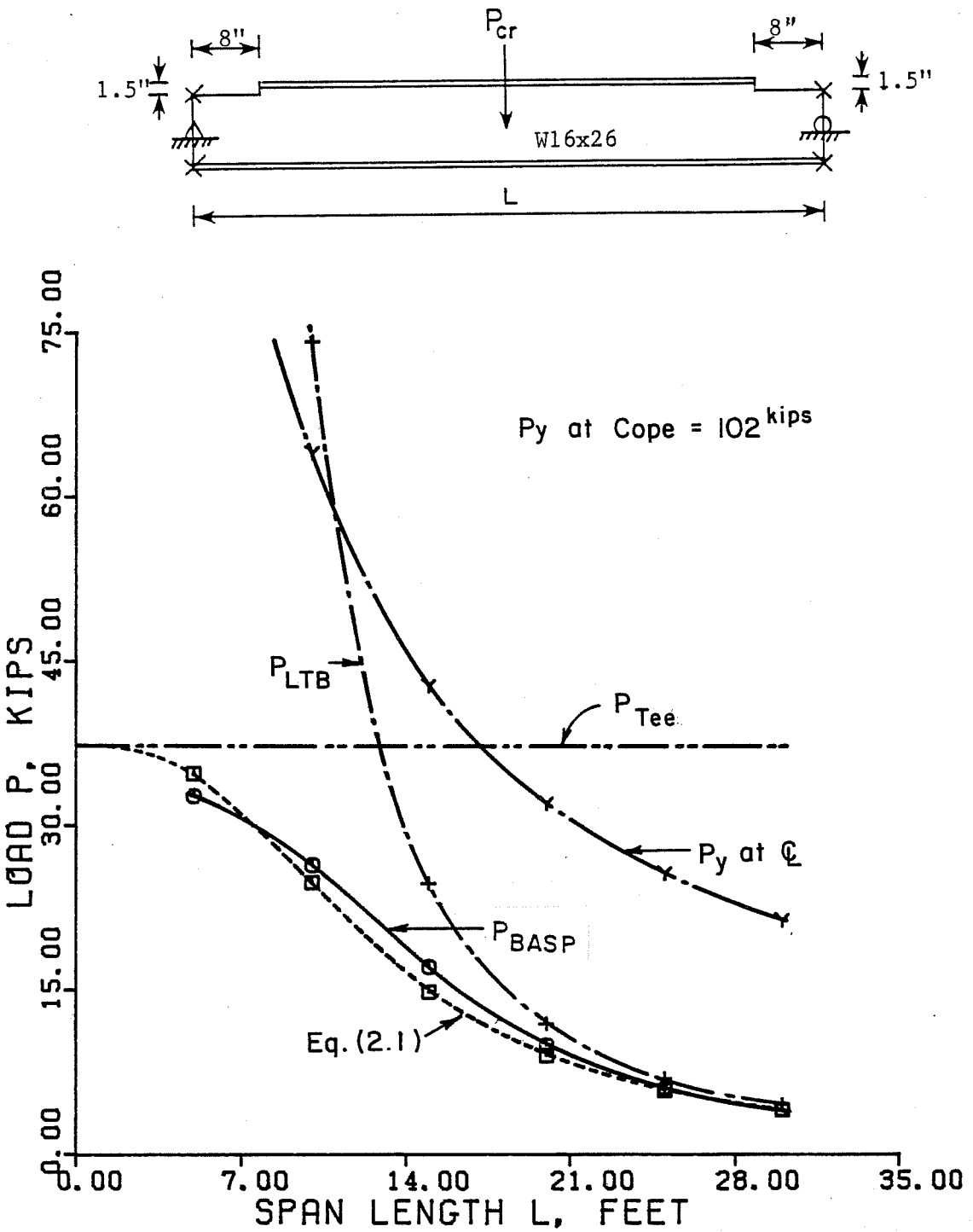

Fig. 2.7 Effect of Span Length for Brace Case 1 of Top Flange Coped Beams

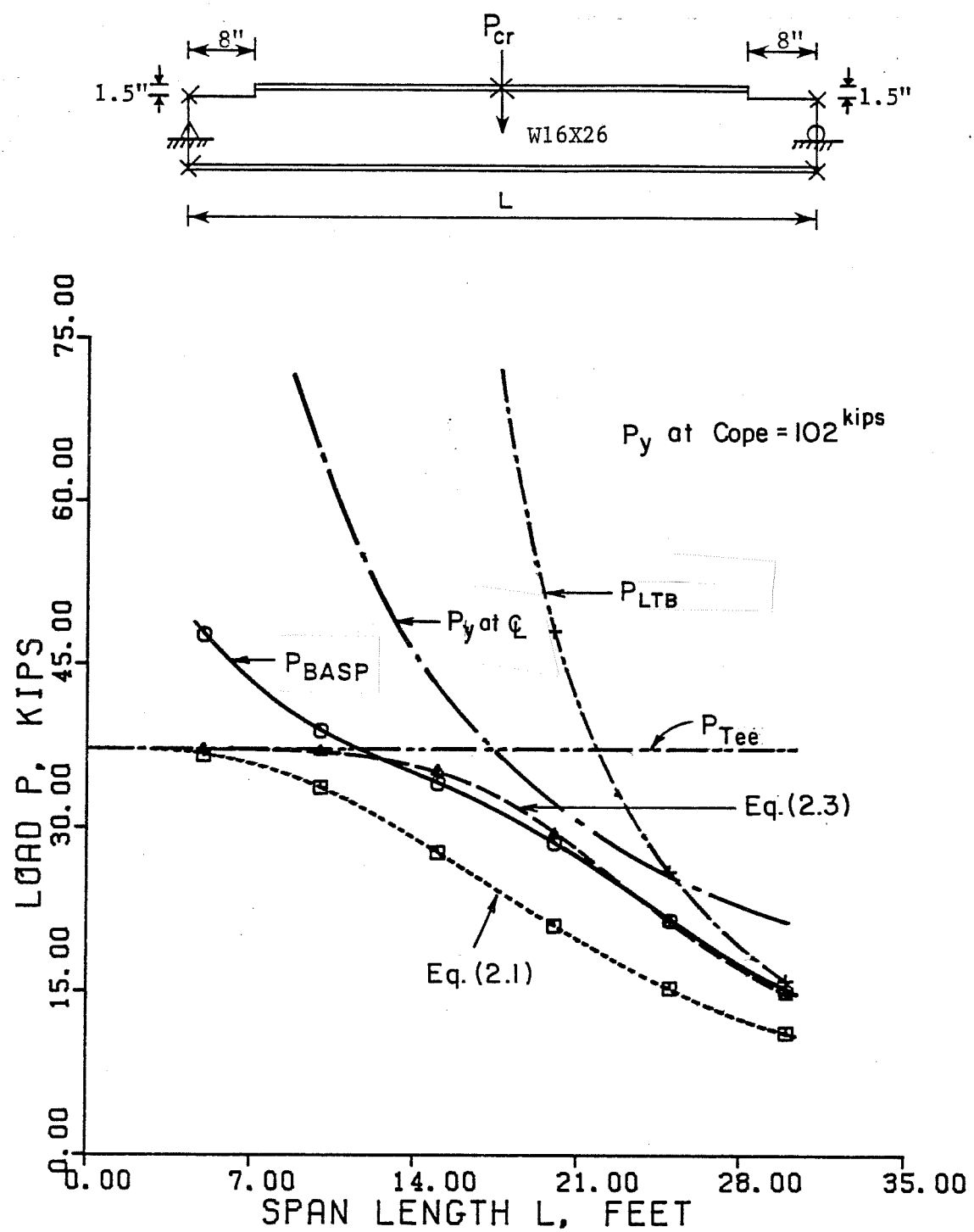

Fig. 2.8 Effect of Span Length for Brace Case 2 of Top Flange Coped Beams

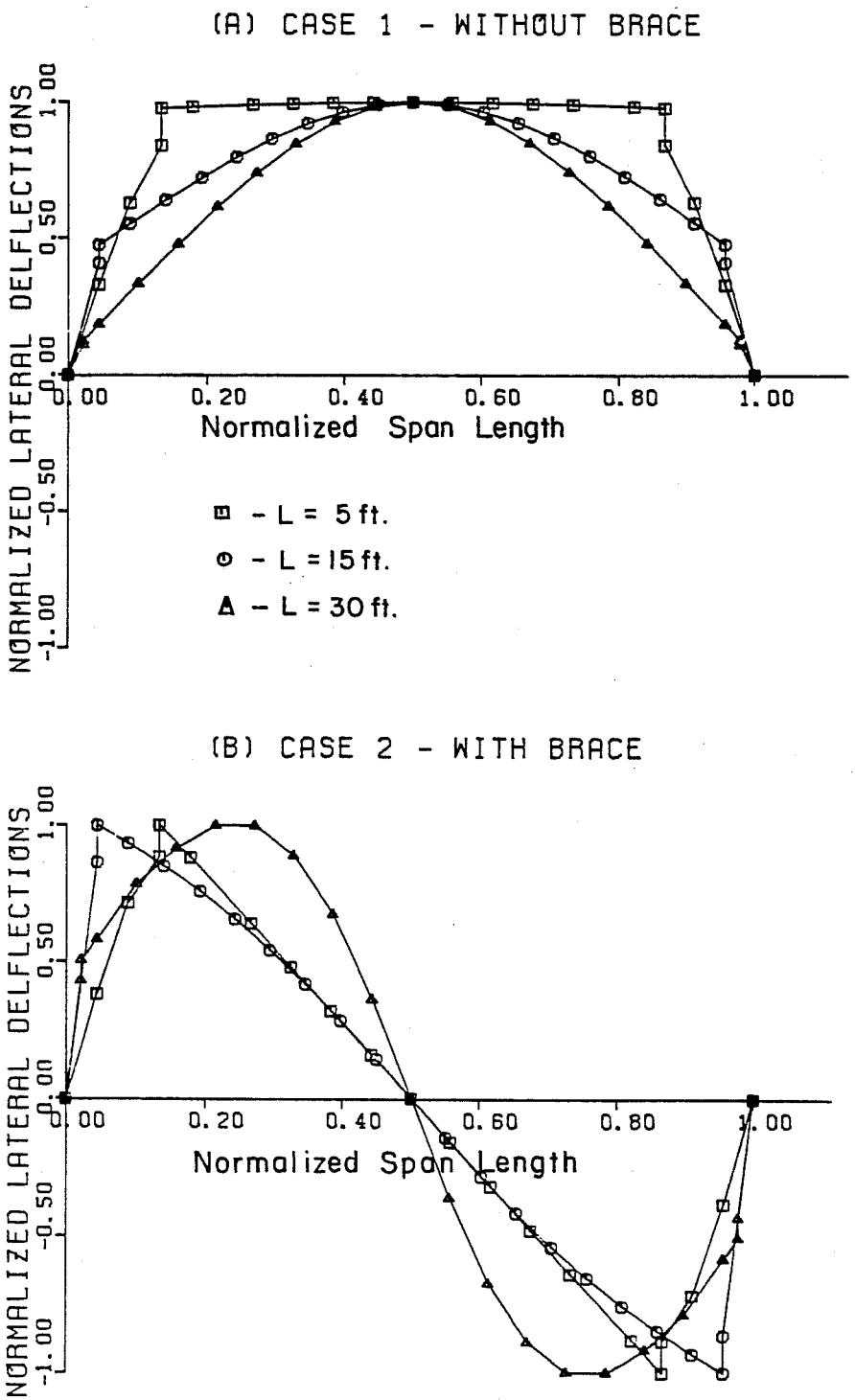

Fig. 2.9 Top Flange Buckled Shapes of Varied Span Length

combination of the capacity of the coped section (P_{Tee}) and the capacity of the uncoped section (P_{LTB}) defined by Eq. (2.1). However, when a lateral brace is present at midspan as shown in Fig. 2.8, Eq. (2.1) gives very conservative results compared with BASP solutions. The main reason is that in this case the unbraced span (L_b) has coping at one end only which will decrease the effects of the coped region and increase the buckling load. Equation (2.3), as follows, is proposed to reduce the interactive effects of the coped and uncoped regions for a

$$1/(P_{Tee})^2 + 1/(P_{LTB})^2 = 1/(P_{cr})^2 \qquad (2.3)$$

beam with coping only at one end of unbraced span. The differences between Eq. (2.3) and BASP solutions are shown in Fig. 2.8. The BASP solutions for short beams when P_{Tee} is dominate (L < 10 ft in Fig. 2.8) are higher than the Eq. (2.3) results because P_{Tee} is calculated assuming uniform moment along the unbraced length, 2c, whereas P_{BASP} considered the actual moment diagram. No moment gradient coefficient, C_b, is available for tee sections.

It should be noted that in Figs. 2.7 and 2.8, the buckling loads of the coped beams are smaller than the yielding of the beams. In other words, coped beams will buckle elastically even for very short spans. This can be easily understood from Fig. 2.9, which shows that lateral buckling is controlled by the coped region for short beams and is relatively independent of the span length.

2.5.2 Variation of Cope Length. The cope length was varied from 0 to 32 in. to check the proposed design formulas (Eqs. (2.1) and (2.3)). The coped depth = 1.5 in. and span length = 20 ft were chosen for this study. The BASP solutions of both cases are compared with the proposed design equations in Figs. 2.10 and 2.11, respectively. The yielding of the coped and uncoped region using Gr. 50 material are also shown. In Fig. 2.10, the yield load of the coped region (P_y at cope) is off the graph. It can be seen in Fig. 2.11. The buckled shapes of the top flange for the two bracing cases are shown in Fig. 2.12.

In Fig. 2.10, Eq. (2.1) gives reasonable solutions compared with P_{BASP}. For the second brace case, Eq. (2.3) gives better results compared with P_{BASP} while Eq. (2.1) yields conservative results. When the 20 ft span is unbraced (Case 1), lateral buckling takes place before yielding. For Case 2 with a brace at midspan, yielding controls when the cope length is $\leq$ 7 in. or 6 percent of the unbraced length of 10 ft. For longer copes, buckling controls.

2.5.3 Variation of Coped Depth. The cope depth was varied from 0 to 7.5 in. to check the proposed design equations for situations in which the beam is coped up to one half of beam depth. A cope length = 8 in. and span length = 20 ft were used for this study. The BASP solutions of both cases are compared with Eqs. (2.1) and (2.3) in Figs. 2.13 and 2.14, respectively. Since all the buckling loads are smaller than the yield load for Gr. 50 material,

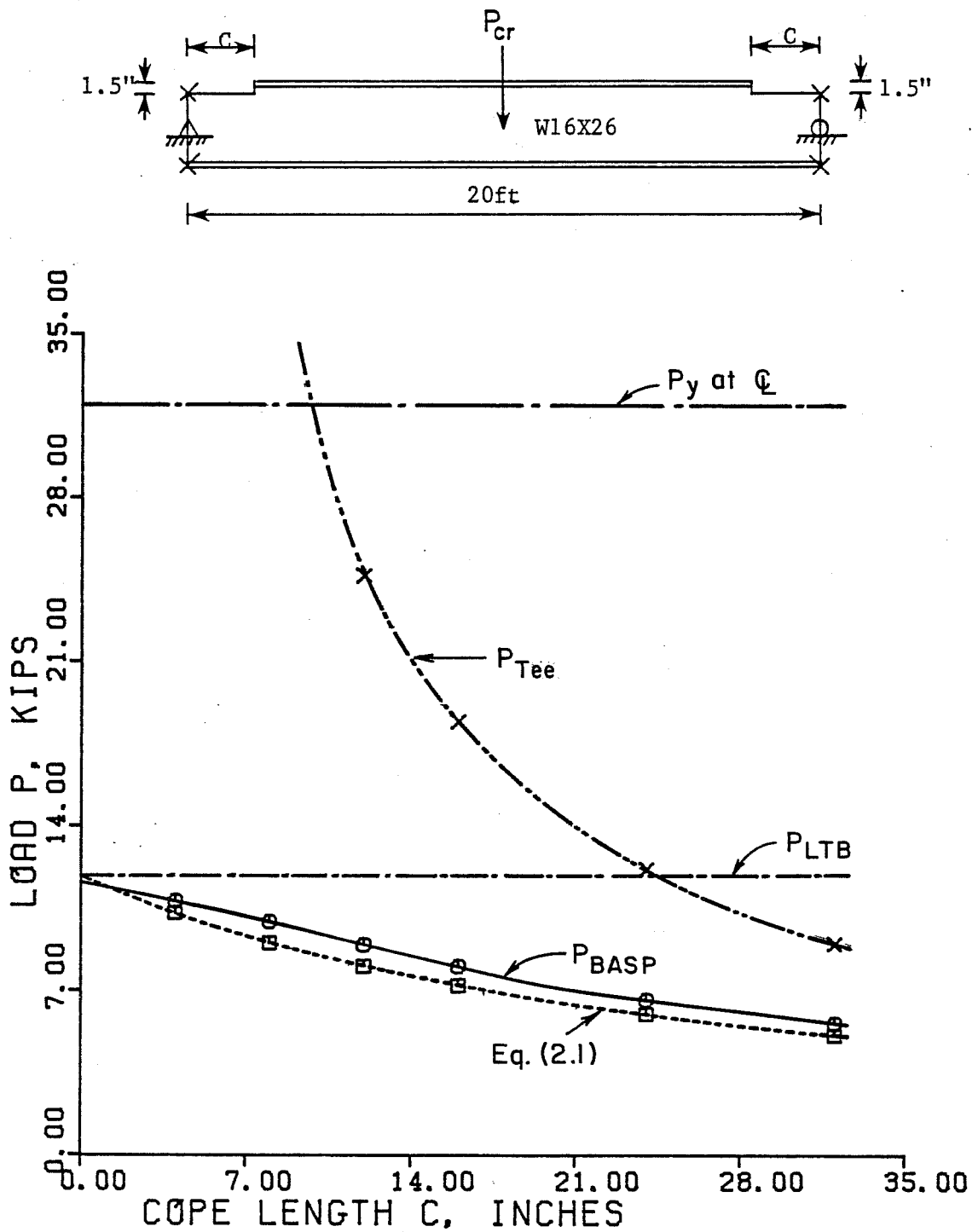

Fig. 2.10 Effect of Cope Length for Brace Case 1 of Top Flange Coped Beams

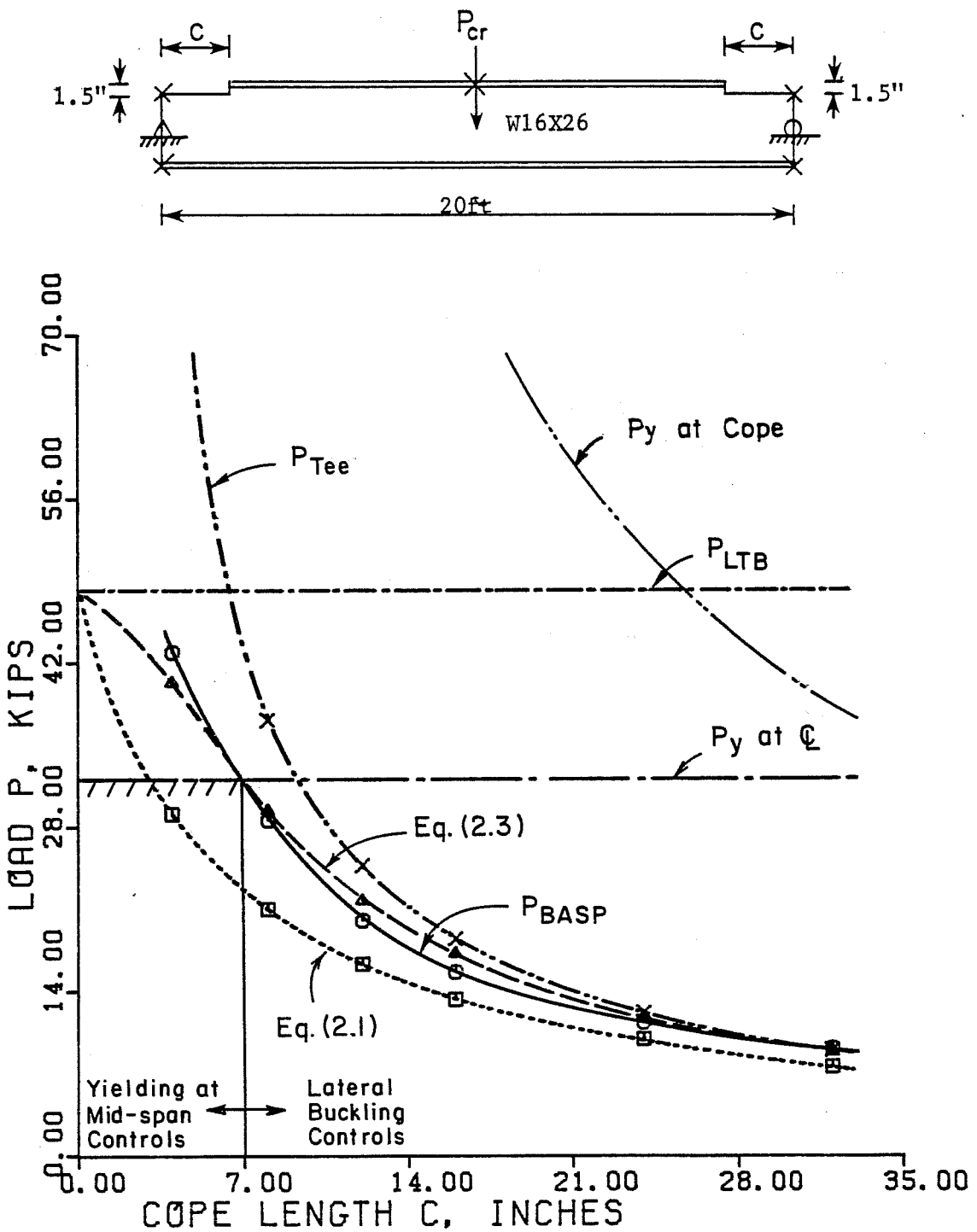

Fig. 2.11 Effect of Cope Length for Brace Case 2 of Top Flange Coped Beams

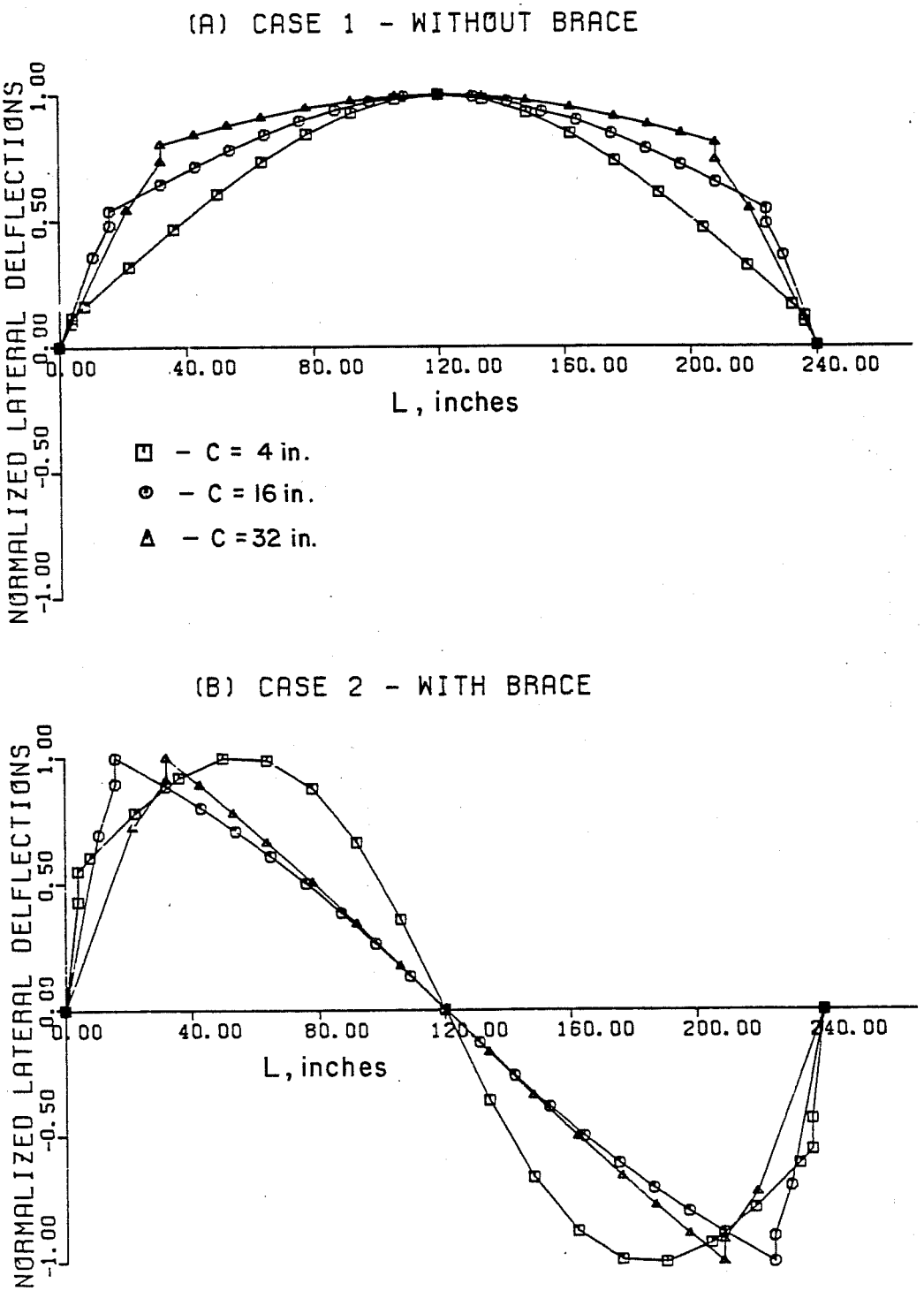

Fig. 2.12 Top Flange Buckled Shapes of Varied Cope Length

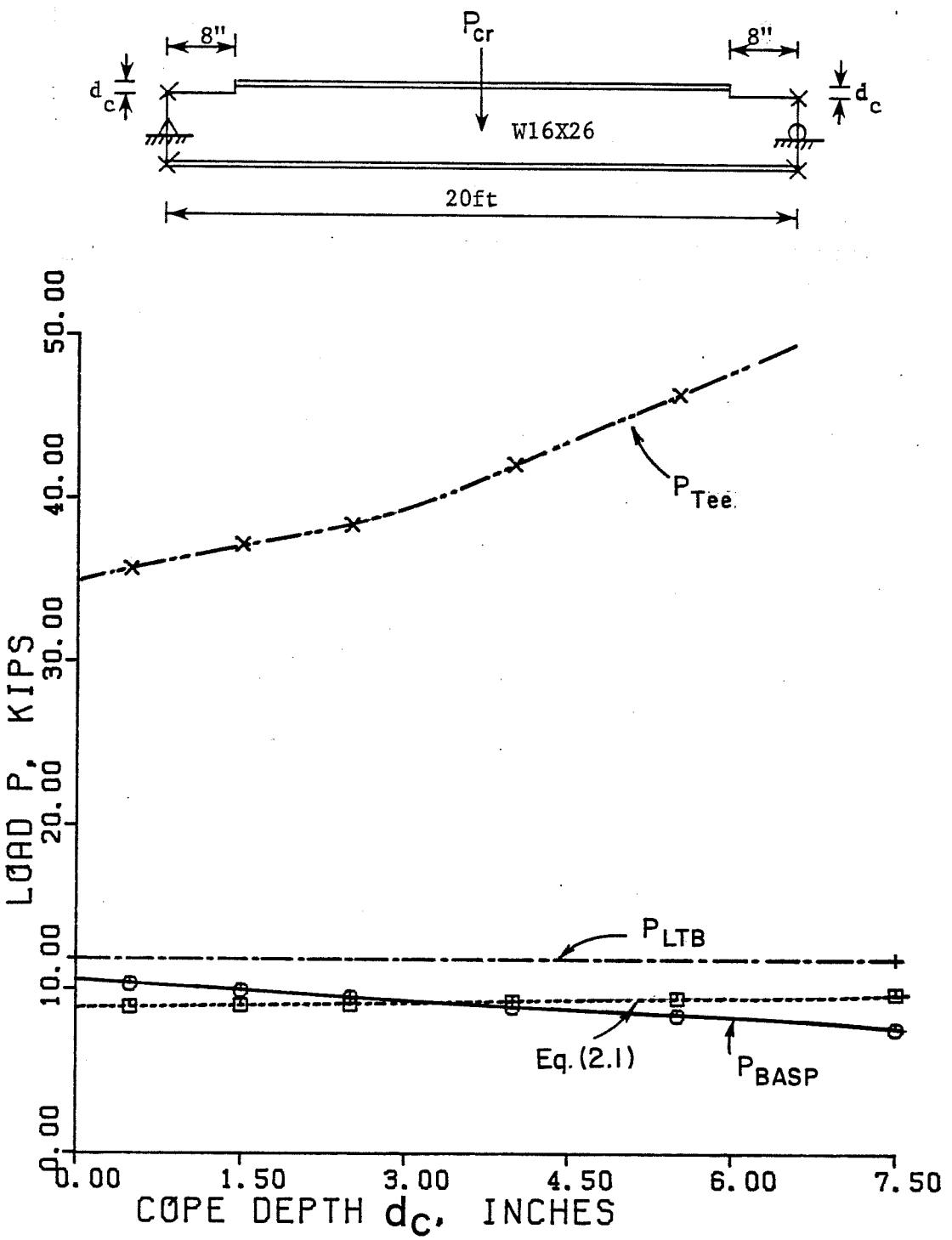

Fig. 2.13 Effect of Cope Depth for Brace Case 1 of Top Flange Coped Beams

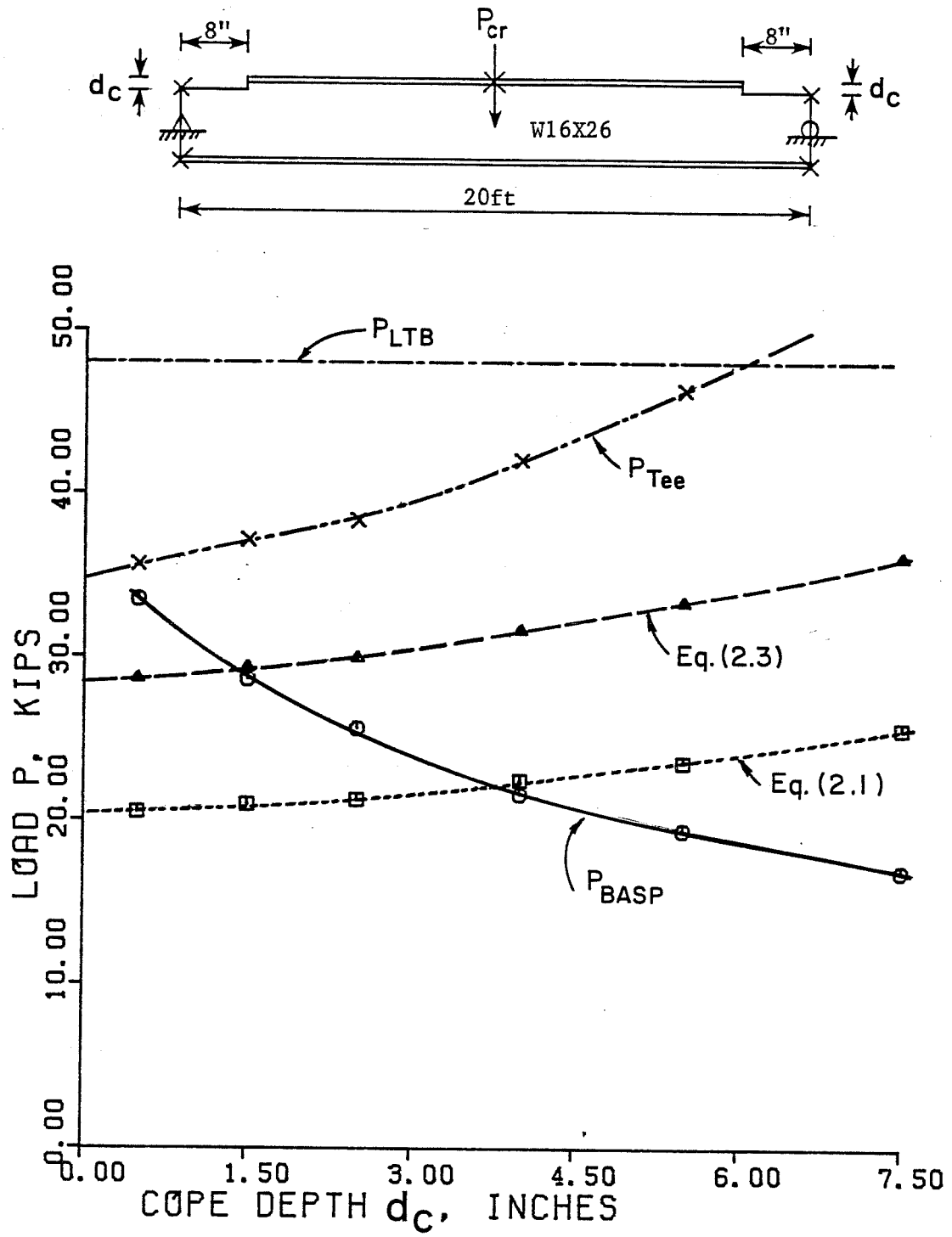

Fig. 2.14 Effect of Cope Depth for Brace Case 2 of Top Flange Coped Beams

the yield loads of the coped and uncoped regions are not shown in the figures.

In Figs. 2.13 and 2.14, both Eqs. (2.1) and (2.3), respectively, become unconservative as coped depth increases. This is due to an inadequate model for the calculation of P_{LTB} and P_{Tee} as indicated by the lateral deflections of the cross section at A for two brace conditions shown in Fig. 2.15. Due to lack of lateral restraint at coped depth position A, the top flange tends to tip over at the coped region which decreases the buckling load of the uncoped region. This movement creates a lateral force on the coped (tee) region that will also decrease the buckling capacity of the coped region. The buckled shapes of the top flange for both brace cases are shown in Fig. 2.16. In Fig. 2.15, the lateral deflections of Case 2 have the same shape for the three different coped depths because the maximum lateral deflection for all three cope depths occurs at the A position and the lateral deflections are normalized. However, Figs. 2.14 and 2.16b show that the buckling capacities and the top flange buckled shapes are affected by coped depth. In order to use Eqs. (2.1) and (2.3), modification must be made for calculating P_{LTB} and P_{Tee} to account the effects of coped depth.

2.5.3.1 Modification of P_{LTB}. Two models as shown in Fig. 2.17 were developed for the two bracing cases to account for cross section distortion as cope depth increases. The results are compared with the BASP solutions in Fig. 2.18.

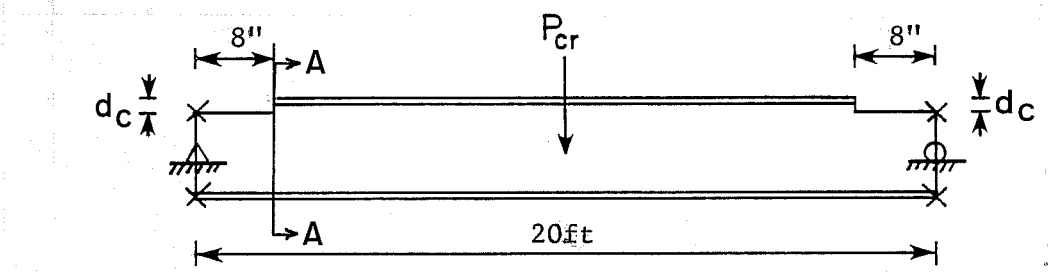

Case 1 – Without Brace

Case 2 – With Brace

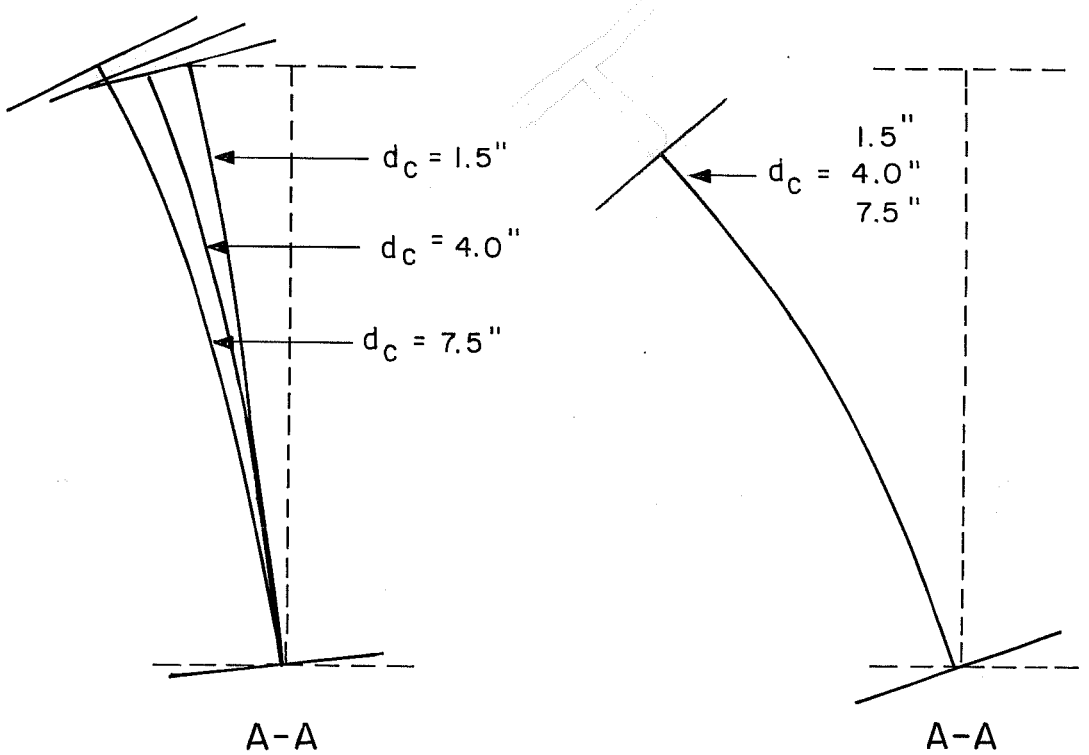

Fig. 2.15 Lateral Deflection of Varied Cope Depth at the Section A

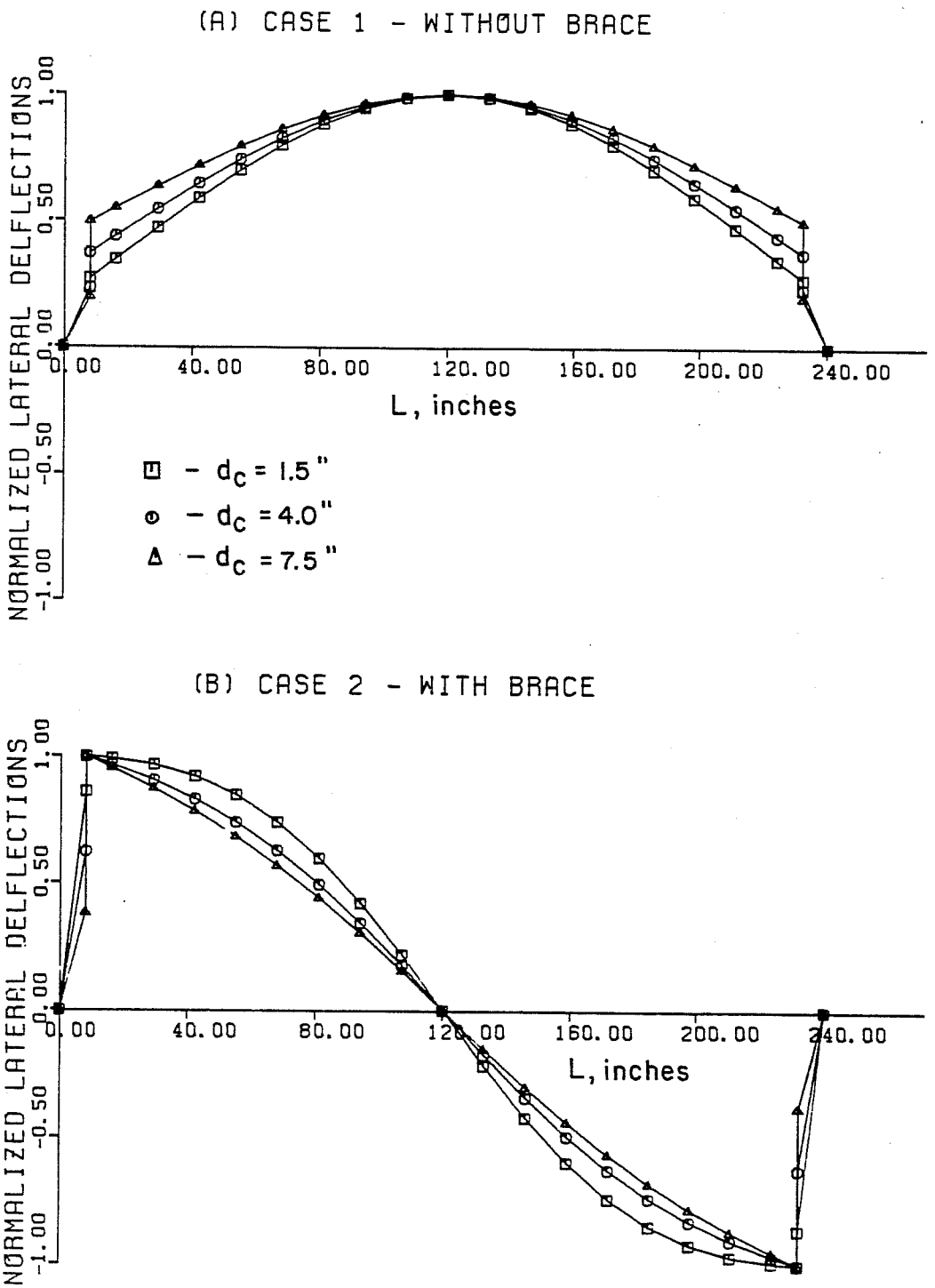

Fig. 2.16 Top Flange Buckled Shapes of Varied Cope Depth

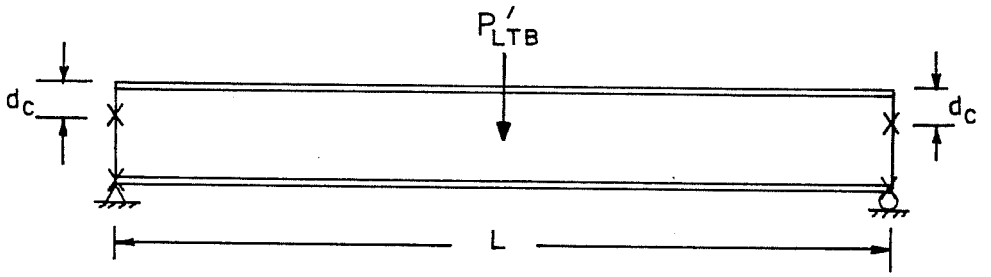

(a) Column Analogy

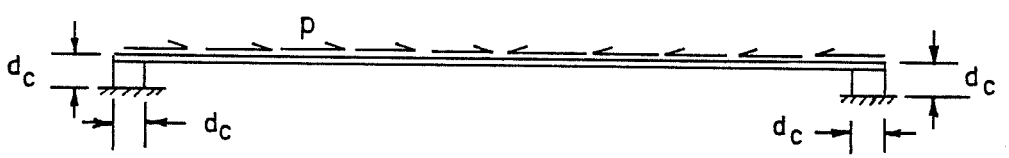

(b) Model 1 – Without Brace

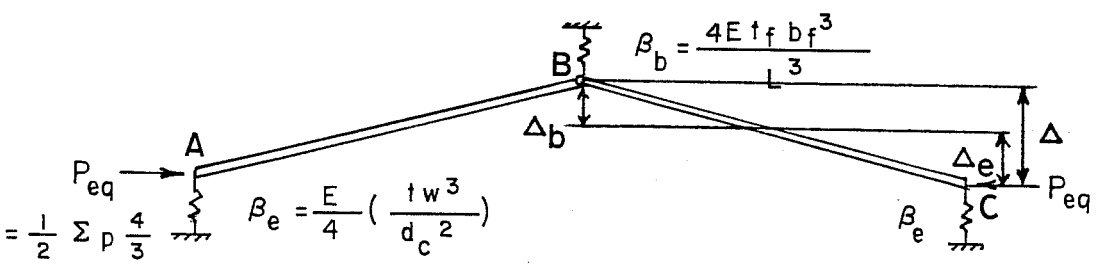

(c) Model 2 – With Brace

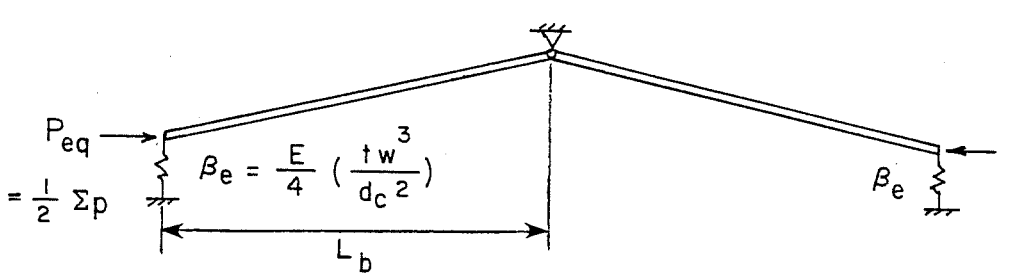

Fig. 2.17 Modified Models for Lateral-Torsional Buckling Capacity of Uncoped Length

In Fig. 2.17, the top flange of the beams was modeled as a column with lateral restraints at both ends. The lateral restraint is represented by a spring stiffness, $\beta_e = (E/4)\,(t_w^3)/(d_c^2)$, which is established by assuming cantilever action of the web plate above the cope line with length, d_c, and an effective plate width also chosen as d_c as shown in Fig. 2.17(a). β_e implies that for deep copes and thin webs, the lateral buckling loads of coped beams will decrease very rapidly. To further simplify the column analogy, the rigid body models as shown in Figs. 2.17(b) and (c) are used. In Fig. 2.17(b), $\beta_b = (4\,Et_f b_f^3)/L^3$ is the stiffness of the flange and P_{eq} is the equivalent axial force which causes the buckling of the top flange of the beam. The maximum axial force (Σp) in the top flange at midspan can be approximated by dividing the applied moment by the beam depth. In the P_{eq} calculation, the 1/2 factor in Figs. 2.17(b) and (c) accounts for the linear variation in flange force due to the applied moment gradient. The 4/3 factor in Fig. 2.17(b) was obtained by calculating the buckling load of Model 1 with $\beta_e = \infty$ and comparing the result with the BASP solution for the case of uniform moment. Thus, the 4/3 factor is a correction which is primarily due to the difference between the straight line buckling shape of the model and the sine curve shape of the actual beam. In the case 1 model which has no bracing at load point, the buckling load calculated by the model includes both lateral buckling of the top flange and the tipping effect of the unrestrained cope depth. The critical buckling load P'_{LTB} is $= 4\,M'_{LTB}/L$ where

$$M'_{LTB} = \Sigma p \cdot d = 3/2\ P_{eq} \cdot d$$

Cutting the structure at point B in Fig. 2.17(b) and ΣM gives

$$P_{eq} \cdot \Delta = \beta e \cdot \Delta_e \cdot L/2 \qquad (a)$$

Summation of vertical forces gives

$$\beta_b \cdot \Delta_b = 2\ \beta_e \cdot \Delta_e$$

therefore

$$\Delta_b = 2\ (\beta_e/\beta_b)\ \Delta_e$$

Defining

$$n = \beta_b/\beta_e$$

and noting that

$$\Delta = \Delta_e + \Delta_b$$

gives $\Delta=((n + 2)/n)\ \Delta_e$

Therefore,

$$\Delta_e = (n/(n+2))\Delta \qquad (b)$$

Substituting (b) into (a) gives

$$P_{eq} = (n/(n+2)) \cdot \beta_e \cdot L/2$$

and

$$M'_{LTB} = (3/16)\ (n/(n+2))\ ELd\ ((t_w^3)/(d_c^2)) \qquad (2.4)$$

where $$n = \beta_b/\beta_e = (16\ t_f\ b_f^3\ d_c^2)/(L^3 t_w^3) \qquad (2.4a)$$

In the case 2 model which has bracing at the load point, the buckling load from the model only considers the tipping effects. Thus, an interactive equation is used to calculate the final buckling load P''_{LTB}:

$$1/P''_{LTB} = 1/P_{TIP} + 1/P_{LTB} \qquad (2.5)$$

where $P_{TIP} = 4\ M_{TIP}/L$ is the buckling load calculated by the case 2 model and

$$M_{TIP} = \Sigma p \cdot d = 2\ P_{eq} \cdot d = 2(\beta_e L_b) \cdot d$$
$$= (1/2)\ E\ L_b d\ (t_w^3/d_c^2) \qquad (2.6)$$

Equation (1.1) is used to calculate P_{LTB} and L_b and C_b are defined in Eq. (1.1). The results calculated by Eqs. (2.4) and (2.5) for the two bracing cases with W16x26 sections are compared with the BASP solutions in Fig. 2.18. The simple analytic models show very good agreement with the exact BASP solution. In order to investigate the tipping effect for thin web members and further check the reliability of the design model, Bracing Case 1, with web thickness reduced from 0.25 to 0.10 in. for a W shape with the same flange and beam depth as a W16x26 section, was studied by varying the cope depth d_c. The results shown in Fig. 2.18 indicate that the tipping effect reduces

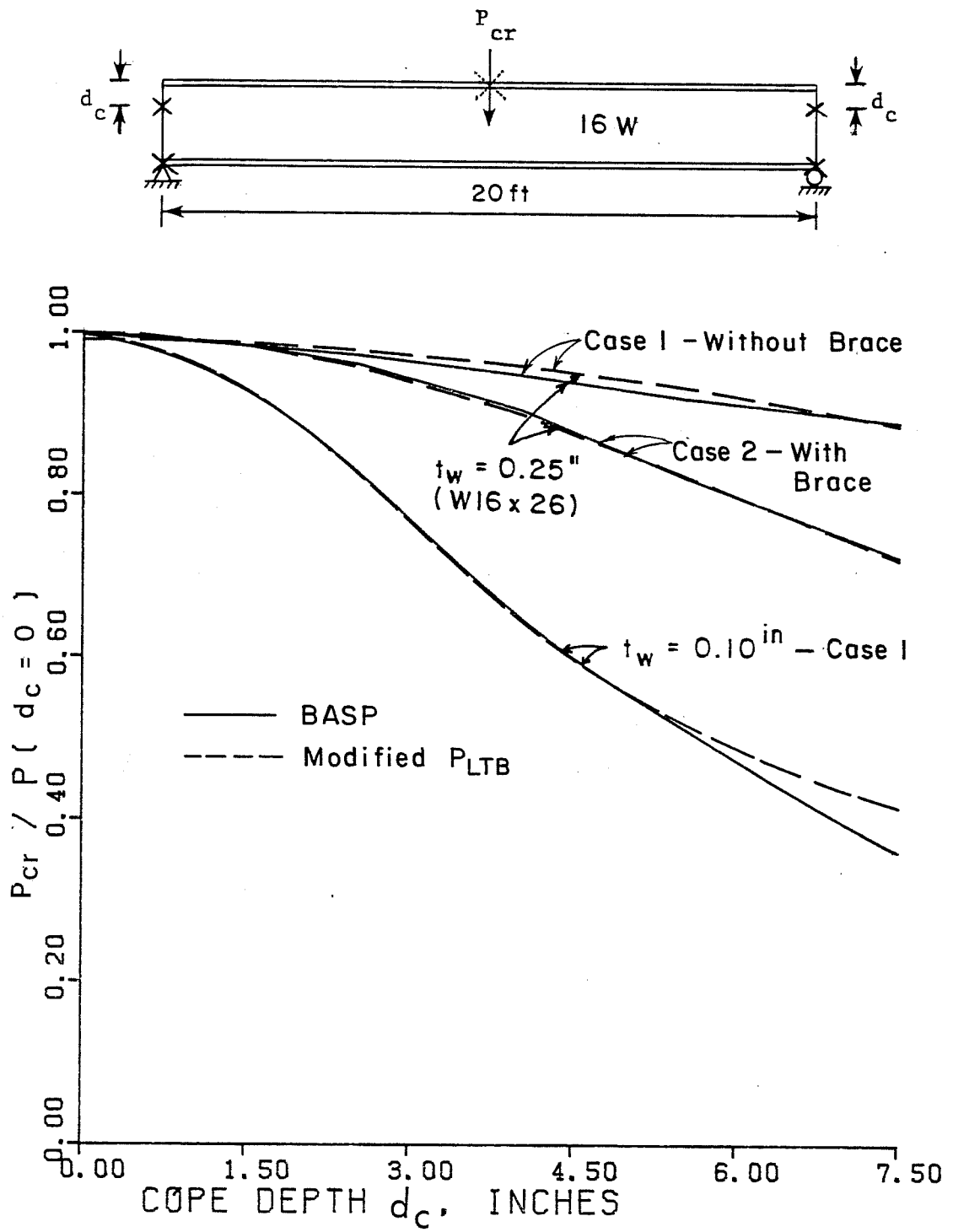

Fig. 2.18 Comparison of BASP Results with Modified P_{LTB}

the lateral buckling capacity of thin web members up to 65 percent of the uncoped lateral buckling capacity with $d_c = d/2$. Again, the simple analytic model gives good correlation with the BASP solutions.

2.5.3.2 Modification of P_{Tee}. A 5 ft long short beam with stiffeners at A position which minimizes the effects of lateral torsional buckling and tipping due to coped depth as shown in Fig. 2.19 was analyzed by using BASP program. The results are plotted in Fig. 2.19. As expected, increases in the cope depth will decrease the capacity of coped region significantly. A simple approximation is used to modify P_{Tee} for cope depth effects as follows:

$$P'_{Tee} = P_{Tee} (1 - 1.5\, d_c/d) \qquad (2.6)$$

where P_{Tee} is the tee-section capacity calculated by Eq. (2.2). The modified tee section capacity P'_{Tee} is shown in Fig. 2.19 for comparison. Equation (2.6) has the same shape as the BASP results but due to the conservative assumption of the tee section buckling load in Eq. (2.2), both Case 1 and Case 2 results are much higher than P'_{Tee}.

Using the modified P'_{LTB}, P''_{LTB} and P'_{Tee} in Eqs. (2.1) and (2.3), the results of both cases are plotted in Figs. 2.20 and 2.21, respectively. Again, after using the cope depth modification for P_{LTB} and P_{Tee}, Eqs. (2.1) and (2.3) work fairly well for cases 1 and 2, respectively.

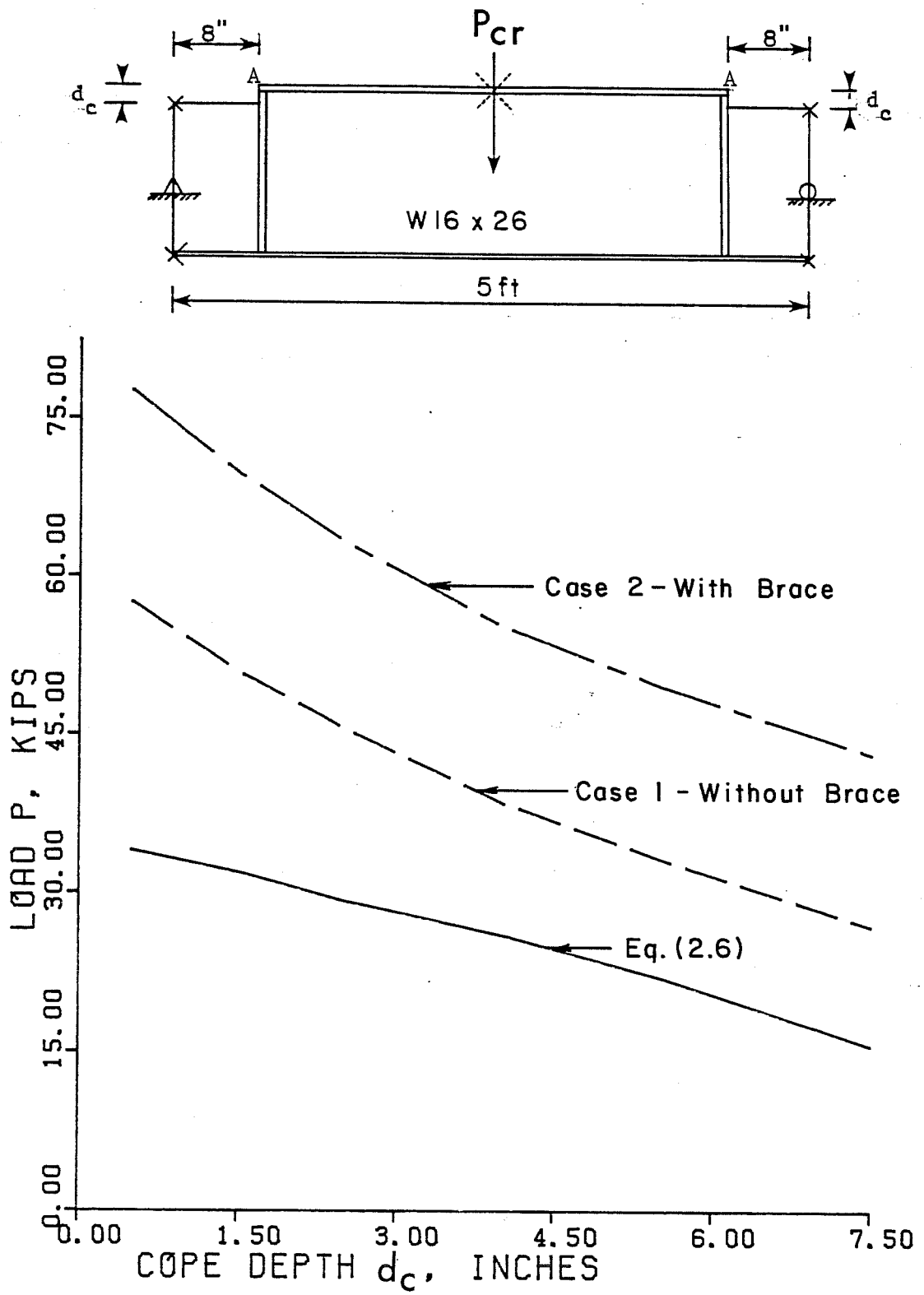

Fig. 2.19 Effect of Cope Depth on Tee Section Capacity P_{Tee}

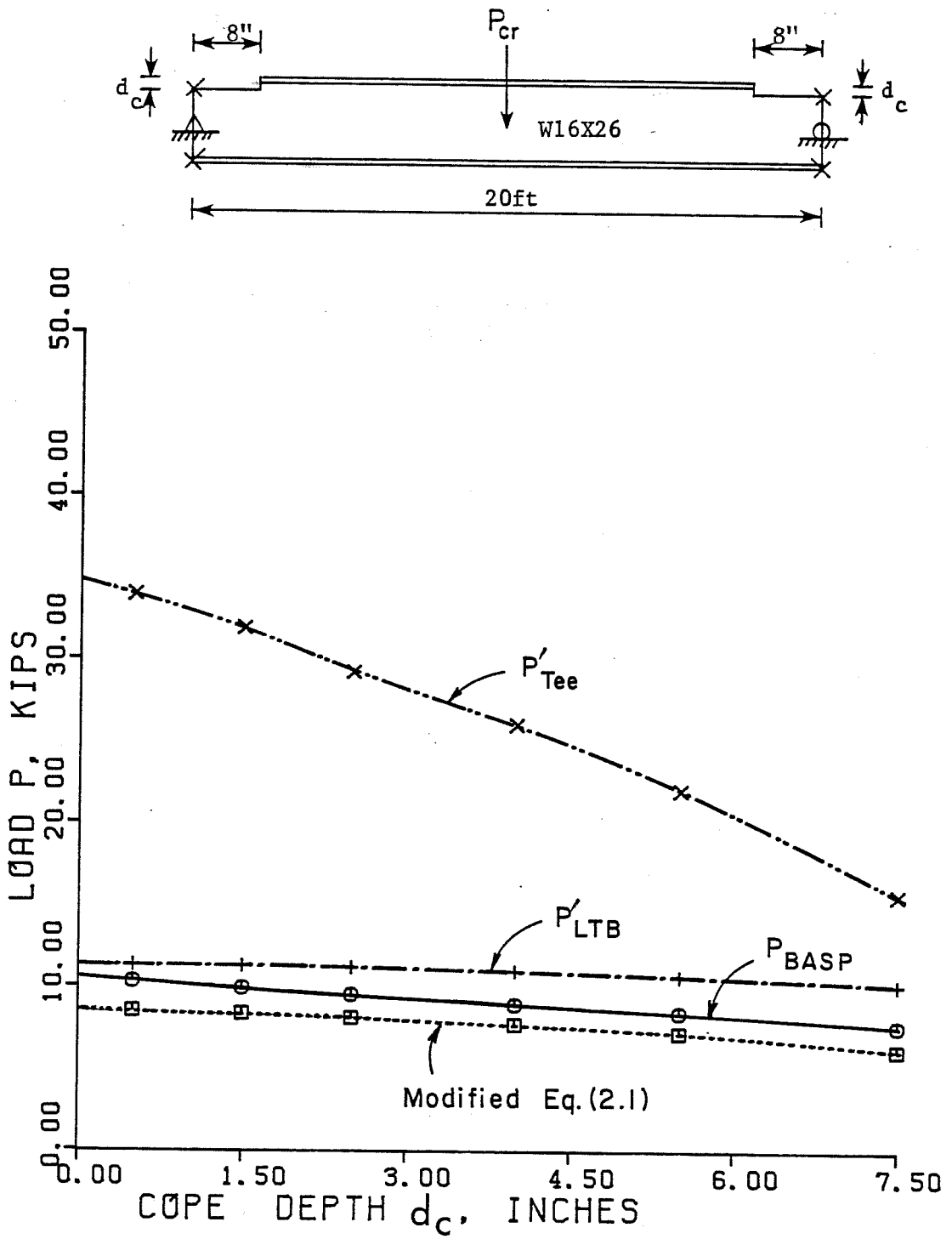

Fig. 2.20 Comparison of BASP Solutions with Proposed Design Equations by Using Modified P_{LTB} and P_{Tee} for Brace Case 1

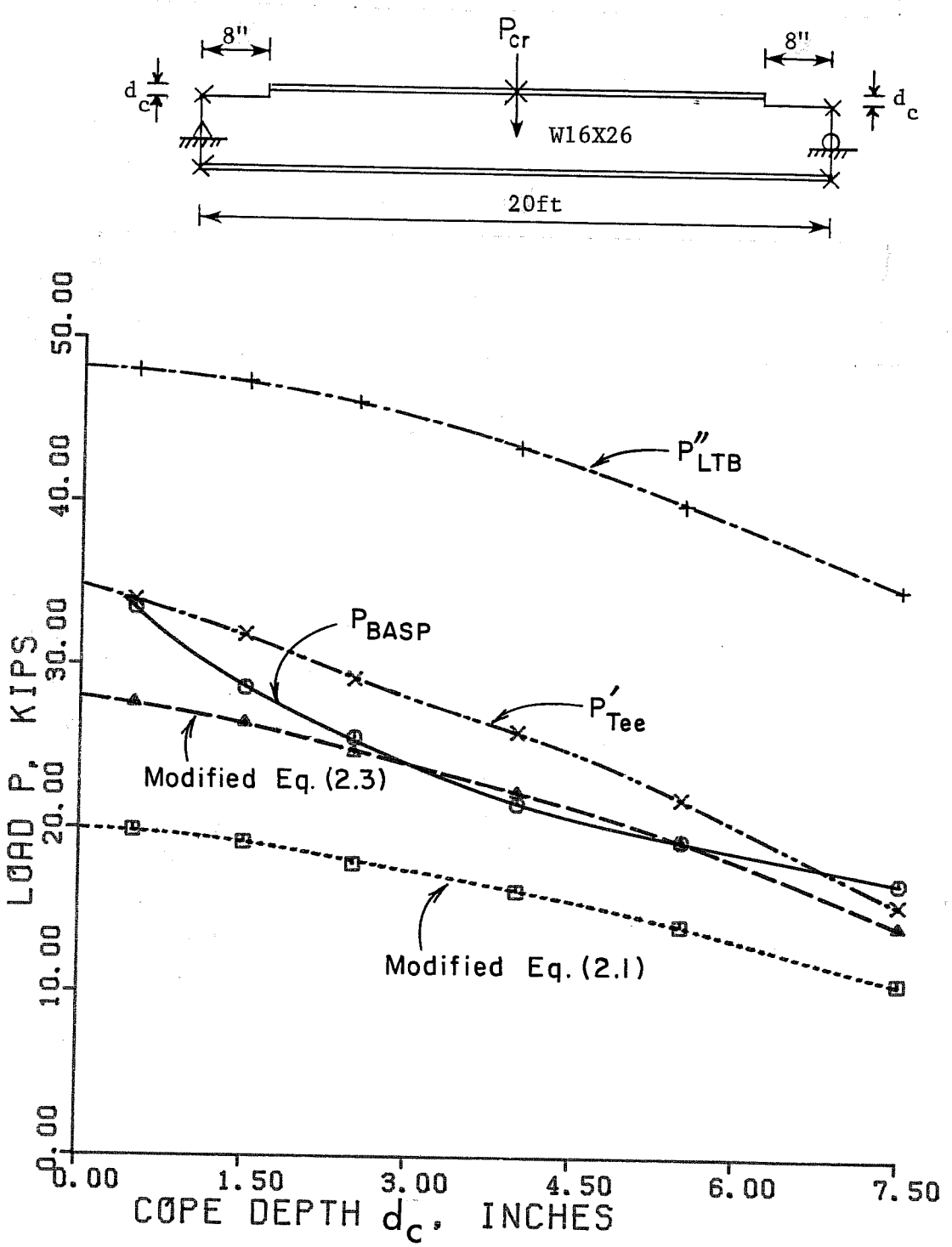

Fig. 2.21 Comparison of BASP Solutions with Proposed Design Equations by Using Modified P_{LTB} and P_{Tee} for Brace Case 2

2.6 Proposed Design Recommendations

The interaction equations (Eqs. (2.1) and (2.3)) are recommended for top flange coped beams. Equation (2.1) is used when the copes are at both ends of the unbraced span and Eq. (2.3) is applied to the unbraced span with the copes at one end of the unbraced span only.

In order to consider the effects of cope depth, according to Figs. 2.13, 2.14, 2.20, and 2.21, modified P_{LTB} and P_{Tee} expressions (Eqs. (2.4) to (2.6)) are recommended for the copes at both ends of the unbraced span when $d_c > 0.2d$ and for the copes at one end of the unbraced span when $d_c > 0.1d$. Otherwise, Eq. (1.1) and Eq. (2.3) are used to calculate the P_{LTB} and P_{Tee}. Since all the studies used the W16x26 section ($d/t_w = 62.5$), Eq. (1.1) might produce unconservative results for thin web plate girders due to the cope depth tipping effects as discussed in Sec. 2.5.3.1. Thus, for thin web plate girders ($h/t_w \geq 60.0$), modified P_{LTB} and P_{Tee} (Eqs. (2.4) to (2.6)) are recommended for all cope depths.

The summary of the design recommendations along with examples will be given in Chapter 7.

CHAPTER 3

BOTTOM FLANGE COPED BEAMS

In this chapter a design method for bottom (tension) flange coped beams is developed based on the behavior and results from a parametric study presented in Sec. 3.2. The same analysis program BASP and a W16x26 section were used in this study as described in the previous chapter.

3.1 Preliminary Studies

Two 20-ft beams with different coped lengths at the bottom flange were assumed to cover the important effects of copes on lateral stability. The buckling loads and buckling shapes for coped lengths of 8 in. and 24 in. are shown in Figs. 3.1 and 3.2, respectively. Comparing these results with those shown in Fig. 2.2 for an uncoped beam indicates the buckling shapes of the compression flanges are almost identical, even though cross-section distortion occurs at the coped region. The buckling loads of the two coped beams, 10.6 kips and 10.0 kips, for cope lengths of 8 in. and 24 in, respectively, indicate the cope length is not too important (P_{BASP} = 11.4 kips for the uncoped beam). The beam coped to 24 in. showed a reduction in buckling load of only 10 percent compared to the uncoped beam, as expected, since the coped flange is in tension.

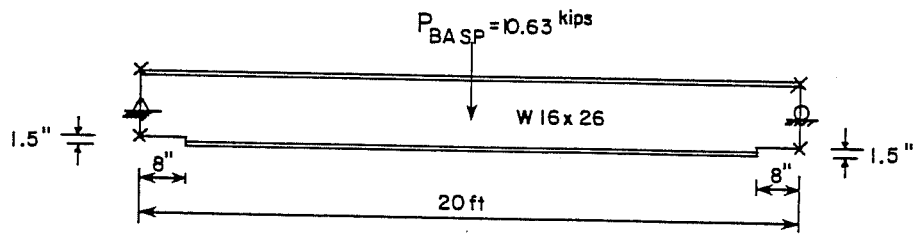

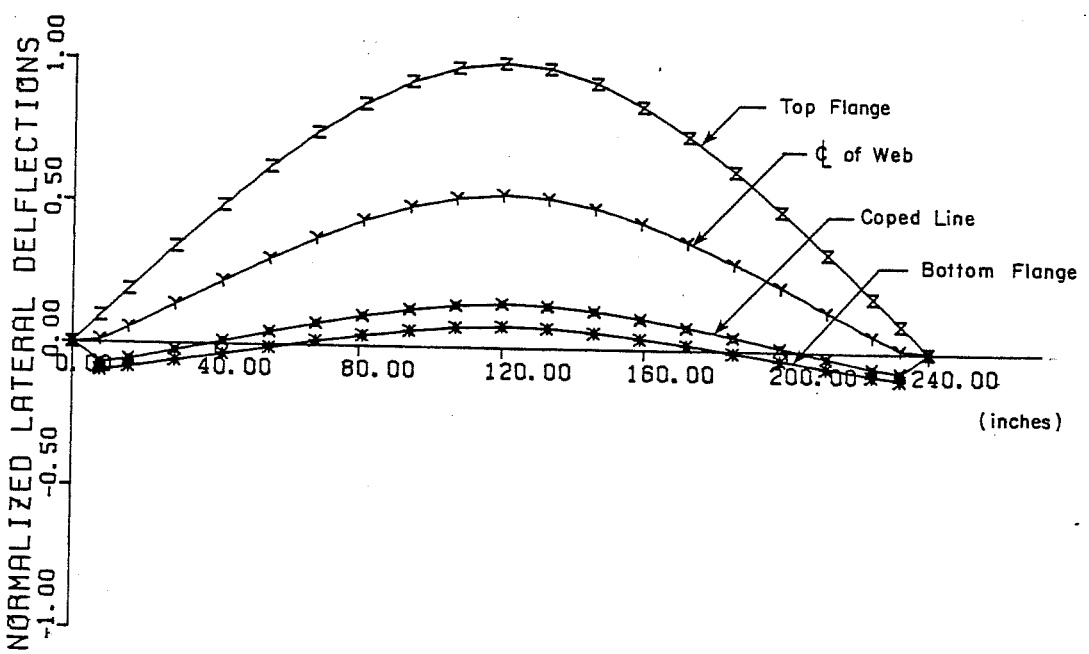

Fig. 3.1 Buckled Shape of 8in. Bottom Flange Coped Beam

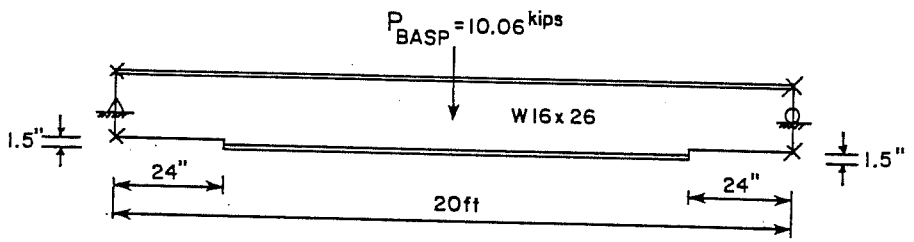

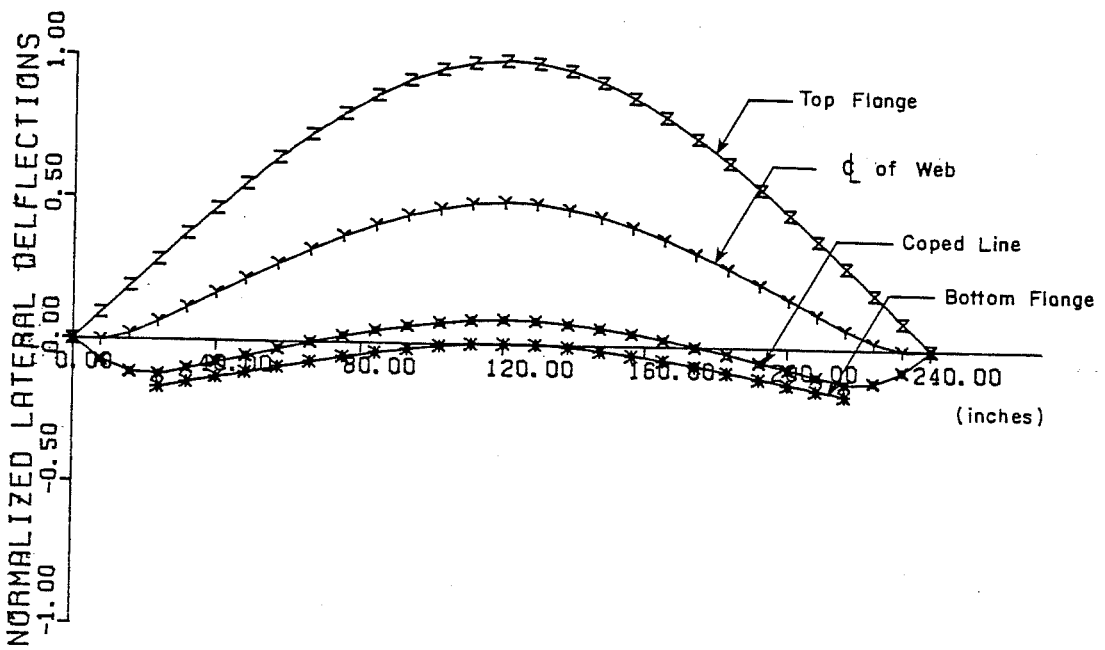

Fig. 3.2 Buckled Shape of 24in. Bottom Flange Coped Beam

Although the reduction of buckling capacity due to bottom flange copes is not as significant as top flange copes, the cross-section distortion in the coped region does decrease the torsional rigidity of the beams. The degree of reduction depends upon the coping details. Thus, further parametric studies were undertaken to investigate the reduction of the lateral buckling capacity due to bottom copes.

3.2 Parametric Studies

Two bracing conditions, with and without a brace at the load position, and three parameters, span length, cope length and cope depth, were studied to develop the design recommendations for bottom flange coped beams. Only coped beams with a cope length less than twice the beam depth ($c \leq 2d$) and with a cope depth less than one-half the beam depth ($d_c \leq d/2$) were considered in this study. The analyzed results, P_{BASP}, are compared to the lateral buckling capacity of the uncoped beam, P_{LTB}, and summarized in Tables 3.1 to 3.3. In Table 3.1, P_{LTB} was calculated by Eq. (1.1) and in Tables 3.2 and 3.3. P_{LTB} was obtained by BASP for proper comparison. For a span length = 5 ft, the BASP solutions are much lower than Eq. (1.1) (uncoped beams) as shown in Table 3.1. The reason is that the short span causes the coped beams to fail in a combination of web flexural and shear buckling instead of the lateral buckling as Eq. (1.1) predicts. Thus, these two cases were not included in the comparison. The buckling loads shown in the tables are elastic lateral buckling

TABLE 3.1 Variation of Span Length (W16x26 Section with c = 8 in. and d_c = 1.5 in.)

	w/o bracing at load position			w/bracing at load position		
Span length, ft	5	15	30	5	15	30
P_y, kips	128	42.7	21.3	128	42.7	21.3
P_{LTB}, kips	544	24.7	4.54	2754	108.5	16.0
P_{BASP}, kips	338.7*	21.6	4.12	740*	99.0	15.95
P_{BASP}/P_{LTB}	0.62*	0.87	0.91	0.27*	0.91	0.98

* The beam failed in a combination of flexural and shear buckling of the web.

TABLE 3.2 Variation of Cope Length (W16x26 Section with d_c = 1.5 in. and L = 20 ft; P_y = 32.0 kips)

	w/o bracing at load position			w/bracing at load position		
Cope Length (C), in.	4	16	32	4	16	32
P_{LTB}, kips	11.43	11.43	11.43	49.4	49.4	49.4
P_{BASP}, kips	10.95	10.24	9.95	47.5	45.0	44.3
P_{BASP}/P_{LTB}	0.95	0.90	0.87	0.96	0.91	0.90

TABLE 3.3 Variation of Cope Depth (W16x26 Section with c = 8 in. and L = 20 ft; P_y = 32.0 kips)

	w/o bracing at load position			w/bracing at load position		
Cope Depth (d_c), in.	1.5	4.0	7.5	1.5	4.0	7.5
P_{LTB}, kips	11.43	11.43	11.43	49.4	49.4	49.4
P_{BASP}, kips	10.63	10.28	9.8	46.1	45.1	43.9
P_{BASP}/P_{LTB}	0.93	0.90	0.86	0.93	0.91	0.89

loads. Inelastic lateral buckling is beyond the scope of this study. The yielding of the cross-section is assumed to be the upper limit of the beam capacity. The yielding loads, P_y, of the beams with Gr. 50 material are also listed in the tables for comparison.

Tables 3.1 to 3.3 show that under the wide range of beam variables that there is a relatively small reduction of buckling capacity for bottom (tension) flange coped beams compared with compression flange coped beams. The reductions range from 0 to 14 percent for varied parameters.

3.3 Proposed Design Recommendations

The parametric study in Sec. 3.2 shows that the bottom cope details reduced the buckling load slightly and wide variations in parameters show almost no change. Therefore, for design it is recommended that a 10 percent reduction of the lateral buckling capacity calculated by Eq. (1.1) be applied to all the bottom (tension) flange coped beams since Tables 3.1 through 3.3 show reductions no greater than 14%.

CHAPTER 4

DOUBLE FLANGE COPED BEAMS

4.1 Preliminary Studies

Two 20-ft simply-supported W16x26 beams with 8-in. and 24-in. cope lengths on both flanges were used to study the effects of double copes. Figures 4.1 and 4.2 show the buckling loads and buckled shapes of both cases. Beam 1, with 8-in. long copes, buckled at a load of 9.1 kips, which is 79 percent of the buckling load of the uncoped beam (Fig. 2.2). However, Beam 2, with a 24-in. coped length, showed severe cross-section distortion at the coped (rectangular) section, and the uncoped (I) section simply rotated due to buckling of the coped region. The copes reduced the buckling capacity of Beam 2 to 32 percent of the uncoped case.

4.2 Proposed Design Model

The behavior of double-coped beams is similar to that found in beams with only the compression flange coped (Chapter 2). However, for double-coped beams, the coped region has a rectangular cross-section which gives a much smaller buckling load compared to the tee section. Therefore, the reduction in buckling strength of the beam will be much larger for double-coped beams if the buckling is controlled by the coped region. The preliminary design model of double-coped beams proposed accordingly is shown in Fig. 4.3. The interaction of the buckling load of the rectangular section in the

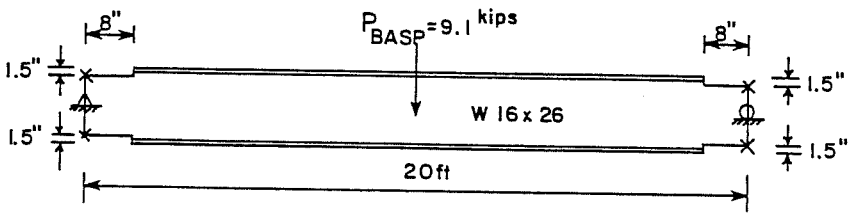

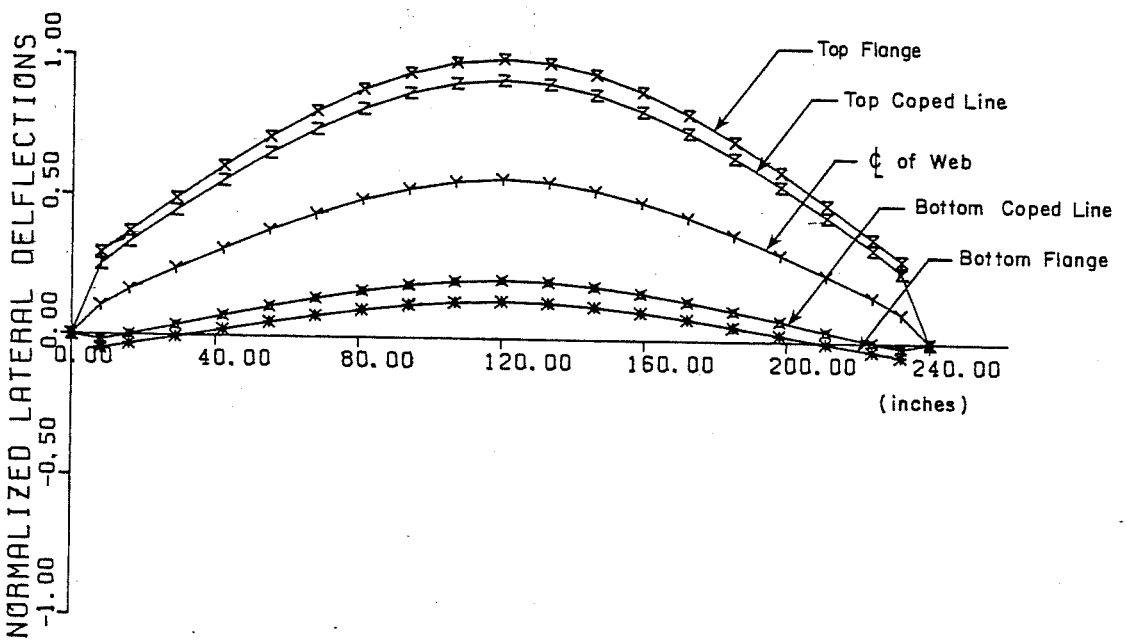

Fig, 4.1 Buckled Shape of 8in. Double Flange Coped Beam

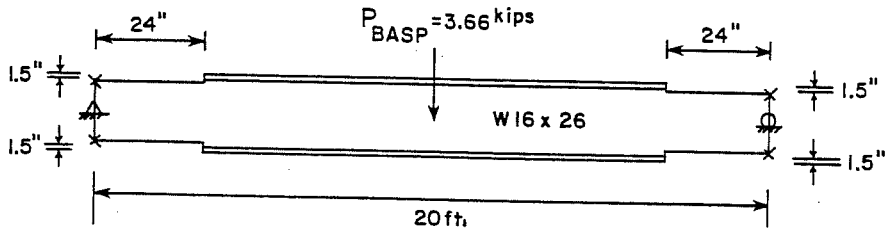

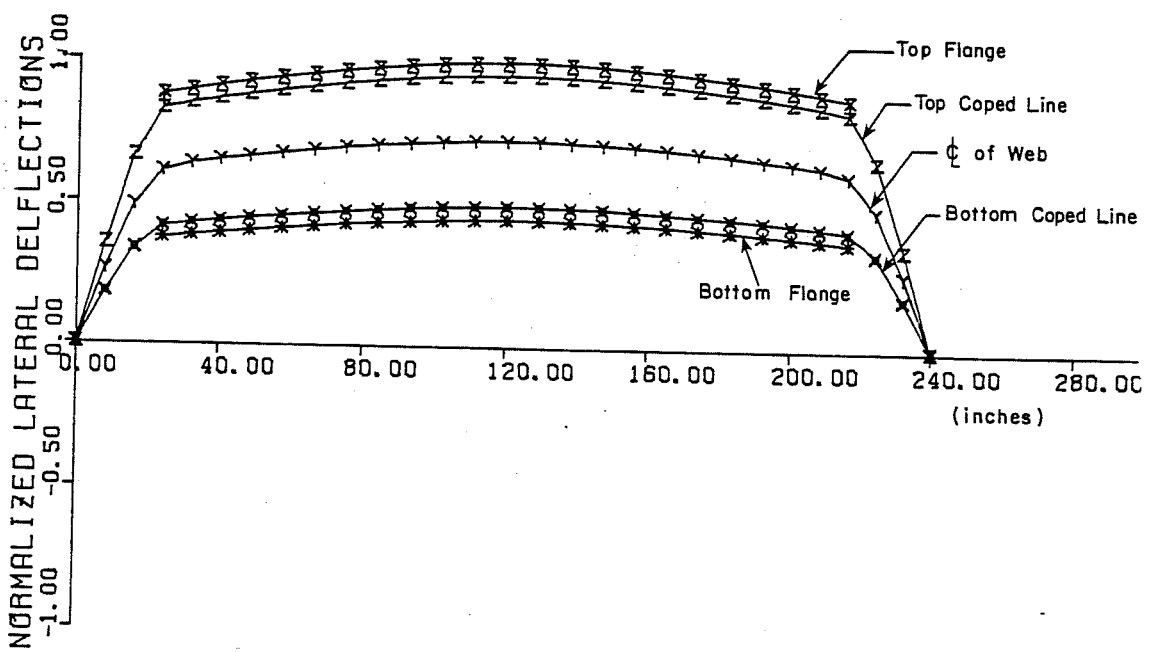

Fig. 4.2 Buckled Shape of 24in. Double Flange Coped Beam

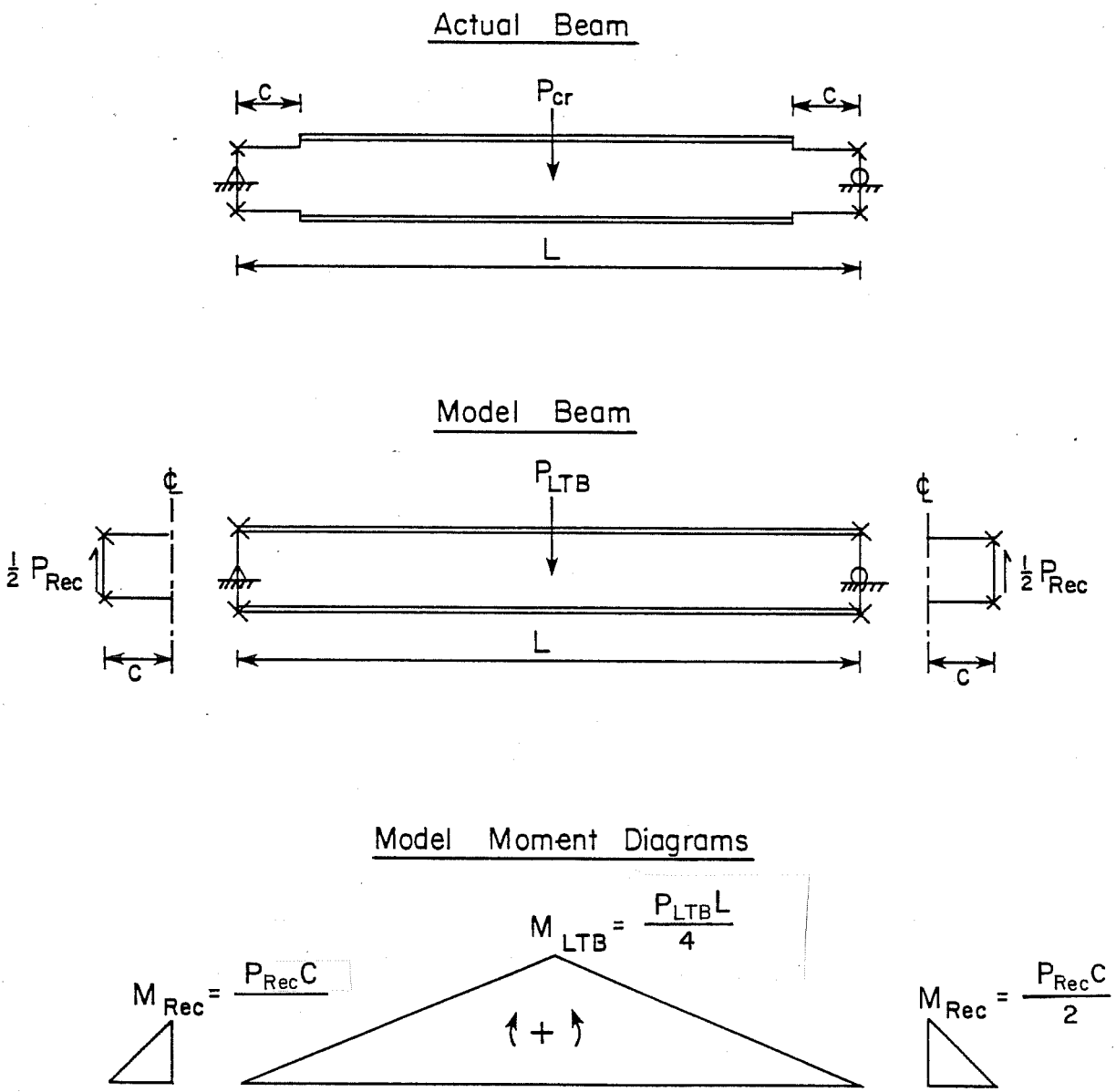

Fig. 4.3 Preliminary Design Model for Double Flange Coped Beams

coped region and the I-section over uncoped region is given by

$$1/P_{Rec} + 1/P_{LTB} = 1/P_{cr} \tag{4.1}$$

P_{Rec} is the buckling load of the coped region which can be calculated from the following equation for critical buckling moment.

$$M_{Rec} = (\pi/L)\sqrt{EI_yGJ} \tag{4.2}$$

where L is taken as 2c. For the P_{LTB} calculation, Eq. (1.1) is used. The two cases given in Figs. 4.1 and 4.2 were used to check the proposed design model, Eq. (4.1). Case 1 with 8-in. copes in both flanges yields P_{cr} = 8.5 kips, which is 7 percent lower than the BASP prediction. Case 2 with 24-in. copes predicts P_{cr} = 2.58 kips, which is 42 percent lower than the BASP solutions.

For the first case, Eq. (4.1) gives a fairly good result compared with the BASP solution; however, Eq. (4.1) underestimates the buckling load of Case 2 by 42 percent compared with the BASP result. The reason for this conservative solution is due to the conservative approach of Eq. (4.2) which assumes uniform moment along the entire span of 2c.

4.3 Parametric Studies

As discussed in Chapter 2, two bracing conditions, with and without brace at the load position, and three parameters, span length, cope length and cope depth, were studied to check and modify the design recommendations proposed above. For practical reasons,

only coped beams with a cope length less than twice the beam depth ($c \leq 2d$) and with a cope depth less than one-fifth the beam depth ($d_c \leq 0.2d$) were considered in this study.

4.3.1 Variation of Span Length. The span length was varied from 5 ft to 30 ft and a coping detail with C = 8 in. and d_c = 1.5 in. on both flanges was adopted for this study. The BASP results for the two bracing cases along with Eq. (4.1) solutions are plotted in Figs. 4.4 and 4.5, respectively.

As in top flange coped beams, Eq. (4.1) gives results very close to the BASP predictions for the case without a brace at the load position. However, when there is a brace at the load position, Fig. 4.5 shows that Eq. (4.1) results in a very conservative solution since only one end of unbraced span is coped in this case. Thus, Eq. (4.3), as follows, is proposed to reduce the interactive effects between the coped and uncoped region for a beam with coping only at one end of unbraced span.

$$1/P_{Rec}^2 + 1/P_{LTB}^2 = 1/P_{cr}^2 \qquad (4.3)$$

The results of Eq. (4.3) shown in Fig. 4.5 give better agreement with BASP than results from Eq. (4.1). However, since Eq. (4.2) conservatively neglects moment gradient in the coped region, Eq. (4.3) underestimates the buckling loads for short beams which are controlled mainly by coped region buckling capacity.

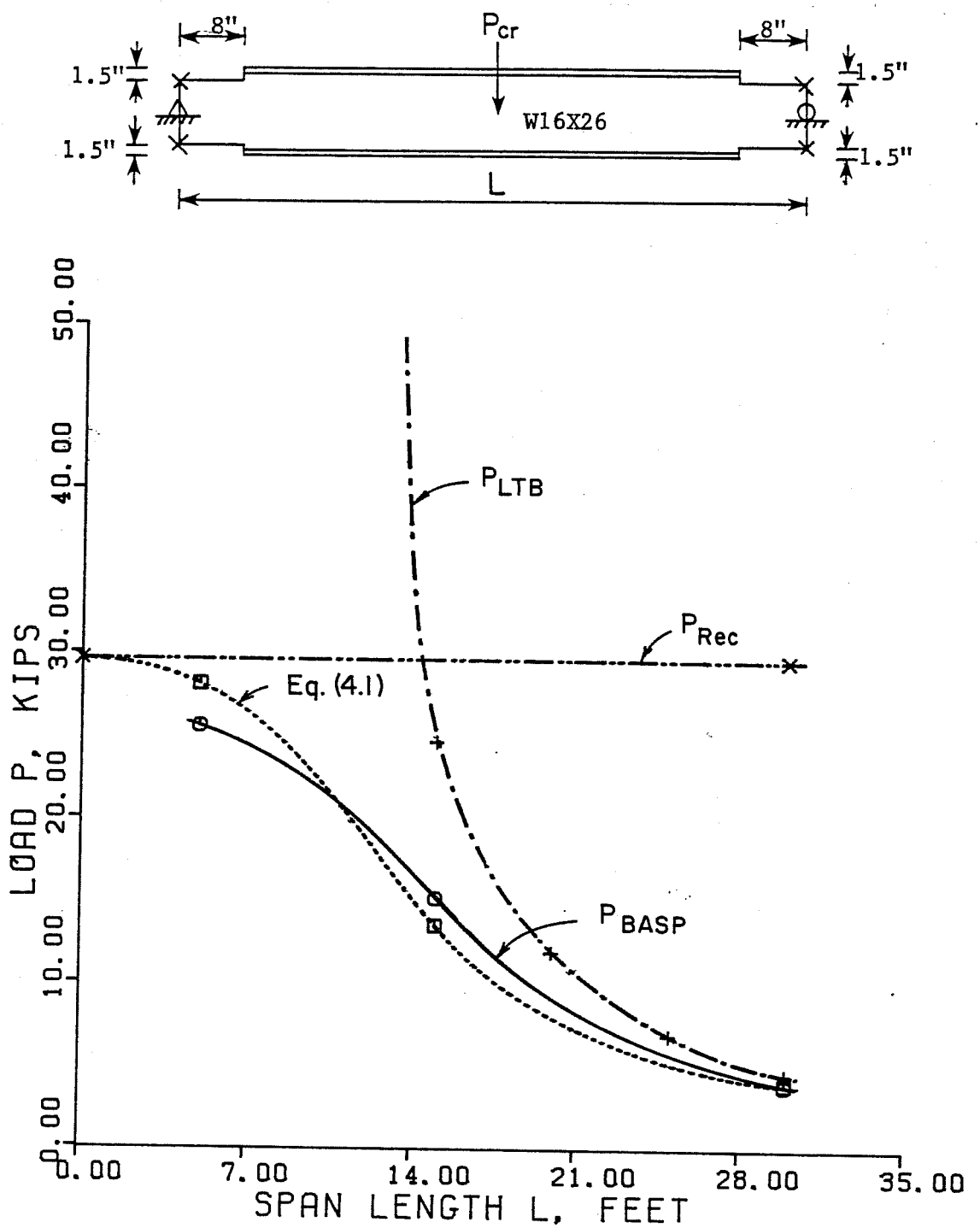

Fig. 4.4 Effect of Span Length for Brace Case 1 of Double Flange Coped Beams

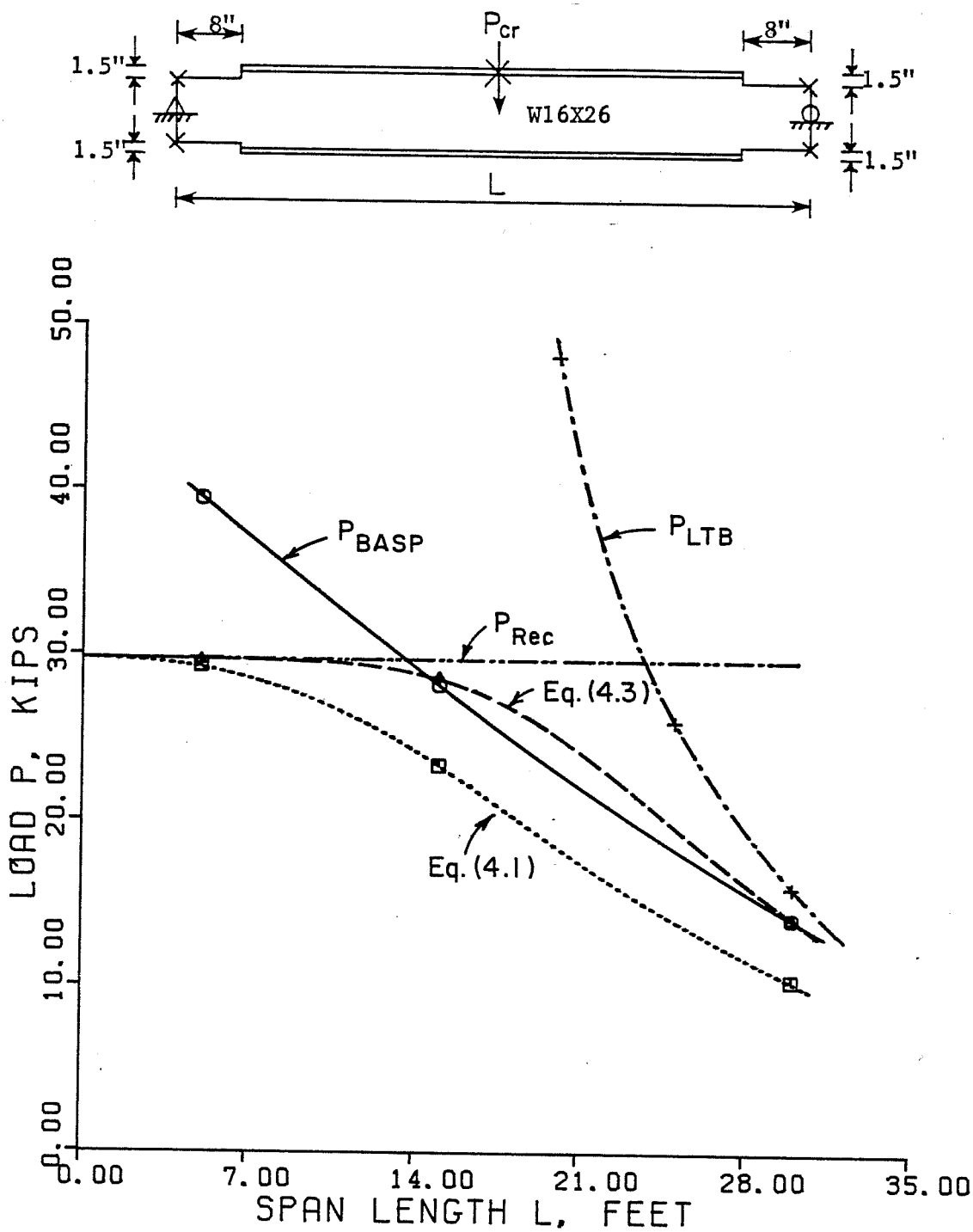

Fig. 4.5 Effect of Span Length for Brace Case 2 of Double Flange Coped Beams

Yielding of the cross-section with Gr. 50 material is not shown in figures since it is much higher than the buckling loads of the studied cases.

4.3.2 Variation of Cope Length. The cope length was varied from 0 to 32 in. to check Eqs. (4.1) and (4.3) for both bracing conditions. A cope depth = 1.5 in. and span length = 20 ft were used in this study. The calculated results compared with BASP results are shown in Figs. 4.6 and 4.7, respectively.

In Fig. 4.6, Eq. (4.1) gives reasonable solutions compared with the BASP results and in Fig. 4.7, Eq. (4.3) shows better agreement with BASP solutions for the Case 2 bracing conditions. Except for the Case 2 condition with a cope length smaller than 6 in., which will be controlled by yielding of the cross-section as shown in Fig. 4.7, the coped beams in this study failed in elastic lateral buckling.

4.3.3 Variation of Cope Depth. The cope depth was varied up to 0.2d to check Eqs. (4.1) and (4.3) for both bracing conditions. A cope length = 8 in. and span length = 20 ft were adopted throughout this study. The theoretical results obtained from BASP are compared with calculated results (Eqs. (4.1) and (4.3)) and shown in Figs. 4.8 and 4.9.

Equation (4.1) shows very good agreement with BASP solutions for the case 1 condition (no bracing at the load position) in Fig. 4.8. However, Eq. (4.3) gives results slightly higher than BASP solutions for the cope depth larger than 1.2 in. for the brace case 2

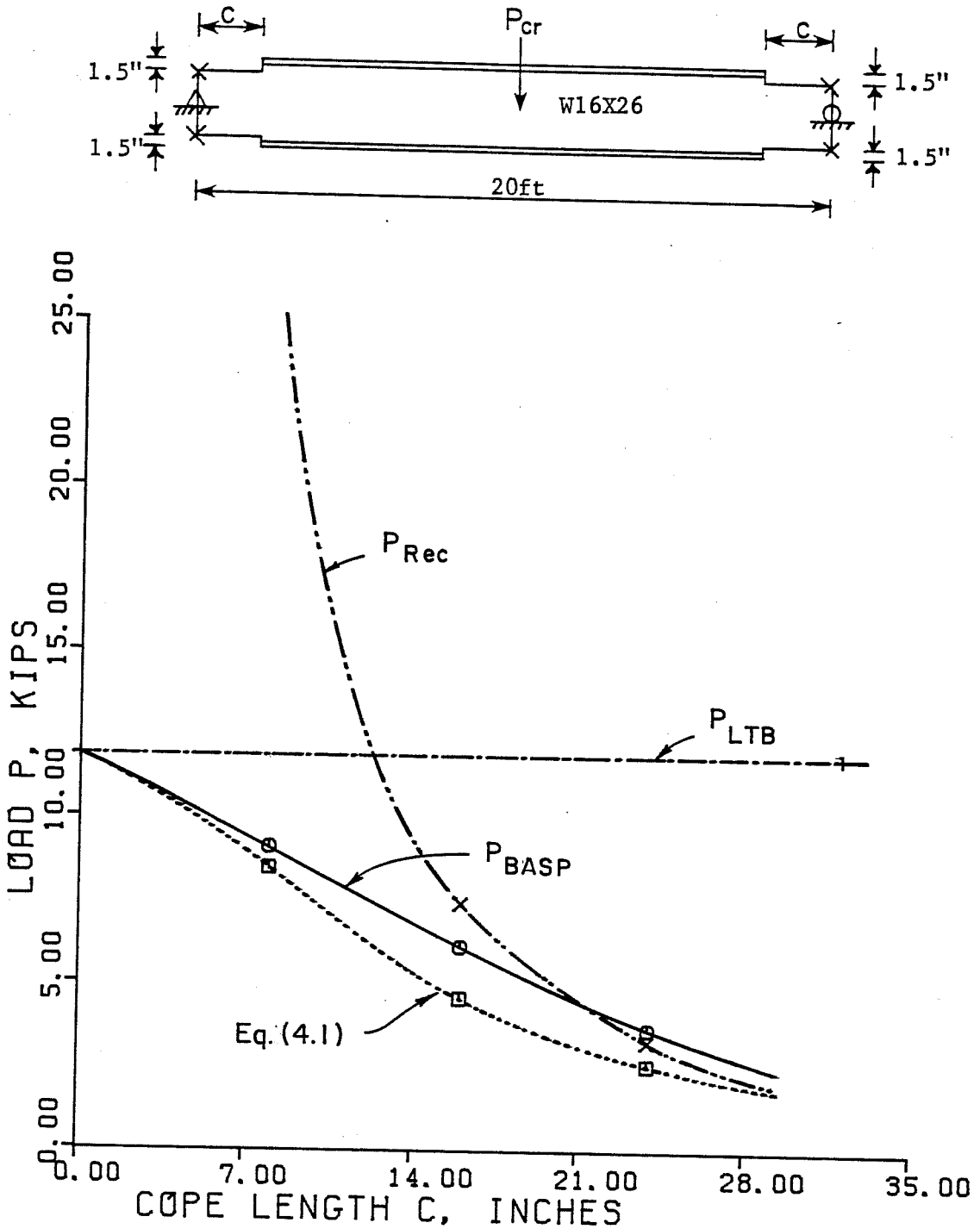

Fig. 4.6 Effect of Cope Length for Brace Case 1 of Double Flange Coped Beams

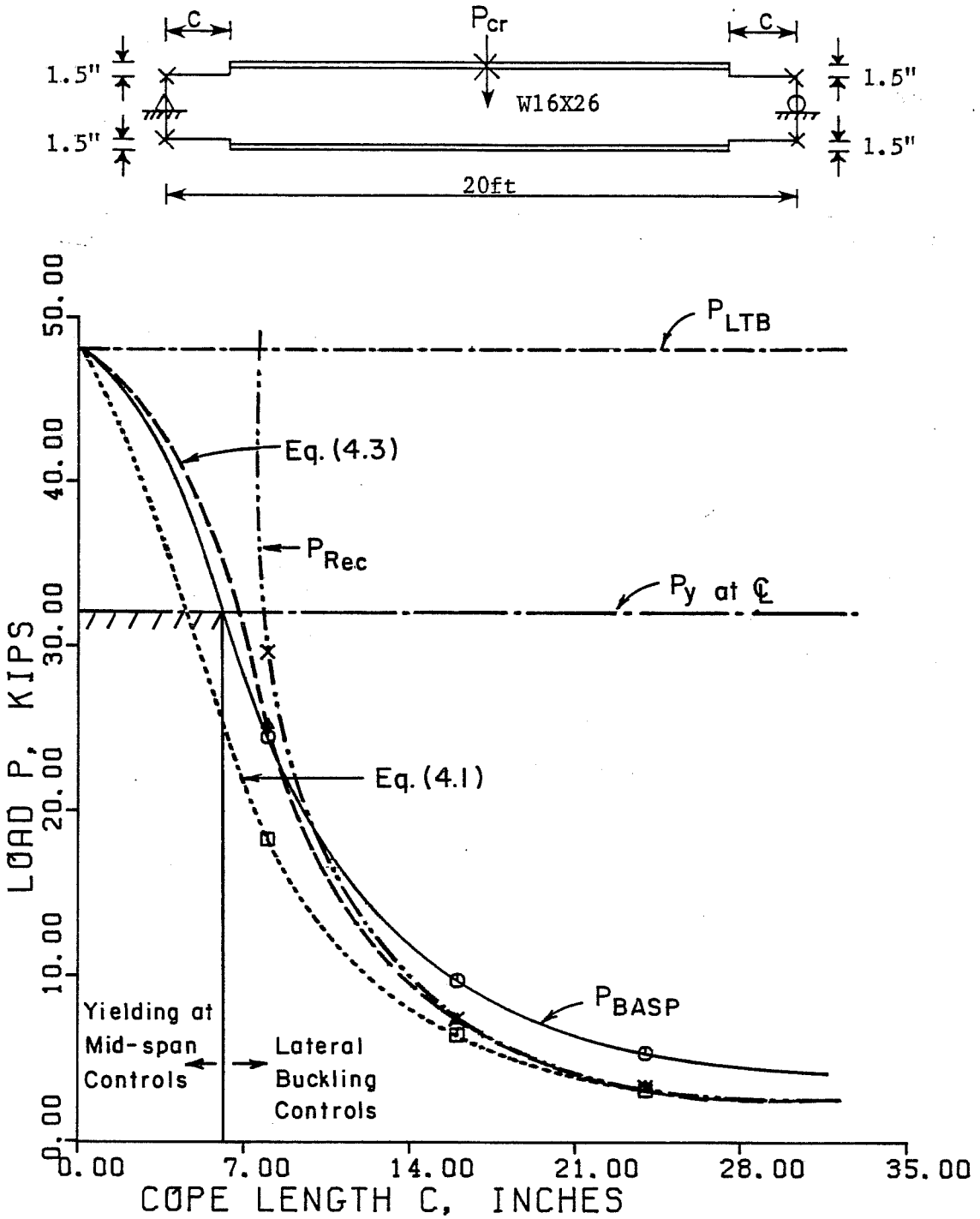

Fig. 4.7 Effect of Cope Length for Brace Case 2 of Double Flange Coped Beams

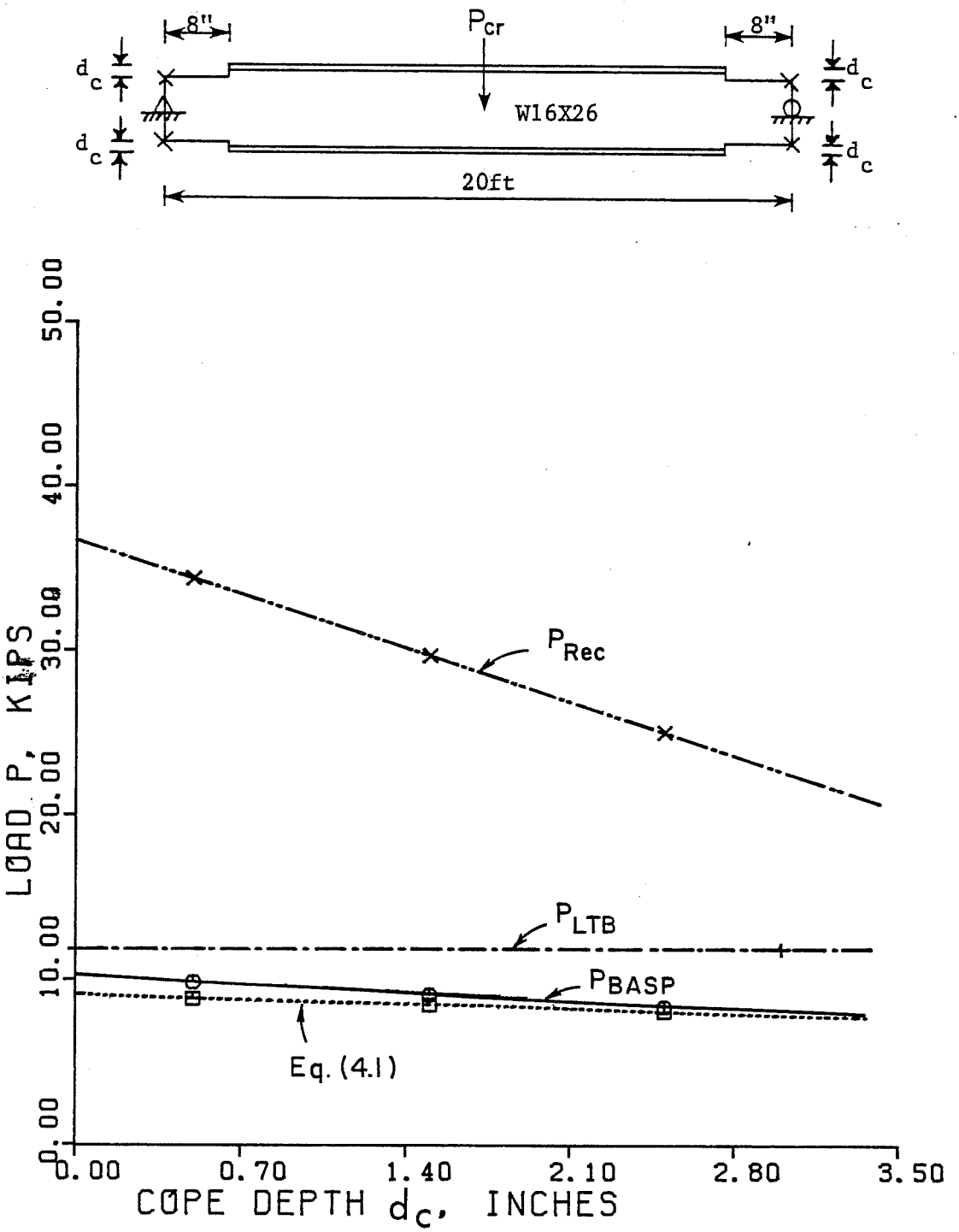

Fig. 4.8 Effect of Cope Depth for Brace Case 1 of Double Flange Coped Beams

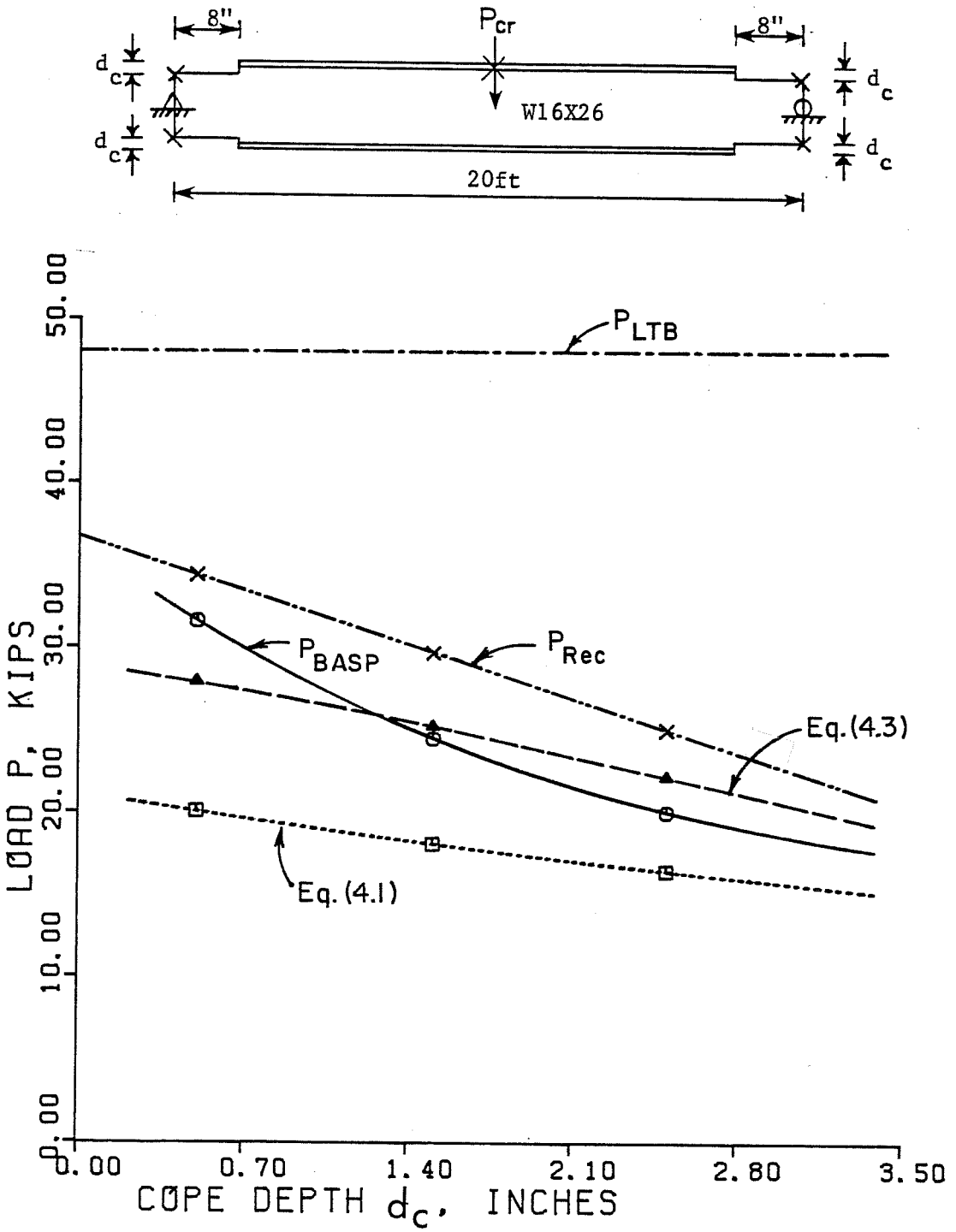

Fig. 4.9 Effect of Cope Depth for Brace Case 2 of Double Flange Coped Beams

(Fig. 4.9) due to the tipping effects caused by deep copes as discussed in Sec. 2.5.3. Nevertheless, since there is a cope depth limit of 0.2d in double coped beams, the tipping effects are much less significant than top flange coped beams with a $d_c \leq 0.5d$. For design purposes, the tipping effects due to cope depth can be neglected in this case.

4.4 Proposed Design Recommendations

The interaction equations (Eqs. (4.1) and (4.3)) are recommended for double flange coped beams. Equation (4.1) is used when the copes at both ends of the unbraced span and Eq. (4.3) is applied to the unbraced span with the cope at one end of the span only. The summary of the design recommendations along with the design examples are given in Chapter 7.

CHAPTER 5

TEST PROGRAM AND RESULTS

Six tests were conducted on top (compression) flange coped beams to check the reliability of the BASP program and proposed design recommendations.

5.1 Test Specimens

A single length of W12x14 section with a nominal yield strength of 50 ksi was used for six elastic lateral-torsional buckling tests. The specified and measured coping details are given in Fig. 5.1. Test LTB1 has no cope and is used for comparison. Tests LTB2 to LTB4 have the same cope depth but different cope lengths, and, conversely, tests LTB5 and LTB6 have the same cope length but different cope depths. The measured section properties of the W12x14 are as follows: b_f = 3.972 in., t_f = 0.239 in., t_w = 0.212 in., d = 11.884 in. Based on these dimensions, the following section properties were calculated: A = 4.317 in.^{2}, I_x = 90.6 in.^{4}, I_y = 2.51 in.^{4}, J = 0.072 in.^{4}. The average static yield strengths of two tensile coupons cut from the flanges and from the webs are 57.4 ksi and 55.3 ksi, respectively.

In order to minimize the end restraints so a conservative pinned-end condition is approached, a shear end-plate connection was used in the tests as shown in Fig. 5.1. The end plates were 10 gage

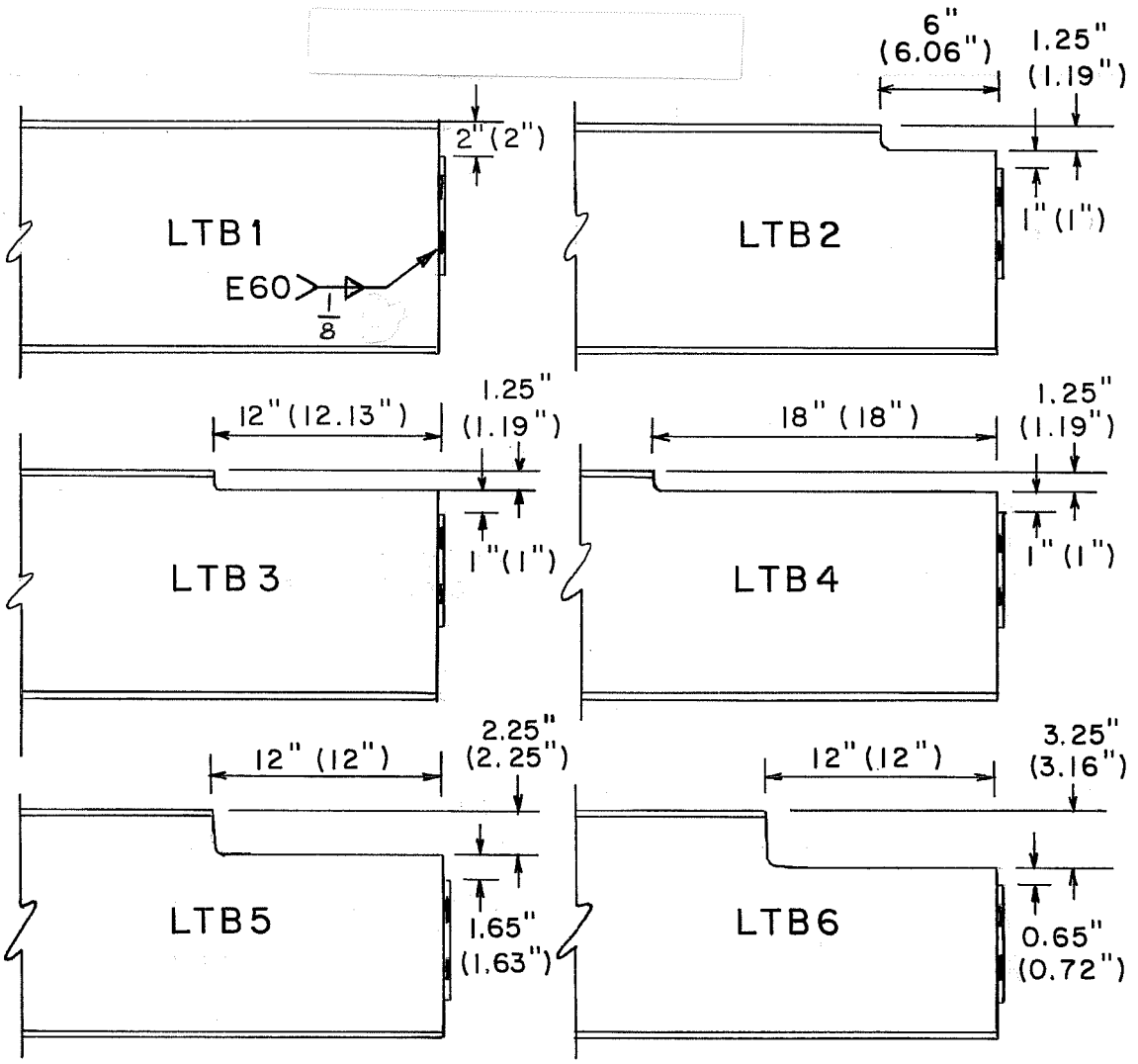

Note :

Thickness of End Plate = 0.1345" (0.1335")

All holes $\frac{13}{16}$" ϕ diameter

Dimensions shown are Specified (Measured)

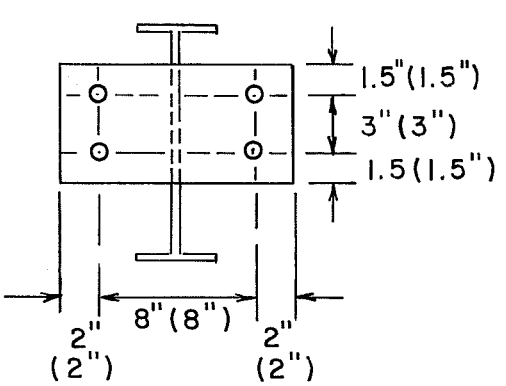

Fig. 5.1 Detail of Coping Connections of Lateral-Torsional Buckling Tests

material (t = 0.1335 in.). An 8 in. gage distance and a 3-in. spacing were used for the four bolts. To further reduce in-plane and lateral end restraint, the end plate and supporting column were separated by placing two washers between them at each bolt location. This has the effect of minimizing connection stiffness resulting from prying action. Standard 13/16 in. diameter holes for 3/4-A325 bolts were used. The fillet weld size is 1/8 in. using E60 electrodes. Turn-of-nut tightening method was used to provide the bolt tension required by 1978 AISC specification.

5.2 Test Setup

The test arrangement shown schematically in Fig. 5.2 was designed to apply determinate forces to the test connection. For simplicity, the beam was loaded upside down. A reaction floor and wall system served as the loading frame. A photograph of the test setup is shown in Fig. 5.3. The stub column to which a test connection was bolted consisted of a W10x89 section with 13/16 in. bolt holes. The stub was bolted to the vertical reaction wall.

Load was applied to the test beam, 114.3 in. from the face of end plate connection, by a 60 ton hydraulic ram. A 50 kip load cell centered underneath the ram measured the applied load. The hydraulic pressure was also monitored to provide a second indication of load. The load position was chosen to produce elastic buckling of the test span while minimizing the restraint of the adjacent span. A roller assembly was placed between the bottom flange of the test beam

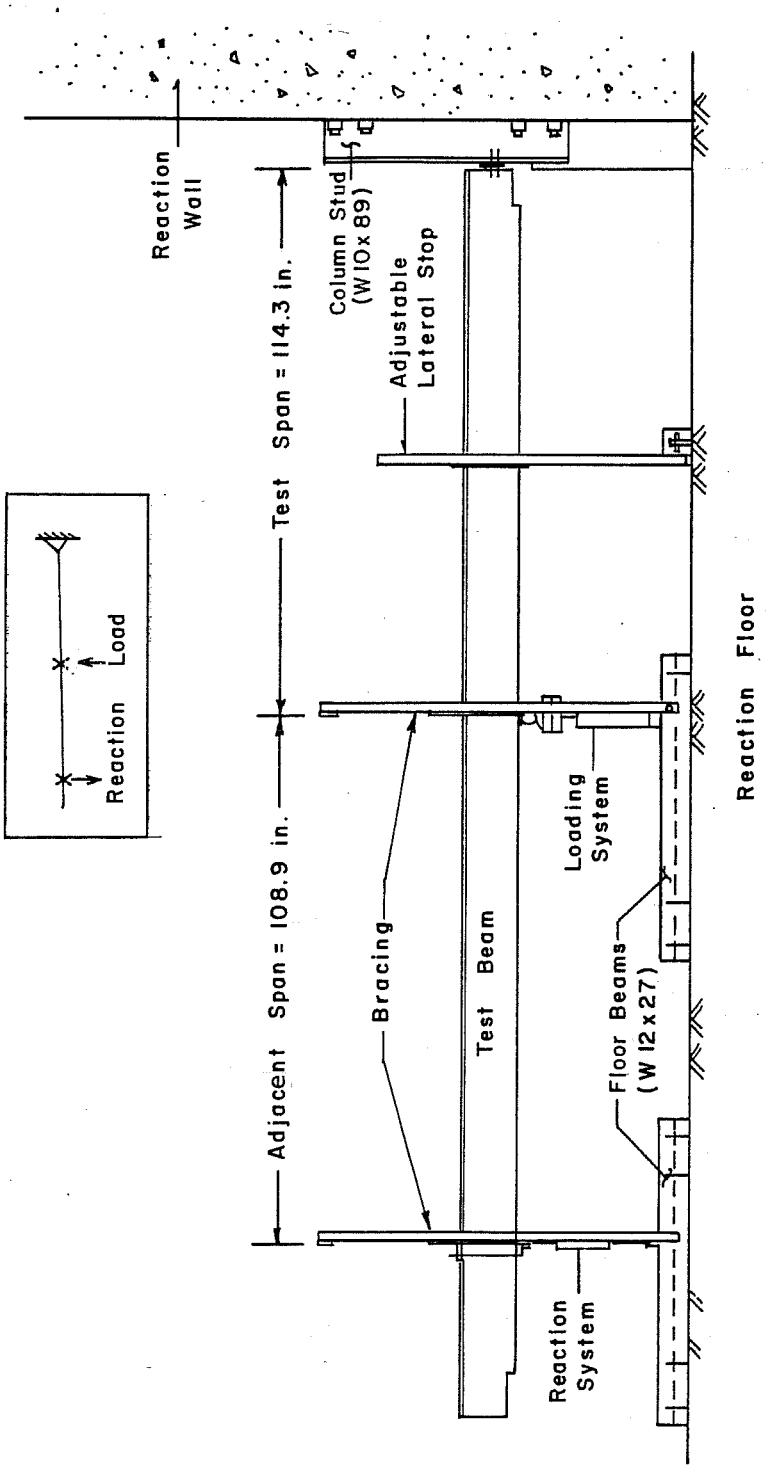

Fig. 5.2 Schematic of Test Setup

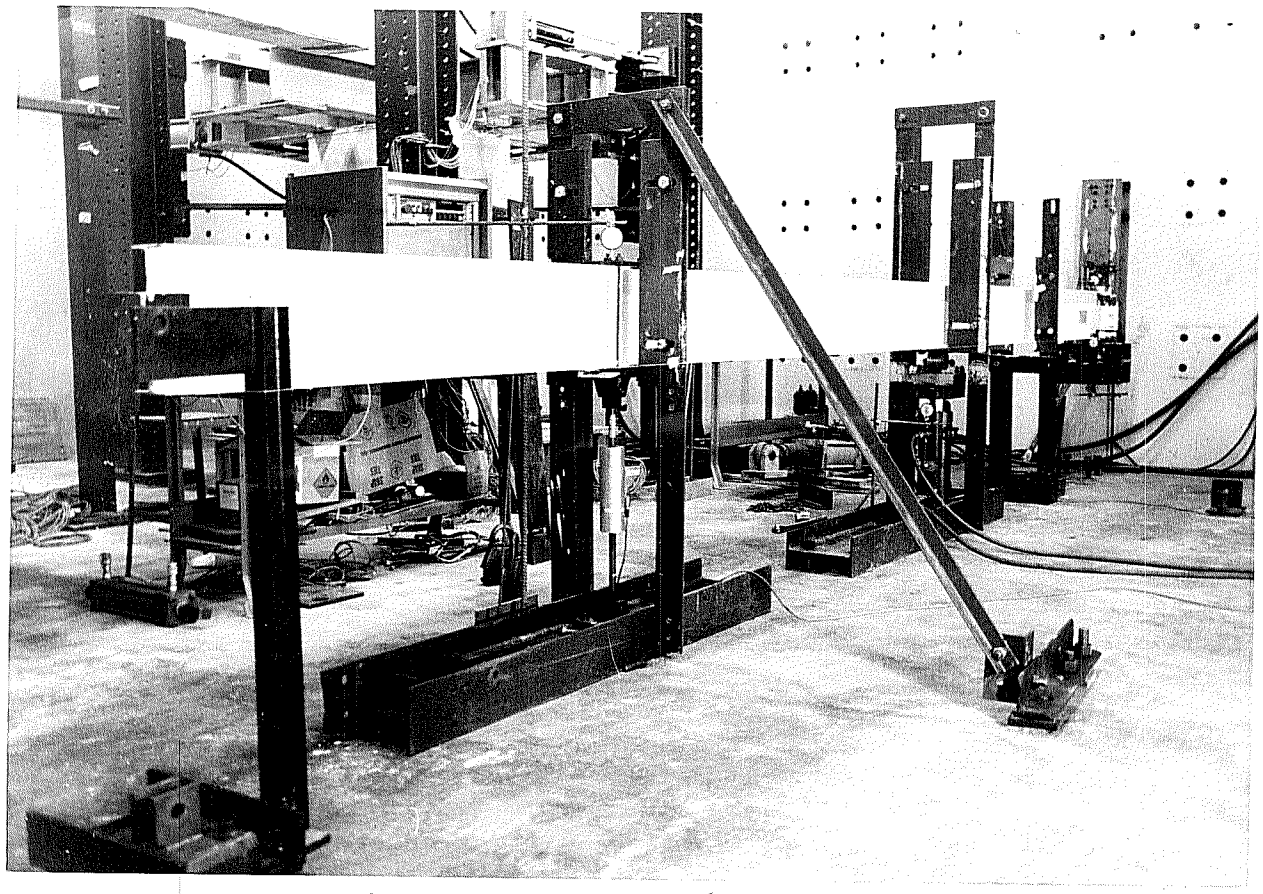

Fig. 5.3 Test Setup

and load ram so that longitudinal movement was permitted. A schematic and photo of the loading system are shown in Figs. 5.4 and 5.5, respectively.

A 10 kip tension load cell was located 108.9 in. from the center of the load ram. The load cell was connected to the test beam and floor beam by a bracket arrangement with pinned end connectors which allowed longitudinal movement of test beam as shown in Figs. 5.6 and 5.7.

The test beam was supported laterally at the load and reaction positions by out-of-plane bracing systems as shown in Figs. 5.4 and 5.6. Adjustable brace plates with slotted holes prevented lateral movement but allowed vertical movement of the beam. Two floor beams were tied onto the reaction floor to support the out-of-plane bracing and to connect the reaction load cell as shown in Fig. 5.2. An additional adjustable stop was placed near the mid-span of test span (Fig. 5.2) to prevent large lateral movement which would cause yielding on the compression flange. The maximum lateral movement allowed at the adjustable stop position was about 3/4 in.

5.3 Instrumentation

The hydraulic ram was controlled with a hand pump. The magnitude of the applied load was determined by the calibrated 50 kip load cell and verified by two pressure transducers, one linked to a strain indicator and a second connected to an x-y plotter. A pressure gage also served as a further check on the pressure to the

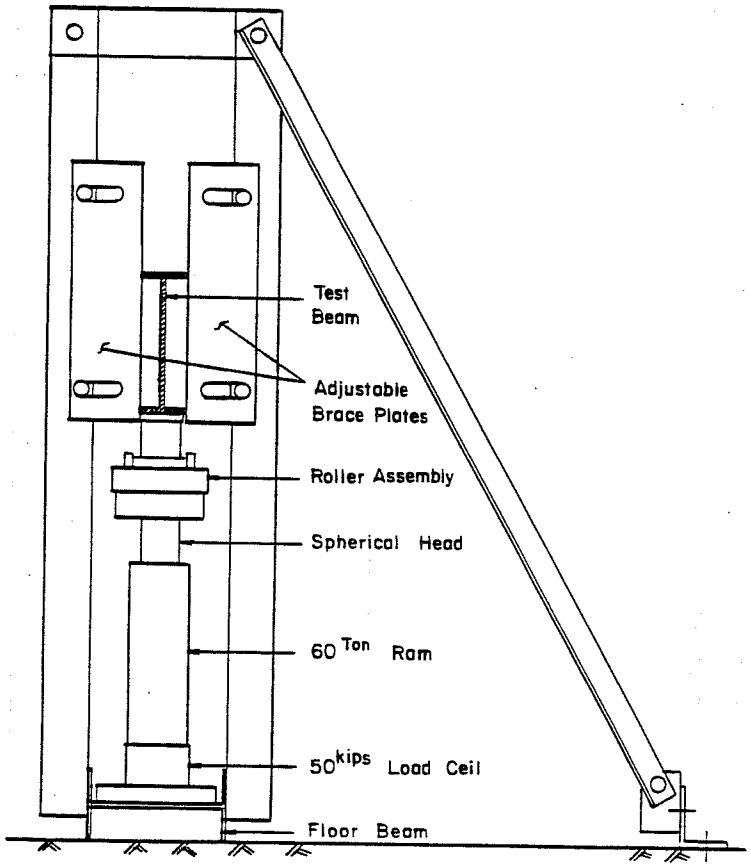

Fig. 5.4 Schematic of Loading System and Out-of-plane Bracing

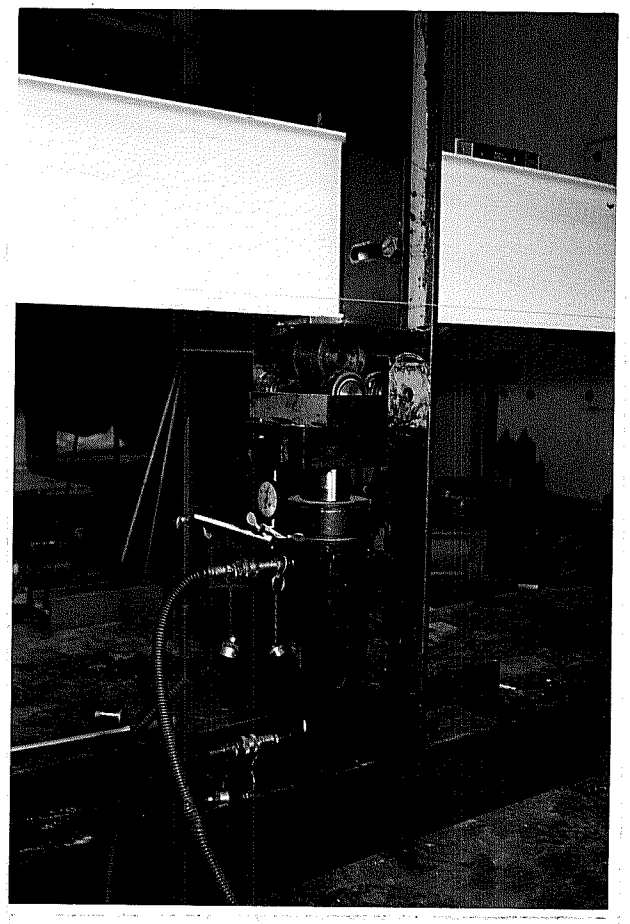

Fig. 5.5 Loading System

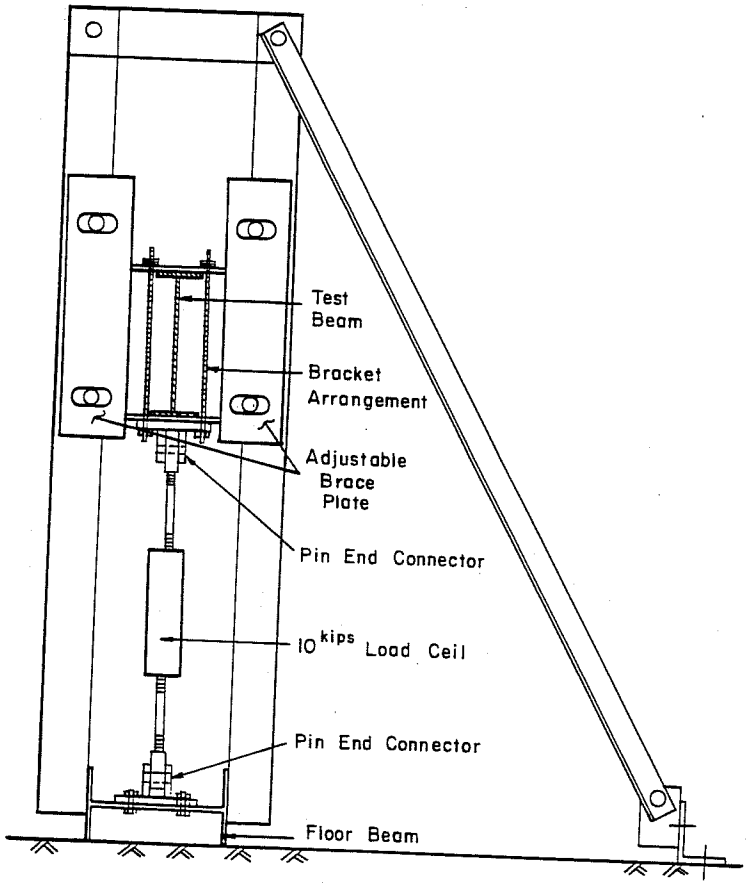

Fig. 5.6 Schematic of Reaction System and Out-of-plane Bracing

Fig. 5.7 Reaction System

ram. The far-end reaction was established by a calibrated 10 kip load cell. With this arrangement the moment and shear at the end plate connection could be determined by statics.

Six dial gages with 0.001 in. interval were used to measure the in-plane deflection and an inclinometer capable of measuring an angle change of 0.00003 radians was used to measure the rotation of the connection. Figure 5.8 shows the arrangement of the in-plane deflection instrumentation.

The out-of-plane deflection instrumentation was arranged as shown in Fig. 5.9. A string was stretched parallel to the beam and a scale with graduations to 0.002 in. was placed perpendicular to the string at eight locations along the length of the compression flange to measure the lateral movement. A potentiometer was also placed at location A in Fig. 5.9 so that an x-y plotter could monitor the load-lateral deflection response. An inclinometer placed 7 in. away from the potentiometer near the mid-span of the test span was used to measure the twist of the compression flange.

The test beam was whitewashed in order to detect any unexpected yielding.

5.4 General Test Procedure

The test procedure was generally the same for all tests. Prior to each test, the dimensions of the cross section, coping details and end plate connection were carefully measured using a micrometer. Before applying load to the test beam, first loading

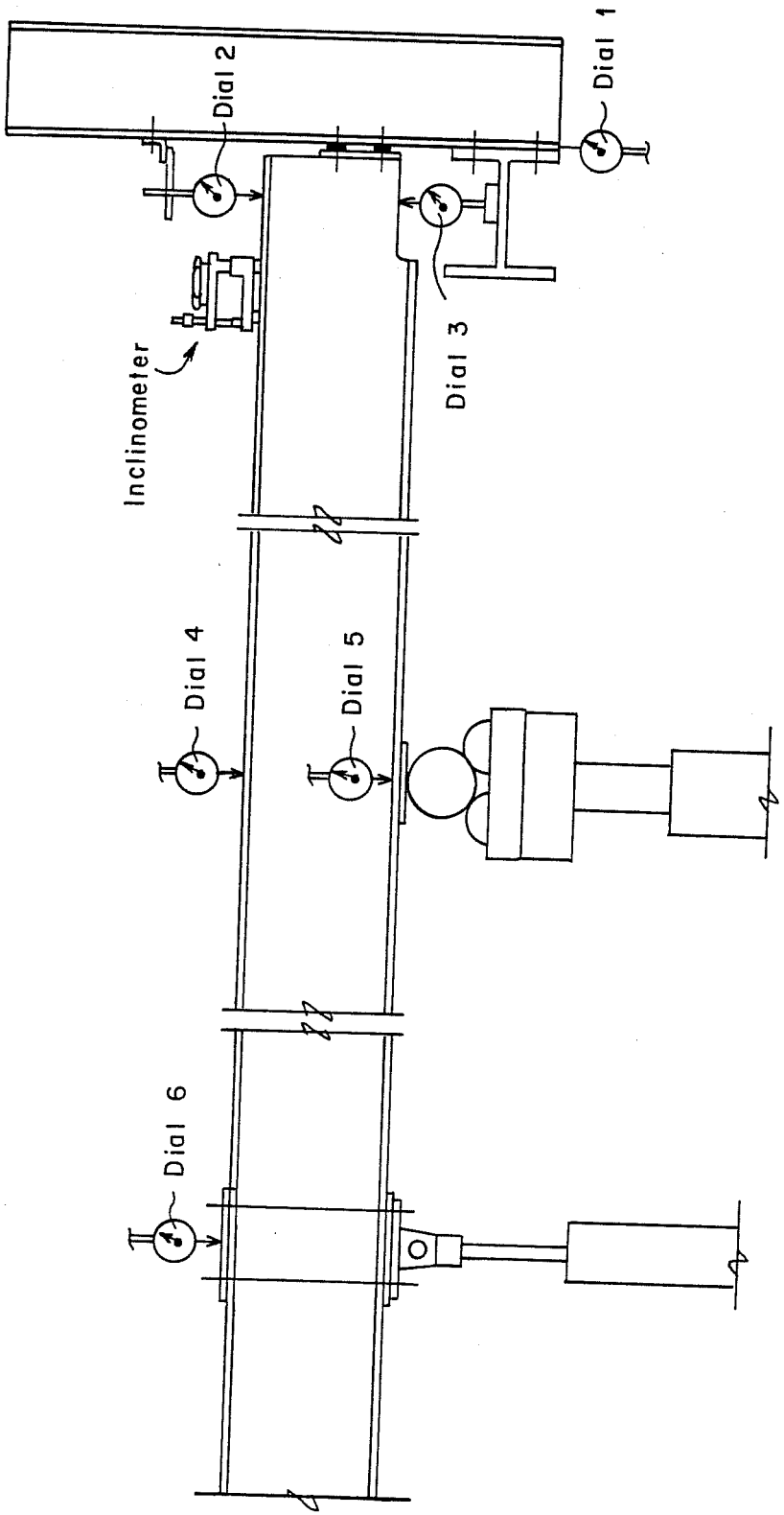

Fig. 5.8 In-plane Deflection Instrumentation

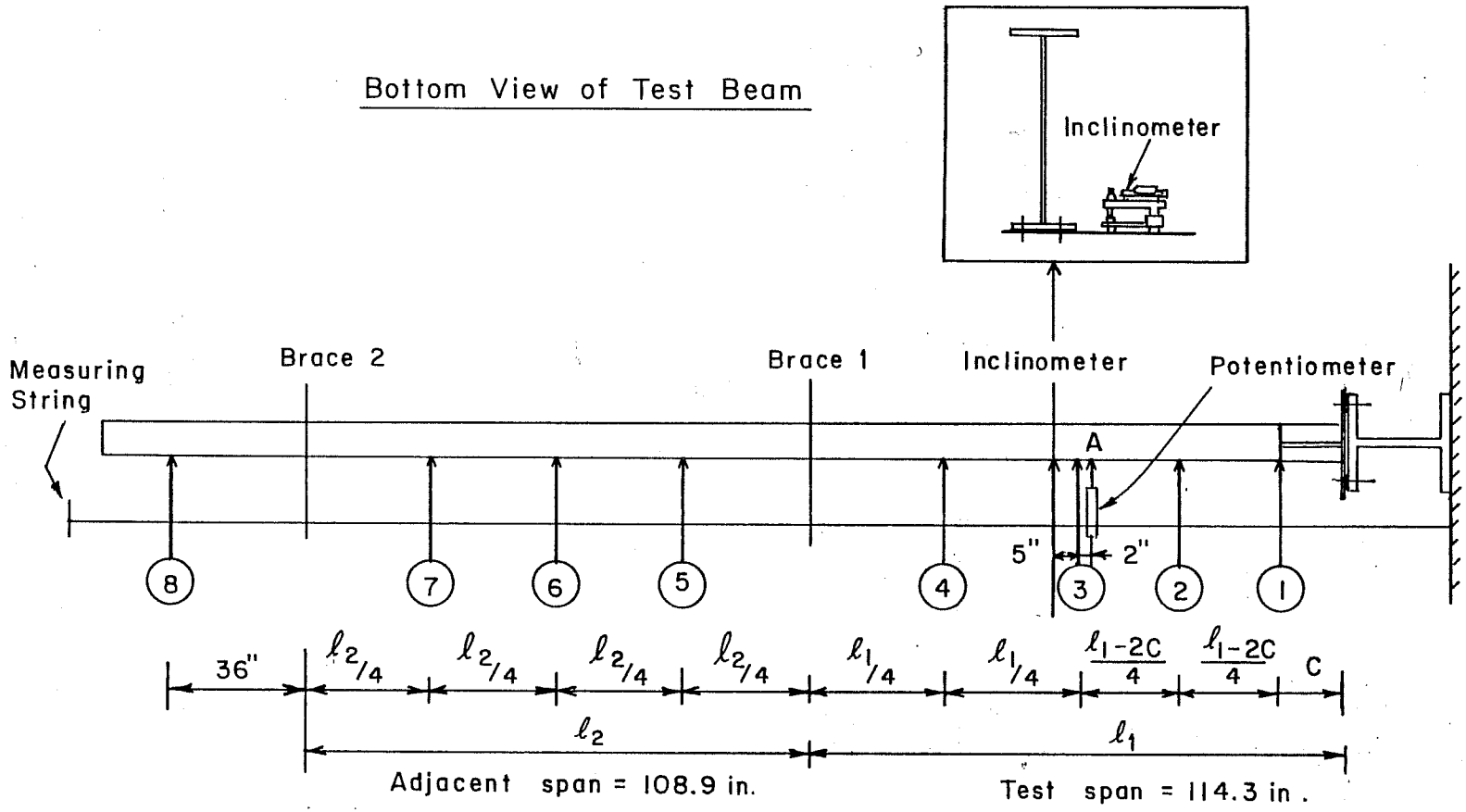

Fig. 5.9 Out-of-plane Deflection Instrumentation

stage data was taken as the self-weight of the beam which was supported by the connection and the far-end reaction.

Loading was applied in increments so that the data points along the load-deflection curve would be nearly equally spaced. The solid lines in Fig. 5.10 show a typical load-lateral deflection curve monitored by the x-y plotter. Since a hand pump was used, the loading between increments gives a wave-like appearance, each wave representing one stroke of the hand pump. When the desired load level was reached, pumping stopped and the load dropped to a stable (static) level after a few minutes. A solid dot indicates the static load at each increment. The test was terminated when the applied load reached at least 85 percent of the buckling load determined by Southwell's method [16] in order to avoid yielding due to large lateral deflection. After completion of each test, the test beam was rotated (there was a connection fabricated on both ends of the beam) or further coped in place, and a new test was conducted.

5.5 Moment-Rotation Characteristics of the Connections

Four tests as shown in Fig. 5.11 were peformed on beams with the same size end plate connection as used in tests LTB1 to LTB6 (Fig. 5.1) to obtain the in-plane and out-of-plane moment-rotation characteristics of connections. Results of the tests are shown in Figs. 5.12 and 5.14. The behavior is represented by a plot of beam moment, which was determined as the product of the dead weight times the distance from the connection face to the centerline of the load,

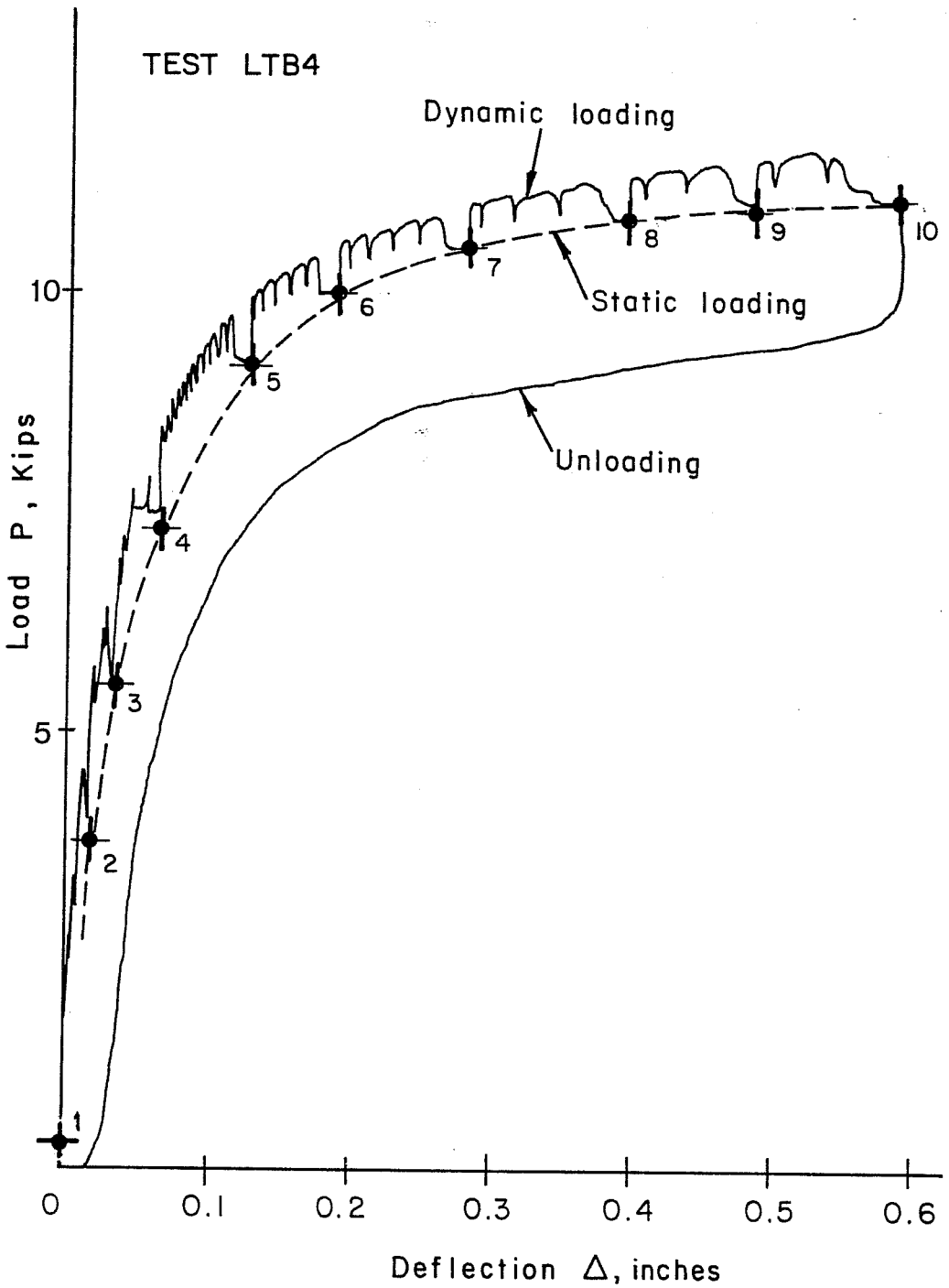

Fig. 5.10 Typical Testing Load-Lateral Deflection Curve

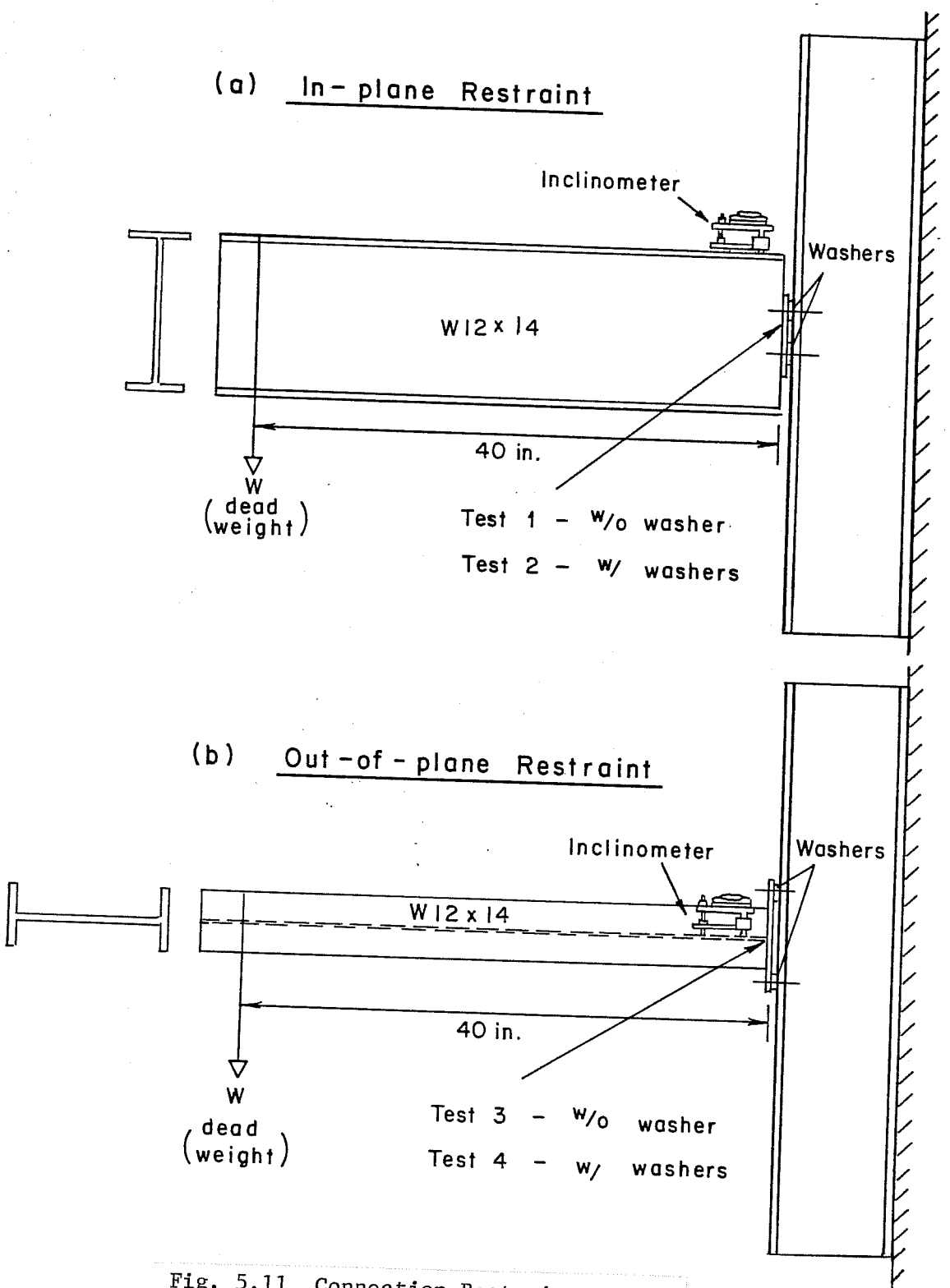

Fig. 5.11 Connection Restraint Tests

versus connection rotation obtained from the inclinometer reading.

Since the beam end moment twists the shear end plate, an elastic torsion analysis of the end plate with two extreme end conditions (warping prevented and free to warp) as shown in Fig. 5.13(c) was performed. When washers were used the top and bottom of the end plate (points A and B) were free to rotate without contacting the framing column as shown in Fig. 5.13(a). Without washers, the bottom of the end plate makes contact with the column and the connection rotates about point B in Fig. 5.13(b). However, probably due to lack of full contact at the bottom of the end plate (point B), the analyzed results are higher than the test results for Test 1 (without washers) as shown in Fig. 5.12. The experimental results of Test 2 (with washers) are located between the two extreme analyzed cases as shown in Fig. 5.13(c) but are closer to the "free to warp" case. The slope of the unloading curve is very close to the "free-to-warp" case. The stiffness of the connections without washers between the end plate and the supporting column is about 2.5 to 3.5 times larger than the connections with washers.

The experimental out-of-plane moment-rotation characteristics of the connections show that both cases (with and without washers between the end plate and the supporting column) give almost the same curve. This may be due to lack of full contact between the plate and column when washers were omitted. An elastic flexural analysis with pinned end conditions as shown in Fig. 5.15 was used for comparison, and the results are plotted in Fig. 5.14. The

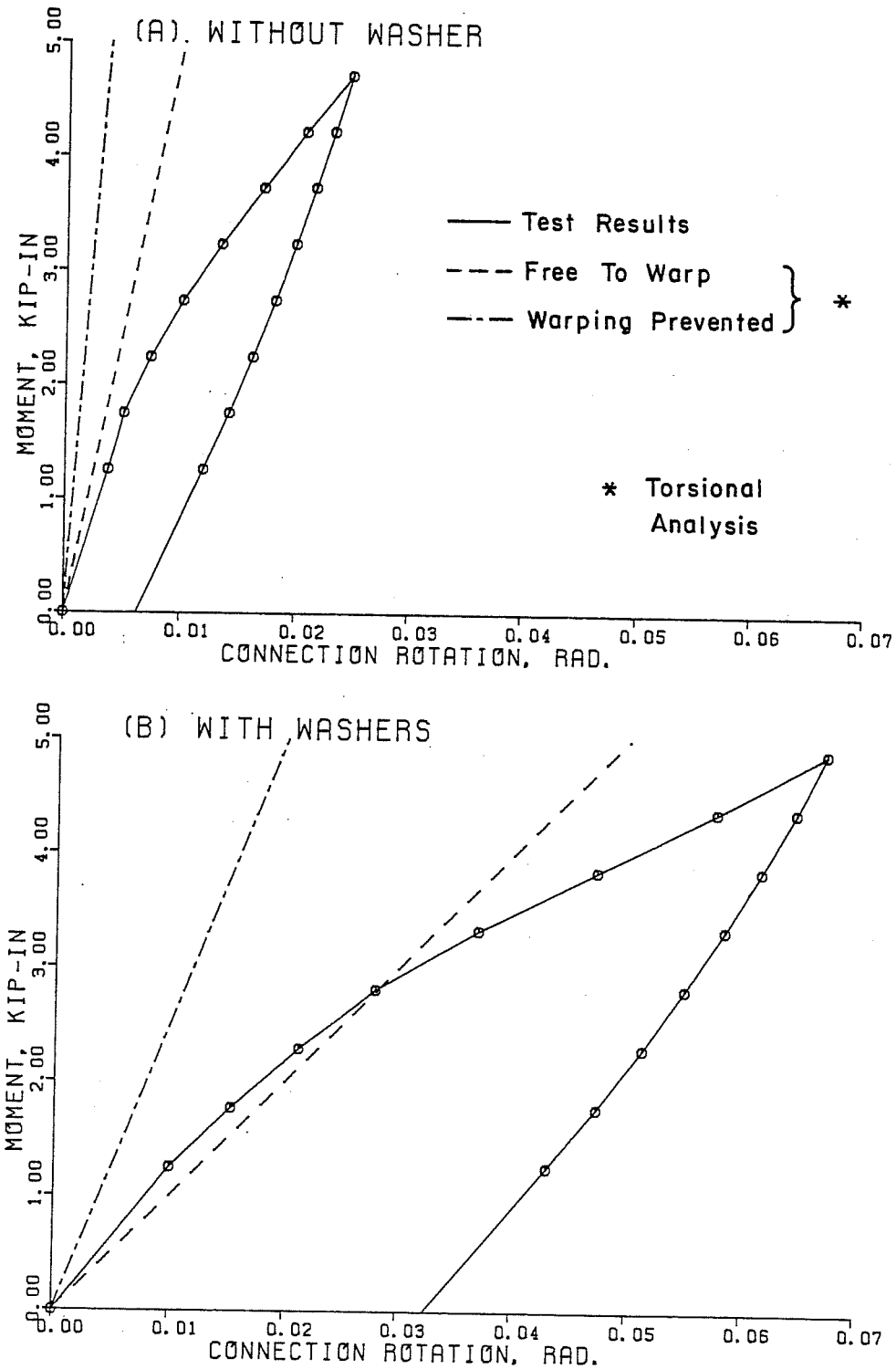

Fig. 5.12 In-plane Moment-Rotation Curves of the Test Connections

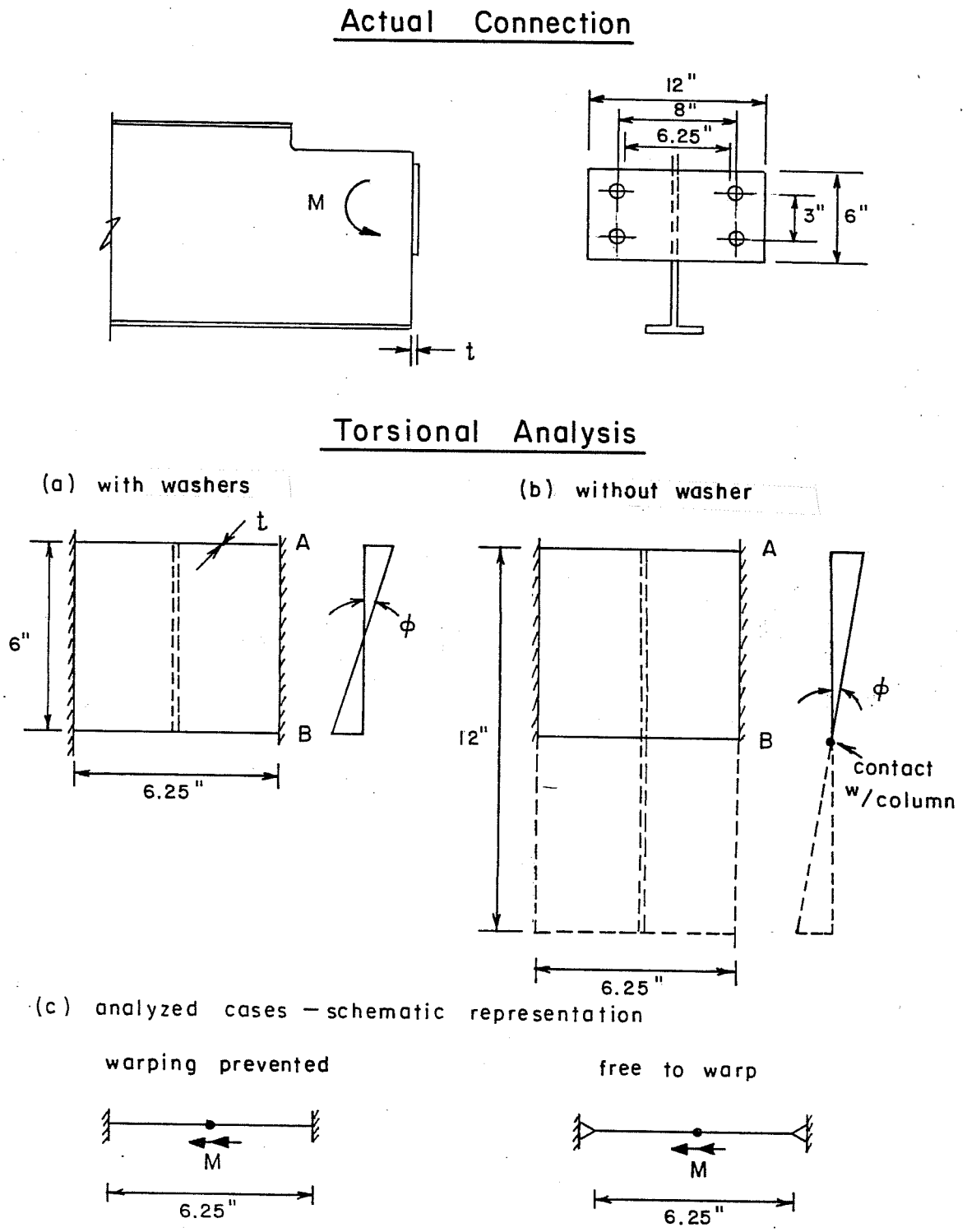

Fig. 5.13 Torsional Analysis of the In-plane Restraint of the End Plate Connections

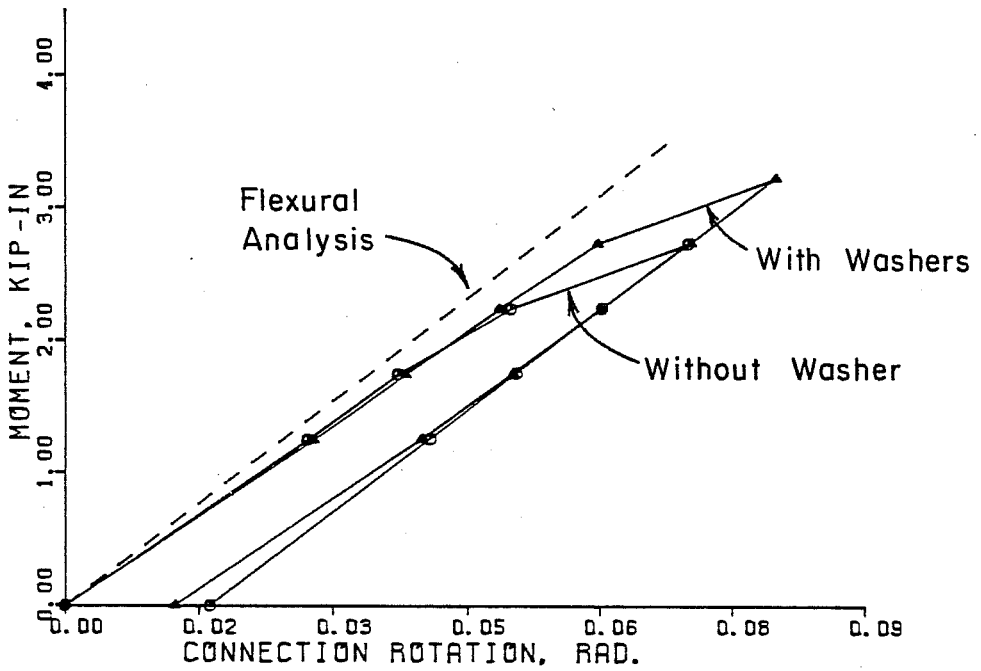

Fig. 5.14 Out-of-plane Moment-Rotation Curves of the Test Connections

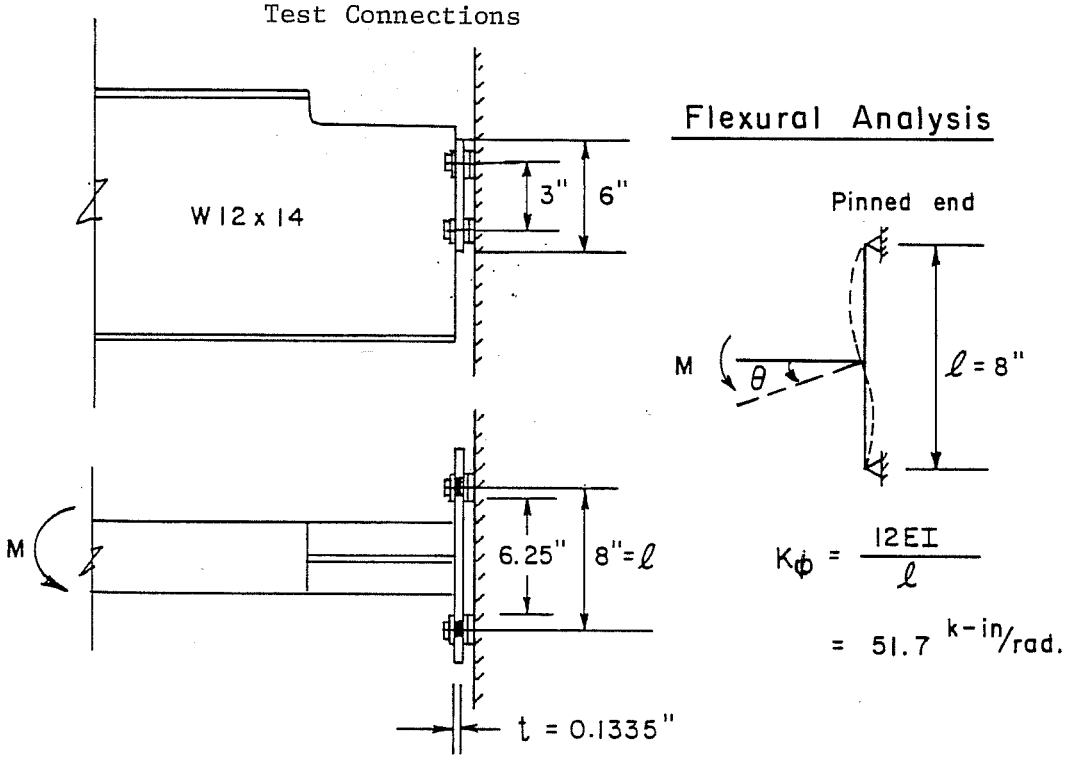

Fig. 5.15 Flexural Analysis of the Out-of-plane Restraint of the End Plate Connections

theoretical results are slightly higher than the test results. The theoretical results are probably higher due to the assumption that the beam is rigid between the end plate and the point at which the rotation is measured.

Both the torsion and the flexural analyses give a good indication of the in-plane and out-of-plane moment-rotation characteristics of the end plate connection.

5.6 Test Results

An examination of the reduced test data showed that a plot of applied load versus average deflection at the load point or rotation measured by the inclinometer gave the best representation of in-plane behavior and a plot of applied load versus critical lateral deflection reading or flange twist afforded the best description of the buckling phenomena of the test beams.

Because the in-plane behavior was similar, only one typical test, LTB4, will be shown and discussed here. Figures 5.16(a) and 5.16(b) show the plot of load versus in-plane deflection and load versus in-plane end rotation, respectively. When the load got close to the buckling capacity, the plots became nonlinear even though the test was still in the elastic range. The non-linear elastic response can be seen in the unloading portion of the x-y plot given in Fig. 5.10.

The plots of load versus lateral deflection and flange twist are shown in Figs. 5.17 and 5.18. The results of six tests were

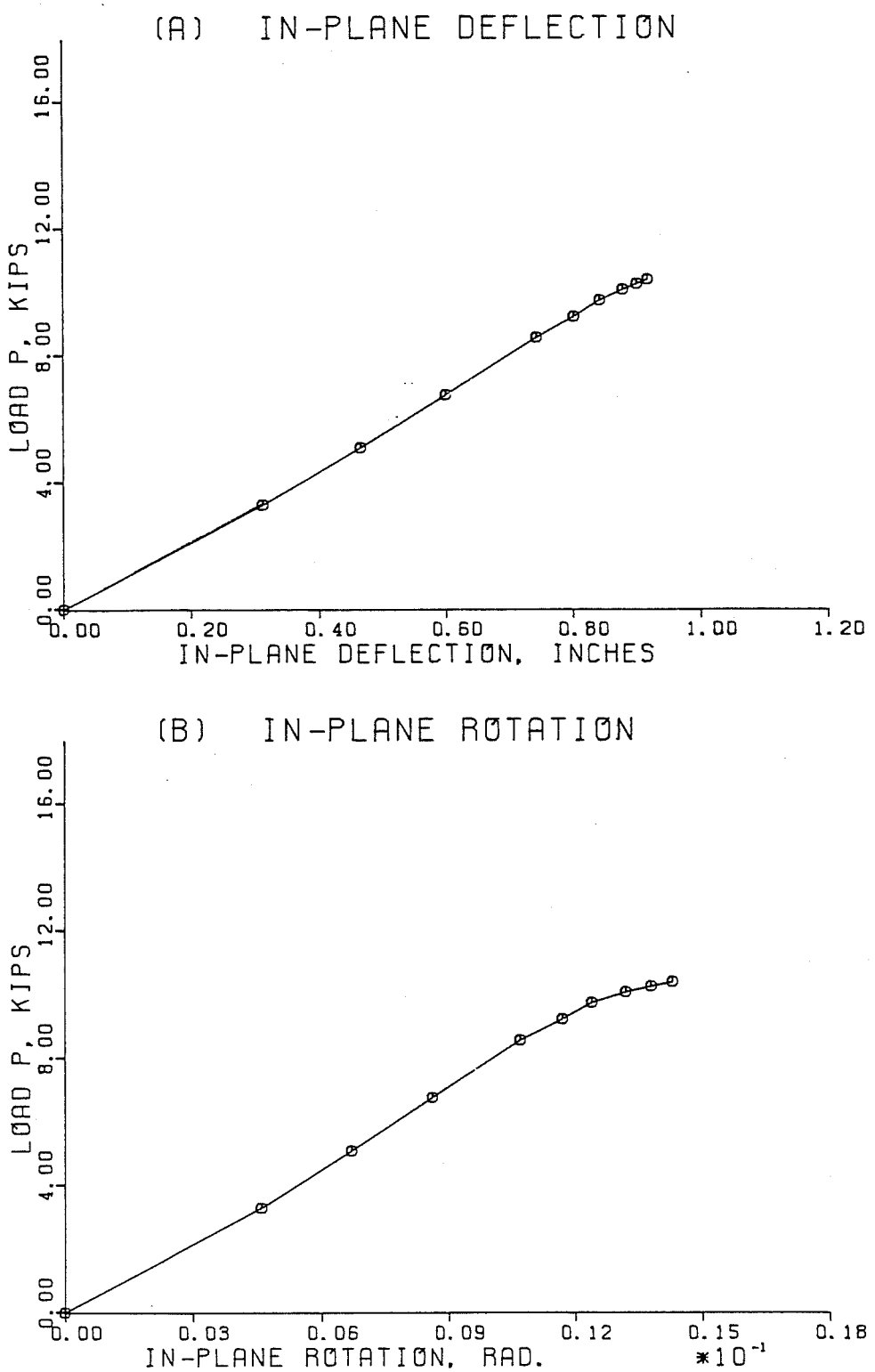

Fig. 5.16 Load vs. In-plane Deflection (Rotation) Curves

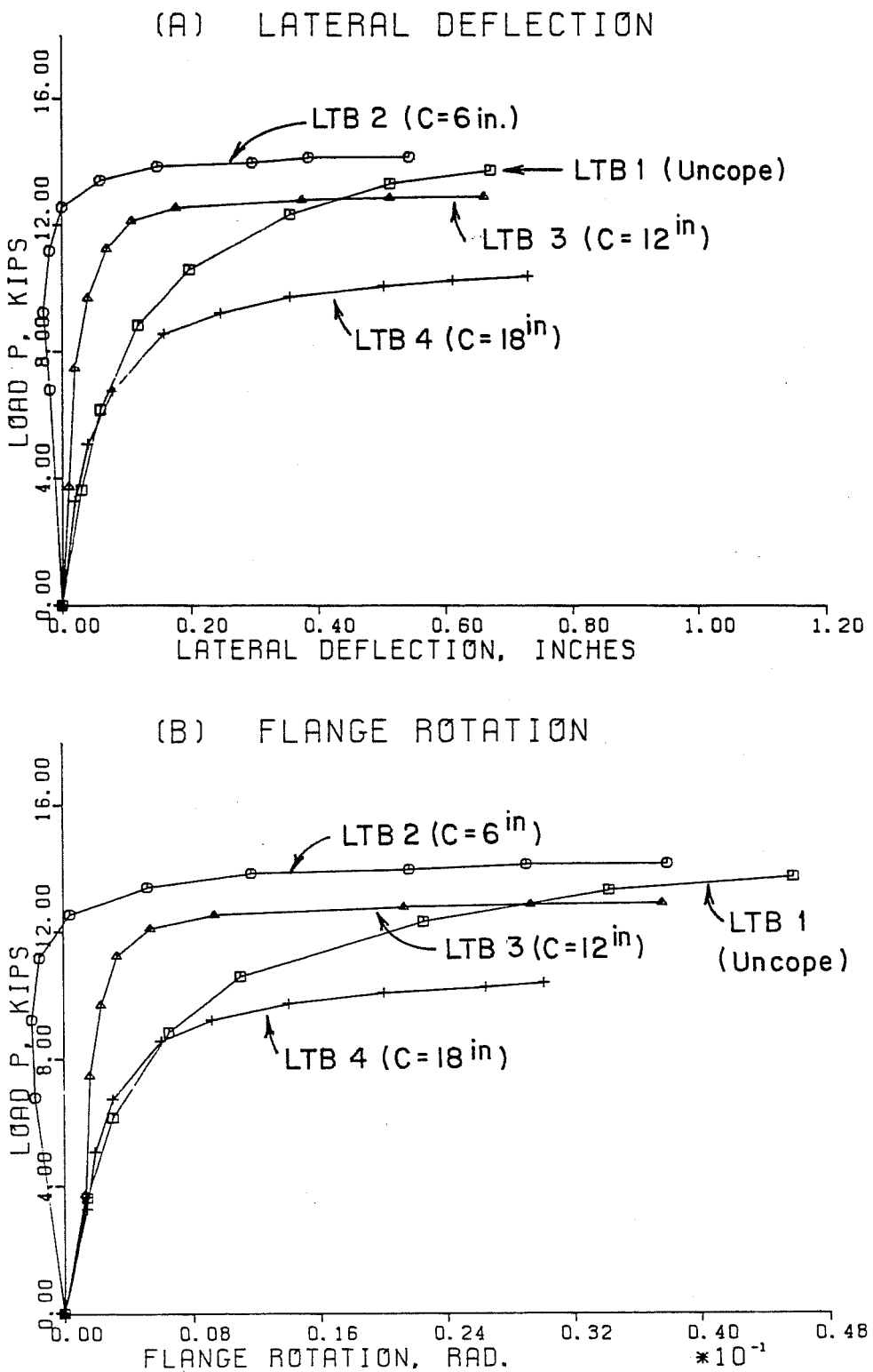

Fig. 5.17 Load vs. Lateral Deflection (Flange Twist) Curves of the Tests with Varied Cope Length

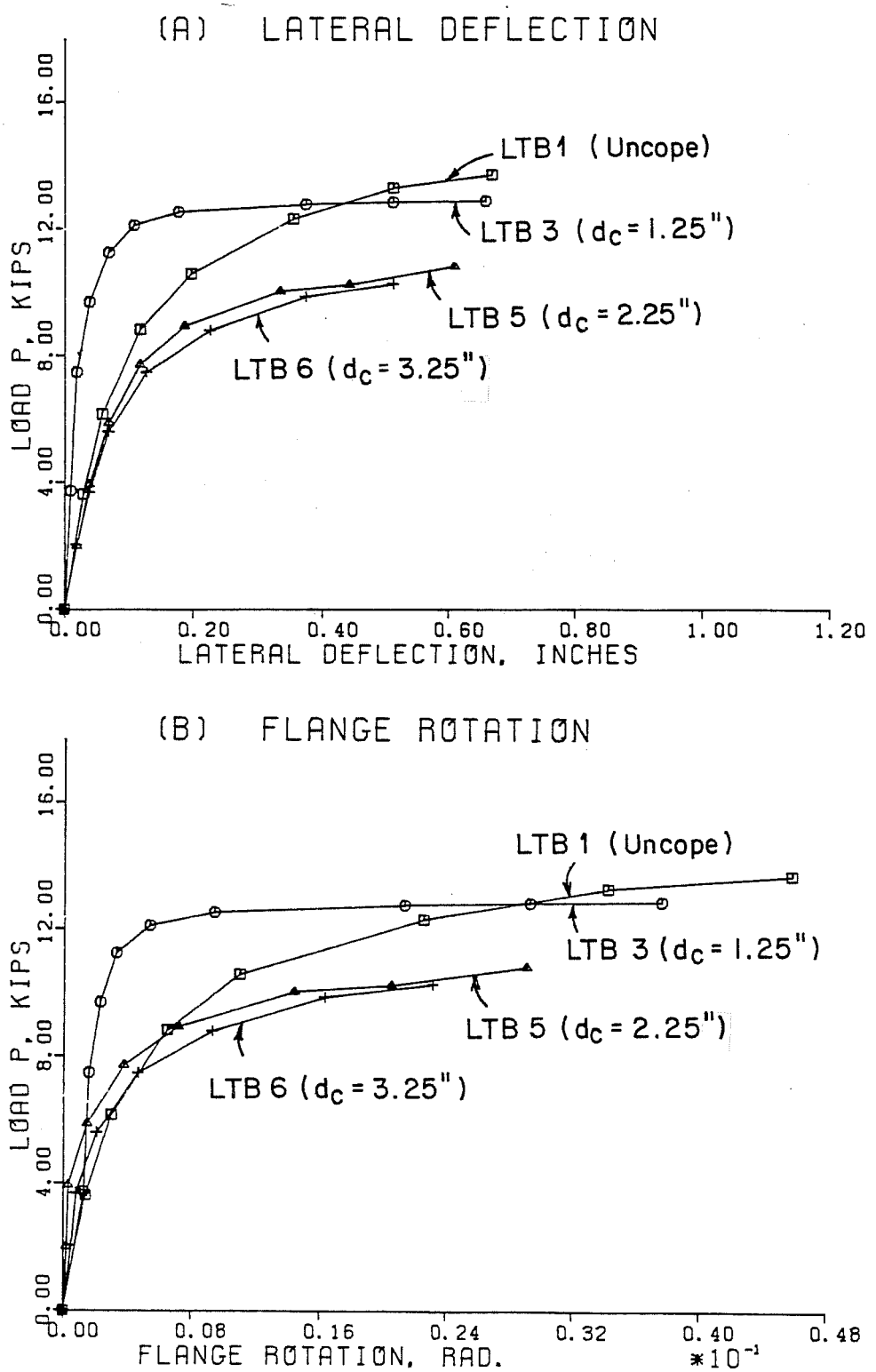

Fig. 5.18 Load vs. Lateral Deflection (Flange Twist) Curves of the Tests with Varied Cope Depth

divided into two groups. Tests LTB2 to LTB4 which were tests with the same cope depth but varied cope length are plotted in Fig. 5.17 and tests LTB3, LTB5, and LTB6 which were tests with the same cope length but varied cope depth are shown in Fig. 5.18. The results of the uncoped beam, LTB1, are also plotted in the four figures for comparison. Both the load versus deflection and the load versus twist curves give very similar behavior. In order to avoid yielding the test beam, the specimen was not loaded to maximum for all six tests. However, it can be seen from Figs. 5.17 and 5.18 that the maximum loads attained were very close to the ultimate loads. The normalized buckled shapes of the compression flange of the six tests are shown in Fig. 5.19. The buckled shapes are similar to those developed theoretically in the previous chapters. For long and deep copes, the test beam was simply rotating out-of-plane at the coped region and the capacity of the beam was controlled by the coped region.

While it is possible to calculate the end moment using statics and the measured load and measured end reaction as described in Section 5.3, this approach proved unsatisfactory. A very small error in the load and/or reaction affects the end moment significantly. Since errors in measurement are inevitable, a wide variation in calculated end moment was determined. Therefore, the in-plane end moment of each test was obtained by using the moment-rotation characteristic curve in Fig. 5.12 with the measured end rotation. The end moment was converted to an eccentricity "e" by

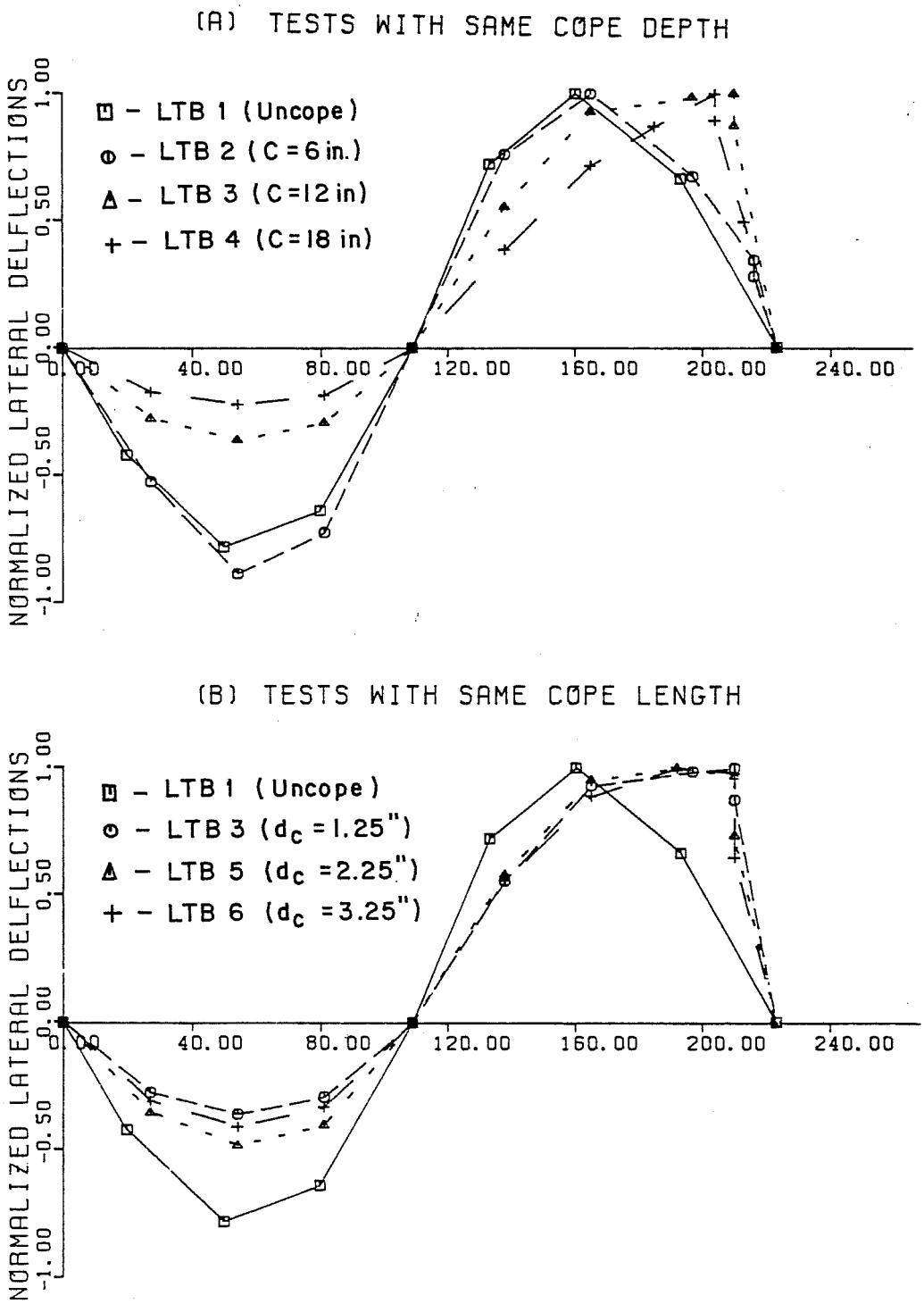

Fig. 5.19 Buckled Shapes of the Compression Flange

dividing it by the reaction at the connection. The average e of each test presented in Table 5.1 is relatively small so that a pinned end was closely approximated. The eccentricity was fairly constant throughout the loading history of each test and the value was consistent for all six tests.

TABLE 5.1 Average In-Plane Eccentricity "e"

Test No.	LTB1	LTB2	LTB3	LTB4	LTB5	LTB6
e (in.)	0.30	0.27	0.31	0.31	0.33	0.31

5.7 Analysis of Test Results

When a column or beam is expected to buckle in the elastic range, it is possible to get an accurate estimate of the experimental buckling load without testing the structure to failure by plotting the measured load and out-of-plane deformation in a particular manner. Three different plotting techniques developed by Southwell, Lundquist and Meck [16,17,18] were used to estimate the experimental elastic buckling loads. However, the results of all three methods gave almost the same results, so only the Southwell results will be shown here. In a Southwell plot lateral deflection (or twist) divided by the load is plotted against the same lateral deformation. In an ideal situation, the data points fall on a straight line whose slope is related to actual buckling load. Two typical Southwell

plots of Test LTB4 are shown in Fig. 5.20(a) and (b) using two different measured deformations, lateral deflection and twist, respectively. The critical buckling load P_{cr} was determined by a straight line passing through these data points using the least squares method. Generally, initial data points were not considered in obtaining P_{cr} due to the effects of small initial restraints of the test setup and experimental error whose effects were more pronounced at small values of load and deflection. The critical loads determined by using lateral deflection or twist for Test LTB4 give almost the same P_{cr}. However, when coped depth increases, localized distortion at the coped region effects flange twist data which increases the differences between P_{cr} obtained from the two test data. Thus, the lateral deflection data was used to determine the P_{cr} given in Table 5.2 since this data are considered more reliable. The highest measured test loads are also given in the table. For reliable Southwell estimates, it is generally suggested that the actual maximum test loads reach levels at least 70 percent of P_{cr} [19]. In this test program, P_{max} reached at least 87 percent of P_{cr}.

In order to check the reliability of the BASP program and the design recommendations proposed in Chapter 2, two computer models as shown in Fig. 5.21 were used. One is the design model which assumes that the coping details and unbraced length are symmetric about the load, defined as $(P_{Design})_{BASP}$, thus eliminating any restraint of adjacent spans which is the usual design assumption. The other is the test model which includes self-weight of the test

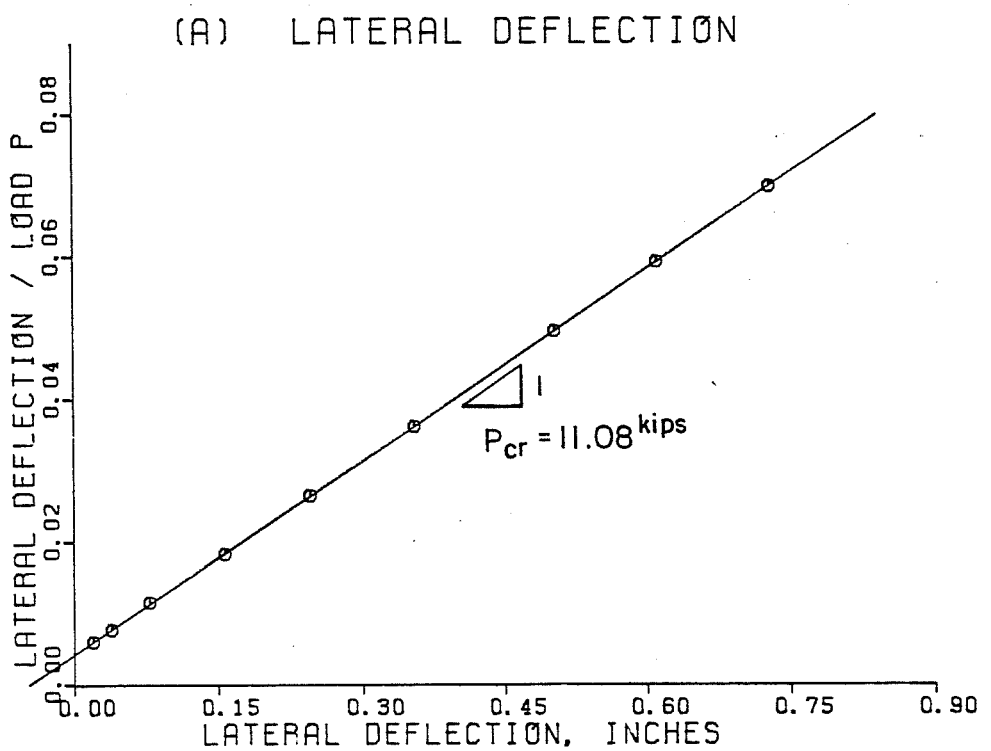

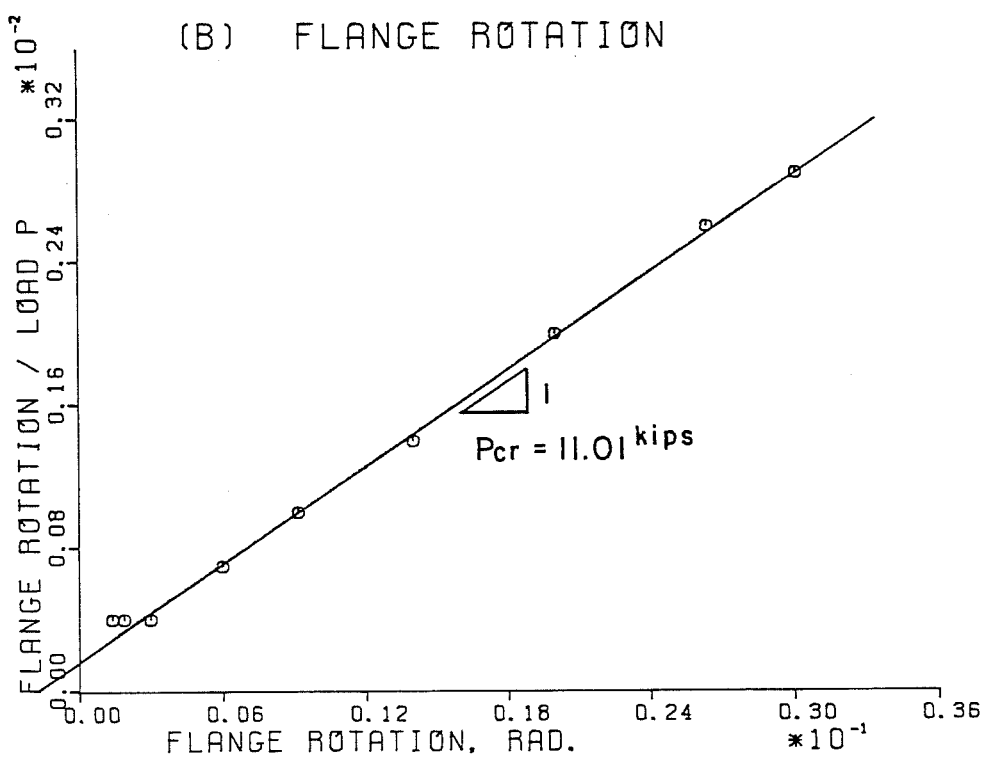

Fig. 5.20 Typical Southwell's Plots

TABLE 5.2 Lateral Torsional Buckling Test Results

Test No.	LTB1	LTB2	LTB3	LTB4	LTB5	LTB6
c, in.	0	6	12	18	12	12
d_c, in.	0	1	1	1	2	3
P_{cr}, kips	15.27	14.20	13.15	11.08	11.95	11.86
P_{max}/P_{cr}	0.89	0.99	0.98	0.94	0.91	0.87
P_{cr}/P_{BASP}	1.15	1.11	1.17	1.23	1.14	1.20
P_{cr}/P_{Design}	1.27	1.33	1.60	1.74	1.72	1.88
$P_{cr}/(P_{Design})_{BASP}$	1.23	1.33	1.67	1.83	1.66	1.77

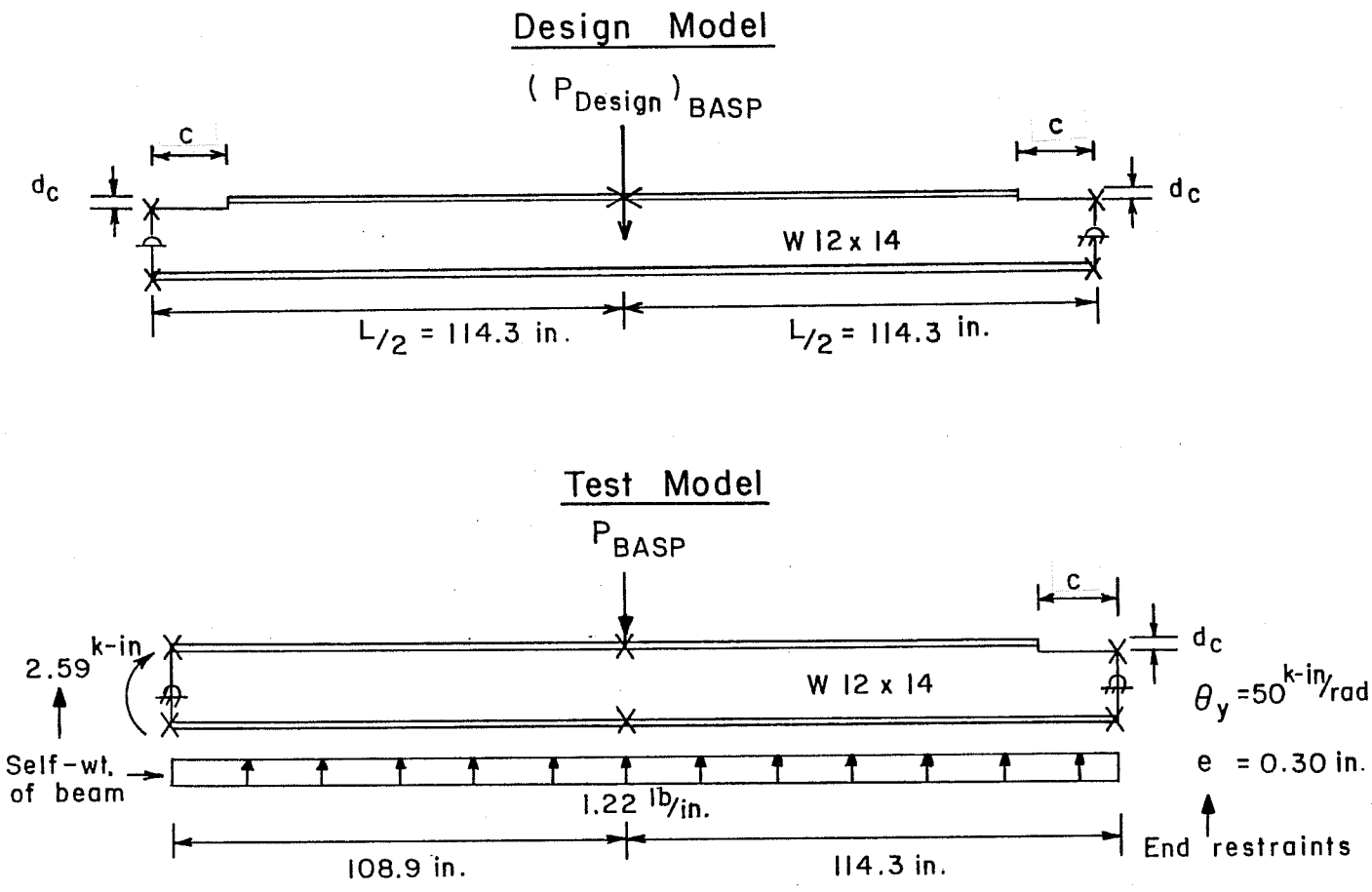

Fig. 5.21 Computer Models of Lateral-Torsional Buckling Tests

beam, in-plane and out-of-plane end restraint and actual span length of the test beam. The beam dead weight is shown upward in Fig. 5.21 because the beams were tested upside down as described earlier. The buckling load of the second model is defined as P_{BASP}. The results of two computer models, $(P_{Design})_{BASP}$ and P_{BASP}, and the design recommendation, P_{Design}, divided by P_{cr} estimated by the Southwell plotting technique are summarized in Table 5.2. The buckled shapes of the compression flange of the P_{BASP} solutions are plotted in Fig. 5.22 for comparison with the test results (Figs. 5.19). Both the BASP results and the test results yield very similar buckled shapes.

The results in Table 5.2 show that both P_{max} and P_{cr} are 10 to 20 percent higher than P_{BASP}. This can be attributed to the restraints at the far end reaction and the load, the friction of the bracing systems and the post buckling capacity of the beams. Comparing the design recommendation, P_{Design}, to P_{BASP} shows that P_{Design} gives very conservative results, especially when cope length and cope depth are large. The reason is that P_{Design} was developed assuming no restraint from adjacent spans. P_{Design} agrees fairly well with $(P_{Design})_{BASP}$ which also has no end restraint.

In summary, both the BASP solutions and the design recommendations give conservative but reasonable results compared with the test results. The buckled shapes developed by BASP also compare favorably with the shapes measured in the experiments.

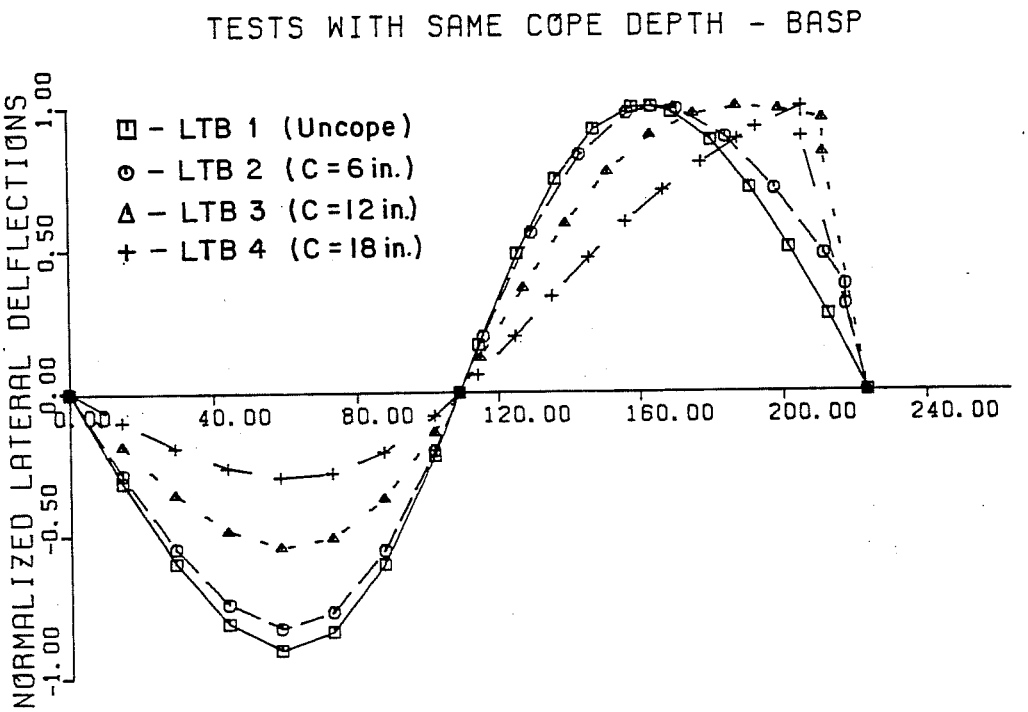

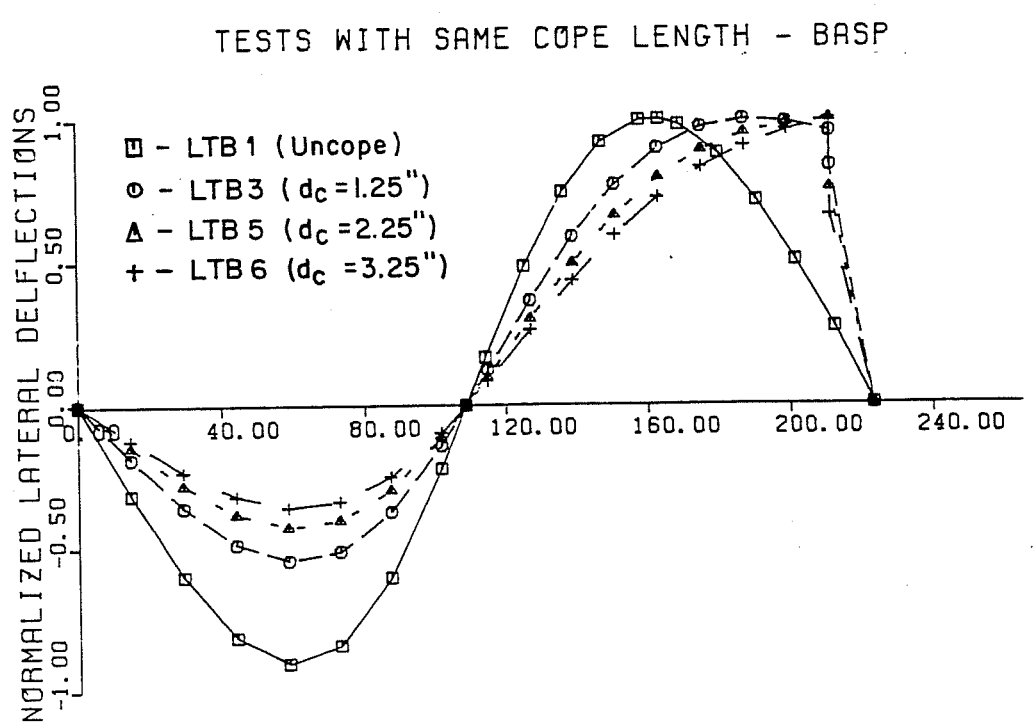

Fig. 5.22 Buckled Shapes of the Compression Flange of the BASP Solutions

CHAPTER 6

REINFORCEMENT AND OTHER DETAILS

6.1 Reinforcement

The BASP solutions indicate that coping the compression flange will decrease the lateral buckling capacity of beams significantly. In some instances the reduction can be more than 90% of the uncoped buckling capacity as discussed in previous chapters. Instead of increasing the beam size so the desired moment capacity can be developed, it may be practical to reinforce the coped area with stiffeners. The purpose of this section is to study the influence of two types of reinforcing detail. The behavior of the reinforced top and double flange coped beams are similar, so only the results of top flange coped beams will be shown and discussed.

A simply supported beam, loaded and braced laterally at mid-span as shown in Fig. 6.1 was chosen for this study. A W16x26 section and a span length = 20 ft were used throughout this investigation. Two types of reinforcement as shown in Fig. 6.1 were studied and the BASP program was used to determine the buckling loads. Doubler plate reinforcement was not considered in this lateral buckling study. The reason is that the lateral buckling strength of coped beams is not only a function of cope length and cope depth, but also the function of span length which will create an infinite variety of situations. The purpose of reinforcement is to

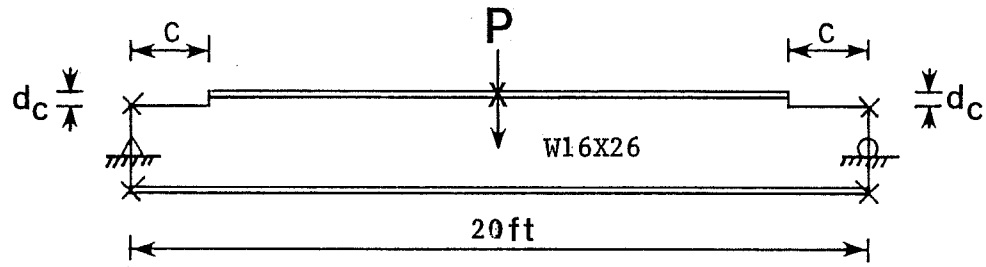

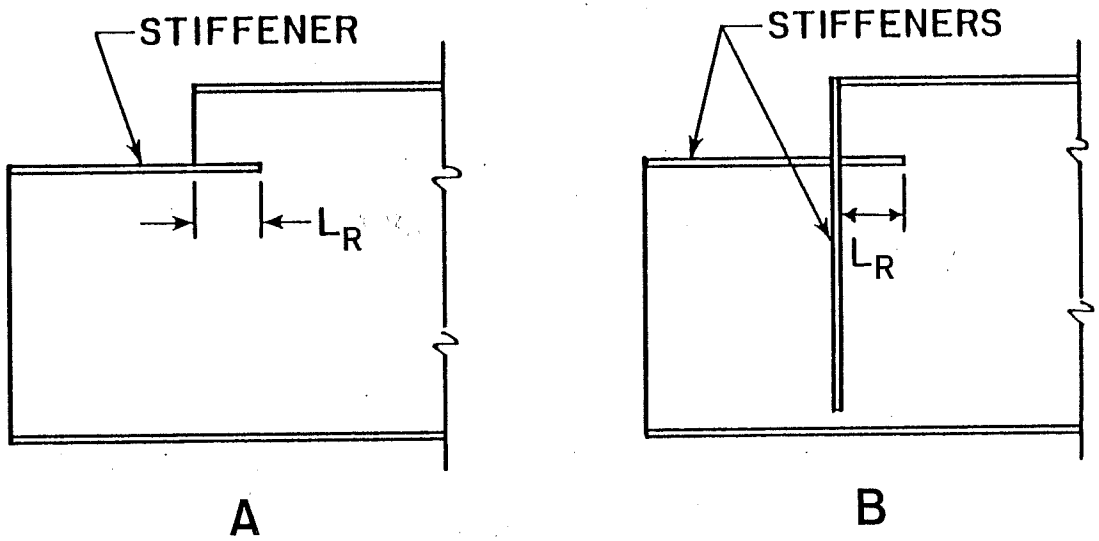

Fig. 6.1 Types of Reinforcement

increase the restraints of the coped region and the effectiveness of the restraint depends upon the torsional strength and stiffness of the coped section. Tee sections are not as effective as wide flange sections in torsional stiffness.

In Fig. 6.2, an extreme cope length, c = 2d, was used so the results could be safely applied to smaller cope lengths. The cope depth and the length of stiffener (L_R) were varied to investigate the behavior of two types of reinforcements as shown in Fig. 6.1. Figure 6.2 shows that Type B reinforcement is more efficient than Type A reinforcement, especially when cope depths are large. This can be explained by the tipping effect of the top flange at the end of the cope as discussed in Section 2.5.3. In both reinforcing details, the buckling loads are very low compared with uncoped beams when $L_R = 0$. This can be attributed to web crippling at the termination of the horizontal stiffener. When L_R increases, the web crippling is eliminated by distributing the concentrated load along the stiffener length L_R. The results show that $L_R \geq c/3$ will be sufficient to eliminate the web crippling problem. Only Type B reinforcement with $L_R = c/3$ was adopted for further study since the Type A detail is not very effective except for very small d_c.

A parametric study with cope length and cope depth varied from 0 to 2d and 0 to d/2, respectively, was undertaken and the results are shown in Fig. 6.3. An unreinforced beam with an 8 in. cope length and varied cope depth is shown dashed in Fig. 6.3 for comparison. The results show that the reinforcement can increase the

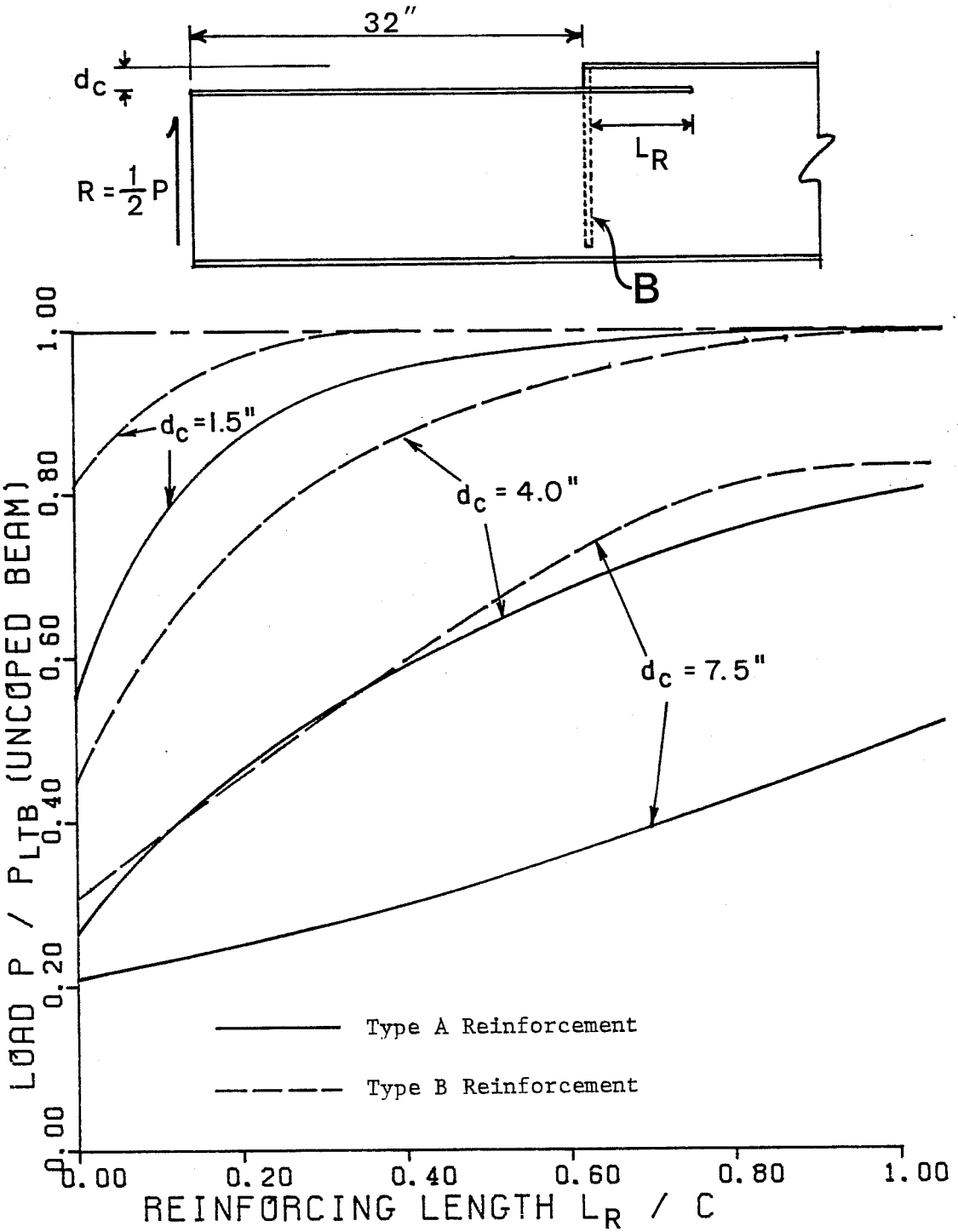

Fig. 6.2 Comparison of the Effectiveness of Two Types of Reinforcement

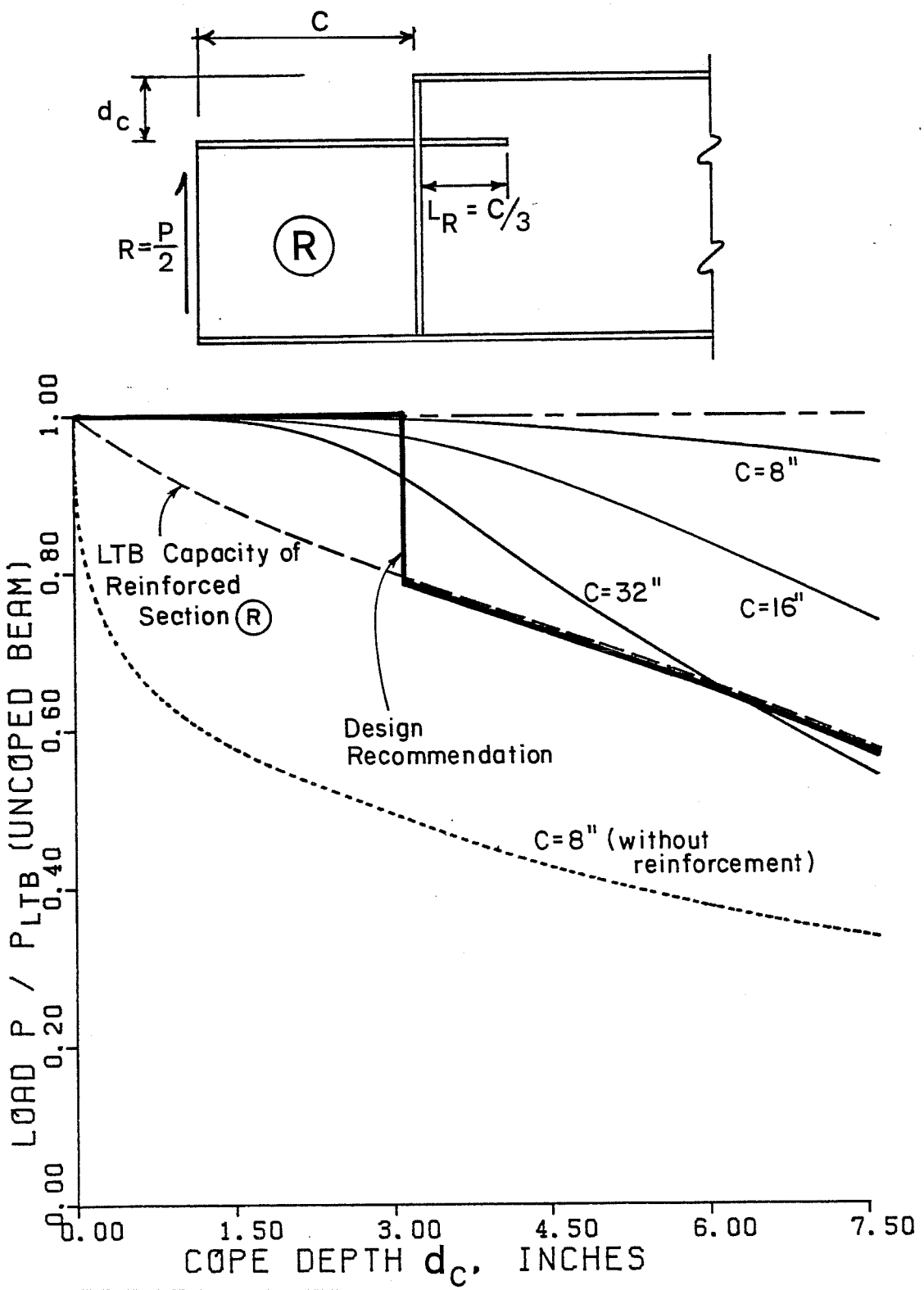

Fig. 6.3 Parametric Study of the Type B Reinforcement

buckling load significantly. In fact, when cope length or cope depth is small, say $c \leq d/2$ or $d_c \leq 0.2d$, the buckling capacity of coped beams with Type B reinforcement can almost reach the original uncoped buckling capacity. However, when cope length and cope depth are increased beyond these limits, the buckling load of reinforced coped beams cannot reach the uncoped buckling load. For design purposes, the lateral buckling loads of the unbraced spans (10 ft in this study) calculated by using the section properties of the reinforced section R as shown in Fig. 6.3 instead of the uncoped section was found to give conservative results. Figure 6.3 shows that the buckling loads calculated by the reinforced section R can be used as the lower bound for long and deep coped beams.

In summary, Type B reinforcing details with $L_R \geq c/3$ is recommended for top and double flange coped beams. No reduction of lateral buckling capacity is needed for the reinforced coped beams if the cope length is smaller than half the beam depth ($c \leq d/2$) or the cope depth is smaller than 0.2 of beam depth ($d_c \leq 0.2d$). Conversely, when $c > d/2$ and $d_c > 0.2d$, the reinforced section R is used to calculate the lateral buckling capacity as shown by heavy solid line in Fig. 6.3. For bottom flange coped beams, Type A reinforcing details with $L_R \geq d_c$ is recommended and no reduction of lateral buckling capacity is needed for the reinforced coped beams.

6.2 Effects of End Restraint

Though most designers treat coped beam connections as "simple" (zero moment), the connection does possess a certain amount of rotational rigidity that may influence the capacity of coped beams. A top flange coped W16x26 beam was used to study the effects of both in-plane and out-of-plane end restraint and the results are shown in Fig. 6.4 and Fig. 6.5, respectively.

In Fig. 6.4, c = 32 in. and d_c = 1.5 in. were used to study the effects of in-plane end restraint. The in-plane end restraint, e, will increase the buckling capacity significantly because the end moment will decrease the maximum applied bending stress at the end of the cope. However, Fig. 6.4 shows that it is unconservative to use the distance between inflection points as the span length L. When e = c, there is still a 20 percent reduction compared to the uncoped beam buckling cpacity as shown in the figure. For bottom and double coped beams, the end moment will produce compression in the bottom which tends to decrease the buckling capacity of the coped region.

A beam fixed out-of-plane means warping is prevented. The buckling strength of a coped beam with and without full warping restraint is compared in Fig. 6.5. The out-of-plane end restraint will increase the buckling capacity of coped beams as expected, but only by about 20 percent. Since the out-of-plane end restraint depends upon the web to restrain the uncoped region, it is not as efficient as in-plane end restraint.

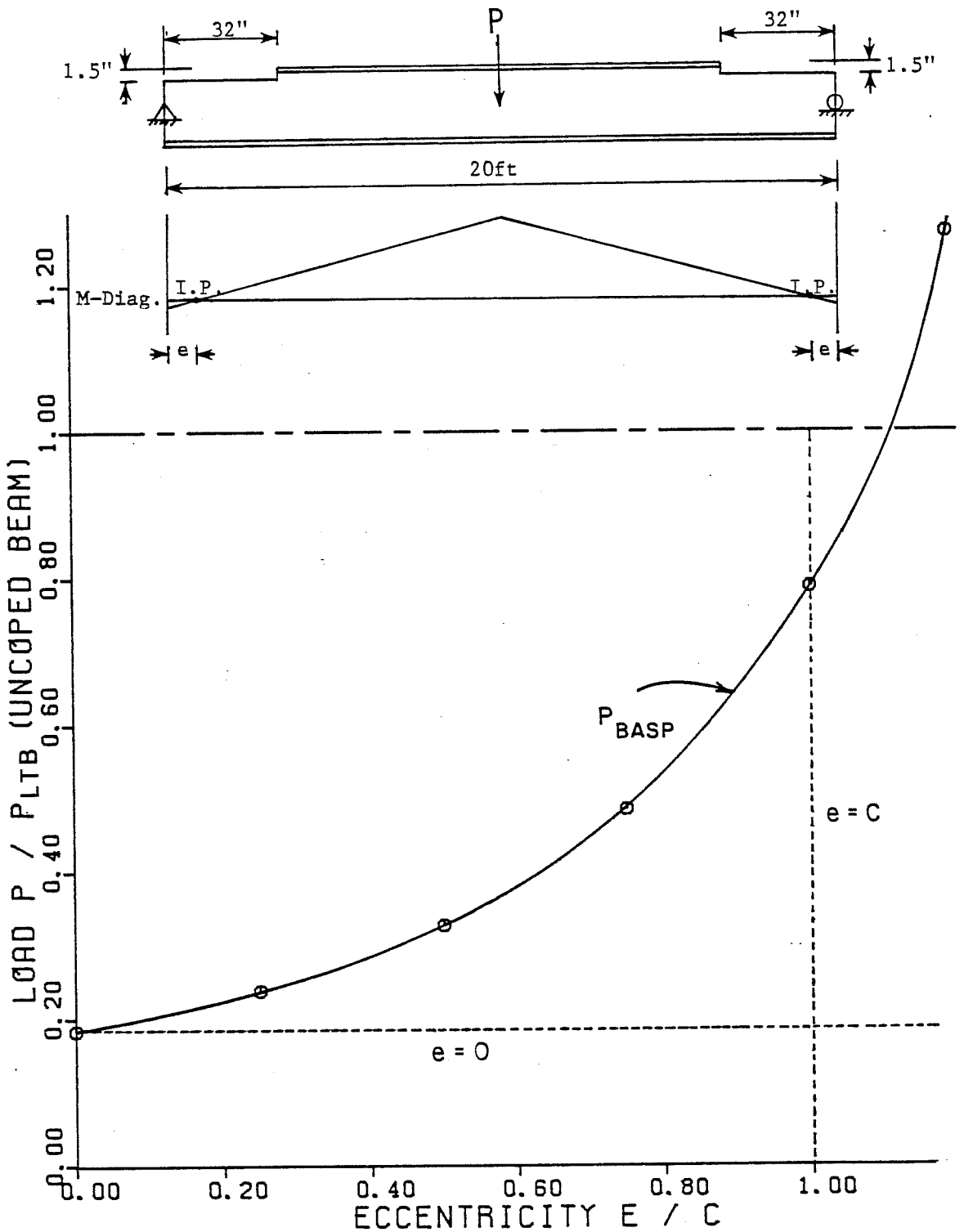

Fig. 6.4 Effects of In-plane End Restraint

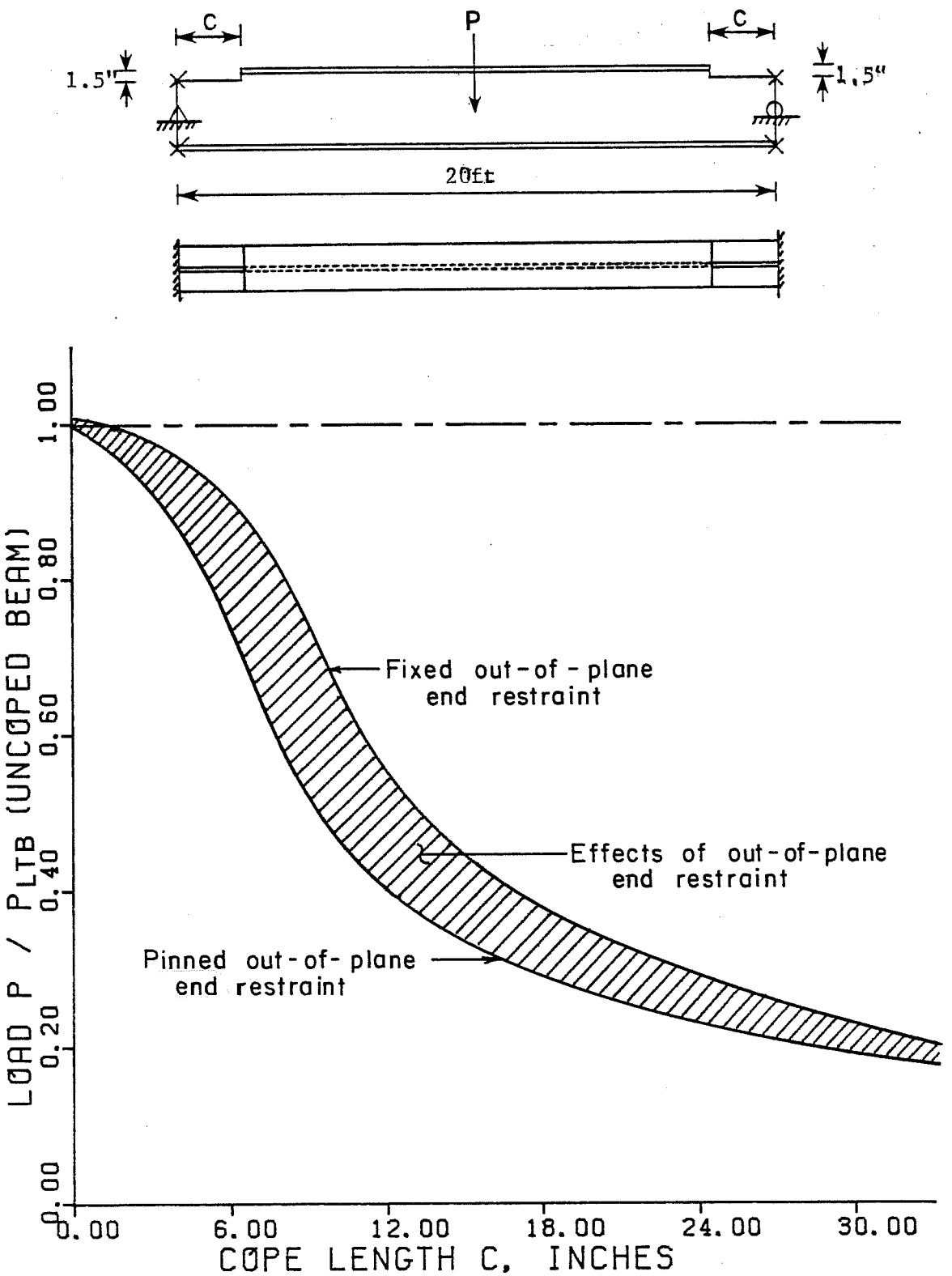

Fig. 6.5 Effects of Out-of-plane end restraint

CHAPTER 7

SUMMARY, RECOMMENDATIONS AND DESIGN EXAMPLES

7.1 Summary

The lateral torsional buckling capacity of coped beams has been investigated by a parametric theoretical study and tests. The theoretical analysis considered parameters such as cope length, cope depth, span length, and end restraints, of top (compression), bottom (tension) and double flange coped beams. Web reinforcing details have also been studied for different copes. Six tests on a W12x14 beam with different top flange coping details were used to check the reliability of the theoretical results. The following is a summary of the findings.

1. Top (compression) flange coped beams: the lateral buckling capacity of the beams is controlled by the interaction of the coped (tee) and the uncoped (I) section. In other words, if copes are small, the behavior of coped beams is similar to uncoped beams. Conversely, if copes are long and deep, the capacity of coped beams is controlled by coped region and the uncoped region simply buckles with rigid body motion. An unbraced length with copes at both ends has less capacity than the same length with only one end coped as represented by Eqs. (2.2) and (2.3), respectively.

2. Bottom (tension) flange coped beams: the cross section distortion at the coped region causes a reduction of buckling capacity.

However, the effects of bottom flange copes are much less than top and double flange copes.

3. Double flange coped beams: the behavior of double flange coped beams is similar to top flange coped beams except the coped section of double coped beams is a rectangular section.

4. End restraints from connections and reinforcement can increase the buckling capacity of coped beams significantly.

5. The theoretical results give conservative but reasonable results compared with test results. The conservatism is due to neglecting of the restraints from adjacent spans and restraint provided by the test fixtures.

7.2 Design Recommendations

In order to apply the previous recommendations to more general design conditions, critical moments instead of critical loads are used in the final design equations below to account for various loading arrangements. The design recommendations for lateral torsional buckling of coped beams are applicable to copes with a length less than twice the beam depth ($c \leq 2d$) and with a depth less than one-half the beam depth ($d_c \leq d/2$) (for double copes $d_c \leq 0.2d$ in each flange). Equations (1) to (6) below are used to define the nomenclature used in the final design equations as follows:

$$M_{LTB} = (C_b \pi/L_b) \sqrt{EI_yGJ + E^2I_yC_w \pi^2/L_b^2} \qquad (1)$$

where C_b is a bending coefficient depending upon the loading conditions under consideration; C_b = 1.0 for uniform moment

and $C_b = 1.75 + 1.05\ M_{sm}/M_{lg} + 0.3\ (M_{sm}/M_{lg})^2 \leq 2.3$ for linear moment diagram. For other loading cases, C_b can be found in the SSRC Guide [1].

$$M'_{LTB} = (3/16)(n/(n+2))\ E\ L_b\ d\ (t_w^3/d_c^2) \tag{2}$$

$$\text{where } n = (16 t_f b_f^3 d_c^2)\ /\ (L_b^3 t_w^3) \tag{2a}$$

$$1/M''_{LTB} = 1/M_{Tip} + 1/M_{LTB} \tag{3}$$

$$\text{where } M_{Tip} = (1/2)\ EL_b d\ (t_w^3/d_c^3) \tag{3a}$$

$$M_{Tee} = (\pi/2c)\sqrt{EI_y GJ}\ \ [\sqrt{1 + (\pi\gamma_m/2)^2} + \pi\gamma_m/2] \tag{4}$$

$$\text{where } \gamma_m = (\beta_x/2c)\sqrt{EI_y/GJ} \tag{4a}$$

$$\beta_x = -\ [\frac{1}{I_x}\ [\frac{t_w}{4}\ [(h_o - \bar{y})^4 - (\bar{y} - t_f)^4] \tag{4b}$$

$$- (\bar{y} - \frac{t_f}{2})\ [\frac{b_f^3 t_f}{12} + b_f t_f\ (\bar{y} - \frac{t_f}{2})^2\ ] + 2\bar{y} - t_f]$$

$$M'_{Tee} = M_{Tee}\ (1 - 1.5\ d_c/d) \tag{5}$$

$$M_{Rec} = (\pi/2c)\sqrt{EI_y GJ} \tag{6}$$

1. <u>TOP (COMPRESSION) FLANGE COPED BEAMS</u>:

   a. Copes at both ends

   $$1/M_{LTB} + 1/((L_b/2c)\ M_{Tee}) = 1/M_{cr}$$

   for rolled sections and $d_c \leq 0.2d$

$$1/M'_{LTB} + 1/((L_b/2c)\ M'_{Tee}) = 1/M_{cr}$$

for thin web members ($h/t_w \geq 60.0$ or $d_c > 0.2d$)

b. Copes at one end only

$$1/(M_{LTB})^2 + 1/((L_b/c)\ M_{Tee})^2 = 1/M_{cr}^2$$

for rolled sections and $d_c \leq 0.1d$

$$1/(M''_{LTB})^2 + 1/((L_b/c)\ M'_{Tee})^2 = 1/M_{cr}^2$$

for thin web members ($h/t_w \geq 60.0$ or $d_c > 0.1d$)

2. BOTTOM (TENSION) FLANGE COPED BEAMS: a 10 percent reduction of lateral torsional buckling capacity of uncoped beams (Eq. (1)) is used for all bottom flange coped beams.

$$M_{cr} = 0.9 \times M_{LTB}$$

3. DOUBLE FLANGE COPED BEAMS:

a. Copes at both ends

$$1/M_{LTB} = 1/((L_b/2c)\ M_{Rec}) = 1/M_{cr}$$

b. Copes at one end only

$$1/(M_{LTB})^2 + 1/((L_b/c)\ M_{Rec})^2 = 1/M_{cr}^2$$

4. WEB REINFORCEMENT:

a. Top and double coped beams:

Top Flange Coped Beams

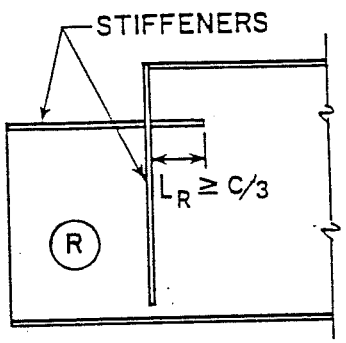

Double Flange Coped Beams

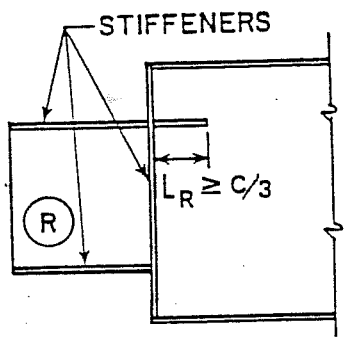

If $c \leq d/2$ or $d_c \leq 0.2d$, no reduction of capacity required for reinforced beams.

If $c \geq d/2$ and $d_c \geq 0.2d$, the cross section properties in zone R should be used in the LTB formulas along with the total unbraced length L_b (not 2c).

b. Bottom flange coped beams:

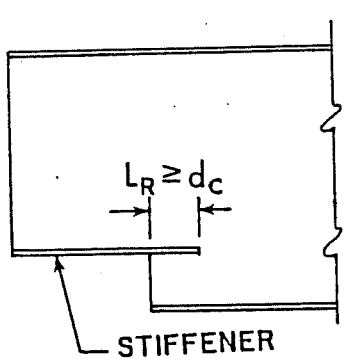

No reduction is required for reinforced beams.

7.3 Design Examples

Test LTB6 is used to illustrate the design procedure of top and bottom flange coped beams. Test LTB3 with the same bottom flange copes as top flange copes was used for a design example of double flange coped beams.

In the following example problems, it is assumed that P is a factored ultimate load. For allowable stress design where P is a service load, a factor of safety of 1.67 is recommended so that $P_{allow} = P_{cr}/1.67$.

Illustrative Example 1

Top (Compression) Flange Coped Beam--Test LTB6

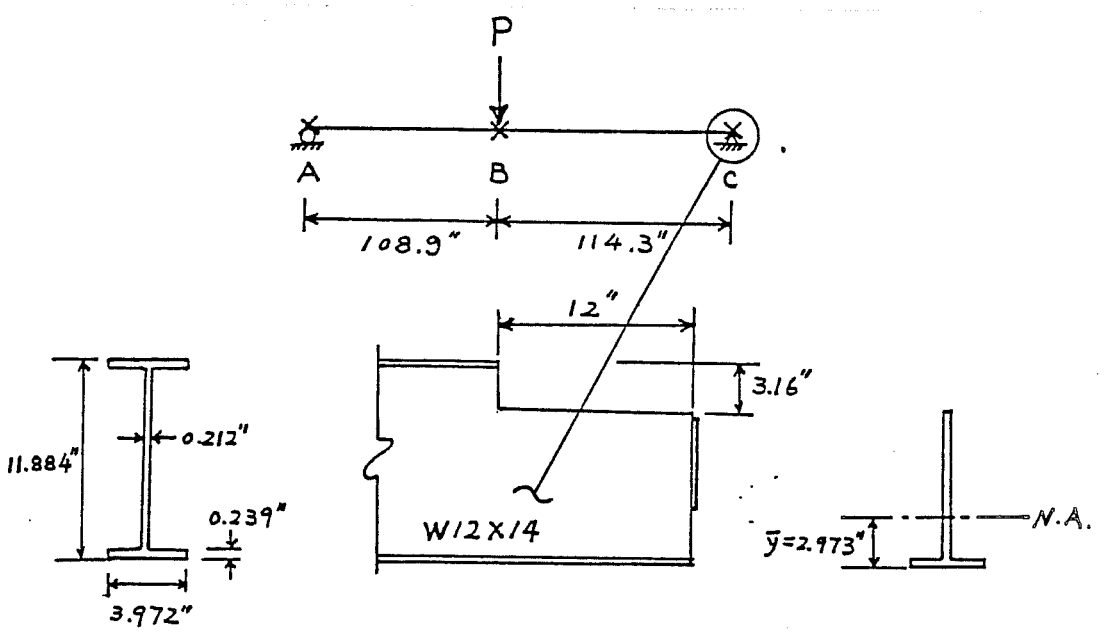

$A = 4.317 in^2$

$I_x = 90.6 in^4$

$I_y = 2.51 in^4$

$J = 0.072 in^4$

$c_w = 84.6\ in^6$

$A = 2.748 in^2$

$I_x = 22.62 in^4$

$I_y = 1.26 in^4$

$J = 0.045 in^4$

Critical span $\overline{BC}$, cope at one end of unbraced span only.

Since $\frac{dc}{d} = 0.266 > 0.1$, and $h/t_w = 53.8 \leq 60$

Therefore, Eq (3) and Eq. (5) are used

Eq. (1) $M_{LTB} = C_b \frac{\pi}{L_b}\sqrt{EI_y\ GJ + E^2 I_y\ C_w\ \pi/L_b^2} = 673^{k-''}$

Eq. (1a) $C_b = 1.75$ was used for the critical span BC.

Eq. (3a) $M_{Tip} = E/2L_b d(t_w^3/d_c^2) = 18793.6^{k-''}$

Eq. (3) $1/M''_{LTB} = 1/M_{Tip} + 1/M_{LTB} \longrightarrow M''_{LTB} = 649.7^{K-''}$

Eq. (4b) $\beta_x = -\left[(1/I_x)\left[(t_w/4)\left[(h_o-\bar{y})^4 - (\bar{y}-t_f)^4\right] - (\bar{y}-t_f/2)\right.\right.$

$\left.\left.[b_f^3 t_f/12 + b_f t_f(\bar{y} - t_f/2)^2]\right] + 2\bar{y} - t_f\right]$

$= -7.004$

Eq. (4a) $\gamma_m = (\beta_x/2C)\sqrt{EI_y/GJ} = -2.437$ (G=11600 ksi was used)

Eq. (4) $M_{Tee} = (\pi/2C)\sqrt{EI_y GJ}\ (\sqrt{1 + (\pi\gamma m/2)^2} + \pi\gamma m/2)$

Eq. (5) $M'_{Tee} = M_{Tee}\ (1-1.5\ d_c/d) = 44.06^{k-''}$

Therefore $\dfrac{1}{(M''_{LTB})^2} + \dfrac{1}{(L_b/c\ M'_{Tee})^2} + \dfrac{1}{M_{cr}^2}$

$\longrightarrow M_{cr} = 352.5^{k-''}$

$\therefore\ P_{cr} = (223.2/108.9).(M_{cr}/114.3) = \boxed{6.32^{kips}}$

Illustrative Example 2

Bottom (Tension) Flange Coped Beam--same coping details, span length and section properties as Illustrative Example 1 except the copes are in the bottom flange.

$L_b = 114.3"$, $C = 12"$, $d_c = 3.16"$

From Example 1 $\longrightarrow$ $M_{LTB} = 673^{k-"}$

10% reduction $\longrightarrow$ $M_{cr} = 0.9\ M_{LTB} = 606^{k-"}$

$$P_{cr} = \frac{223.2}{108.9} \cdot \frac{M_{cr}}{114.3} = \boxed{10.9\ \text{kips}}$$

Illustrative Example 3

Double Flange Coped Beam--same coping details, span length and section properties as Test LTB3 except the copes are in both flanges as shown below.

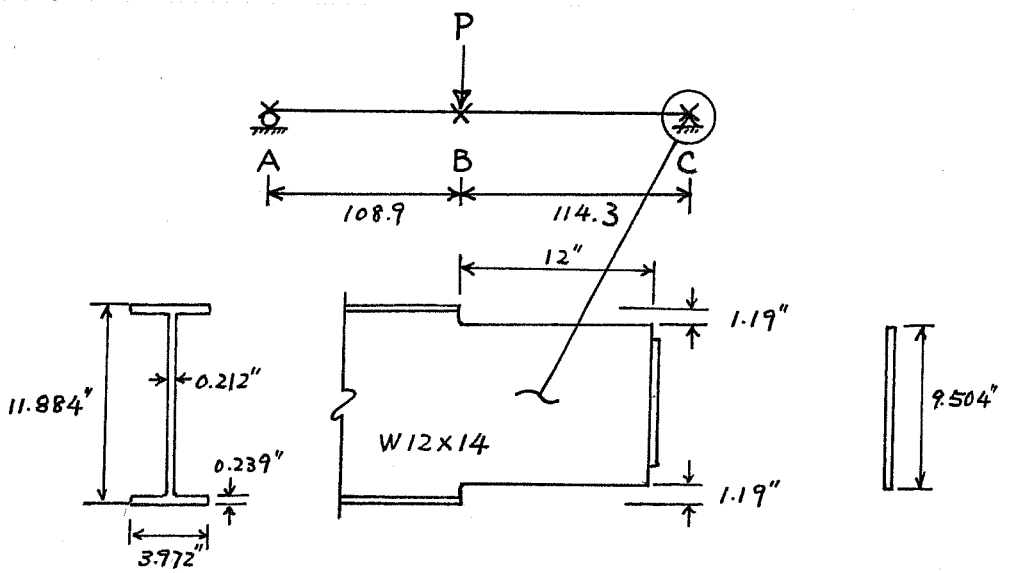

$A = 4.317\ in^2$

$I_x = 90.6\ in^4$

$I_y = 2.51\ in^4$

$J = 0.072\ in^4$

$C_w = 84.6\ in^6$

$A = 2.015\ in^2$

$I_x = 15.17\ in^4$

$I_y = 0.0075\ in^4$

$J = 0.03\ in^4$

Critical span $\overline{BC}$, cope at one end of unbraced span only.

Eq. (1) $M_{LTB} = 673^{k-''}$ (same as previous two examples)

Eq. (6) $M_{Rec} = \left(\frac{\pi}{2c}\right) \sqrt{EI_y GJ} = 36.2^{k-''}$

$$\frac{1}{(M_{LTB})^2} + \frac{1}{\left(\frac{L_b}{c} M_{Rec}\right)^2} = \frac{1}{M_{cr}^2}$$

$$\longrightarrow M_{cr} = 306.9^{k-''}$$

$$P_{cr} = \frac{223.2}{108.9} \cdot \frac{M_{cr}}{114.3} = \boxed{5.50^{kips}}$$

7.4 Future Research

Further research should be conducted on the lateral-torsional buckling of coped beams for the following conditions:

1. Study the buckling capacity of tee sections and rectangular sections which include the effects of moment gradient, coped depth and load position.
2. Investigate the moment-rotation characteristics of other types of connections and study their effects on lateral buckling capacity of the coped beams.
3. Investigate the effects of adjacent restraining span. Test results show that adjacent restraining spans will increase the buckling capacity of coped beams significantly, especially when copes are long and deep.
4. Study the post-buckling behavior of coped beams.
5. Extend the investigation to inelastic buckling of coped beams, especially when the load point is not braced.
6. Investigate the effectiveness of the connection clip angles in reinforcing the web, especially for the rolled sections.
7. Some experimental studies to verify the recommended reinforcement details for improving the lateral-torsional buckling capacity of coped beams are necessary. Also, a few experiments should be used to check the theoretical buckling solutions of double coped and bottom coped beams.

Part II

LOCAL WEB BUCKLING

CHAPTER 8

TOP FLANGE COPED BEAMS

In Section 1.2, some discrepancies between actual behavior and current practice related to local web buckling of coped beams were discussed. The purpose of the following chapters is to investigate the web buckling behavior of beams with different coping details and to develop reasonable and conservative design models and recommendations.

8.1 Analysis Program

The computer program BASP as described in Sectin 2.1 was used to determine elastic web buckling loads. For inelastic buckling, a plastic bifurcation buckling analysis was used. The procedure for determining the buckling load is as follows. At some trial loading, the stress state is calculated and bending stiffness $[K_B]$ and geometric stiffness $[K_G]$ are computed based on these stresses. The eigenvalue equation $[K_B]\{\Delta\} = -[K_G]\{\Delta\}$ is then solved and the lowest eigenvalue obtained. If $\lambda = 1$, the trial loading is the critical one. If the λ is greater (less) than one, the trail loading is less (greater) than the buckling load. Thus, the load is incremented or decremented and the procedure is repeated until $\lambda = 1$. The general computer program ABAQUS written by Hibbit and Karlsson, Inc. [14] was used to compute the in-plane stresses by using tri-linear

isotropic material properties [20] as shown in Fig. 8.1(a) and the bi-linear material properties [21] as shown in Fig. 8.1(b) was used in the bifurcation buckling analysis. The value of tangent modulus, E_T =500 ksi, was estimated from the tensile coupon tests discussed in Chapter 10.

8.2 Scope and Simplified Computer Model

The local web buckling of coped beams in which the compression flange is braced laterally was considered in this study. Bracing systems other than a continuously braced compression flange were not considered in developing design provisions. However, a brief discussion of other bracing systems can be found in Chapter 11. In addition, only top (compression) and double flange coped beams were studied since bottom (tension) flange coped beams could not have local web buckling if no end moment is presented.

For practical purposes, only beams with a coped length less than twice the beam depth ($c \leq 2d$) and with a coped depth less than one-half the beam depth ($d_c \leq d/2$) (for double coped beams, $d_c \leq d/5$) will be considered. These same limitations were used in the lateral buckling study presented previously. End restraints of the connection are not included in the design model in order to obtain conservative results. However, the effects of end restraint are discussed in Chapter 11.

The simplified web-buckling model shown in Fig. 8.2 consisting of a short piece of the end of a beam in which the compres-

(a) Stress-Strain Curve for In-plane Analysis

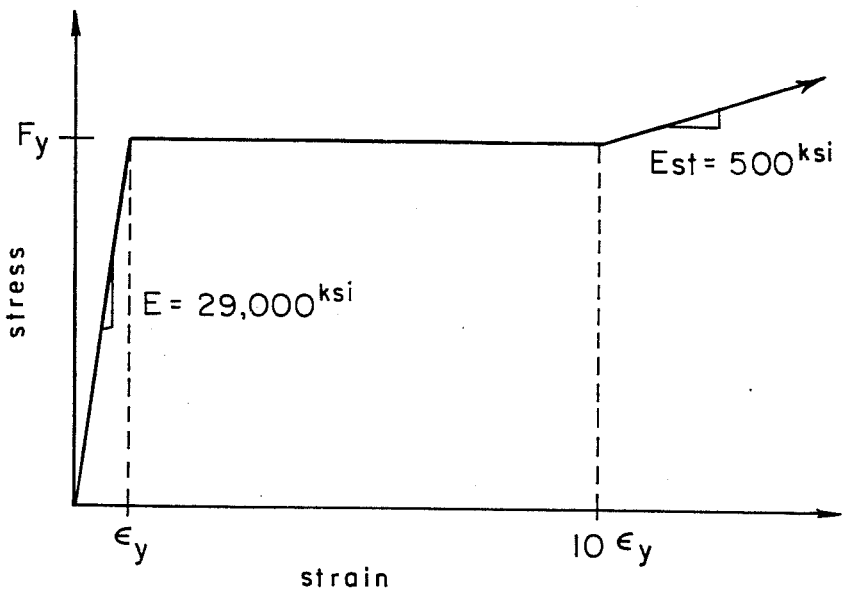

(b) Stress-Strain Curve for Buckling Analysis

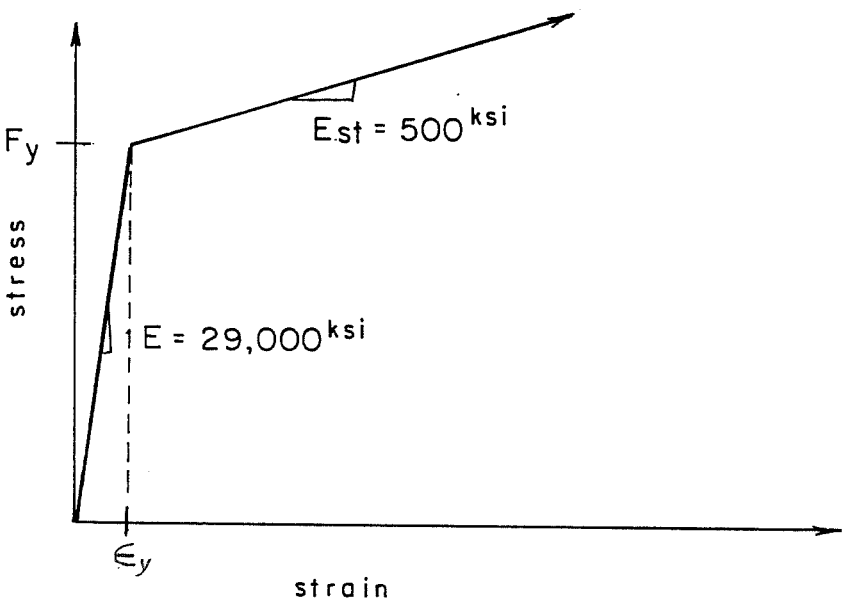

Fig. 8.1 Stress-Strain Curves of the Material

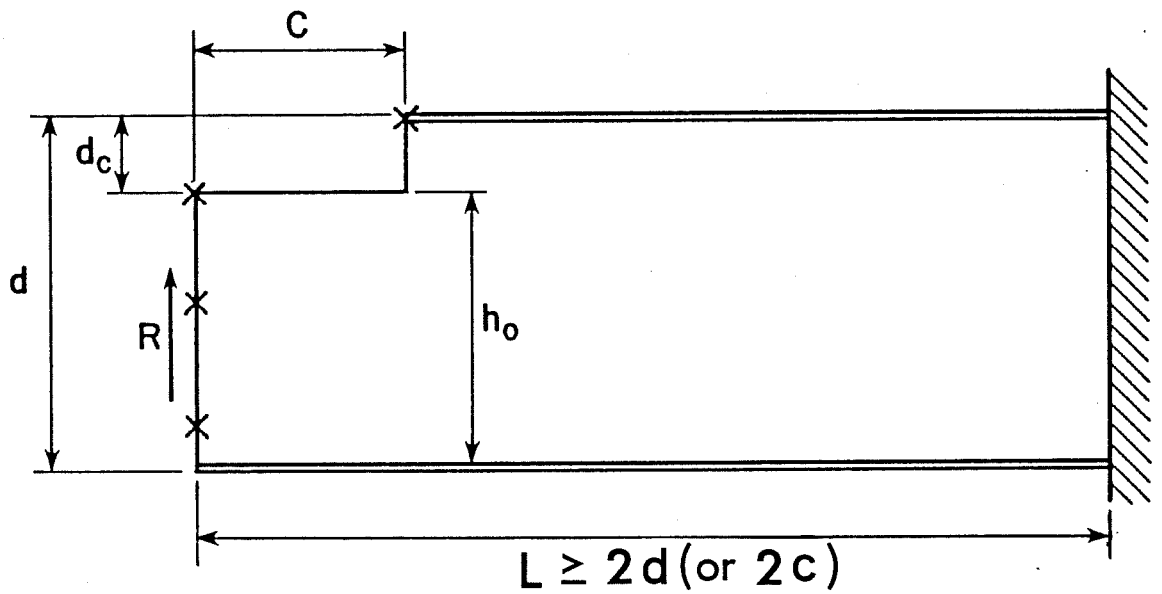

Fig. 8.2 Simplified Local Web Buckling Model

sion flange was not permitted to move laterally (flange braced at the cope) was used throughout this study. The grid used in the finite element model varied from problem to problem, depending on the cope detail and beam size, so computational effort could be accurate yet economical. For a particular problem, the element grid was refined keeping the element aspect ratio constant. The difference in buckling loads was negligible. Some preliminary analysis showed that this simplified model (Fig. 8.2) in which $L \geq 2d$ or $2c$, whichever is larger, gives a very good approximation for local buckling of full length beams while greatly reducing the computational effort. The difference between analysis on full length beams and the short computer model was about 2 ~ 5%.

8.3 Elastic Local Web Buckling Analysis

A W16x26 beam with a 1.5 in. cope depth and three cope lengths which varied between d/2 to 2d was analyzed to study the behavior of elastic local web buckling of top-flange coped beams. The buckled shapes and results of three different coped lengths are shown in Figs. 8.3 through 8.5 which provide many important structural characteristics. The cross-section buckled shape at the maximum lateral deflection positions in the coped region is also plotted in the figures. The approximate buckling lines and the buckling orientation are also shown in the figures.

Since the neutral axis of the cross section is very close to the bottom flange in the coped region, the cross section deflection

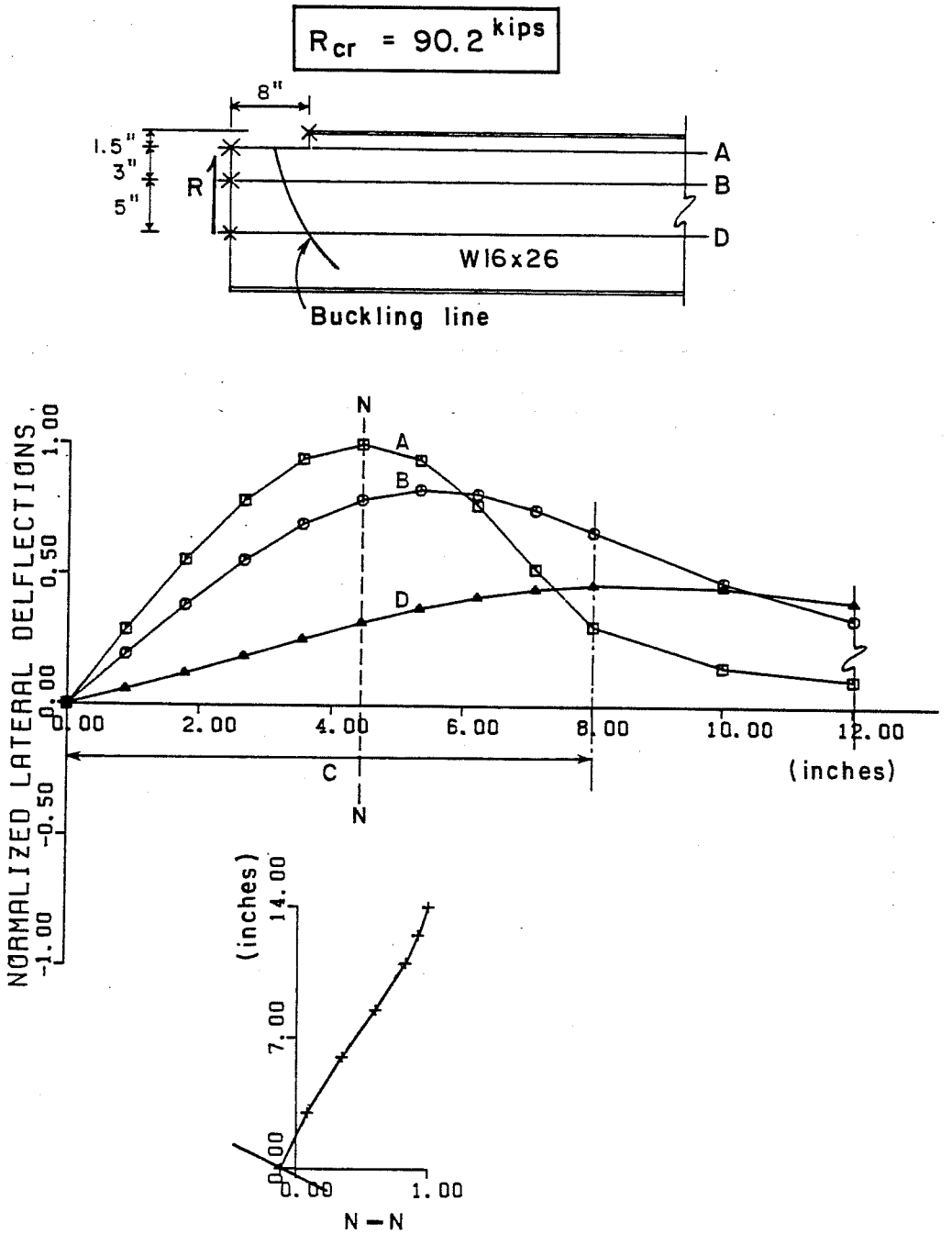

Fig. 8.3 Buckled Shapes - Case 1 with c = 8in.

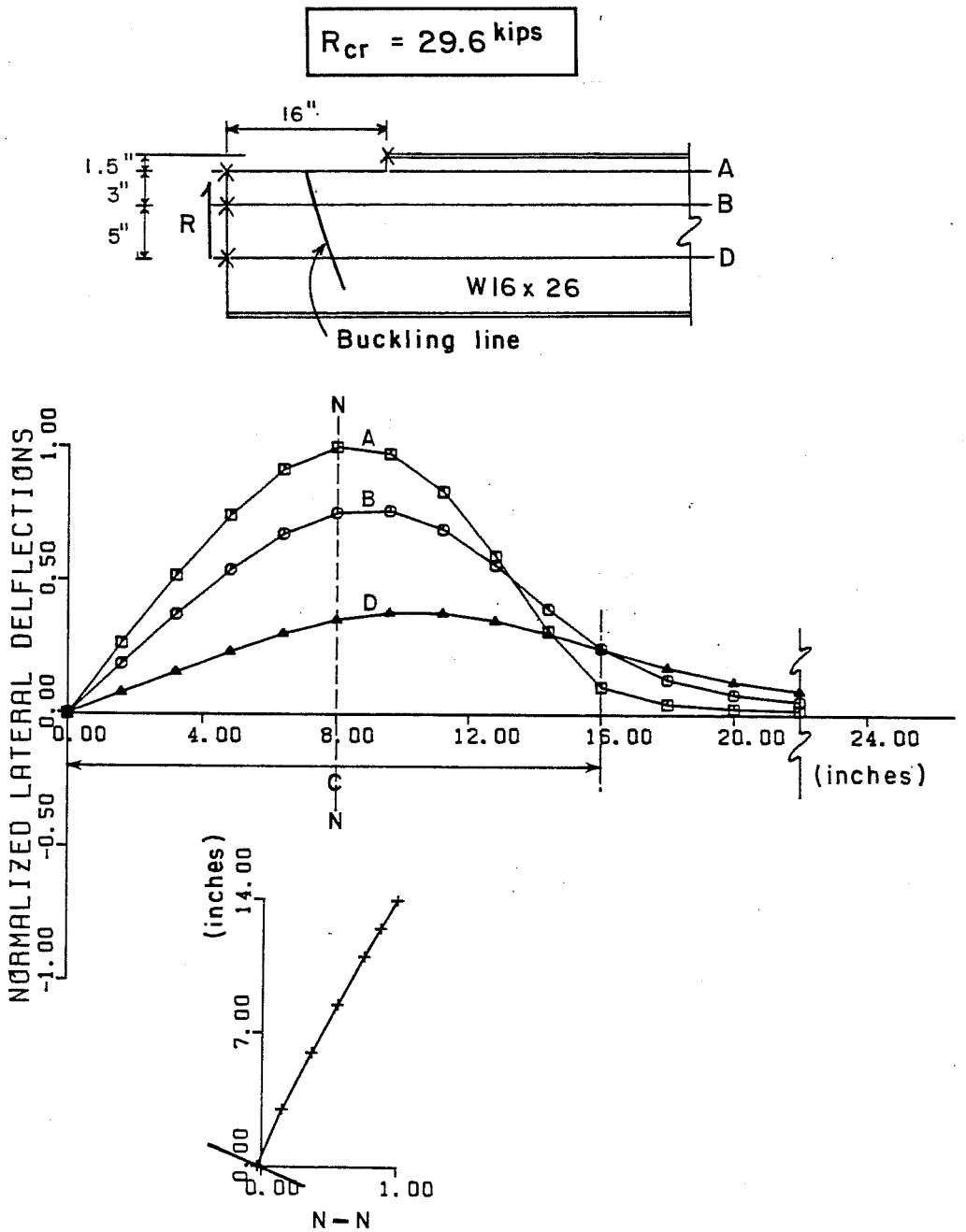

Fig. 8.4 Buckled Shapes - Case 2 with c = 16in.

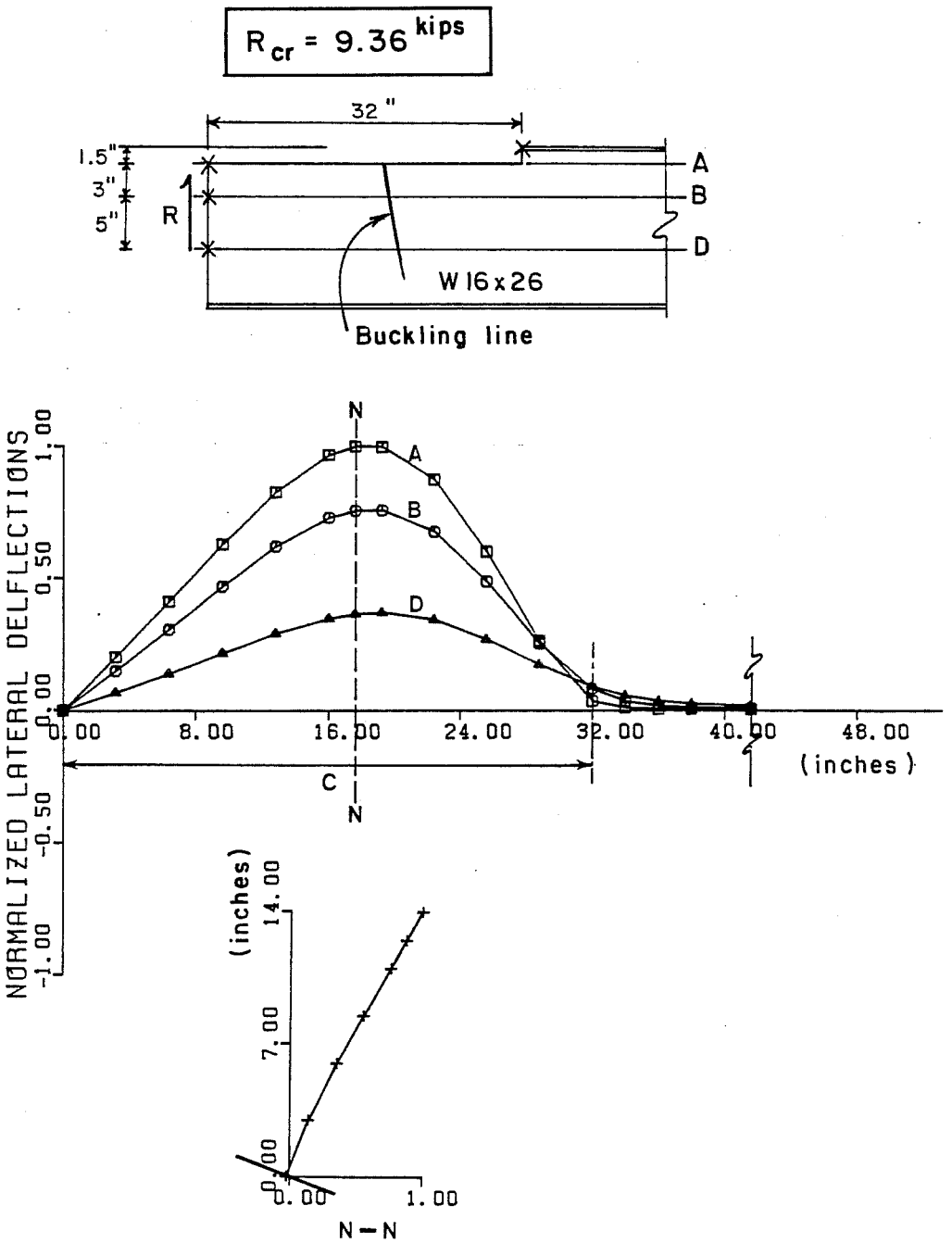

Fig. 8.5 Buckled Shapes - Case 3 with c = 32in.

shapes in Figs. 8.3 through 8.5 show very little lateral movement but signficant twist near the bottom flange. This suggests that a plate buckling model in which the top edge is free and simple supports are assumed at the bottom flange, the end of the beam and a vertical line at the end of the cope as shown in Fig. 8.6 might accurately predict the buckling load. A triangular load distribution is used at the right end to approximate the bending stress distribution as shown in Fig. 8.6. At the node points, bending stresses were input to provide a linear distribution of stress for a zero moment at the left end and the maximum moment at the right end. The bending stresses were applied as the input data to eliminate the possible effect of shear stresses. However, the buckled shape from the plate buckling model in Fig. 8.6 shows significant deviation from the shapes given in Figs. 8.3, 8.4 and 8.5, especially for small cope lengths. The critical end reactions based on the BASP solutions for beams with the three cope lengths and the simple plate buckling model are given in Table 8.1. The comparison shows the plate buckling model overestimates the buckling loads of short coped beams ($c < d$) and underestimates the buckling loads of beams with long cope ($c > d$). The discrepancies between the actual behavior of coped beams and the plate buckling model are discussed below.

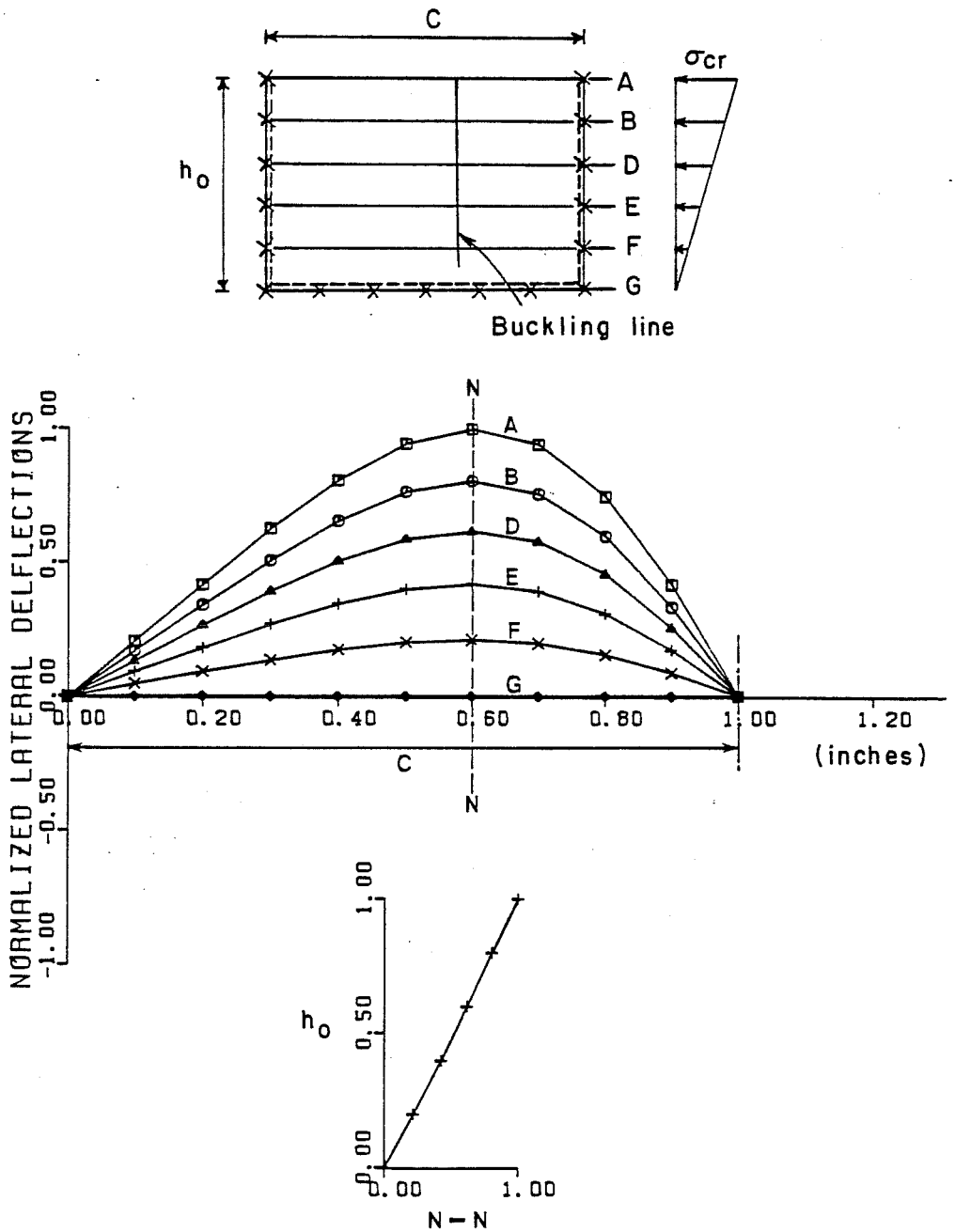

Fig. 8.6 Buckled Shapes of Plate Buckling Model

TABLE 8.1 Buckling Loads for Coped Beams and the Plate Model.

	Critical End Reactions (kips)		
	Cope Length (in.)		
	8	16	32
BASP	90.2k	29.6k	9.36k
Plate Model	142.9k	24.6k	6.16k

8.3.1 Effect of Stress Concentration. The bending stress distributions at the cope line of the three cases studied are plotted in Fig. 8.7 along with Mc/I calculated values. The two discontinuous Mc/I solutions shown for each case are caused by the different section properties on both sides of section A-A. The stress distributions in Fig. 8.7 were determined using a 1.5 in. x 1.6 in. finite element mesh size. The SCF at the cope, the BASP solution divided by the Mc/I solution using I of the coped section, gets smaller as the cope length increases. Also, as the cope length increases, the stress concentration effect is limited to a small length at the end of the cope. For the short cope length, Case 1, the actual stresses are significantly greater than the Mc/I stresses all along the cope length. Thus, the effect of stress concentration decreases if the cope length increases, not only due to the magnitude of SCF but also the extent of stress concentration.

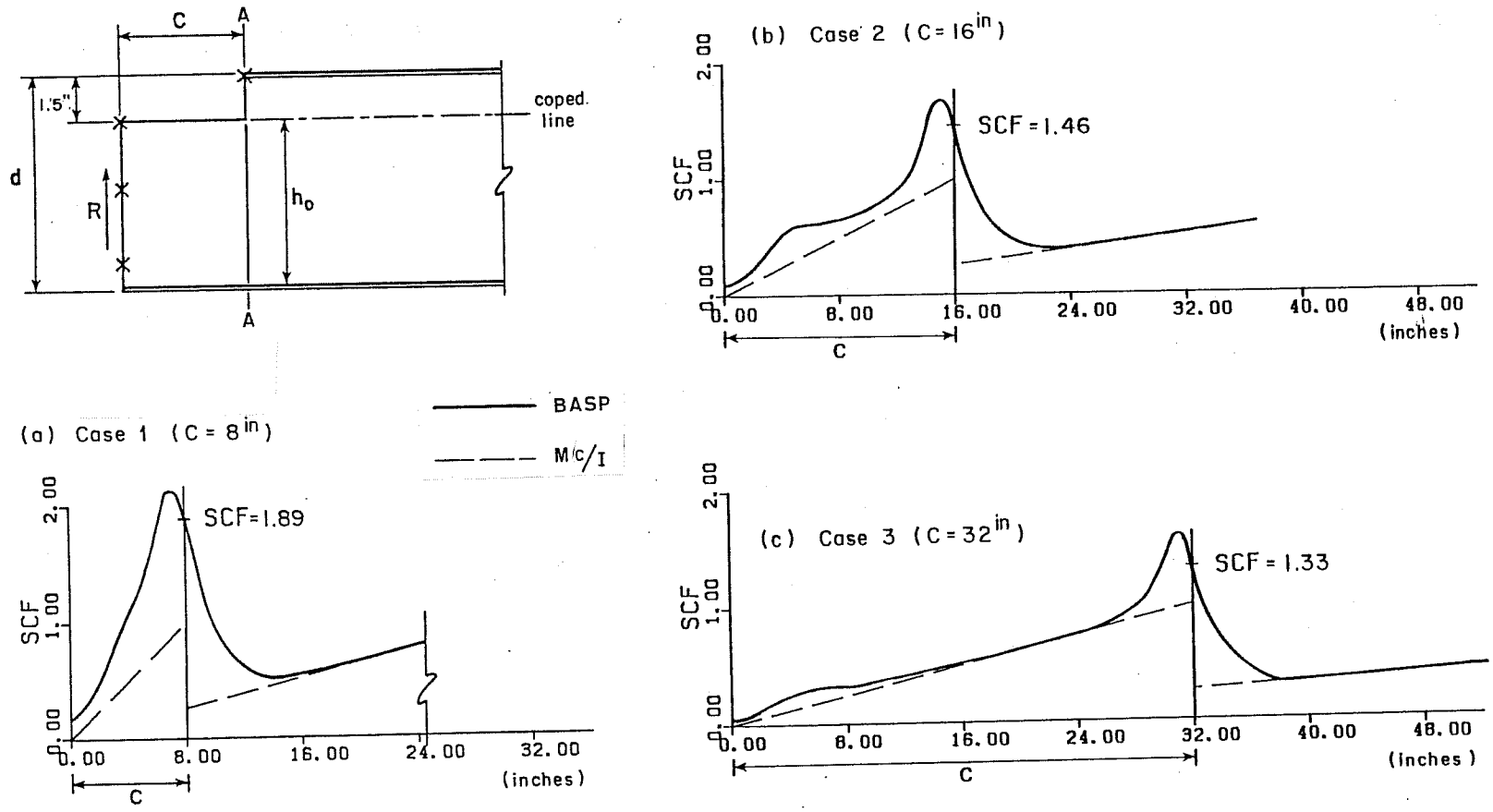

Fig. 8.7 Bending Stress Distributions at Coped Line for Top Flange Coped Beams

8.3.2 Effect of Shear Stress. Figure 1.2 shows that both bending stresses and shear stresses are high at the cope. Therefore, it may be unconservative to neglect the shear effect on local web buckling. If shear stresses dominate the buckling behavior, the buckle should be oriented at about a 45 degree angle from a vertical line. If bending stresses cause the web to buckle, the buckling line should be vertical. Since the buckling load decreases as the cope length increases, the effect of shear stresses on local web buckling should also decrease when cope length increases. This can be seen in Figs. 8.3 through 8.5 where the angle of the buckling line approach a vertical orientation as the coped length increases which implies a decreasing shear effect.

8.3.3 Effect of Cope Depth. Normalized buckled shapes at the top (cope line) for the three cases studied and free edge deflected shape of the plate model are plotted in Fig. 8.8. It shows that the shorter the cope length, the larger the lateral movement at the coped corner. This implies that cope depth will have a greater influence for the copes that are short. To study this influence, a simple model was examined as shown in Fig. 8.9 in which the coped corner is restrained laterally by a spring. The spring stiffness was established by assuming cantilever action of the web plate above the cope, d_c, with a plate length also chosen as d_c as shown in Fig. 8.9(b). The spring constant for a cope depth of 1.5 in. is 50 kip/in. for a web thickness of 0.25 in.

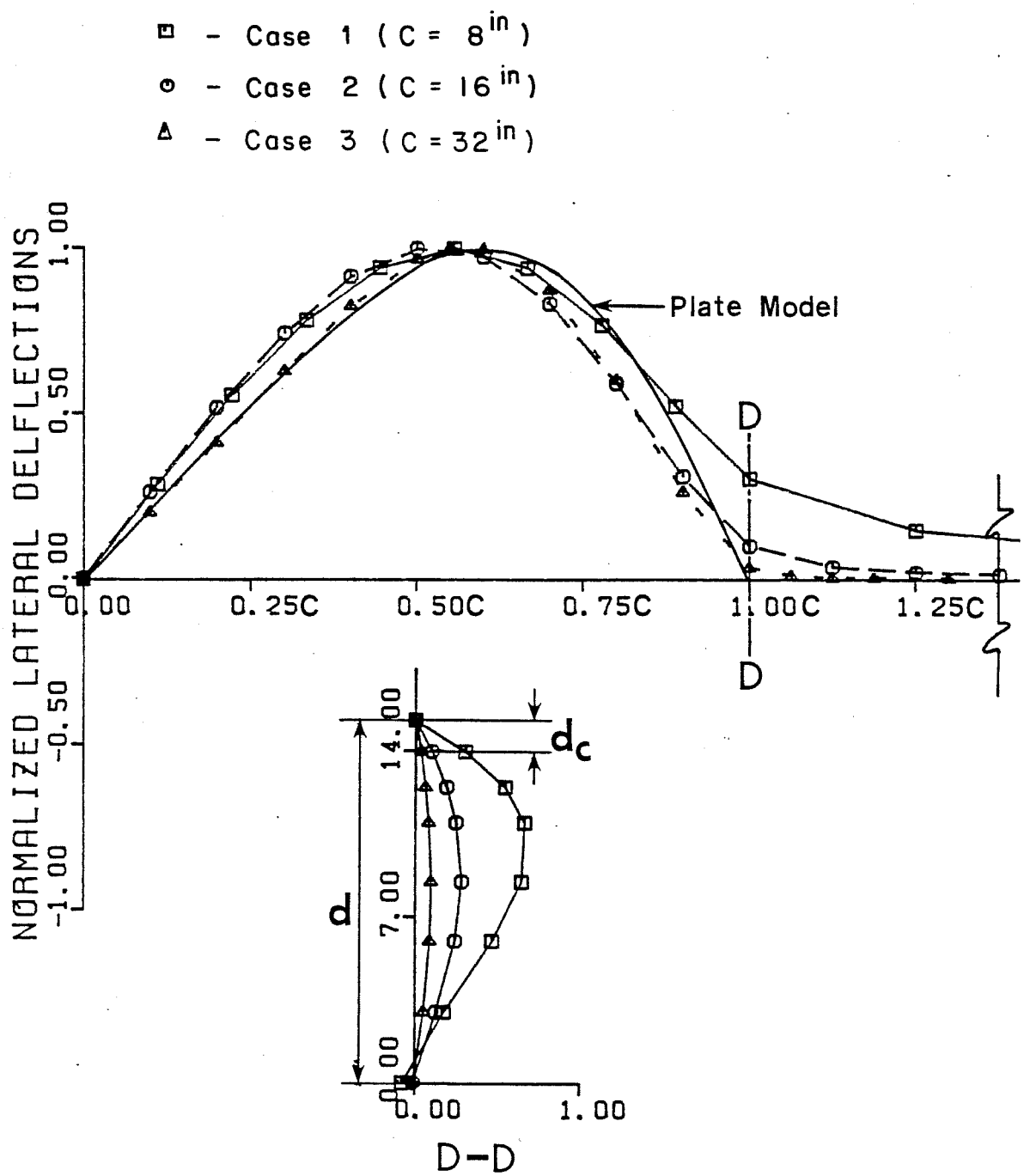

Fig. 8.8 Coped Line Buckled Shapes

(a) Actual Beam

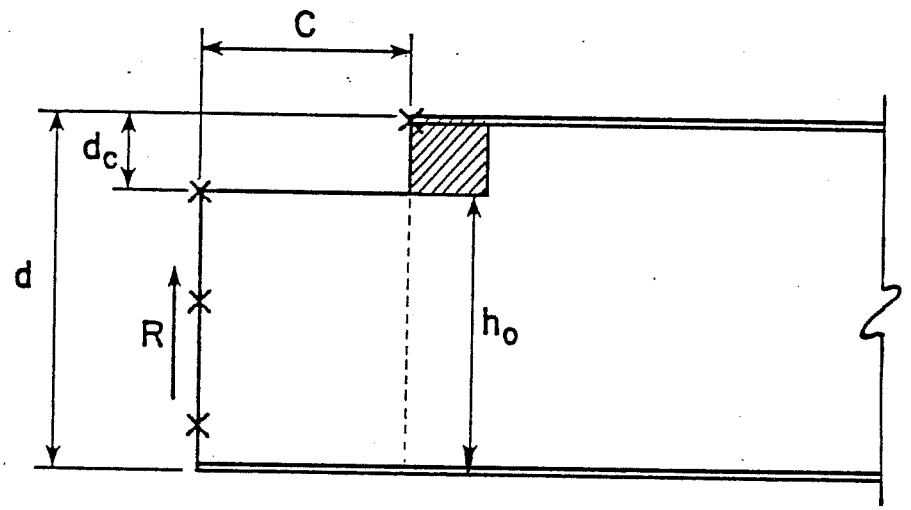

(b) Lateral Restraint Model

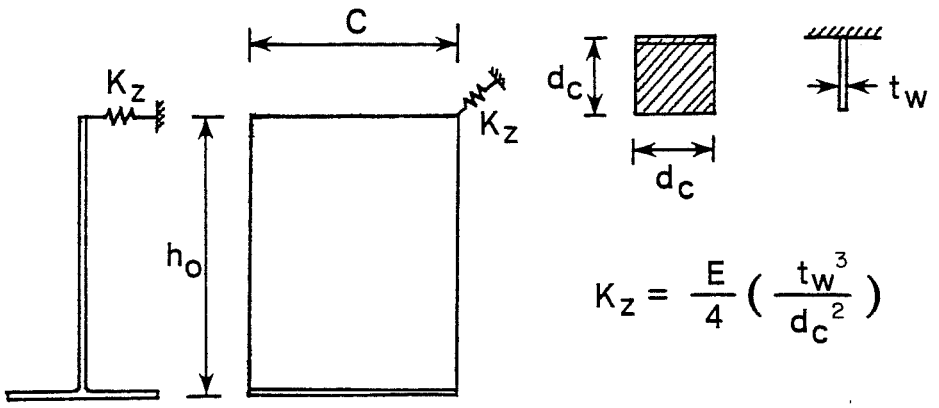

Fig. 8.9 Lateral Restraint Model of Cope Depth

The plate model was analyzed to study the effect of cope depth and the results are shown in Fig. 8.10. The reduction in buckling load due to increases in cope depth is greater for short cope lengths (c/h_o = 1.0) than for long cope lengths (c/h_o = 2.0). In either case, however, the effect of cope depth does not appear to be very significant since changing dc from 1.5 in. to 7.5 in. (almost d/2) in the W16x26 section results in a reduction of 4 percent for c/h_o = 2.0 and 17 percent for c/h_o = 1.0.

8.3.4 Effect of Rotational Restraint. The buckled shapes at section D-D in Fig. 8.8 show that there is some rotational restraint of the uncoped region which will increase the buckling capacity of the plate model. A simple plate model as shown in Fig. 8.11, in which the line A-A is restrained out-of-plane by uniform rotational springs, was used to study the effect of rotational restraint. When the rotational restraint $K_\phi = \infty$ (fixed out-of-plane rotational restraint), the buckling loads of the short plate show a larger relative increase than the long plate (1.76 vs. 2.48 for the short and long, respectively). However, when K_ϕ is small (say < 50 k-in./rad./in.), the relative differences between buckling loads for various plate lengths are small. Since the rotational restraint depends upon the thickness of the web and the magnitude of the cope depth, the buckling shapes in Fig. 8.8 show that the rotational restraints are small for coped beams. Besides, a uniform rotational restraint and fixed lateral movement at the line A-A are conservative assumptions. Therefore, as shown in Fig. 8.11, the effect of

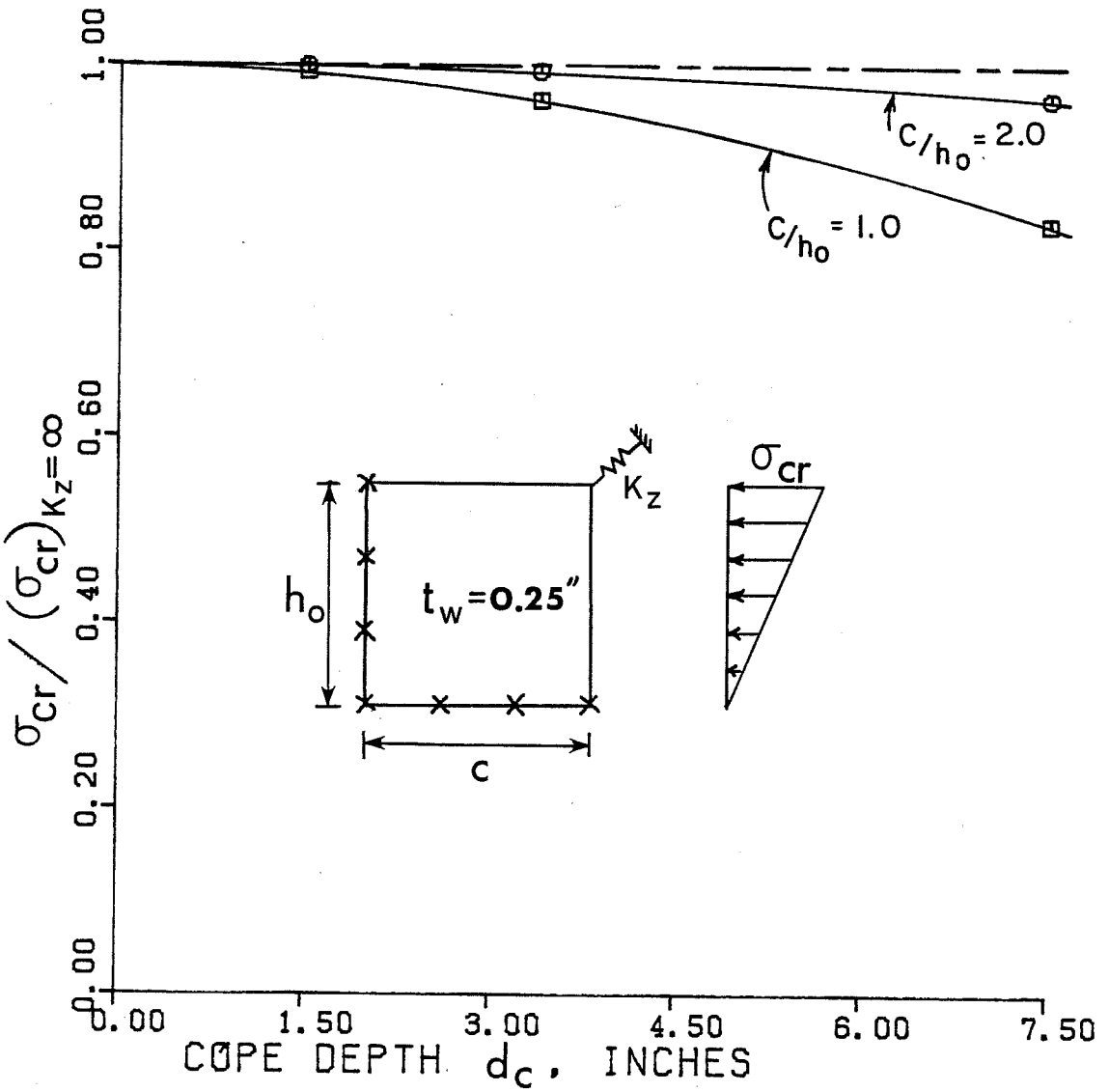

Fig. 8.10 Effect of Lateral Restraint

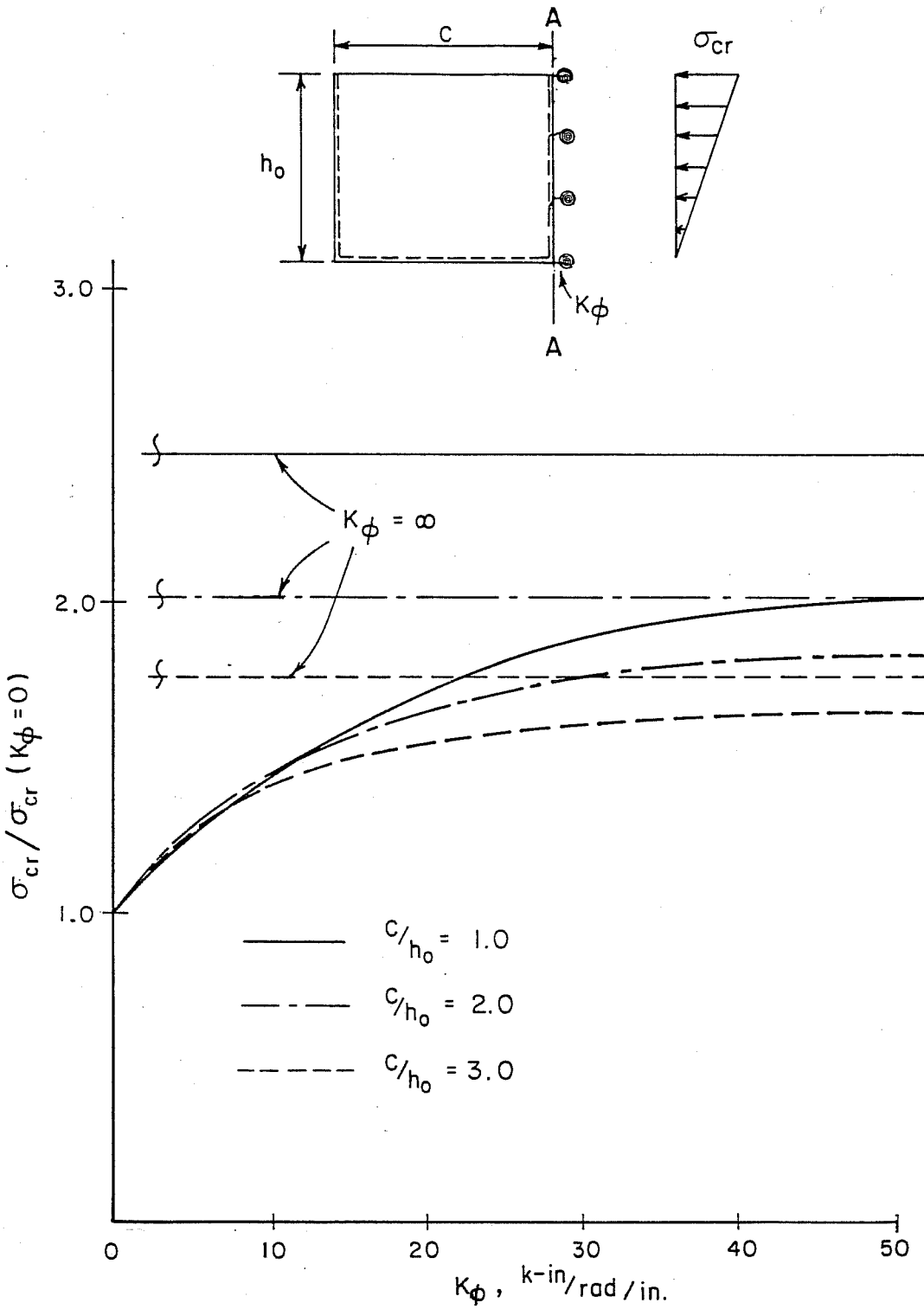

Fig. 8.11 Effect of Out-of-plane Rotational Restraint

rotational restraint on buckling of coped beams is not as much as shown by the plate model and the relative increase in buckling load for the coped beams with various coped lengths is similar when K_ϕ is small.

The discussion above shows that the SCF, shear and cope depth will decrease the buckling capacity of coped beams, especially when cope length is short, and the rotational restraint will increase the buckling capacity. This explains why the simple plate model in Fig. 8.5 will predict higher buckling loads than the actual buckling loads for short coped beams and lower loads for long copes. Modification of the plate model will be made according to a parametric study undertaken in Section 8.5.

8.4 Inelastic Local Web Buckling Analysis

The elastic bending stress distribution discussed in Section 8.3.1 (Fig. 8.7) shows a high stress concentration factor at the coped region for top flange coped beams. The high stresses cause localized yielding at the coped region which will reduce the stiffness of the web and force the beams to buckle in the inelastic range as discussed in Chapter 1. The purpose of this section is to determine whether localized yielding at the coped region will affect the beam capacity. Before failure can occur by inelastic buckling, the maximum Mc/I stress calculation in the coped region may reach the yield strength which is also a structural limit for design.

A W10x22 section with c = 9 in., d_c = 1.5 in., and F_y = 50 ksi (Fig. 8.12) was analyzed for in-plane stresses using the ABAQUS program and an eigenvalue analysis as described in Sectio 8.1 was then performed . For this problem, the critical end reaction was found to be 30.0 kips. The elastic critical load for this same problem is 94.1 kips indicating a 68 percent reduction in buckling capacity due to inelastic action. The in-plane plastic stress distributions are given in Fig. 8.12 for the critical buckling load of 30 kips. Yielding spreads from the top of the cope to a distance 0.13d below the top. Strain hardening develops at the corner which gives a maximum stress of 51 ksi. The elastic stress distributions, Mc/I and $V/h_o t_w$ values with 30 kips load, are also shown in the figure. The localized yielding at the coped region reduces the stress concentration and forces the actual stress distribution closer to the Mc/I and $V/h_o t_w$ calculations in the coped region. The plastic shear stress distribution at line A is different from VQ/It distribution but similar to average shear stress distribution ($V/h_o t_w$) except at the top of the cope. The discontinuity at the coped corner region produces high bending and shear stresses which causes localized yield as shown by the shaded zone in Fig. 8.13. As yielding spreads, the beam fails in inelastic local web buckling at R = 30 kips. The buckled shape shows that the maximum displacement occurs much closer to the cope corner than that developed for elastic buckling (see Fig. 8.3).

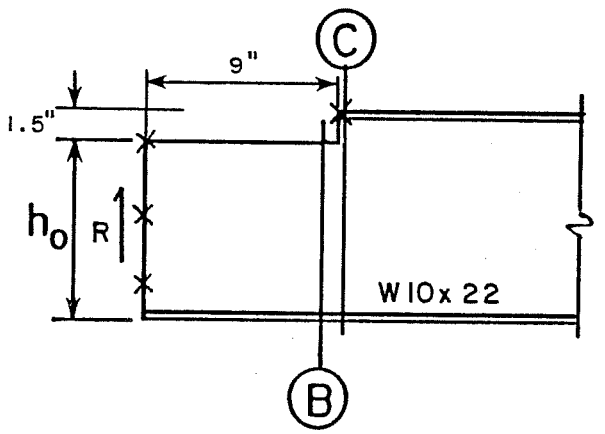

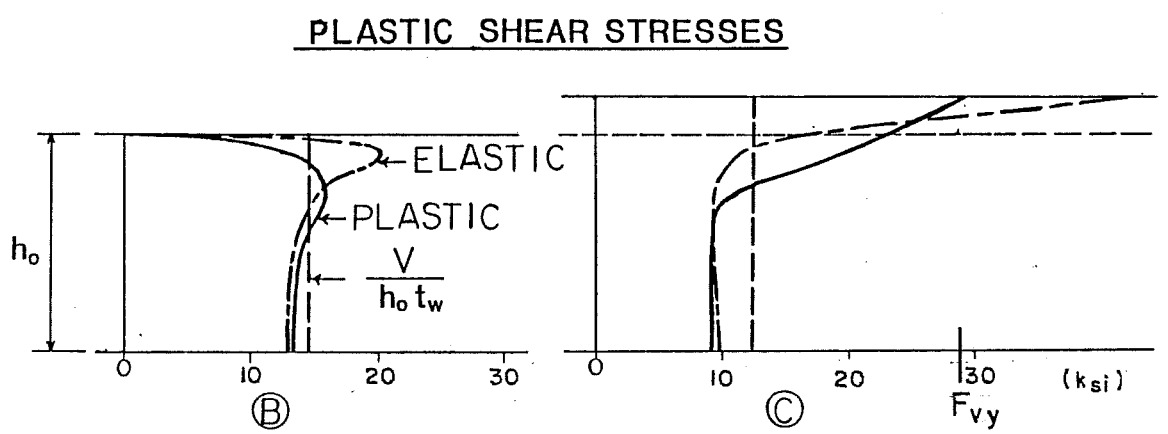

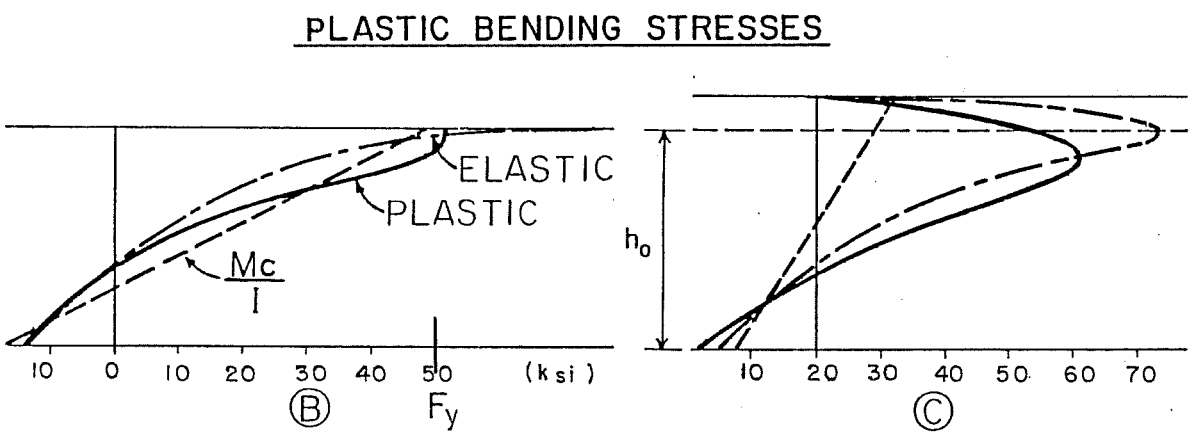

Fig. 8.12 Plastic Stress Distributions at Coped Region

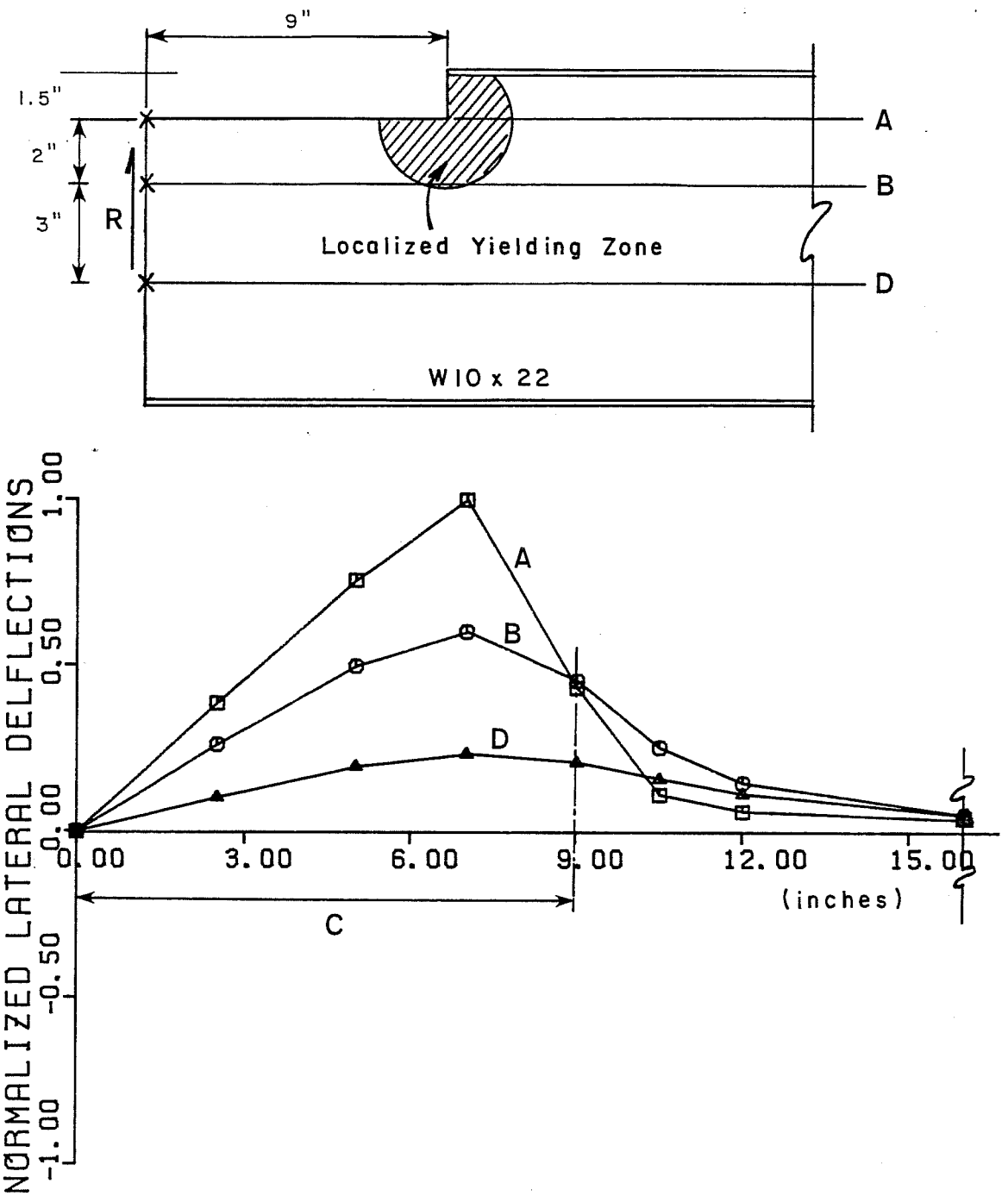

Fig. 8.13 Buckled Shape of Inelastic Local Web Buckling

It is common practice to check for yielding in bending and shear in the coped region neglecting stress concentrations. For this problem, the Mc/I stress will reach the yielding stress when the reaction is 26.7 kips. Since this load is less than the inelastic web buckling load, yielding controls. By studying other cases it was found that the yield load using Mc/I and $V/h_o t_w$ to calculate stresses always provided a lower bound when compared to the inelastic web buckling solutions. Therefore, for design, checking yielding will give a lower bound to the inelastic local web buckling solutions.

8.5 Proposed Design Recommendations

The objective of this research project was to develop relatively simple, conservative design procedures to handle buckling in coped regions. It is apparent from the discussion in the previous sections that the problem is very complex and the number of variables that affect the buckling strength is quite large. Closed form solutions did not appear practical so it was decided to try using a classical plate buckling solution which would be altered by factors representing the principal variables such as cope length and cope depth.

The basic plate model to be used in the design method is given in Fig. 8.14, the plate buckling coefficient k given by the solid line was obtained from the Japanese Column Research Council Handbook [22] and further expanded and checked by BASP solutions.

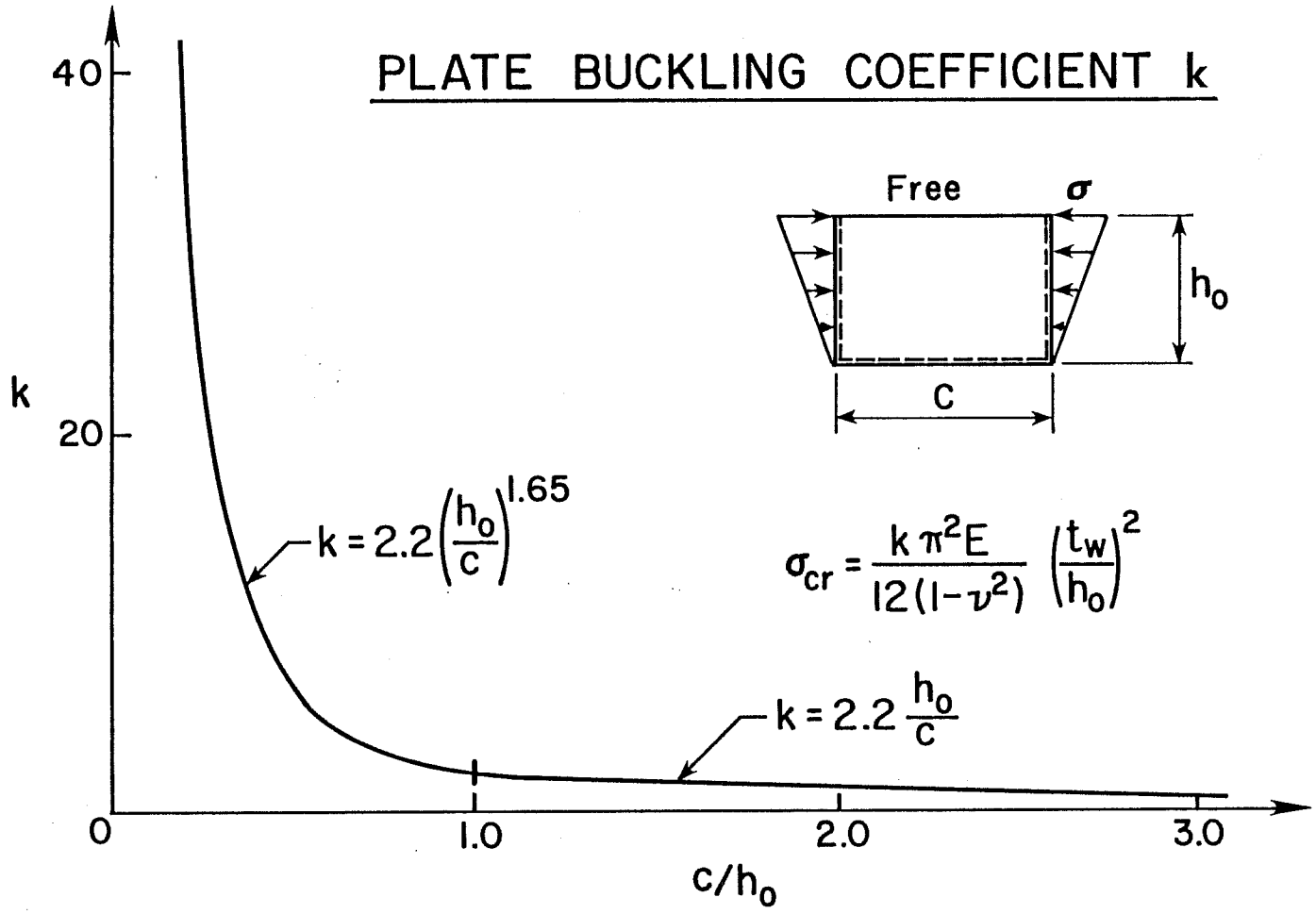

Fig. 8.14 Basic Designing Plate Model

Using curve fitting techniques the plate buckling coefficient can be given by

$$k = 2.2\,(h_o/c)^{1.65} \quad \text{for } c/h_o \leq 1.0$$

$$\text{or} \qquad k = 2.2\,(h_o/c) \quad \text{for } c/h_o \geq 1.0 \tag{8.1}$$

The solution in Fig. 8.14 does not consider important variables such as stress concentration, shear stress, cope depth, and moment variation from the beam end to the end of the cope. It was found that all these factors could be considered by a single adjustment factor, f, to the basic solution as shown below.

$$F_{cr} = k\,\frac{\pi^2 E}{12(1-\nu^2)}\,(t_w/h_o)^2 f \tag{8.2}$$

but not more than F_y, where k is given by Eq. (8.1) and f is defined by

$$f = 2\,c/d \quad \text{for } c/d \leq 1.0$$

$$f = 1 + c/d \quad \text{for } c/d \geq 1.0 \tag{8.3}$$

For a satisfactory design, the maximum Mc/I stress in the coped region must be less than the buckling stress given by Eq. (8.2). Further discussion of the development of the f factor is given below.

The calculated top fiber bending stress varies linearly from zero at the end of the beam to a maximum at the cope corner as shown in Fig. 8.15. This problem was solved and the critical stress, σ_{cr2}, was compared with results given in Fig. 8.14, σ_{cr}. The ratio

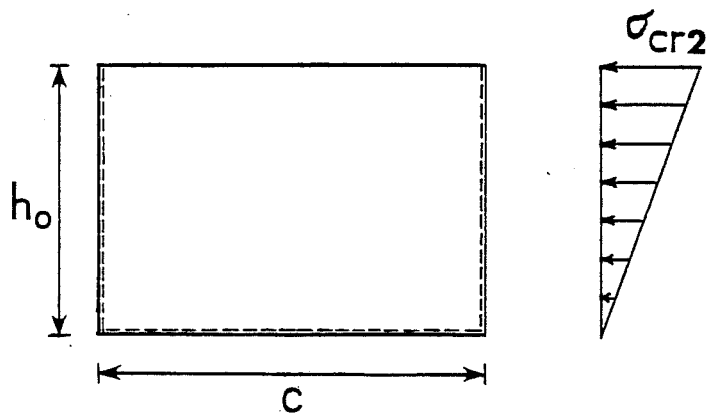

c/h_o	1.0	2.0	3.0
σ_{cr2}/σ_{cr}	1.96	2.01	1.97

Fig. 8.15 Effect of Moment Variation

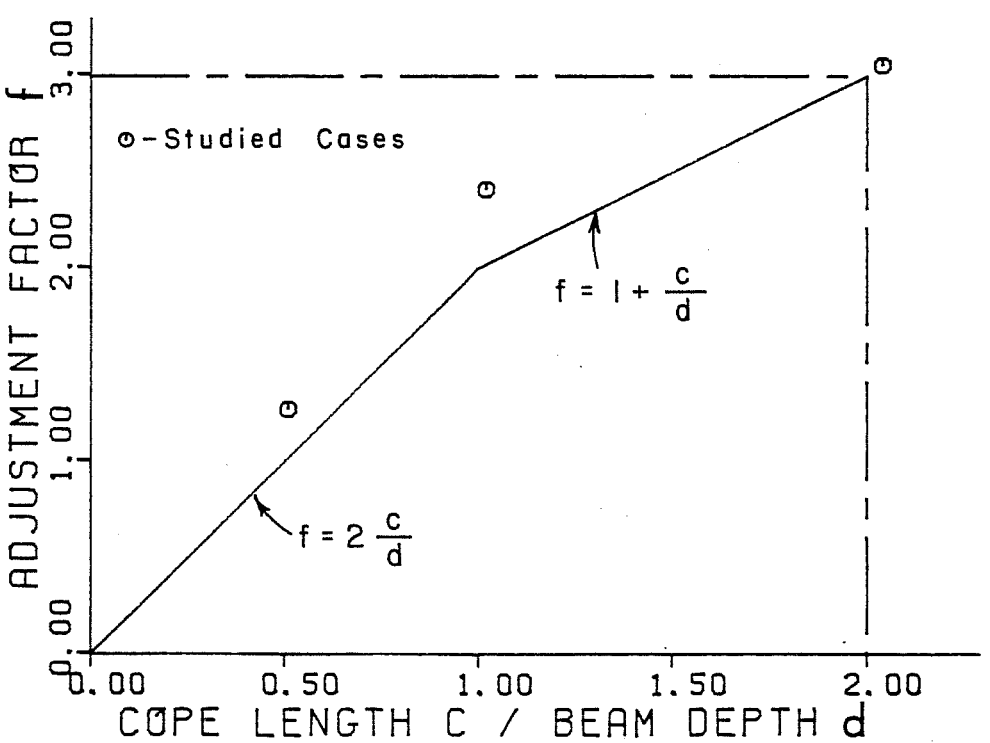

Fig. 8.16 Adjustment Factor f

σ_{cr2}/σ_{cr} given in Fig. 8.15 was found to be almost a constant of 2.0 for the three different aspect ratios, c/h_o, of 1.0, 2.0 and 3.0 considered. Thus, the moment gradient could be handled directly by changing the coefficient 2.2 in Eq. (8.1) to 4.4. However, since the moment gradient effect was found to be a constant, it was decided to include it in the f factor.

The value for f given in Eq. (8.3) was developed from the solutions to the three basic cases given in Section 8.3 The BASP results from these three cases were equated to Eq. (8.2), the value of f was calculated and the results plotted in Fig. 8.16 by the open circles as a function of c/d. A conservative bilinear expression for f given by Eq. (8.3) was fit to these results. A conservative approximation was used for $c/d < 2.0$ to account for the reduction that could occur because of cope depth. Recall that in Section 8.3, Fig. 8.9, reduction up to approximately 20 percent might be expected if cope depths approached d/2.

To check the reliability of Eqs. (8.2) and (8.3), BASP solutions were developed for the cases shown in Figs. 8.17 and 8.18 and the results compared to the design recommendations. In Fig. 8.17, cope length is varied for two different web thicknesses, 0.25 in. and 0.10 in., and a 1.5 in. deep cope for a W shape with the same flange and beam depth as a W16x26 section. The results indicate that the design recommendations are conservative for d/t_w ratios between 62.8 and 157.0. In Fig. 8.18, the cope depth is varied for the same two sections (t_w = 0.25 in. and 0.10 in.), with a constant cope

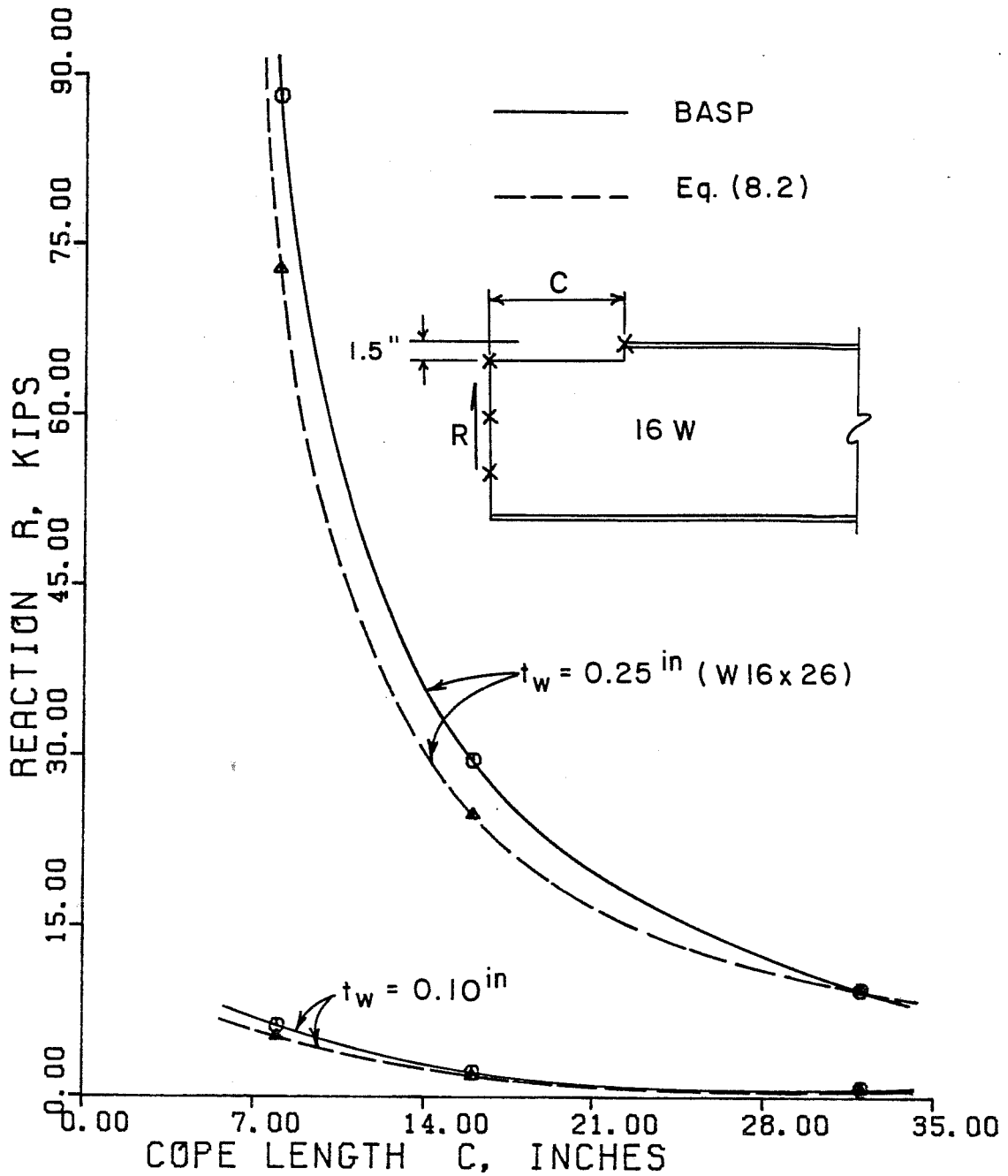

Fig. 8.17 Parametric Studies - Variation of Cope Length

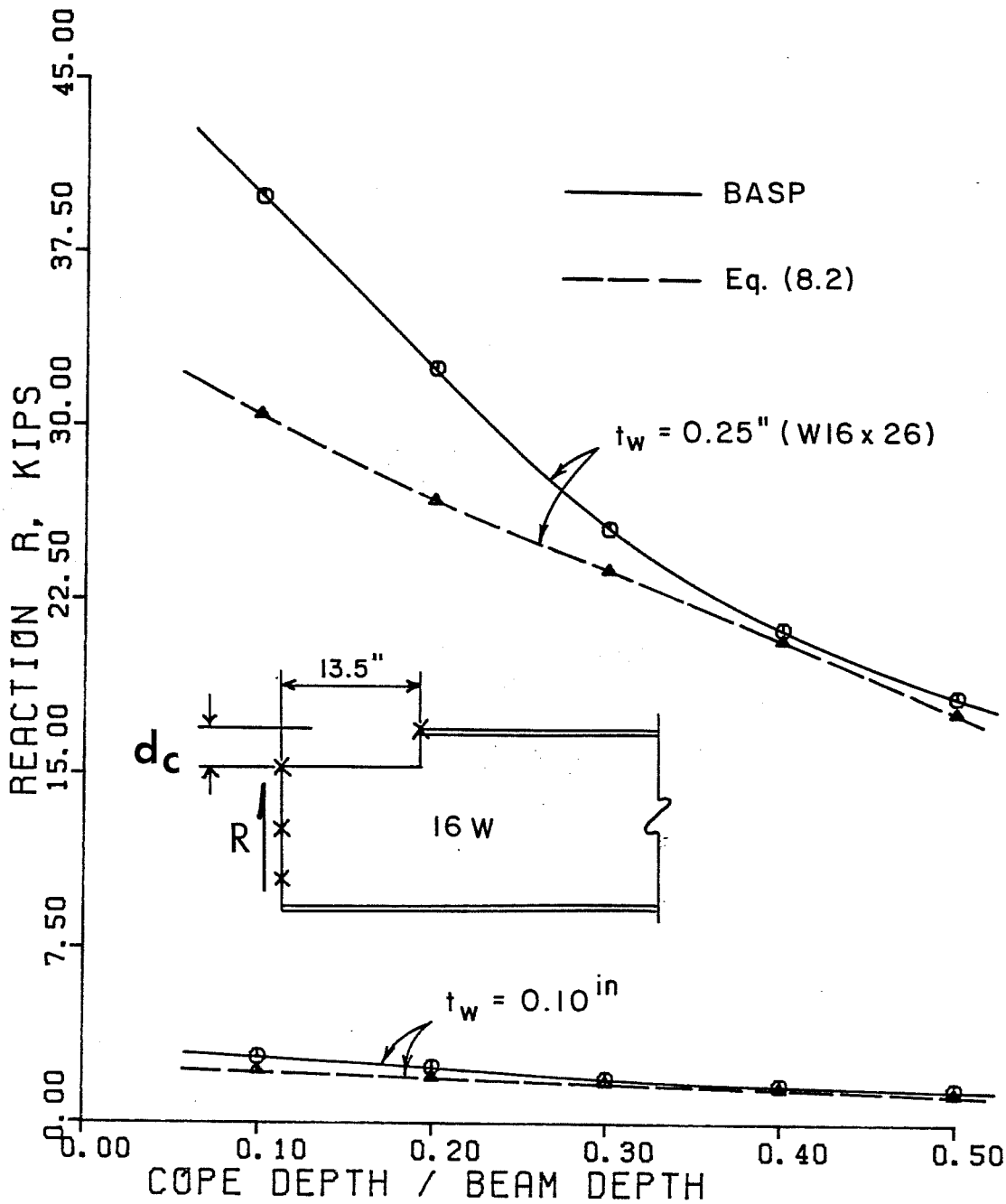

Fig. 8.18 Parametric Studies - Variation of Cope Depth

length of 13.5 in. The design equations are very close to the BASP results for deep copes (large d_c/d) but are about 20 percent conservative for shallow copes. Thus, for a wide range of parameters, the design recommendation gives results close to the theoretical buckling solutions generated by BASP.

In addition to the design buckling equations given by Eqs. (8.2) and (8.3), the maximum Mc/I and $V/h_o t_w$ stresses must also be compared to the yield stress which will be a lower bound to inelastic local web buckling. To give some indication when yielding controls the design, the results from Eq. (8.2) are plotted in Fig. 8.19 for different d/t_w ratios, various c/d and a $h_o = d$ (only the top flange missing). Since almost all rolled W sections have $d/t_w < 60$, the cope lengths must be greater than the depth of the section for steel with $F_y = 36$ ksi for buckling to occur before yielding. As the yield stress increases, the cope detail becomes more susceptible to web buckling. If d/t_w is less than 42 and $c/d < 2.0$, then buckling need not be checked; yielding will control. For built up sections like plate girders with thin webs, web buckling is much more likely to control for common cope lengths. For $d/t_w = 150$ and a cope length equal to 0.2d, the buckling stress will be less than $0.5 F_y$ for A36 steel ($F_y = 36$ ksi).

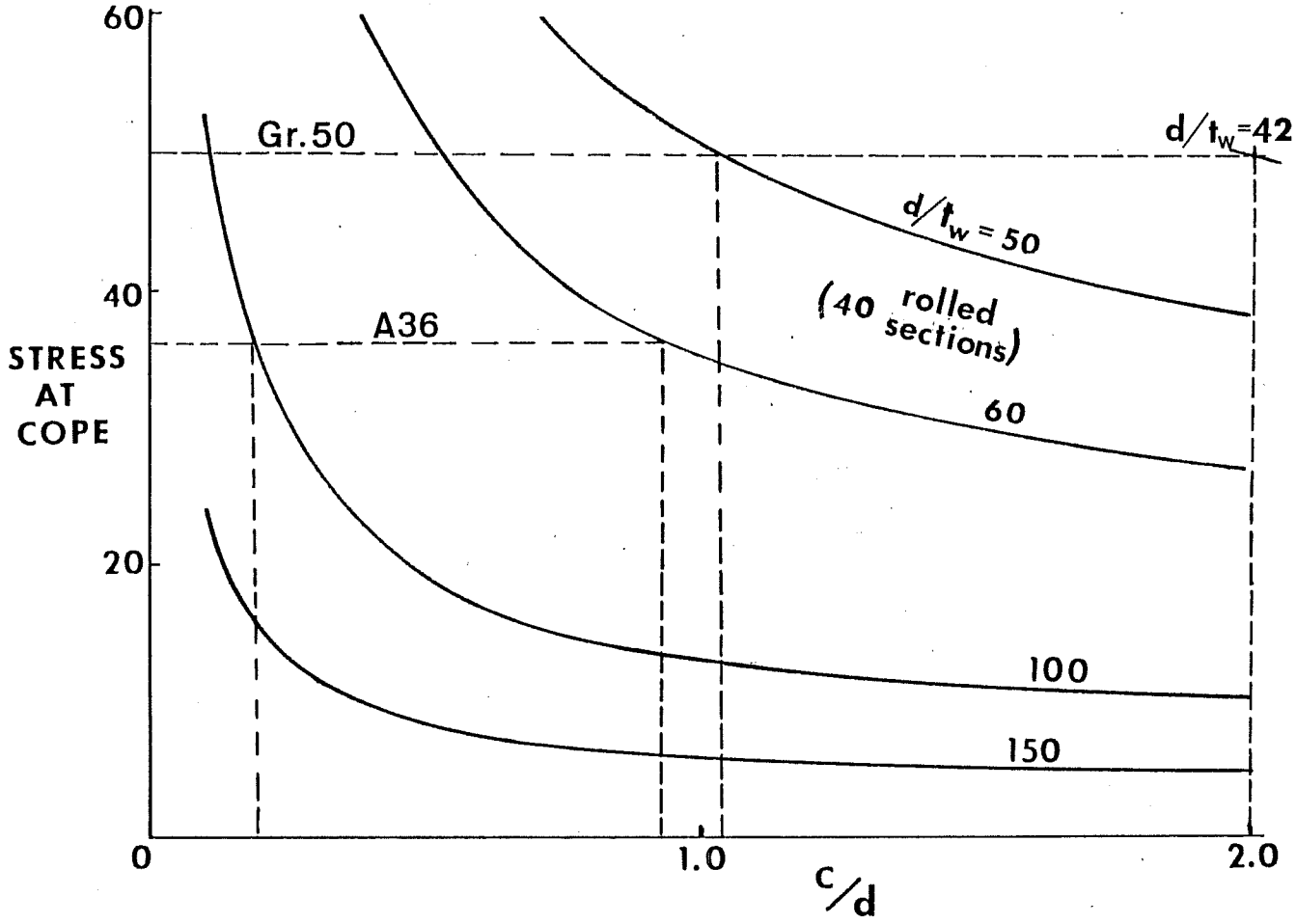

Fig. 8.19 Buckling Strength of Top Flange Coped Beams

CHAPTER 9

DOUBLE FLANGE COPED BEAMS

9.1 General

The same computer programs and simplified model as described in Sections 8.1 and 8.2 were used to study beams with both flanges coped. Beams with a coped length less than twice the beam depth ($c \leq 2d$) and with a coped depth less than one-fifth the beam depth ($d_c \leq d/5$) symmetrically on both flanges were considered. As in the study of top flange coped beams, the effects of end restraints were not included in the design model in order to obtain conservative results.

In Section 8.4 it was found that yield loads using Mc/I and $V/h_o t_w$ to calculate stresses always provided a lower bound when compared to the inelastic local web buckling solution of top flange coped beams. As will be seen later, the effects of stress concentration of double flange coped beams are much less than top flange coped beams. Thus, it is convenient and conservative to use the same criteria as top flange coped beams for inelastic local web buckling of double flange coped beams. Therefore, only elastic local web buckling analysis of double flange coped beams will be studied in this chapter.

9.2 Elastic Local Web Buckling Analysis

A W16x26 beam with a 1.5 in. cope depth and three cope lengths which varied between d/2 to 2d on both flanges were analyzed to study the behavior of elastic local web buckling of double coped beams. The buckling shapes and results of three different cope lengths are plotted in Figs. 9.1 to 9.3. The buckled shapes show that a significant lateral movement of the bottom of the web (tension side) occurs. This is different from the buckled shapes developed for beams with top flange copes where no significant movement occurred at the bottom flange. For top flange copes, treating the web as a plate with simply supported boundaries along the bottom and two vertical sides and a free boundary along the top correlated with actual behavior. But this model cannot represent buckling of double flange coped beams since both the top and bottom of the web move laterally. Also, the neutral axis of the coped region is located at mid-depth.

The buckled shapes given in Figs. 9.1 to 9.3 suggest that the web buckling can be modeled as a lateral-torsional buckling problem of a rectangular section with span c and a moment diagram as shown in Fig. 9.4. The critical buckling moment of simply supported rectangular section beam is

$$M_{cr} = C_b \, (\pi / k_d c) \sqrt{EI_y GJ} \qquad (9.1)$$

where C_b is the moment gradient coefficient and k_d is an effective length factor that reflects the out of plane restraint conditions at the two ends of the span. C_b = 1.75 for the case of linear moment

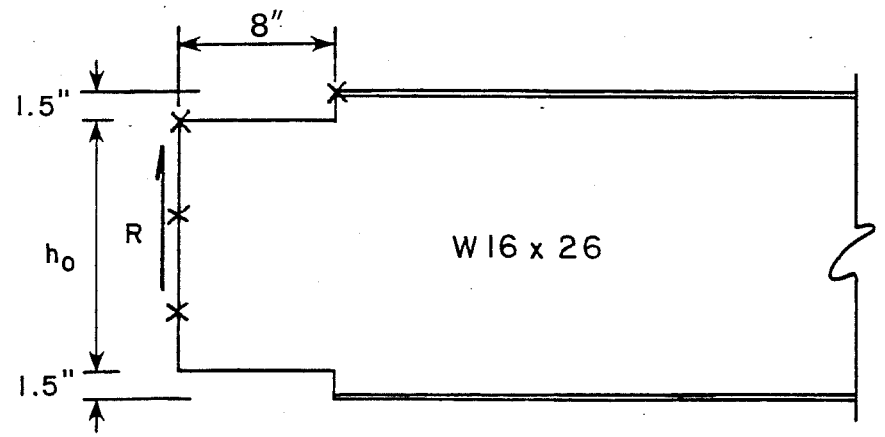

$R_{cr} = 82.0^{kips}$

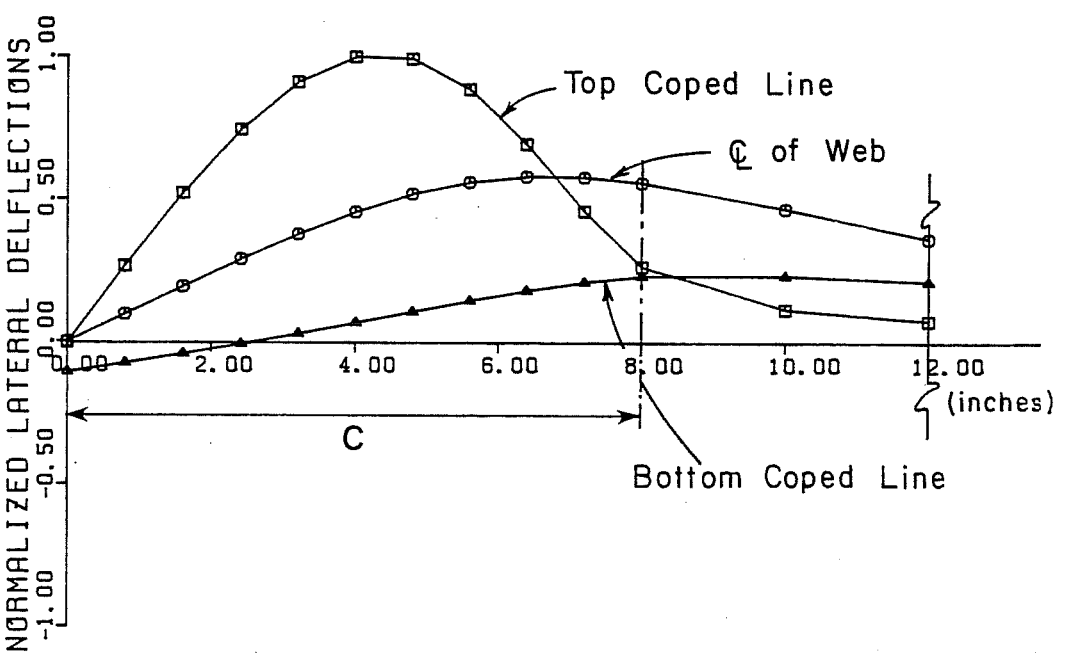

Fig. 9.1 Buckled Shapes- Case 1 with c = 8in.

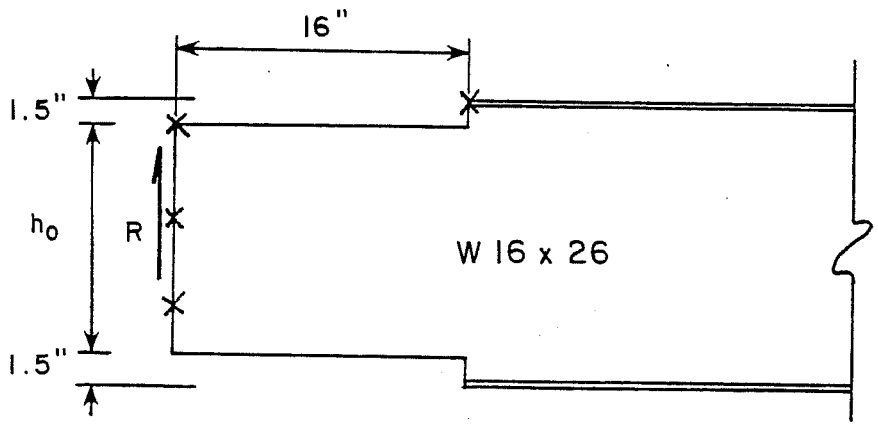

$R_{cr} = 21.2$ kips

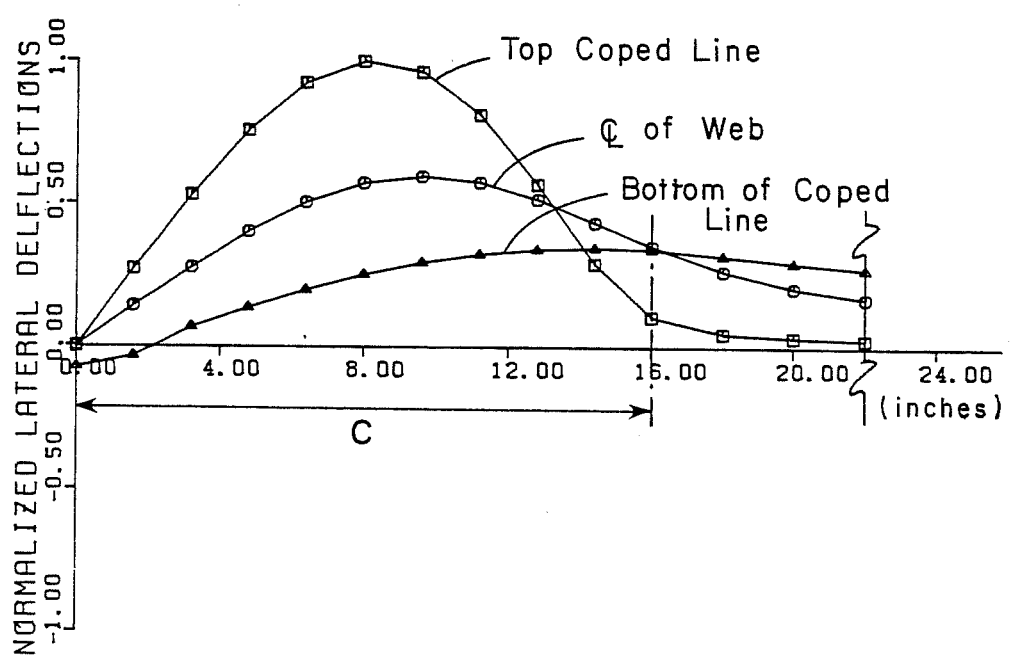

Fig. 9.2 Buckled Shapes - Case 2 with c = 16in.

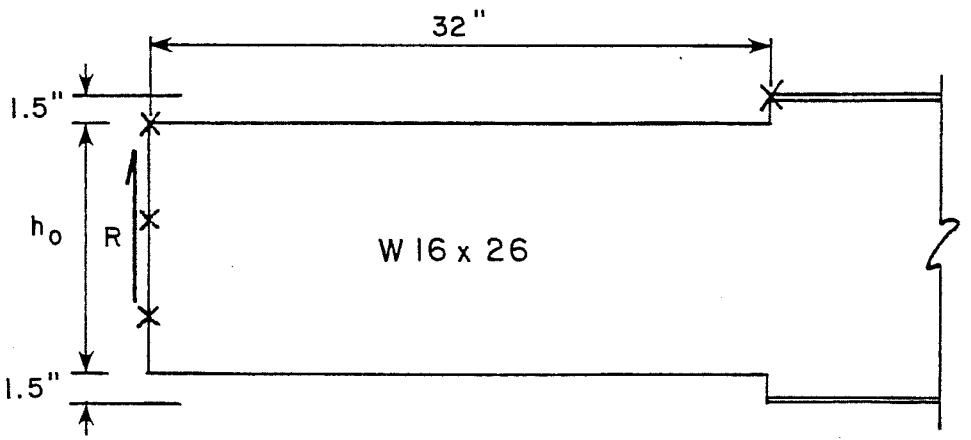

$R_{cr} = 5.18$ kips

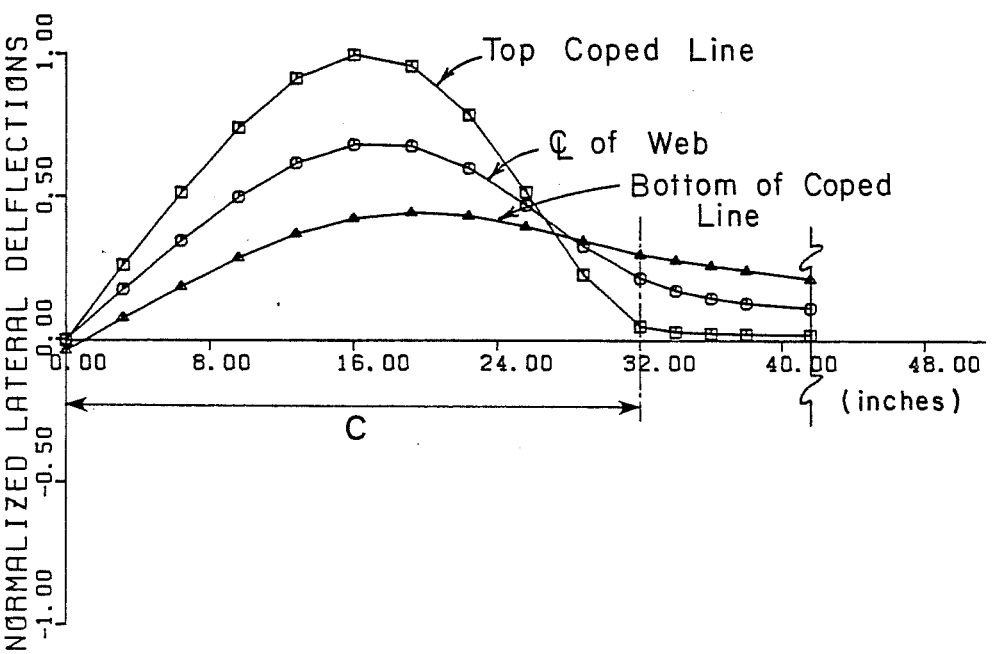

Fig. 9.3 Buckled Shapes - Case 3 with c = 32in.

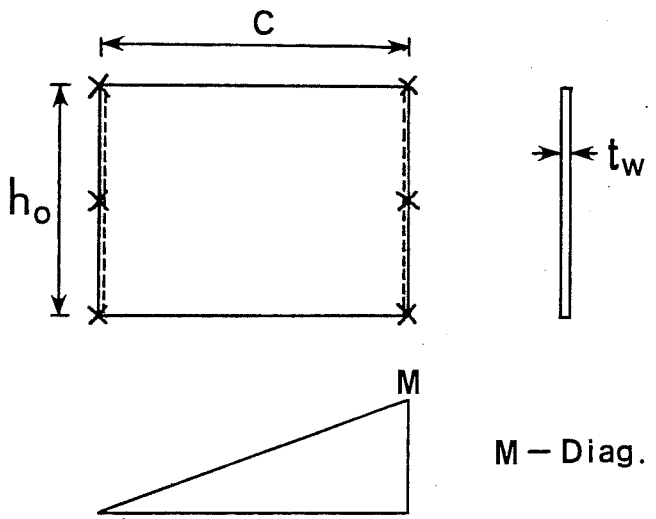

Fig. 9.4 Lateral-Torsional Buckling Model

diagram with zero moment at one end and M_{cr} at the other end. The critical end reactions based on BASP solutions for the three cases studied and the lateral buckling model (Eq. (9.1)) are given in Table 9.1. The comparison shows that the ratios of BASP solutions and Eq. (9.1) are almost the same for the three different cope lengths if C_b/k_d is taken as a constant. This implies that the effects of stress concentration, shear stress, cope depth and rotational restraint are almost the same for different cope lengths. This can be explained by the bending stress distributions of the cases studied as shown in Fig. 9.5. The same finite element mesh size as used for top flange cope beams was used in this analysis. It shows that the SCF at the cope (1.03 to 1.16) is significantly decreased compared to the SCF in top flange coped beams (1.33 to 1.89--see Fig. 8.7). Therefore, the effect of the stress concentrations are smaller in double coped beams as compared to top coped beams. For double flange coped beams all these effects can be considered in a single adjustment factor, f_d, to the basic formula, Eq. (9.1), which is developed later.

9.3 Discussion of the Proposed Design Models

The lateral buckling model (Fig. 9.4) gives good indication of the buckling load of double coped beams. If the moment gradient coefficient C_b is included in the adjustment factor, f_d, which accounts for the effects of SCF, shear stress, coped depth and rotational restraints, the design formula can be written as

TABLE 9.1 Comparison of BASP Solutions with Lateral Torsional Buckling Model

	Critical End Reactions (kips)		
	Coped Length (in.)		
	8	16	32
BASP	82.0	21.2	5.18
Eq. (9.1)	29.5 C_b/k_d	7.38 C_b/k_d	1.84 C_b/k_d
BASP/Eq. (9.1)	2.78/(C_b/k_d)	2.87/(C_b/k_d)	2.81/(C_b/k_d)

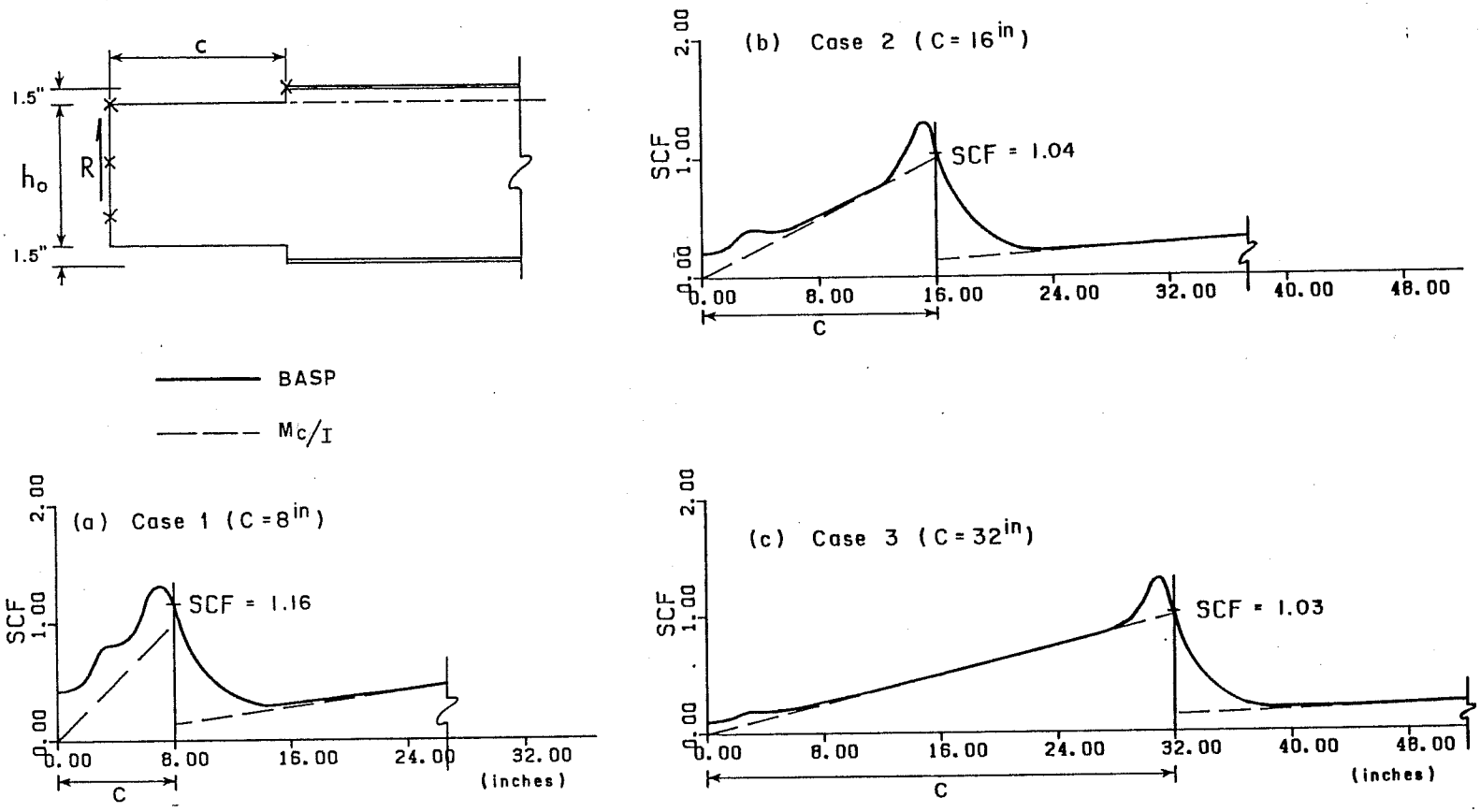

Fig. 9.5 Bending Stress Distributions at Top Coped Line for Double Flange Coped Beams

$$M_{cr} = f_d \, (\pi / c) \sqrt{EI_y GJ} \qquad (9.2)$$

Equation (9.2) can be further simplified by substituting $I_y = (1/12)\, h_o t_w^3$, $J = (1/3)\, h_o t_w^3$ and $G = E/2.6$, to become

$$M_{cr} = f_d \, (\pi E\, h_o t_w^3)/9.67\, c \qquad (9.3)$$

In addition, $F_{cr} = M_{cr}\, h_o/2I_x$ and $I_x = (1/12)\, h_o^3 t_w$, Eq. (9.3) can be rewritten in terms of critical bending stresses,

$$F_{cr} = 0.62 \;\; \pi E \, (t_w^2/c\, h_o)\, f_d \qquad (9.4)$$

Equation (9.4) is similar to Eq. (8.2) (plate buckling model) of top flange coped beams.

To further study the relationship between the plate buckling and the lateral buckling design models, the critical load of a double coped beam is calculated by Eqs. (8.2) and (9.4), and the ratio of these two equations is

$$\text{Eq. (8.2)/Eq. (9.4)} = f/f_d \qquad \text{for } c/h_o \geq 1.0$$

$$\text{Eq. (8.2)/Eq. (9.4)} = (h_o/c)^{0.65}\, (f/f_d) \qquad \text{for } c/h_o \leq 1.0 \qquad (9.5)$$

Equation (9.5) shows that when $c/h_o \geq 1.0$, the only difference between the two design models is the adjustment factors f and f_d. The adjustment factor f is a function of cope length, but f_d almost remains constant for different cope lengths. In other words, the buckling capacities of top flange coped beams are affected by cope

length more than the double cope beams are. When $c/h_o \leq 1.0$, the differences between the two design models are not only the adjustment factors, but also the ratio of h_o/c. The reason is that when the cope length decreases, the plate buckling coefficient k, which is a function of h_o/c, in Eq. (8.2) increases very fast (Fig. 8.14).

Although the two design models (plate buckling model for top flange coped beams and lateral buckling model for double coped beams) used for coped beams appear to have very different foundations, the principal variables in the design equations are the same in both cases.

9.4 Proposed Design Recommendations

The basic web lateral buckling model with an adjustment factor, f_d, (Eq. (9.4)) is recommended as the design method for double flange coped beams. It was found that for various coping details, the adjustment factor, f_d, to the basic Eq. (9.4) could be taken as

$$f_d = 3.5 - 7.5\ (d_c/d) \qquad (9.6)$$

For design the maximum Mc/I stress in the coped region is compared to Eq. (9.4). Further discussion of the development of the f_d factor is given below.

The value of f_d given in Eq. (9.6) was developed from solutions for a W16x26 beam with a constant cope length (8 in.) and various cope depths ($0 \sim 0.2d$) on both flanges. The BASP results of

these cases were equated to Eq. (9.4), the value of f_d was calculated and the results plotted in Fig. 9.6 by solid line as a function of d_c/d. A conservative linear expression for f_d given by Eq. (9.6) was fit to these results. Figure 9.6 shows that f_d decreases as cope depth increases.

To check the reliability of Eqs. (9.4) and (9.6), BASP solutions were developed for the cope geometries studied in Section 9.2 (varied cope length) and above (varied cope depth) but with a web thickness t_w = 0.1 in. (d/t_w = 157). The results are compared with solutions for t_w = 0.25 in. and Eq. (9.6) and are summarized in Tables 9.2 and 9.3, respectively. The comparison shows that the design equations (Eqs. (9.4) and (9.6)) give conservative results which are close to the theoretical buckling solutions obtained by BASP.

In addition to the design buckling equations, Eqs. (9.4) and (9.6), the maximum Mc/I and $V/h_o t_w$ stresses must also be checked with the yield stress which is close to inelastic local web buckling. These same yielding criteria were used in top flange coped beams. The results from Eq. (9.4) with a d_c = 0.1d, but different d/t_w ratios and various c/d are plotted in Fig. 9.7 to give some indication when yielding controls. Figures 9.7 and 8.19 for top flange coped beams show a lot of similarity. In fact, the same design rules mentioned in Section 8.5 can be applied to double coped beams. For example, for all rolled W sections with $c \leq d$ and F_y = 36 ksi, or sections with $d/t_w \leq 42$ and $c/d \leq 2.0$, the buckling need not

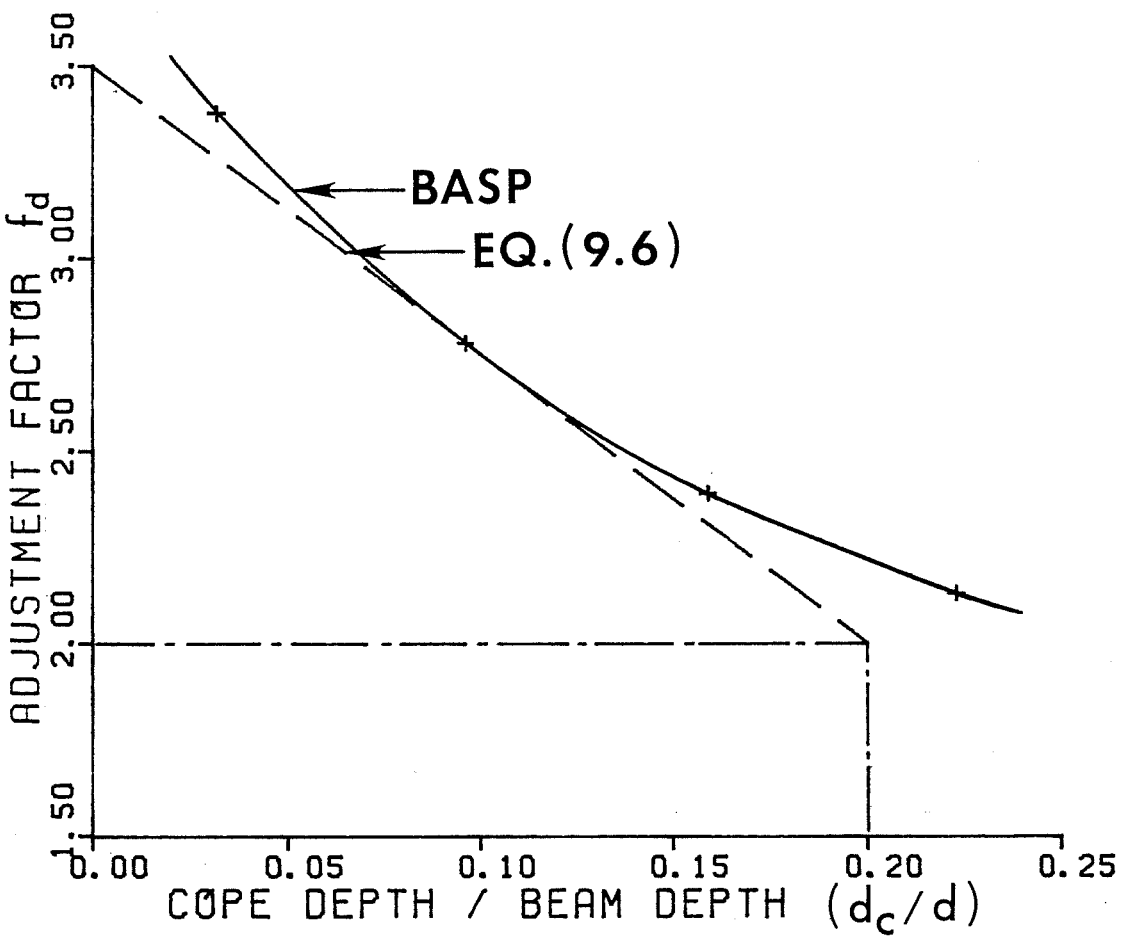

Fig. 9.6 Adjustment Factor f_d

TABLE 9.2 Double Flange Coped Beams--Variation of Cope Length

Cope Length (in.)		8	16	32
f_d (BASP)	t_w = 0.1 in.	2.89	2.92	2.88
	t_w = 0.25 in.	2.78	2.87	2.81
f_d (Eq. 9.6)		2.78	2.78	2.78

TABLE 9.3 Double Flange Coped Beams--Variation of Cope Depth

Cope Depth (in.)		0.5	1.5	2.5	3.5
f_d (BASP)	t_w = 0.1 in.	3.54	2.89	2.57	2.31
	t_w = 0.25 in.	3.38	2.78	2.39	2.13
f_d (Eq. (9.6)		3.26	2.78	2.30	1.83

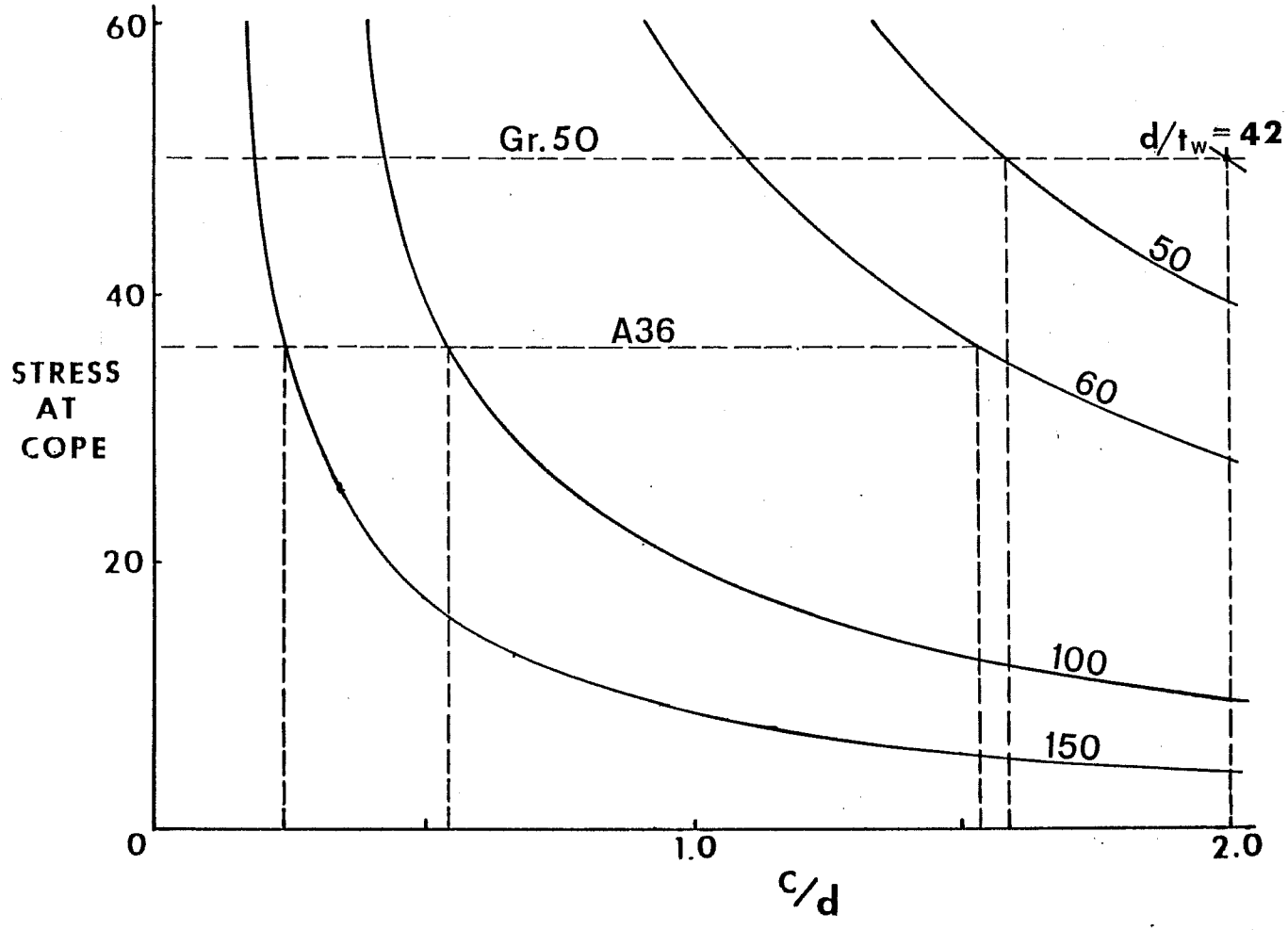

Fig. 9.7 Buckling Strength of Double Flange Coped Beams

be checked; yielding controls. For thin web plate girders, local web buckling is much more likely to control for common cope lengths. It should be noticed that, for thin web plate girders, the buckling stress for $c/d \leq 1.0$ of double coped beams is higher than top flange coped beams. This is due to the difference in section properties of the coped region and the different adjustment factors for the two types of coped beams.

CHAPTER 10

TEST PROGRAM AND RESULTS

10.1 Test Specimens

A total of ten tests were performed to study local web buckling in top (compression) flange coped beams. No tests were conducted on beams with double copes. The specified connection details can be seen in Fig. 10.1 and actual measured coping details are listed in Tables 10.2 and 10.3 later. The first five connections, labeled W1, W2, W3, RB18A, and RB12A, deal with the problem of inelastic local web buckling. These five tests were designed to study shear and flexural inelastic web buckling and the effects of end restraints. The remaining five connections were designed to fail by elastic local web buckling. The principal parameters considered in preparing these test specimens were cope length, cope depth, ratio of cope length to beam depth and elastic shear web buckling effects. Tests W1 through W3 have welded clip angle connections and the other seven tests have end plate shear connections. The connections were designed to carry the ultimate buckling load only.

All test specimens were fabricated with one connection detail at each end of the beams. The test beams for tests W1 through W3 and RB18A are 10 ft long W18x35 sections with A36 material. Tests RB12A through RB12D were fabricated from 12 ft long W12x14 sections with A572 Gr. 50 material. The test beam for tests PB26A and 26B was

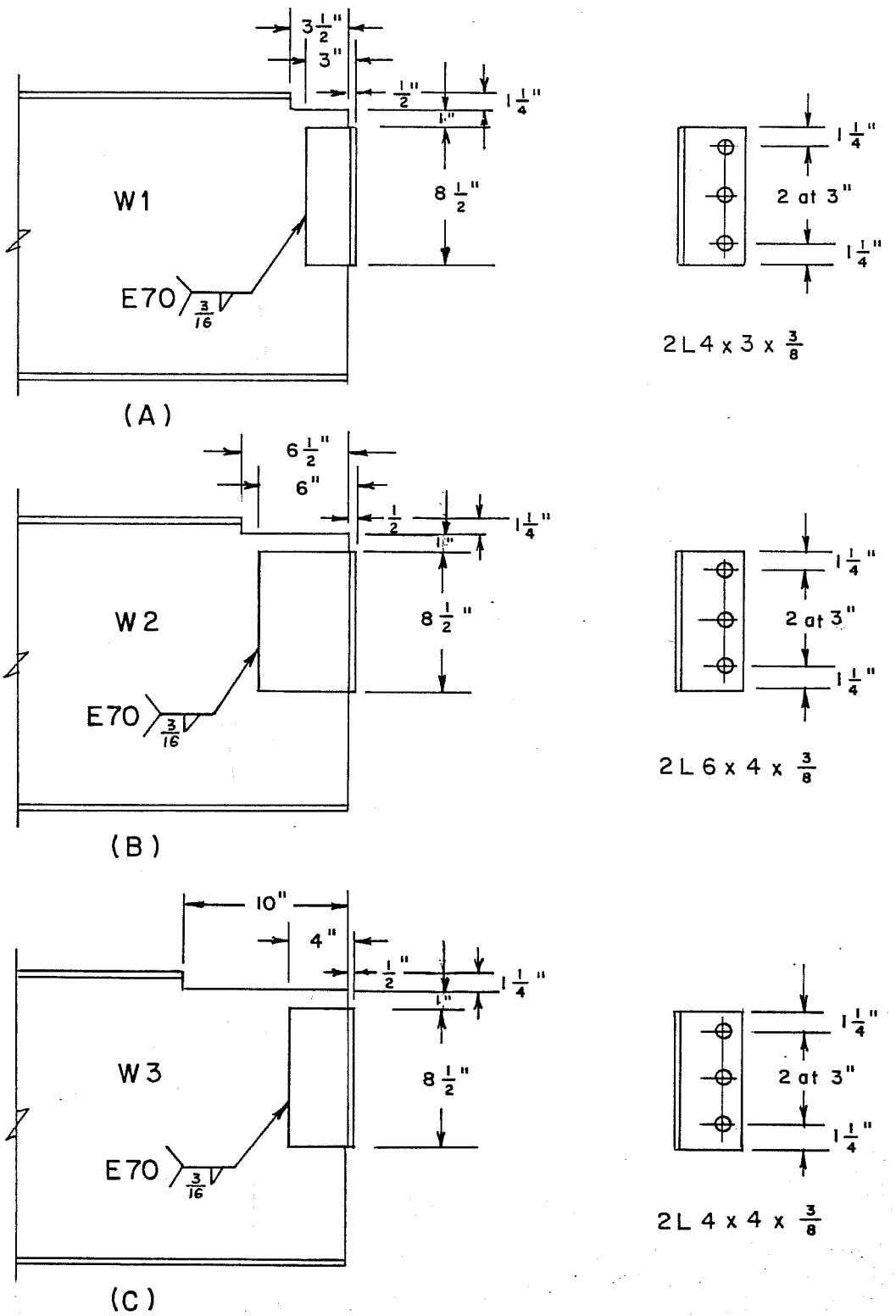

Fig. 10.1 Detail of Coping Connections of LocalWeb Buckling Tests

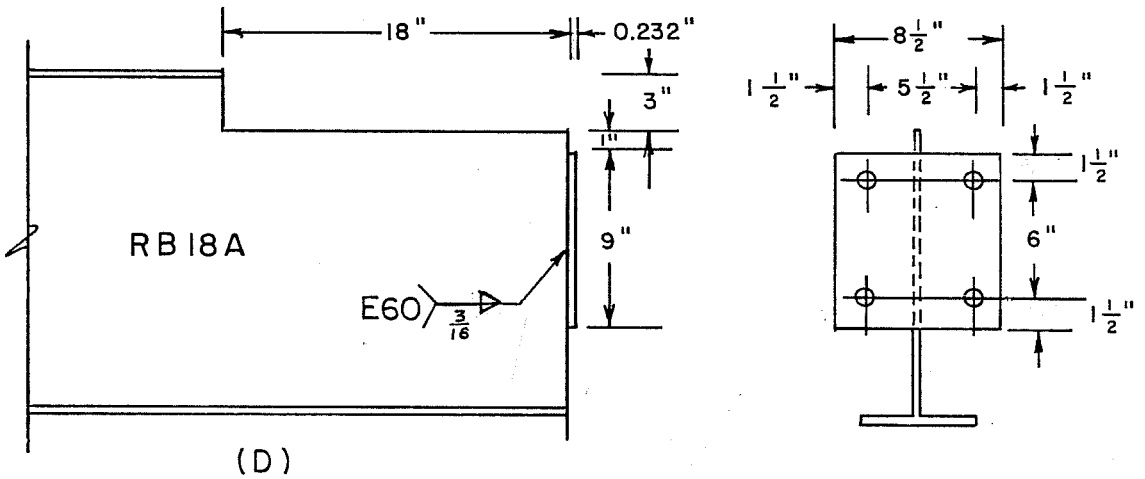

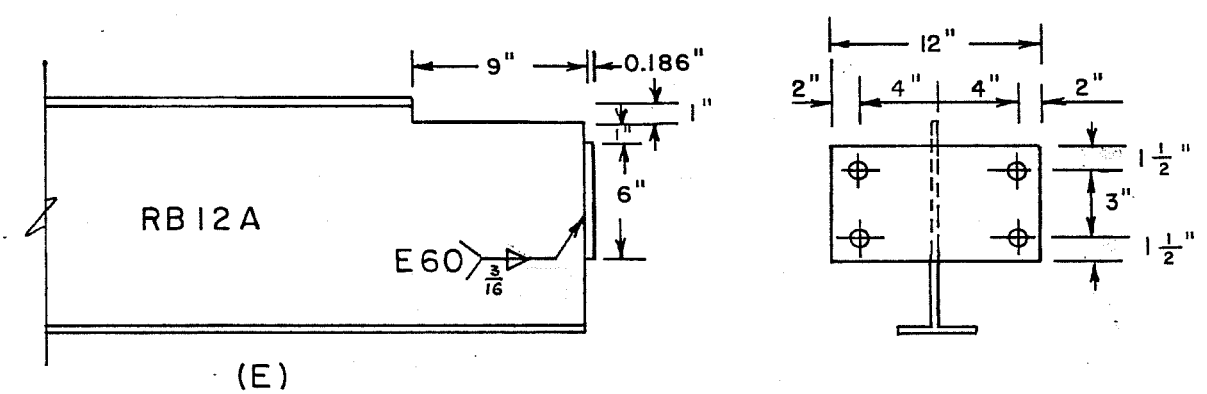

Fig. 10.1 (Cont'd)

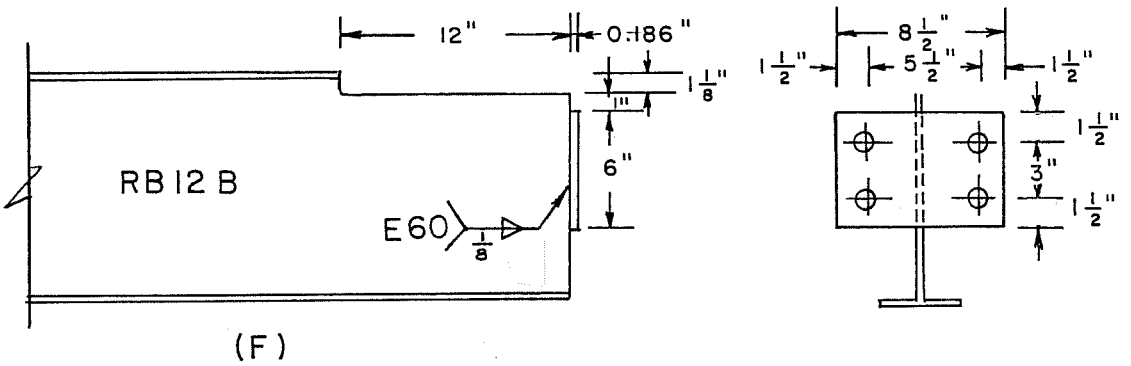

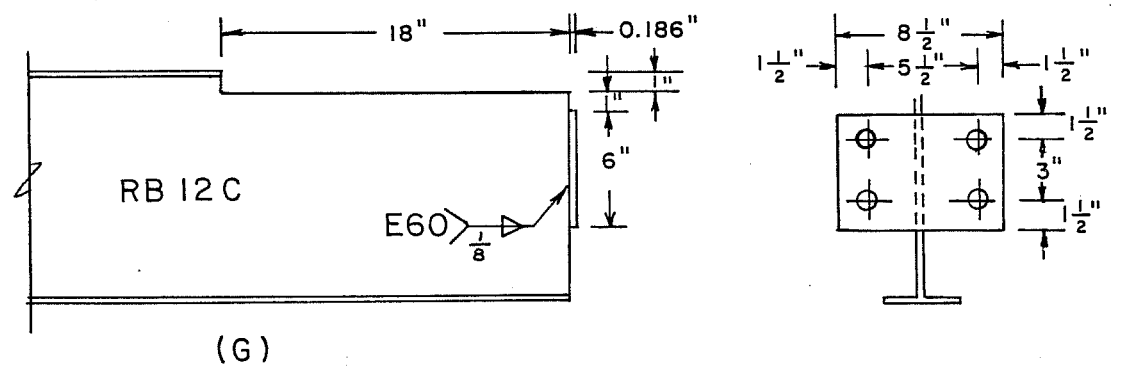

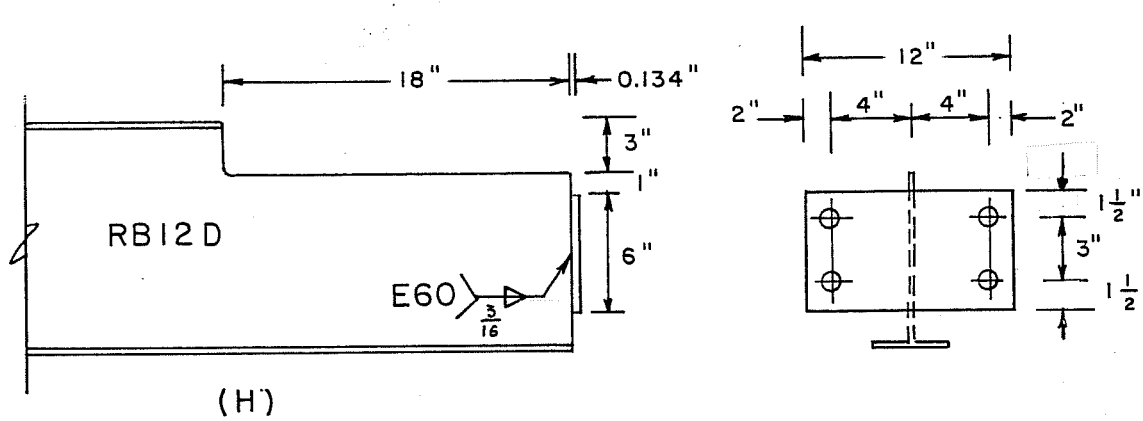

Fig. 10.1 (Cont'd)

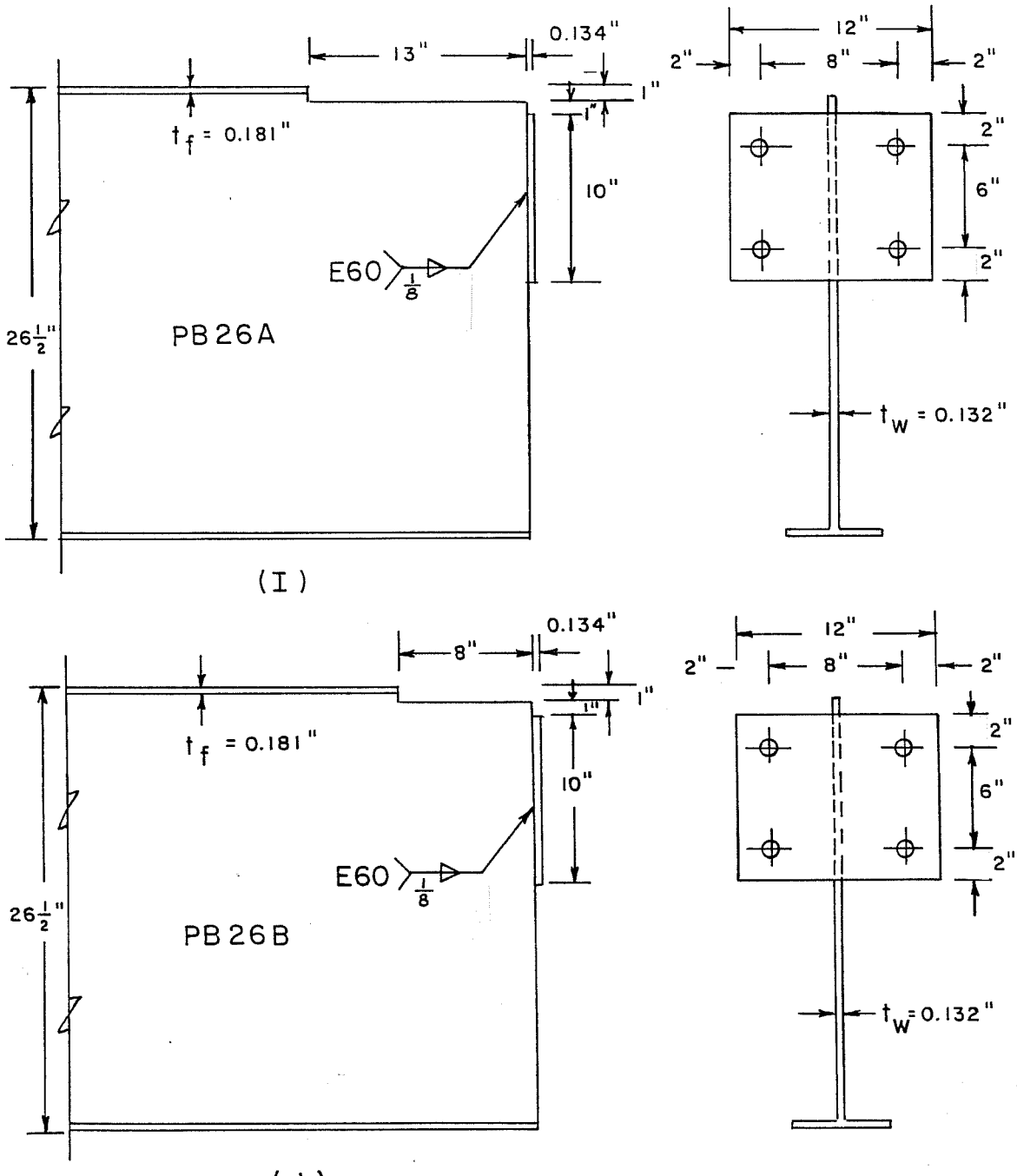

Fig. 10.1 (Cont'd)

a 13.7 ft long plate girder with h = 26 in., h/t_w = 197 and Gr. 50 material. The measured section properties and the tensile coupon tests results from the specimens are summarized in Table 10.1.

In order to minimize the end restraints, an 8 in. vertical bolt line distance (see Fig. 10.1) was used and and washers were placed between the end plate and supporting column in tests RB12A, RB12D, PB26A and PB26B. The other connections had a 5.5 in. vertical bolt line distance and no washers. In tests W1, W2 and W3, 15/16 in. diameter holes for 7/8-A325 bolts were used and 13/16 in. diameter holes for 3/4-A325 bolts were used for other tests. Minimum weld size was used for all test connections as shown in Fig. 10.1. The turn-of-nut tightening method was used to provide the bolt tension required by 1978 AISC Specification.

10.2 Test Setup

The test arrangement shown schematically in Fig. 10.2 is similar to the lateral-torsional buckling test setup (Fig. 5.2) which allowed the application of determinate forces to the test connection. However, the out-of-plane braces were designed to prevent lateral-torsional buckling; thus, the bracing systems were not located exactly at load and reaction positions. Also, there was an extra brace at the end of the copes to prevent the compression flange from moving laterally. Except for test PB26B, the load position was chosen not only to produce failure in the coped region but also to minimize the effect of the load itself on the stress distribution in

TABLE 10.1 Material and Section Properties

Tensile Coupon Test Results

Test Specimens	Flange Static Yield (ksi)	Flange Static Ultimate (ksi)	Web Static Yield (ksi)	Web Static Ultimate (ksi)	Strain Hardening Modulus (Est.) (ksi)
Tests W1-W4 RB18A	37.6	60.3	39.4	62.3	Flange 504 Web 590
Tests RB12A, RB12D	54.9	78.7	57.3	79.7	Flange 502 Web 468
Tests RB12B, TB12C	57.4	80.2	55.3	77.7	Flange 510 Web 530
Tests PB26A, PB26B	57.0	79.2	59.4	66.7	--- ---

Measured Section Properties

Test Specimens	Beam Depth d (in.)	Flange Width b_f (in.)	Flange Thickness t_f (in.)	Web Thickness t_w (in.)
Tests W1-W4, RB18A	17.85	6.00	0.439	0.304
Tests RB12A, RB12D	11.88	3.97	0.239	0.212
Tests RB12B, RB12C	11.96	4.00	0.239	0.217
Tests PB26A, PB26B	26.50	6.00	0.181	0.132

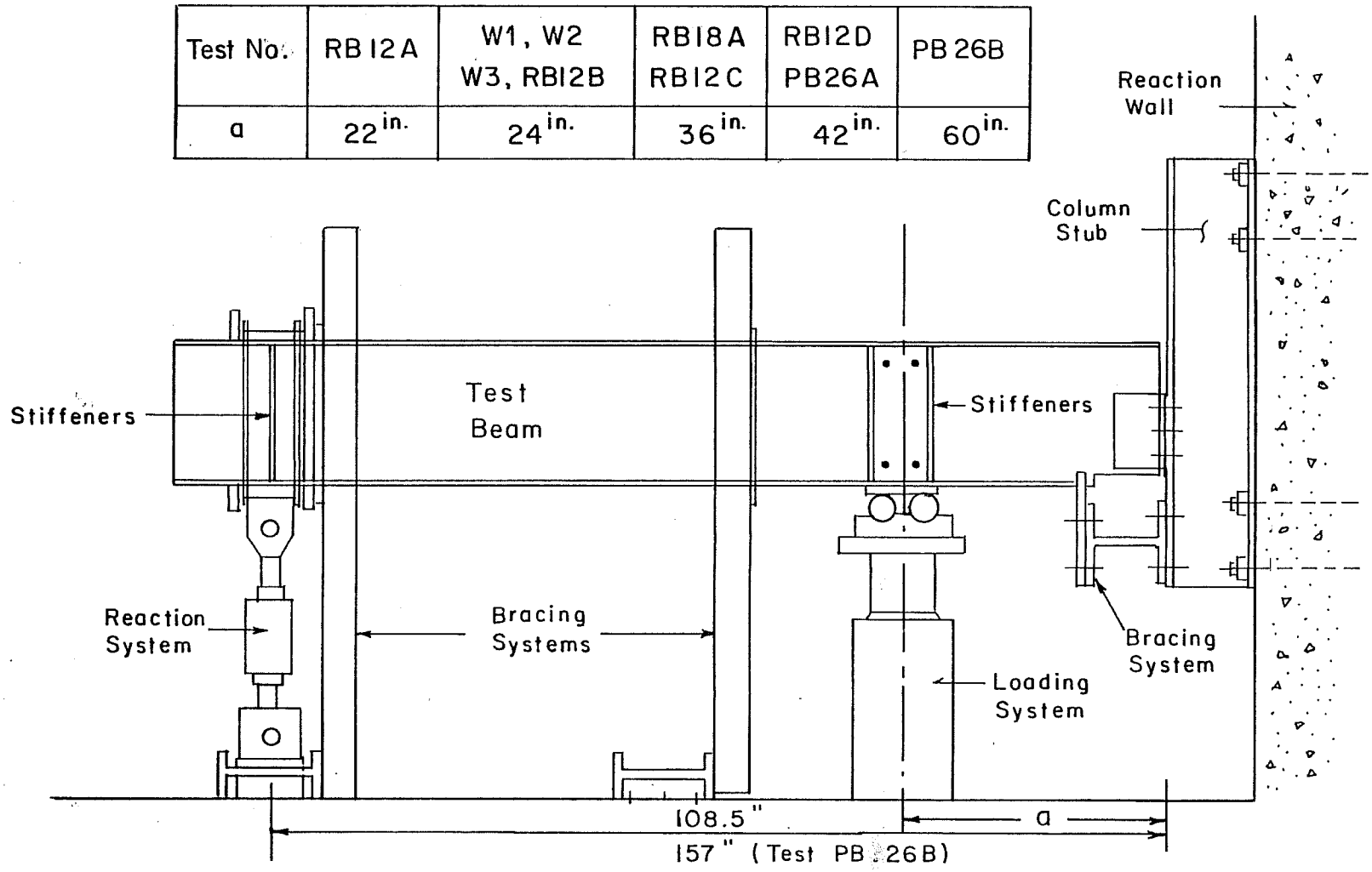

Fig. 10.2 Schematic of Test Setup

the coped region. The distance from the load position to the face of the supporting column is summarized in Fig. 10.2. The end reaction was 108.5 in. from the face of supporting column for all tests except Test PB26B in which the distance was 157 in. The reason that Test PB26B was different from the others was because it was designed to fail in elastic shear web buckling instead of local flexural web buckling. Channel sections or 2x4 wood stiffeners were bolted or clamped to both sides of the web at the ram and the reaction locations to prevent web crippling. A photograph of the test setup is shown in Fig. 10.3.

The arrangement of the loading system was the same as for the lateral-torsional buckling tests (Figs. 5.4 and 5.5). However, 30 ton, 60 ton and 200 ton hydraulic rams were used in these tests. As for the reaction system, the same arrangement as shown in Figs. 5.6 and 5.7 was used with 10 kip or 100 kip load cells depending on the test beam capacity. Figures 10.4 and 10.5 are photographs of the 200 ton loading system and the 100 kip reaction system, respectively.

The test beams were prevented from lateral movement in the vicinity of the load, reaction and end of cope positions by an out-of-plane bracing system as shown in Fig. 10.6, which is similar to that used in the lateral buckling tests. However, if the coped length of the test beam was smaller than 12 in., a bracing system as shown in Fig. 10.7 was used to control lateral movement of the compression flange near the cope.

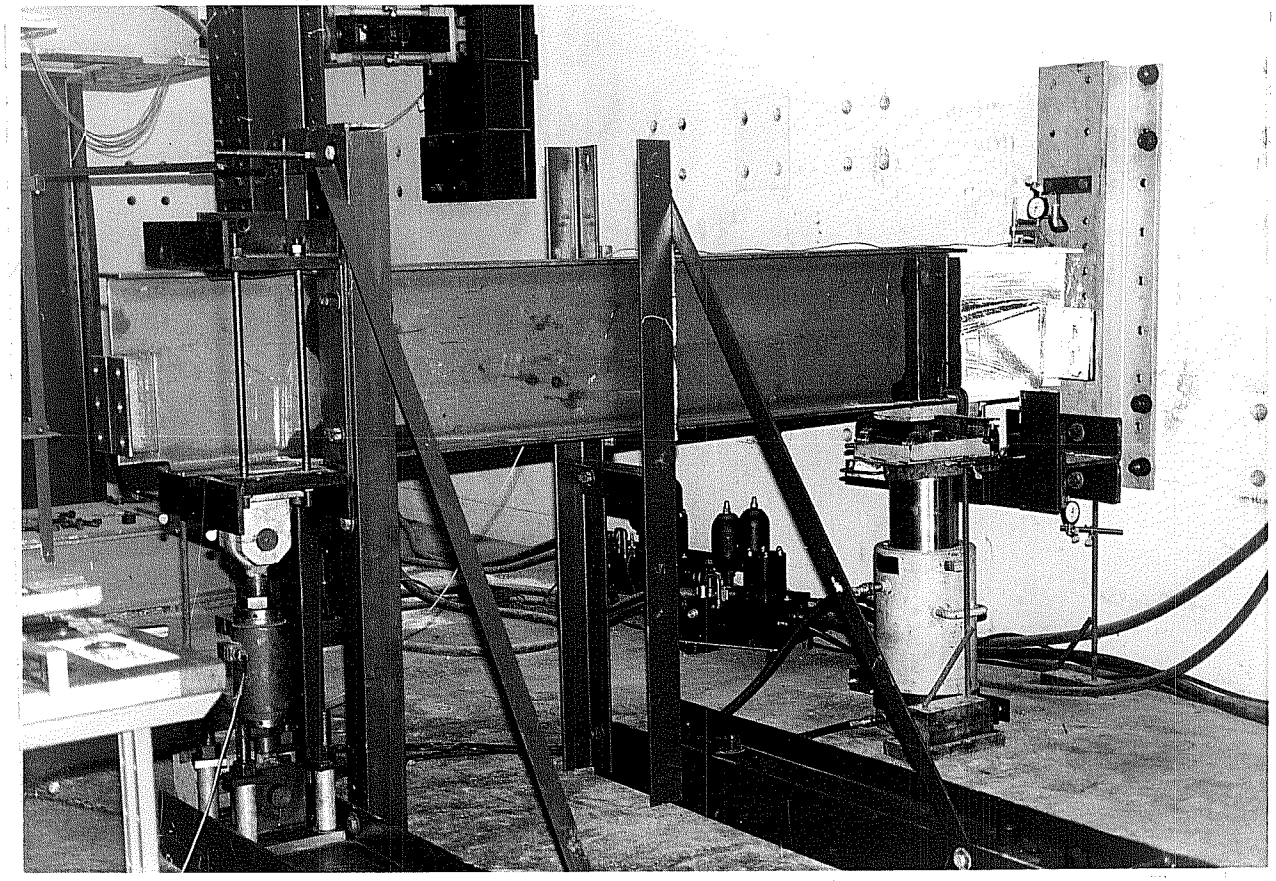

Fig. 10.3 Test Setup

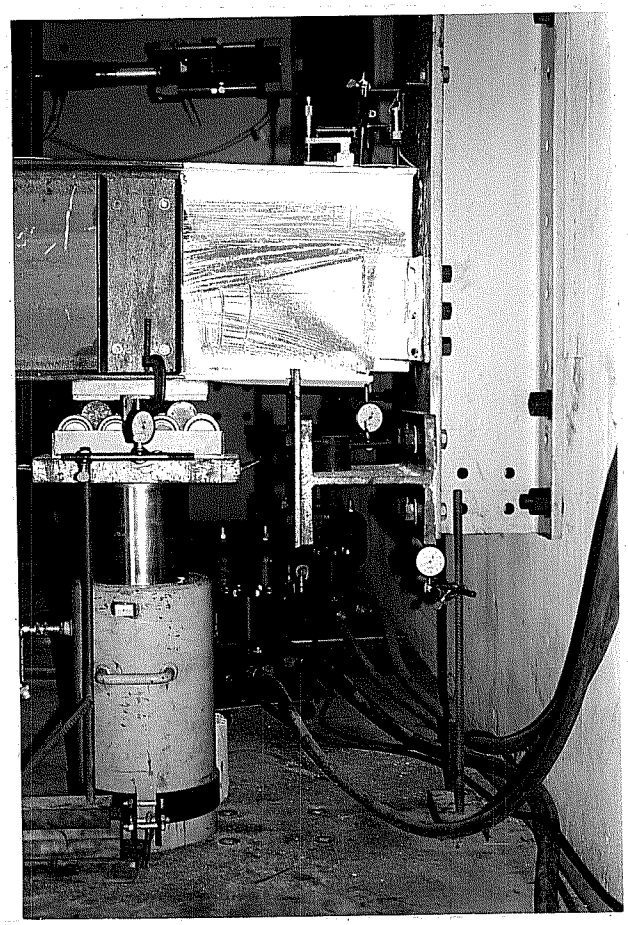

Fig. 10.4 200 ton Loading System

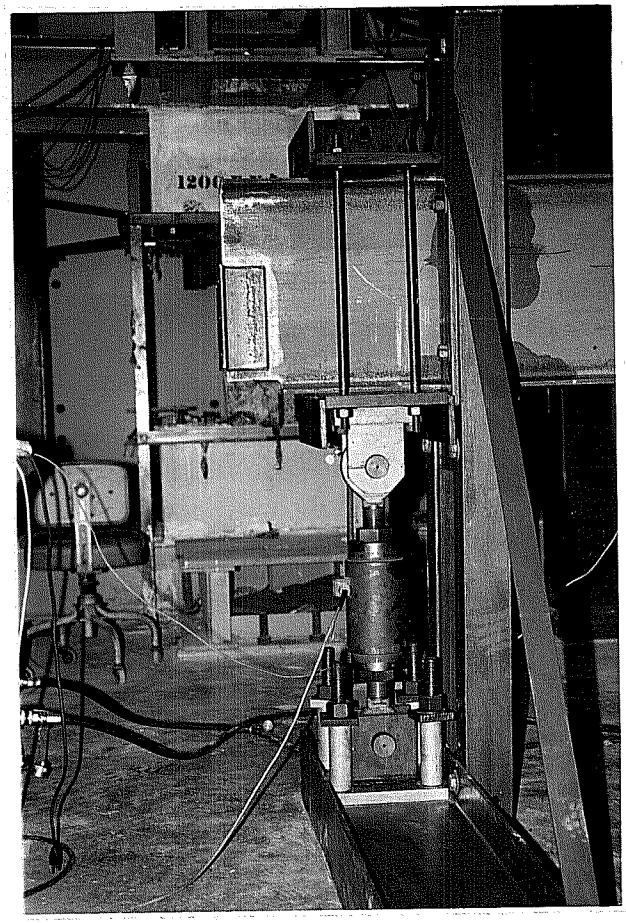

Fig. 10.5 100 kip Reaction System

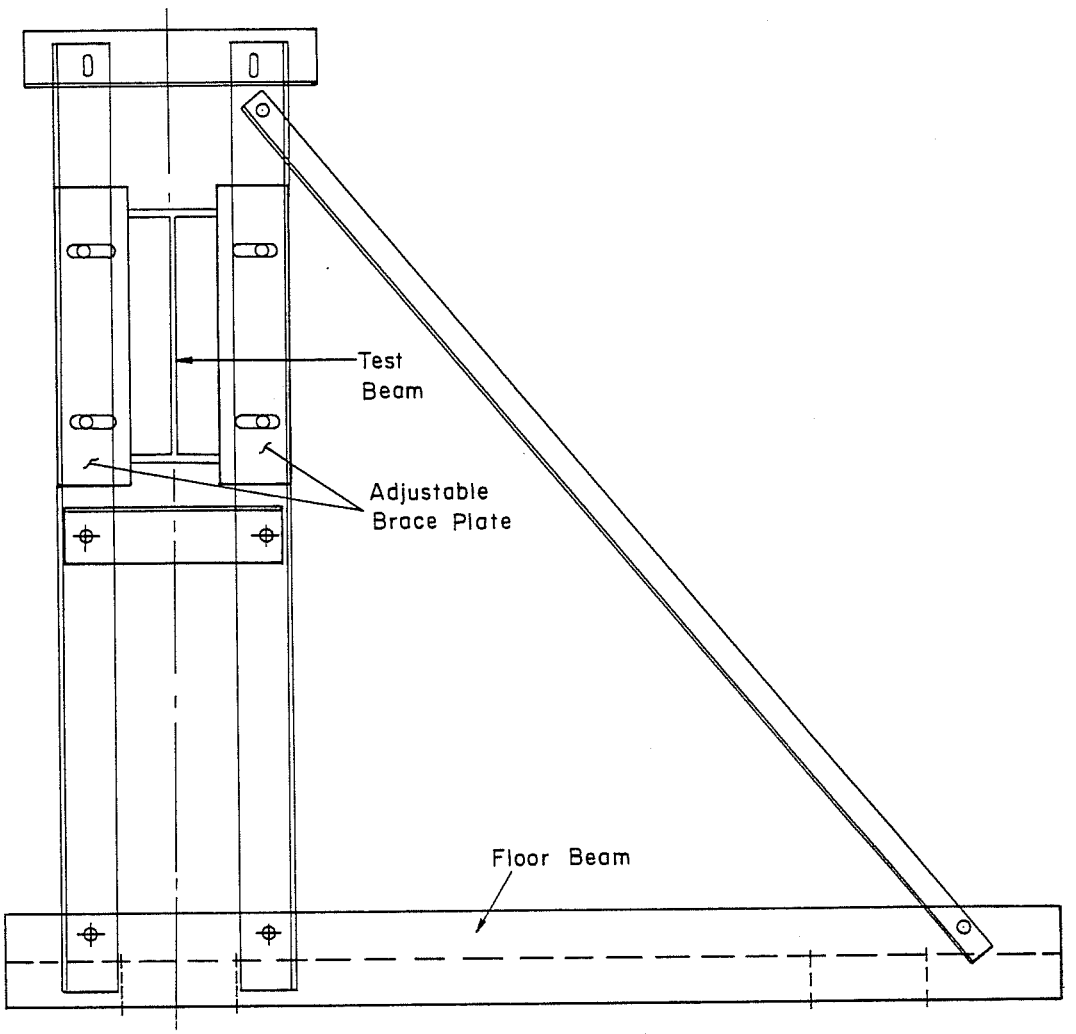

Fig. 10.6 Schematic of Out-of-plane Bracing System

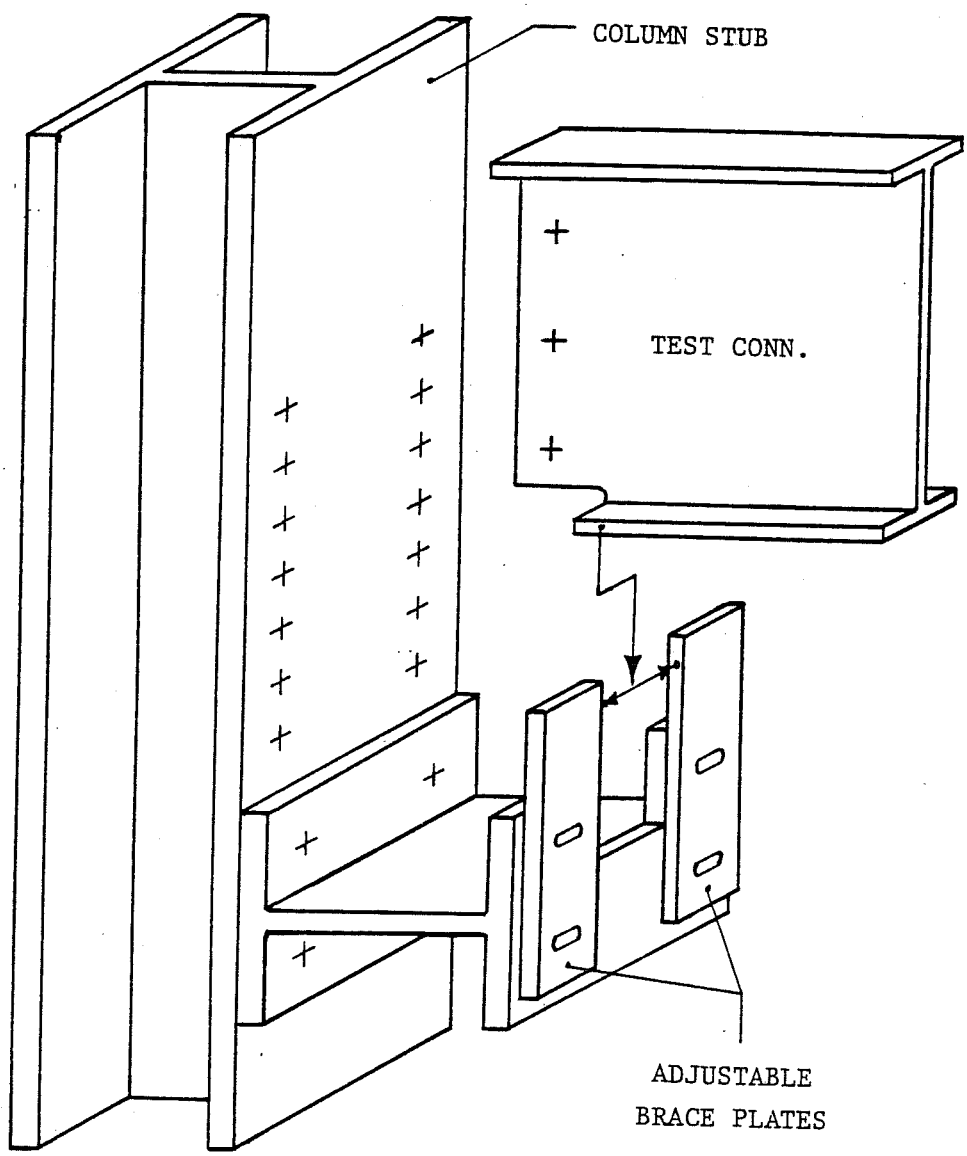

Fig. 10.7 Bracing System at the End of Cope Position

10.3 Instrumentation

The magnitude of the applied load was determined by two pressure transducers, one linked to a strain indicator and a second connected to an X-Y plotter. When the 30 ton ram was used, a load cell checked the load measured by the pressure transducer. No load cell was used with the other rams since there was good correlation between the loads determined from the pressure readings and the load cell. The far-end reaction was determined from the calibrated load cell.

The in-plane deflection measurements were exactly the same as those used in the lateral-torsional buckling tests (Fig. 5.8), six dial gages and one inclinometer. In addition, a potentiometer monitored by an X-Y plotter measured the vertical movement at the load position. Web deflections were measured for all beams except W1, W2 and W3 with the apparatus shown in Fig. 10.8 using 0.001 in. dial gages.

Except in Test W1, strain gages with a gage length of 0.32 in. were spaced equally along the line A as shown in Fig. 10.9 to study the stress distribution at the copes. In Test RB12D, two extra pairs of strain gages were attached at lines B and C to check the stress distribution away from the copes. Gages were placed at both sides of the web. The rectangular rosette gages were used at the corner of the copes to provide further information at the copes. All strain gages, except rosette gages, were oriented parallel to the longitudinal axis of the test beams. The rectangular rosette gages

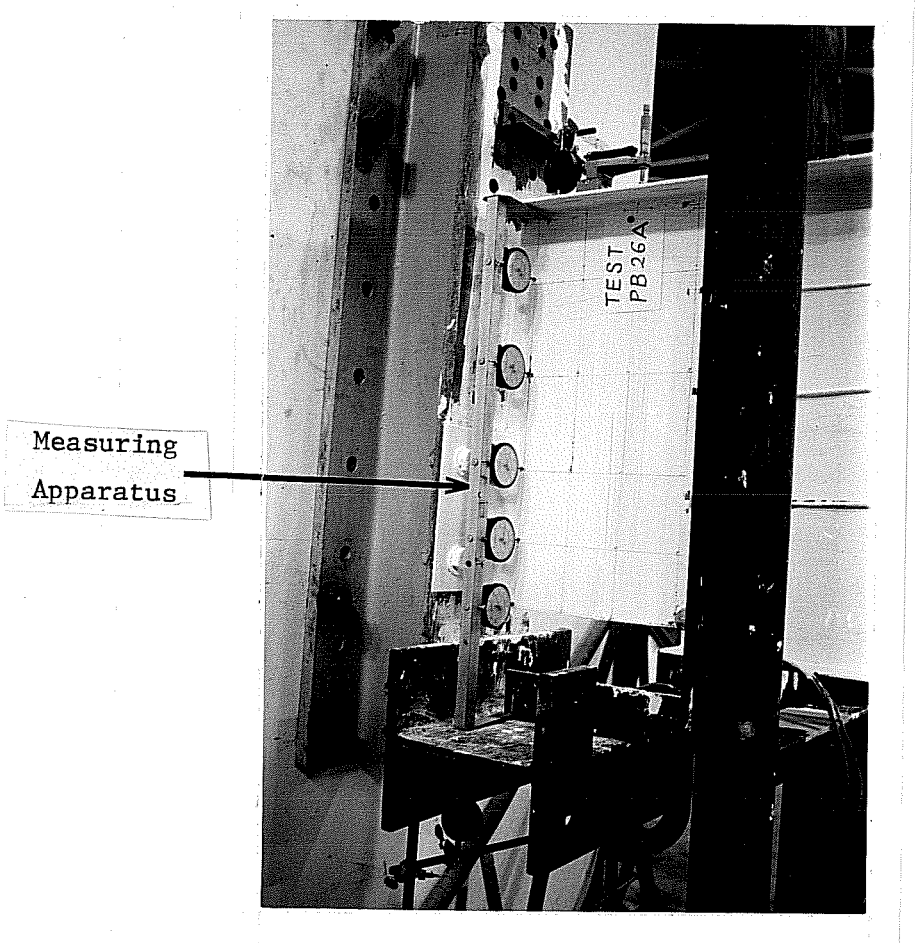

Fig. 10.8 Web Deflection Measuring Apparatus

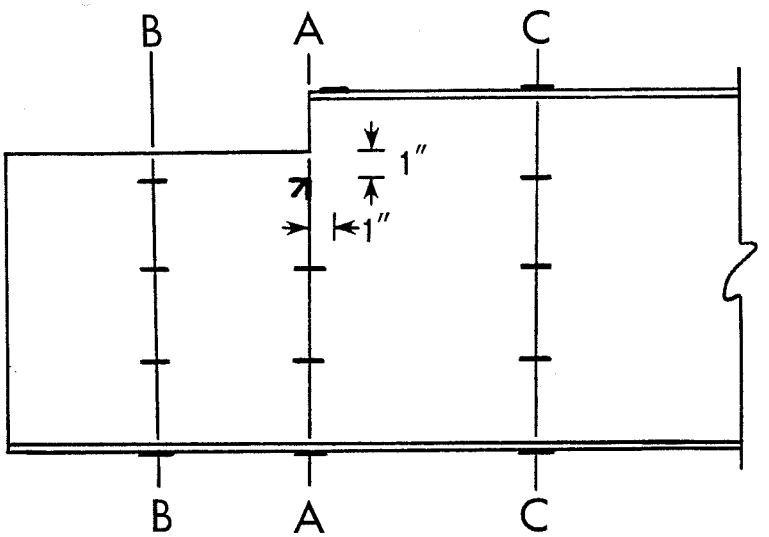

Fig. 10.9 Strain Gage Locations

were oriented so that one gage was at 45 degrees to the test beam longitudinal axis and two other gages were parallel and vertical.

The test beams were whitewashed from the connection to the load position to detect the formation of yield lines.

10.4 General Test Procedure

The test procedure was similar to that described for the lateral-torsional buckling tests except the tests were terminated when the maximum load was reached and unloading occurrred.

10.5 Test Results

Loads, deflections, rotations and strain gage readings were reduced from the recorded data. Examination of these test data showed that reaction at the connection versus average deflection at the load position curves, final buckled shapes (out-of-plane deflection), and stress distribution curves gave very important characteristics of the failure due to local web buckling.

In each reaction versus deflection curves, the reaction determined by Eq. (8.2) for web buckling or for yielding, whichever controls, is plotted on the figures for comparison. The symbol R_{vy} indicates shear yielding of the web and R_y denotes flexural yielding. It should be noted that these recommended values for design are smaller than the BASP exact solutions which will be discussed in the next section.

The results of the tests are divided into four groups. The inelastic local web buckling will be discussed first, followed by

elastic local web buckling. Photographs of the test specimens are included in the discussions.

10.5.1 Inelastic Local Web Buckling--Shear Yielding (Tests W1, W2). Tests W1 and W2 were designed to fail in local web buckling after shear yielding occurred in the coped sections. The reaction versus deflection curves are shown in Fig. 10.10. Photographs of the test beams are shown in Fig. 10.11. Figure 10.12 shows the bending stress distributions at line A of Test W2, measured by the strain gages.

Figure 10.10 shows that the shear yielding criterion predicts beam capacity fairly well. As expected, due to the larger cope length of Test W2 which would increase the bending stress at the coped region, Test W2 had slightly less buckling capacity and post buckling strength than Test W1. However, both tests showed that even with a thicker web at the coped region due to the presence of the clip angles, the web had little capacity after the whole coped region reaching shear yield. The buckling occurred very suddenly after the coped regions were severely yielded as shown in Fig. 10.11. Figure 10.11 also shows that clip angles will affect the stress distribution of the coped region as confirmed by the bending stress distribution given in Fig. 10.12. Two load stages are plotted in Fig. 10.12. One is in the elastic range and the other is in the inelastic range. The stress distributions are different from Fig. 8.15 because of the clip angles.

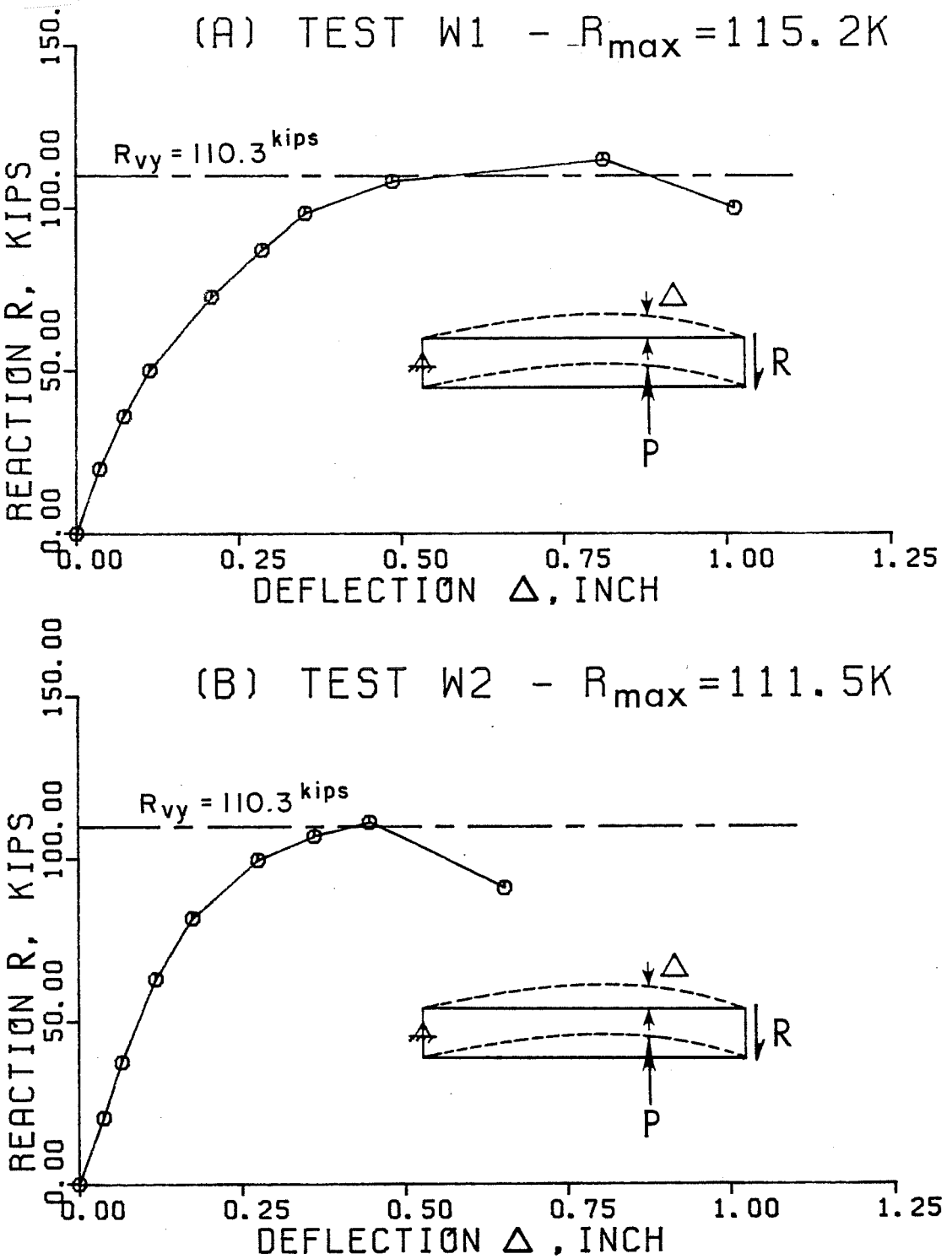

Fig. 10.10 Reaction vs Deflection Curves of Inelastic Local Web Buckling - Shear Yielding

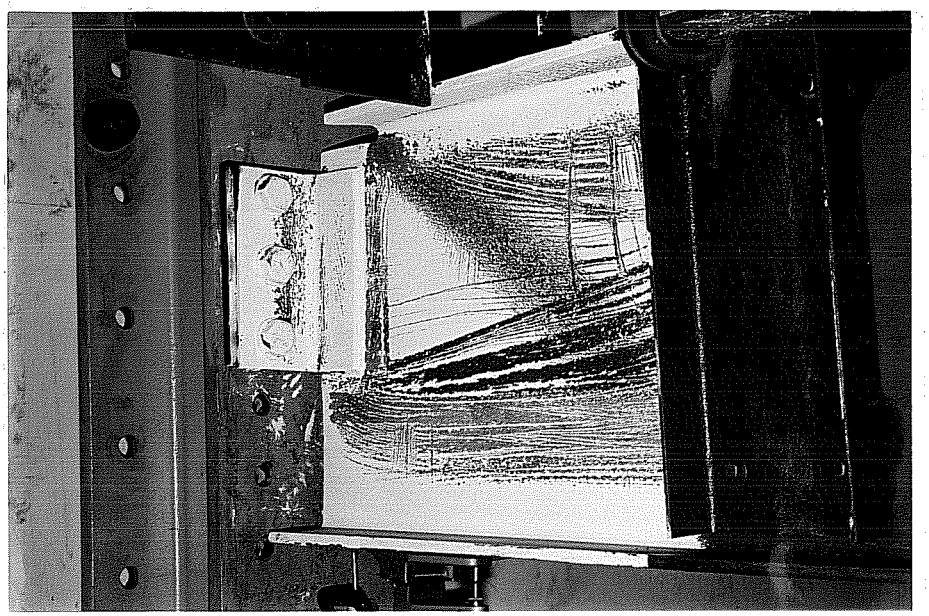

West Side

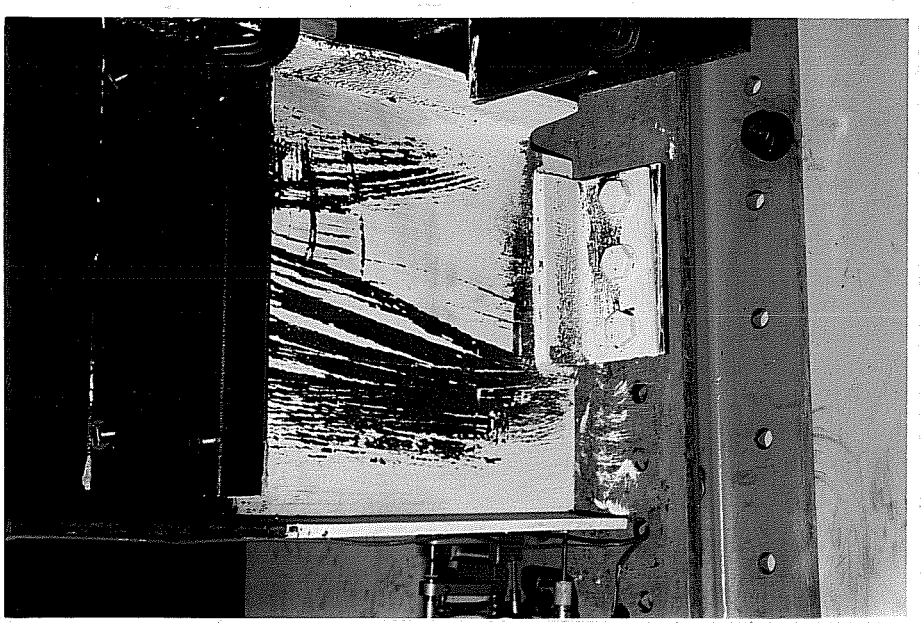

East Side

(a) Test W1

Fig. 10.11 Inelastic Local Web Buckling - Shear Yielding

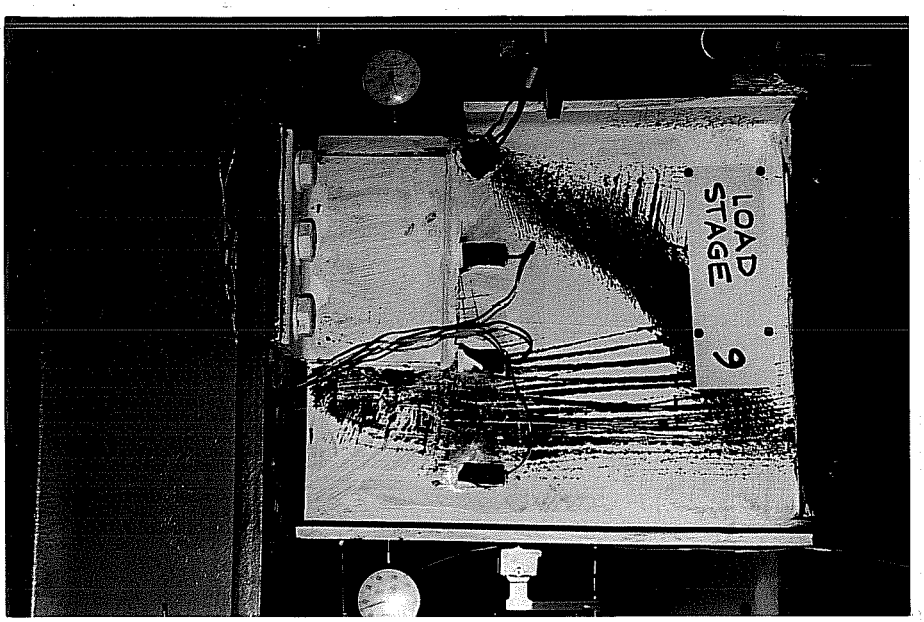

West Side

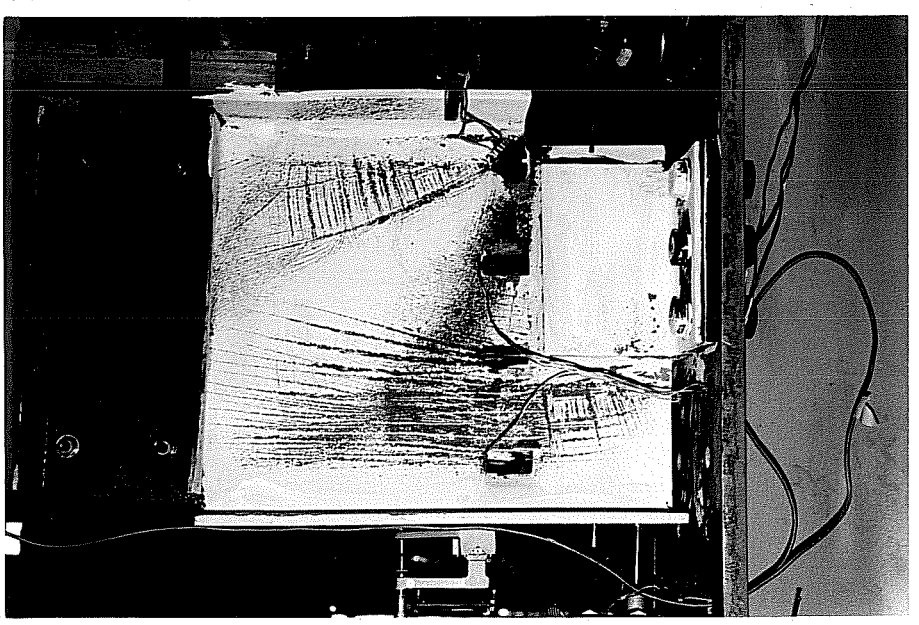

East Side

(b) Test W2

Fig. 10.11 (Cont'd)

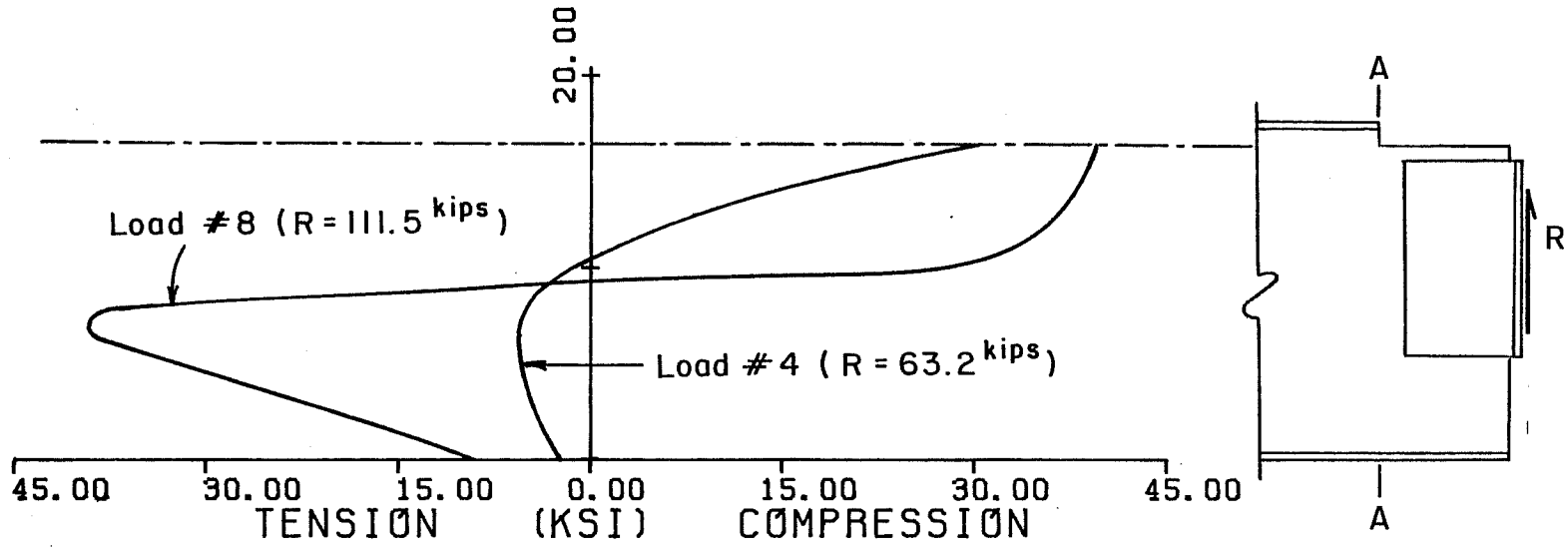

Fig. 10.12 Bending Stress Distributions of Test W2 at Line A

10.5.2 Inelastic Local Web Buckling--Flexural Yielding (Tests W3, RB18A, RB12A). Tests W3, RB18A and RB12A were used to check the bending stress yield criterion. Test RB12A with washers between the end plate and supporting column was designed to minimize the end restraint effects. The reaction versus deflection curves, buckling shapes, photographs and stress distributions are shown in Figs. 10.13 through 10.16, respectively. Due to the sudden occurrence of the buckling, the maximum loads in the reaction versus deflection curves (Fig. 10.13) were estimated from the recorded X-Y plots.

Tests W3 and RB18A gave higher maximum loads than predicted by the bending stress yield criterion while Test RB12A showed fairly good comparison. The differences occur because of in-plane and out-of-plane end restraint effects. In Test W3, welded clip angles provided both in-plane and out-of-plane end restraints. The measured end moment divided by the end reaction gave an equivalent end eccentricity of 3.9 in. before the beam failed in web buckling. Since the flexural yielding was localized, restraint provided by the clip angles increased the buckling load. In Test RB18A, though the end plate connection reduces the out-of-plane end restraint significantly, test results show very large in-plane end restraint (e = 8 in. before failure) which reduces the stress level at the coped region and eventually increased the buckling capacity. In Test RB12A, the end plate connection was carefully designed to minimize

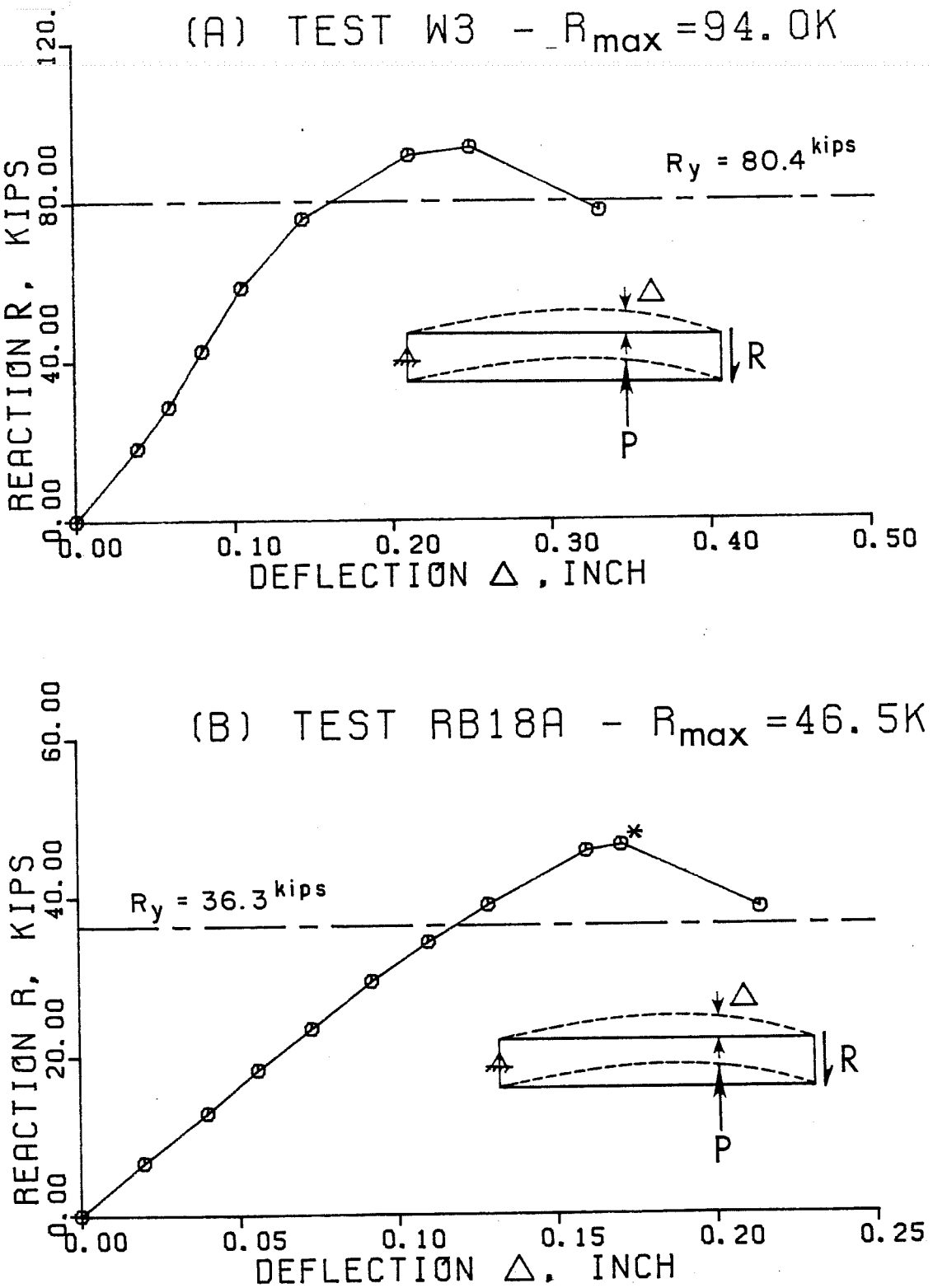

Fig. 10.13 Reaction vs Deflection Curves of Inelastic Local Web Buckling - Flexural Yielding

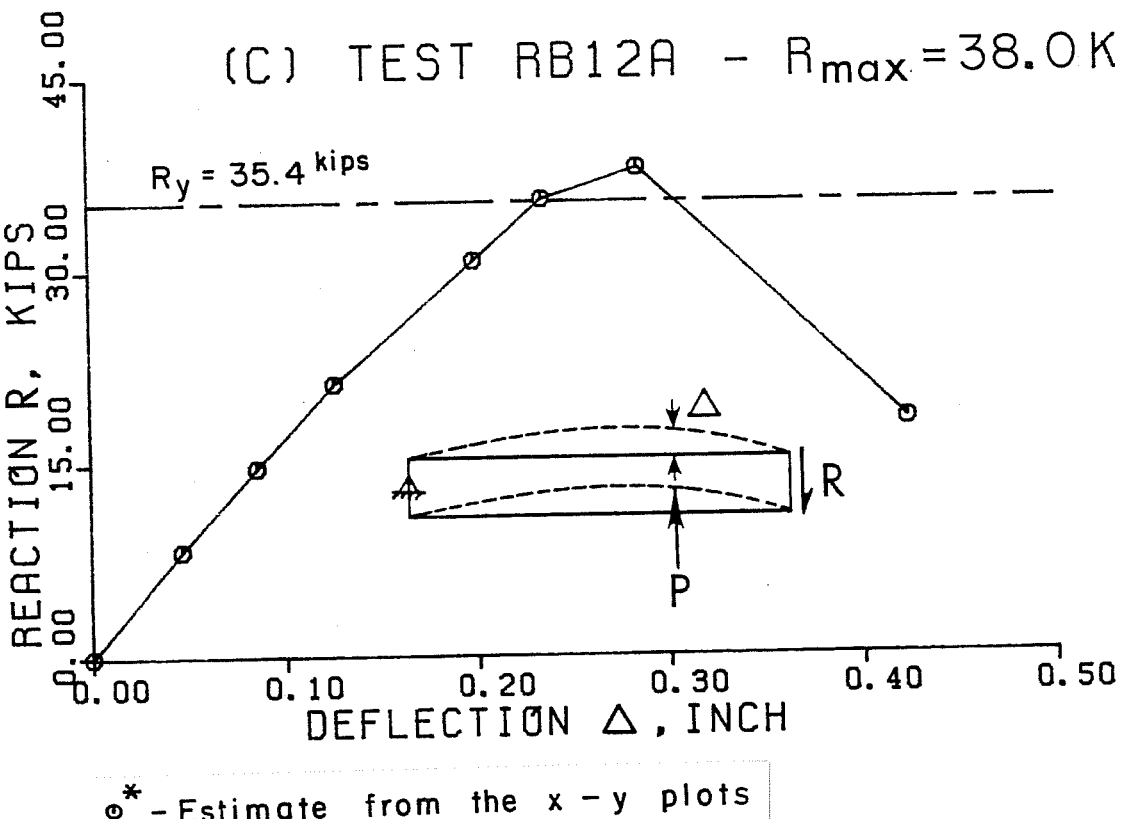

Fig. 10.13 (Cont'd)

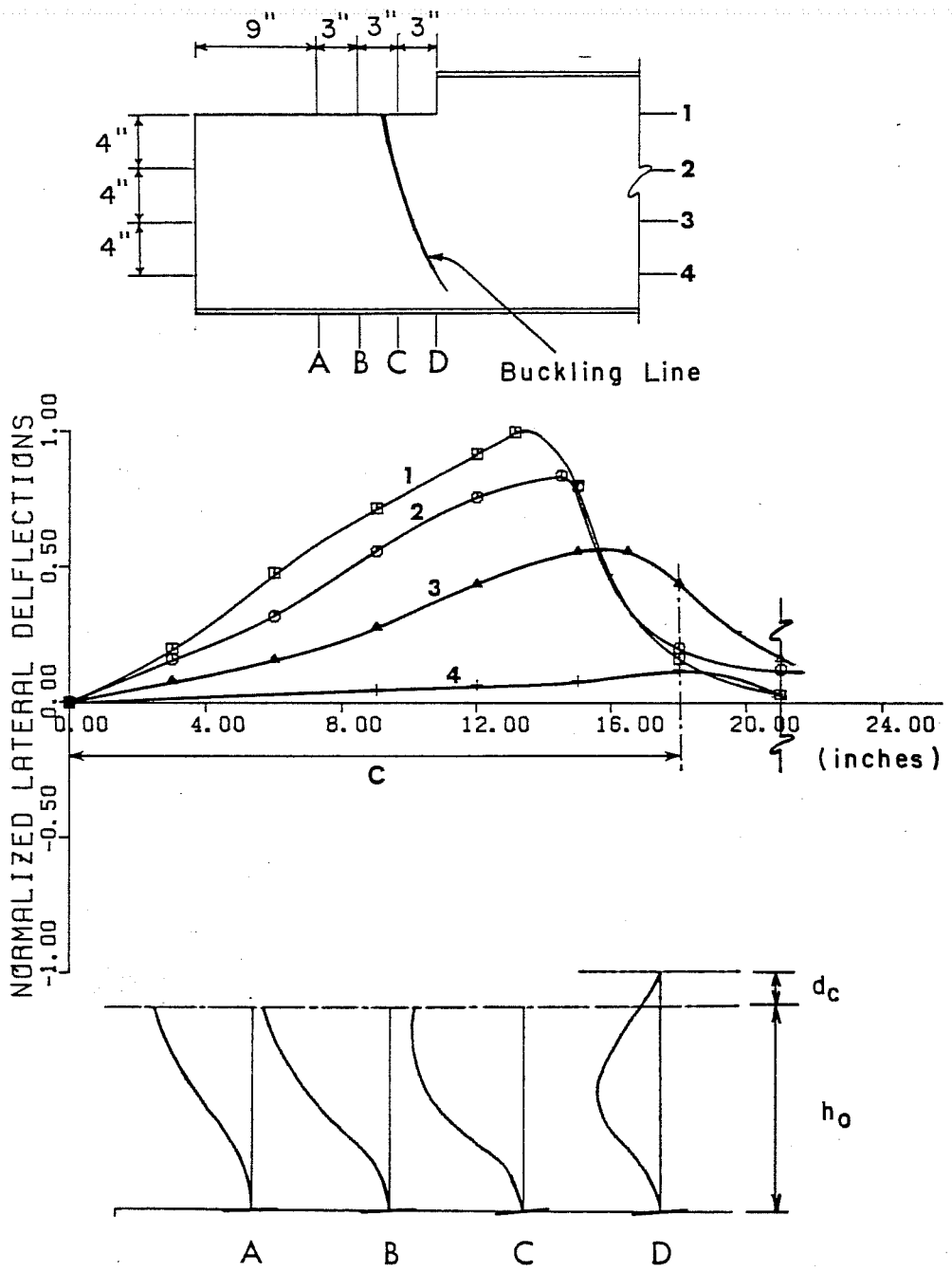

(a) Test RB 18A

Fig. 10.14 Inelastic Local Web Buckling due to Flexural Yielding

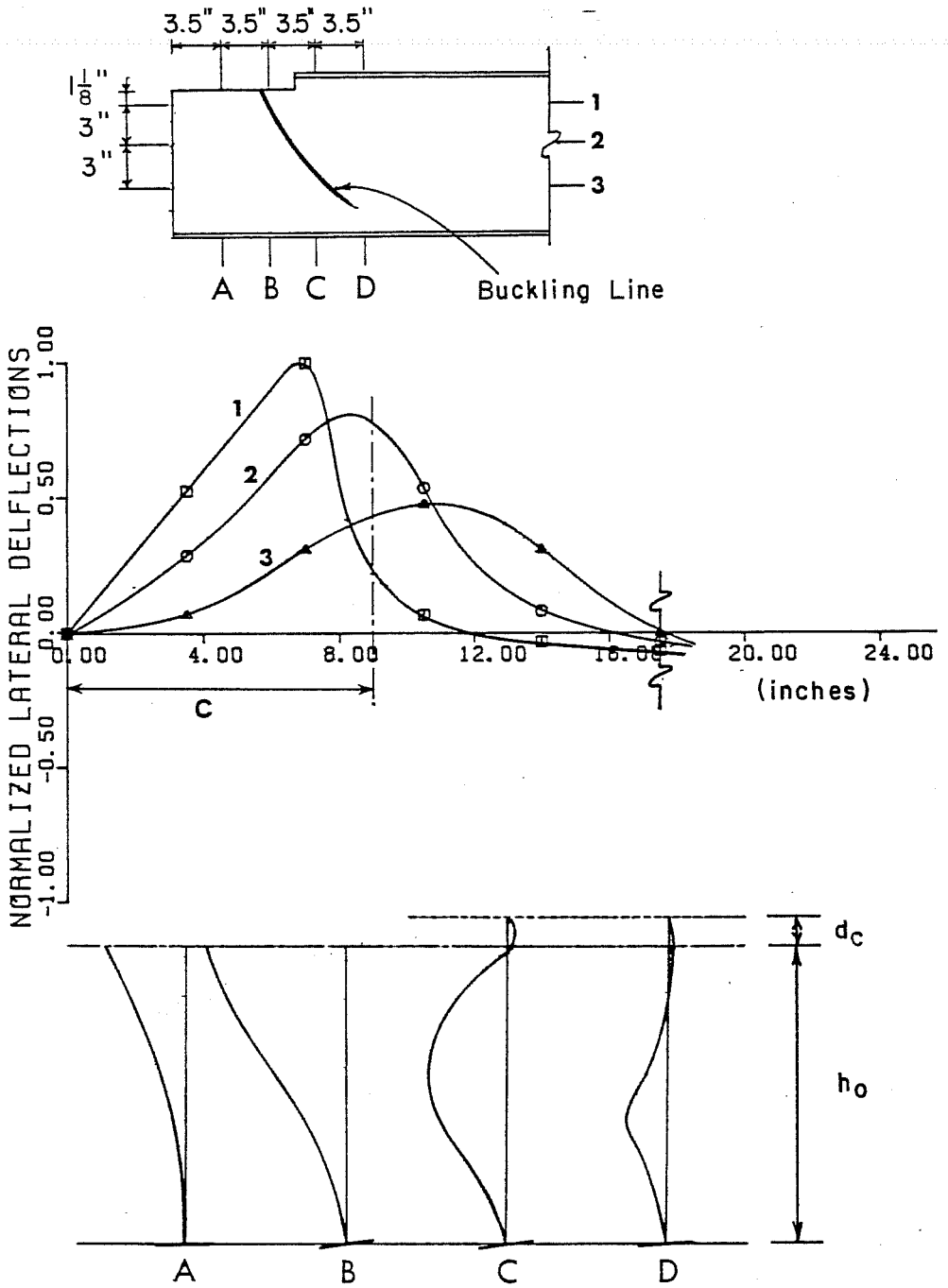

(b) Test RB12A

Fig. 10.14 (Cont'd)

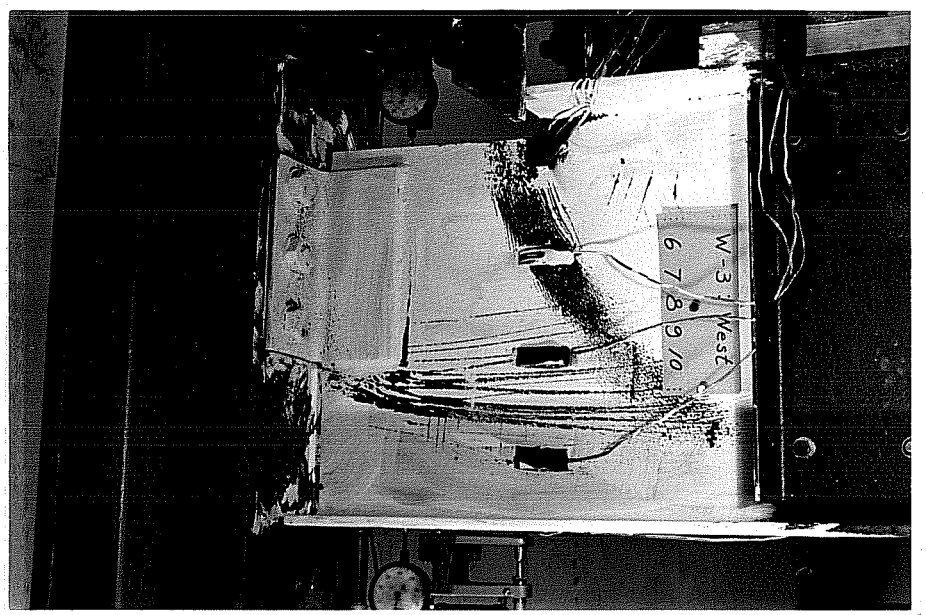

West Side

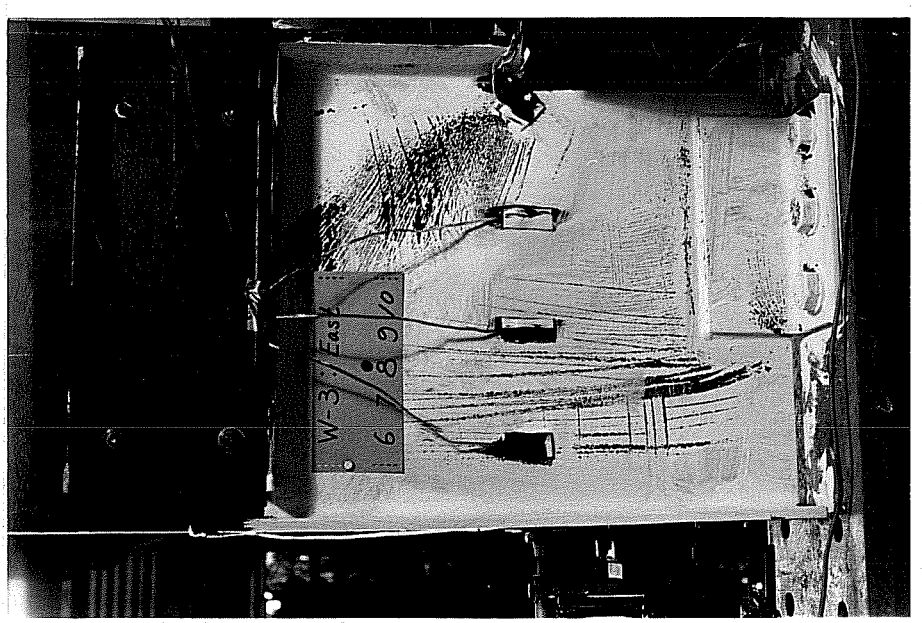

East Side

(a) Test W3

Fig. 10.15 Inelastic Local Web Buckling - Flexural Yielding

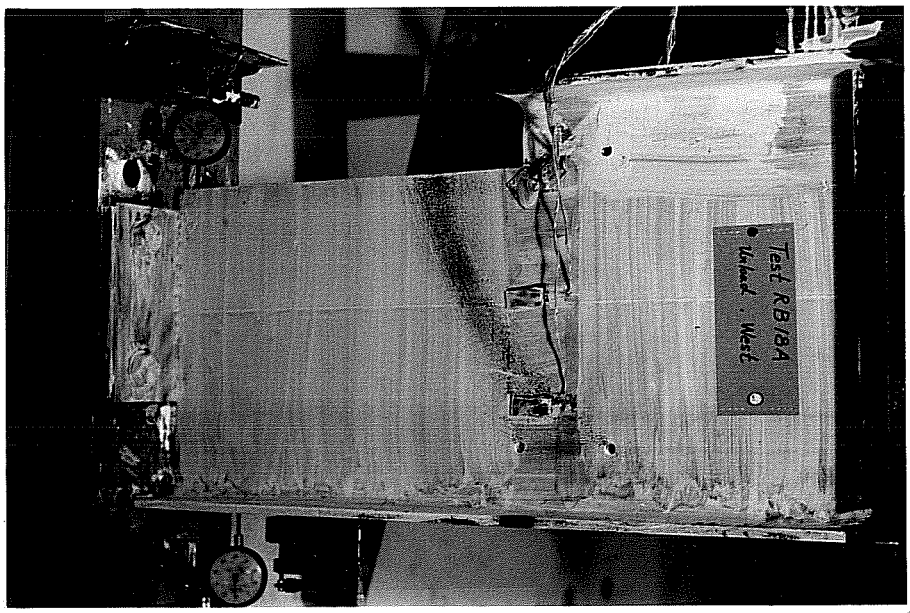

West Side

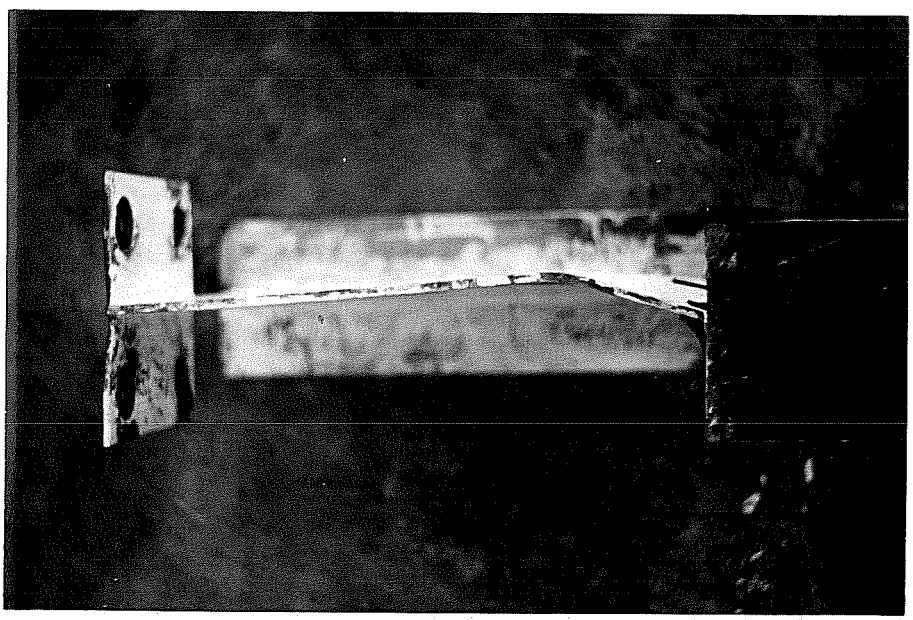

Top View after Unloading

(b) Test RB18A

Fig. 10.15 (Cont'd)

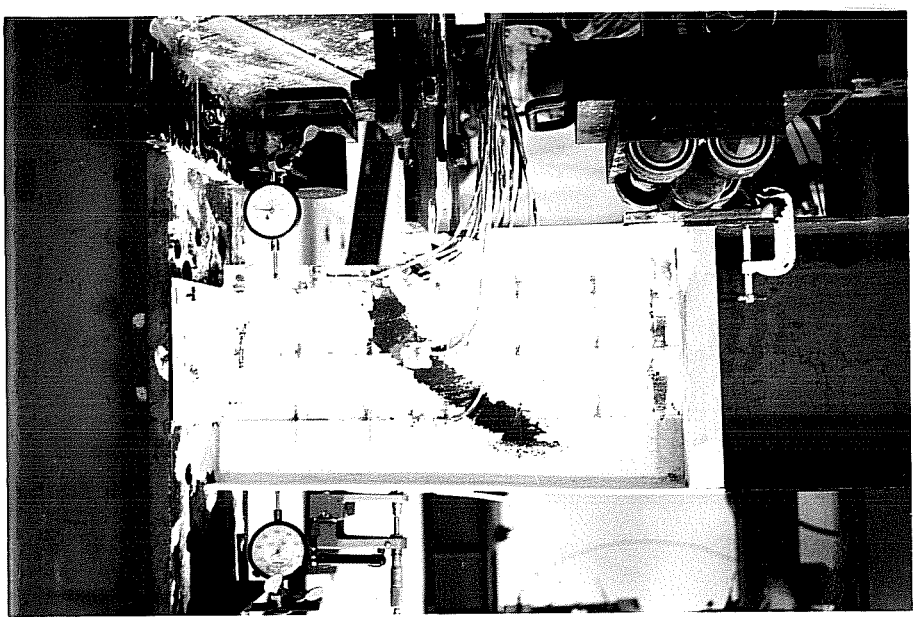

West Side

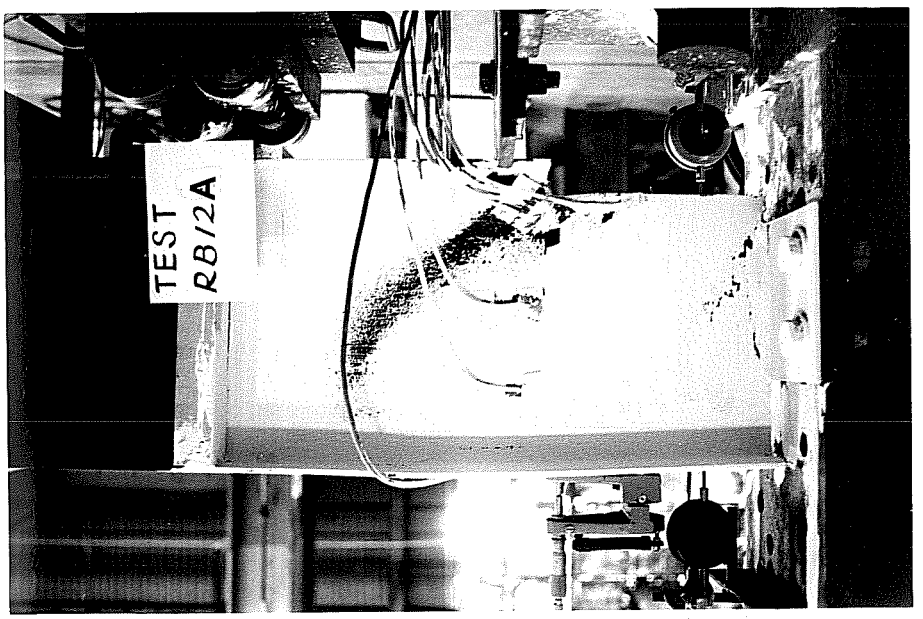

East Side

(c) Test RB12A

Fig. 10.15 (Cont'd)

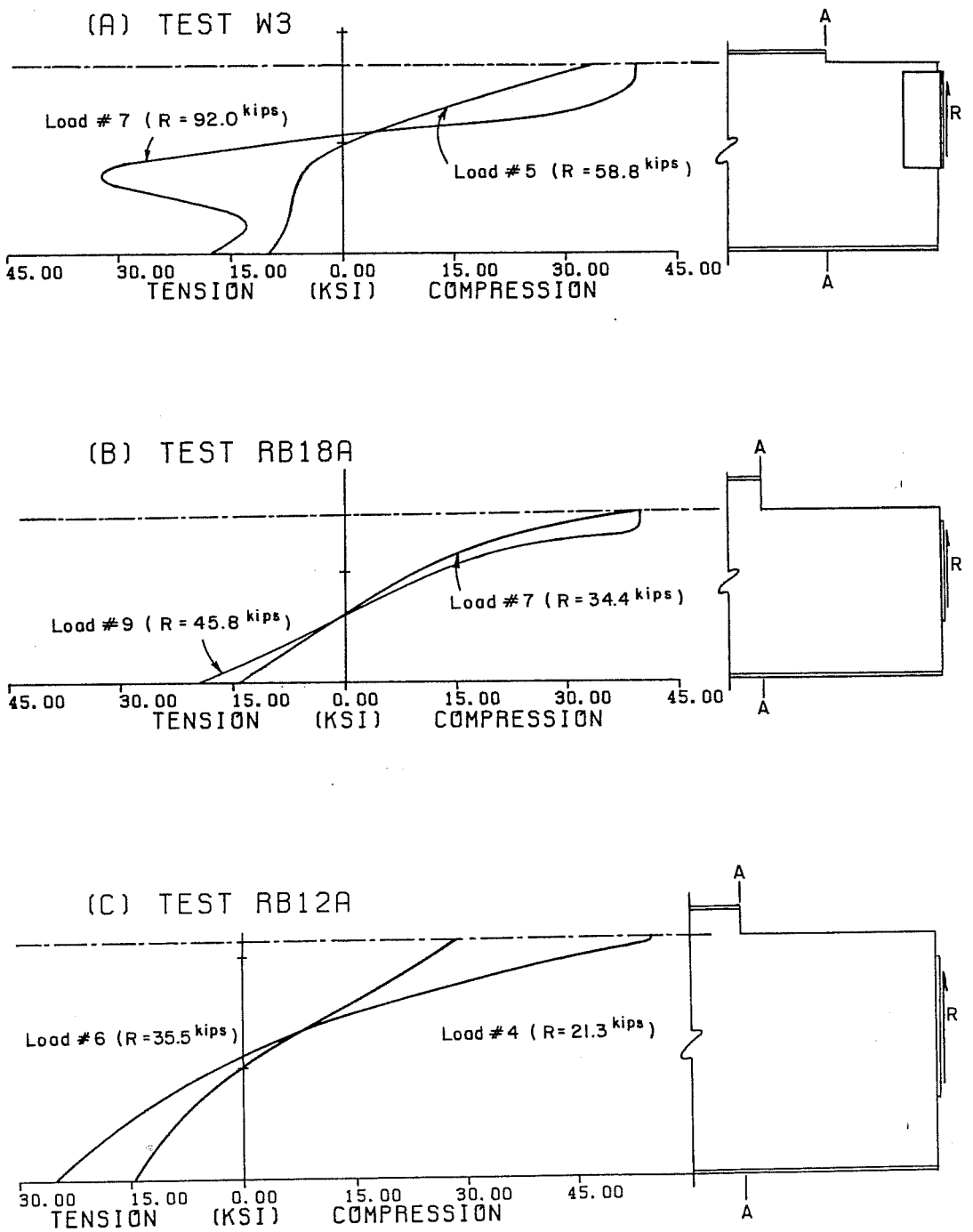

Fig. 10.16 Bending Stress Distributions of Inelastic Local Web Buckling - Flexural Yielding

the in-plane end restraint; thus, the test results agree fairly well with the flexural yield stress criterion.

Normalized buckled shapes in Fig. 10.14 are similar to those developed by BASP solutions as discussed in Sec. 8.4. The angle of the buckling line is related to the magnitude of shear effects. The data show that Test RB12A has higher shear effects than RB18A.

Figures 10.15 and 10.16 show that the clip angle connection affected the web stress distribution of Test W3 as discussed in Tests W1 and W2. However, the measured distributions at line A (Fig. 10.16) of Tests RB18A and RB12A did not appear to be affected by the end plate connections. Two load stages for each test in Fig. 10.16 were chosen as elastic and inelastic loading stages.

10.5.3 Elastic Local Web Buckling--Rolled Sections (Tests RB12B, 12C, 12D). Three W12x14 test beams with different coping details were designed to fail in the elastic local web buckling range. Figures 10.17 through 10.21 give the reaction versus deflection curves, buckling shapes, photographs and stress distributions of Tests RB12B, RB12C and RB12D. All three tests yielded very similar results. The reaction versus deflection curves (Fig. 10.17) show that the test beams behave linearly before reaching the buckling load and have very little post-buckling strength. Equation (8.2), because of the approximations in its development, predicted conservative solutions for all three tests. A more exact analysis will be discussed in the next section.

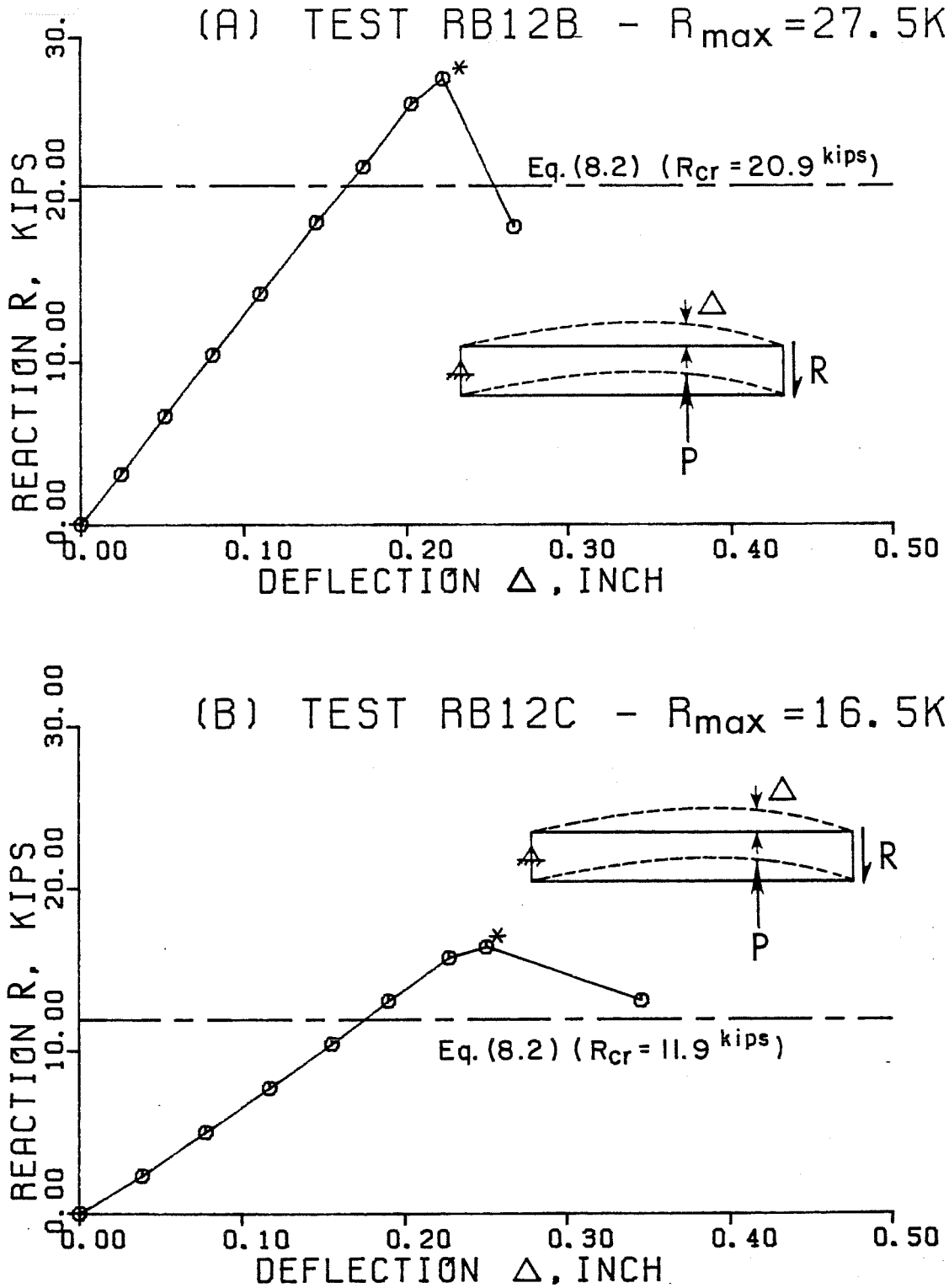

Fig. 10.17 Reaction vs Deflection Curves of Elastic Local Web Buckling - Rolled Sections

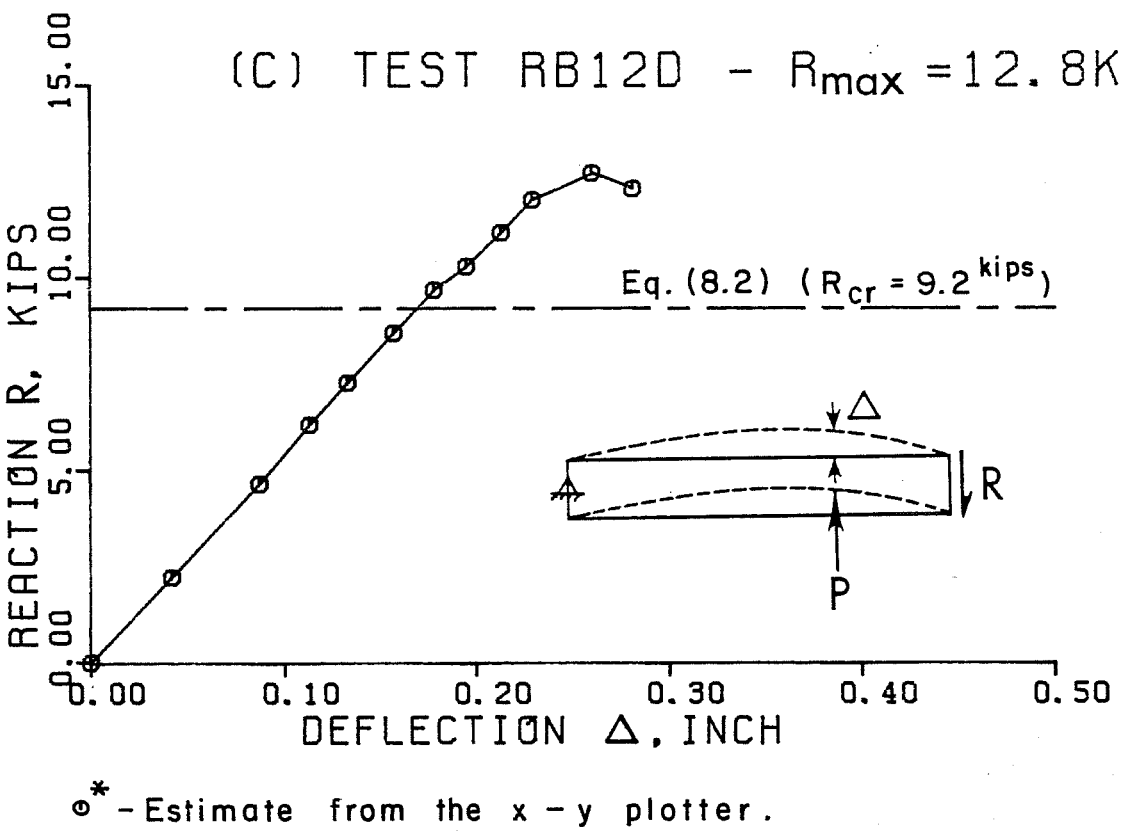

⊙* - Estimate from the x - y plotter.

Fig. 10.17 (Cont'd)

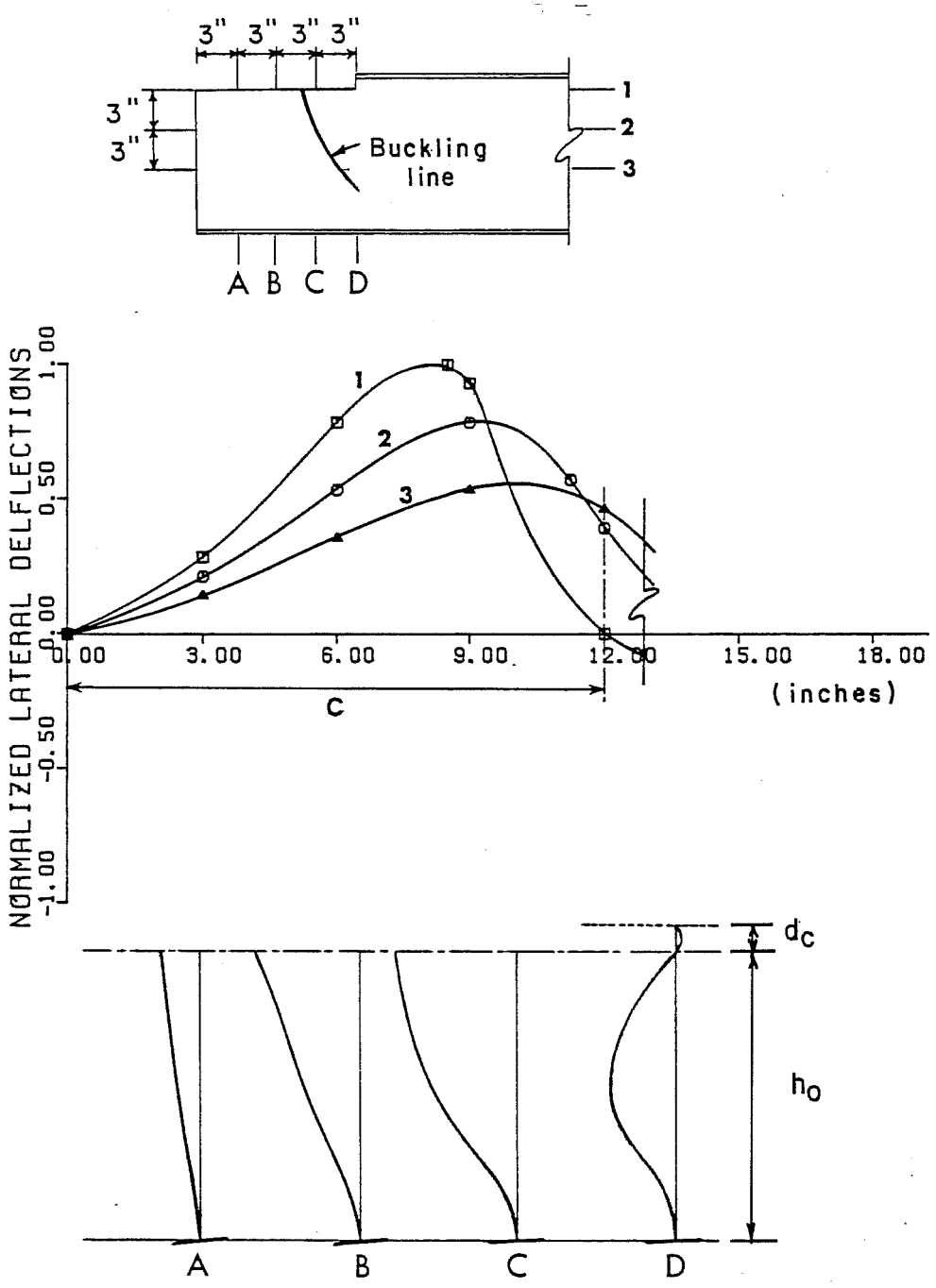

(a) Test RB 12B

Fig. 10.18 Elastic Local Web Buckling Shapes
Rolled Sections

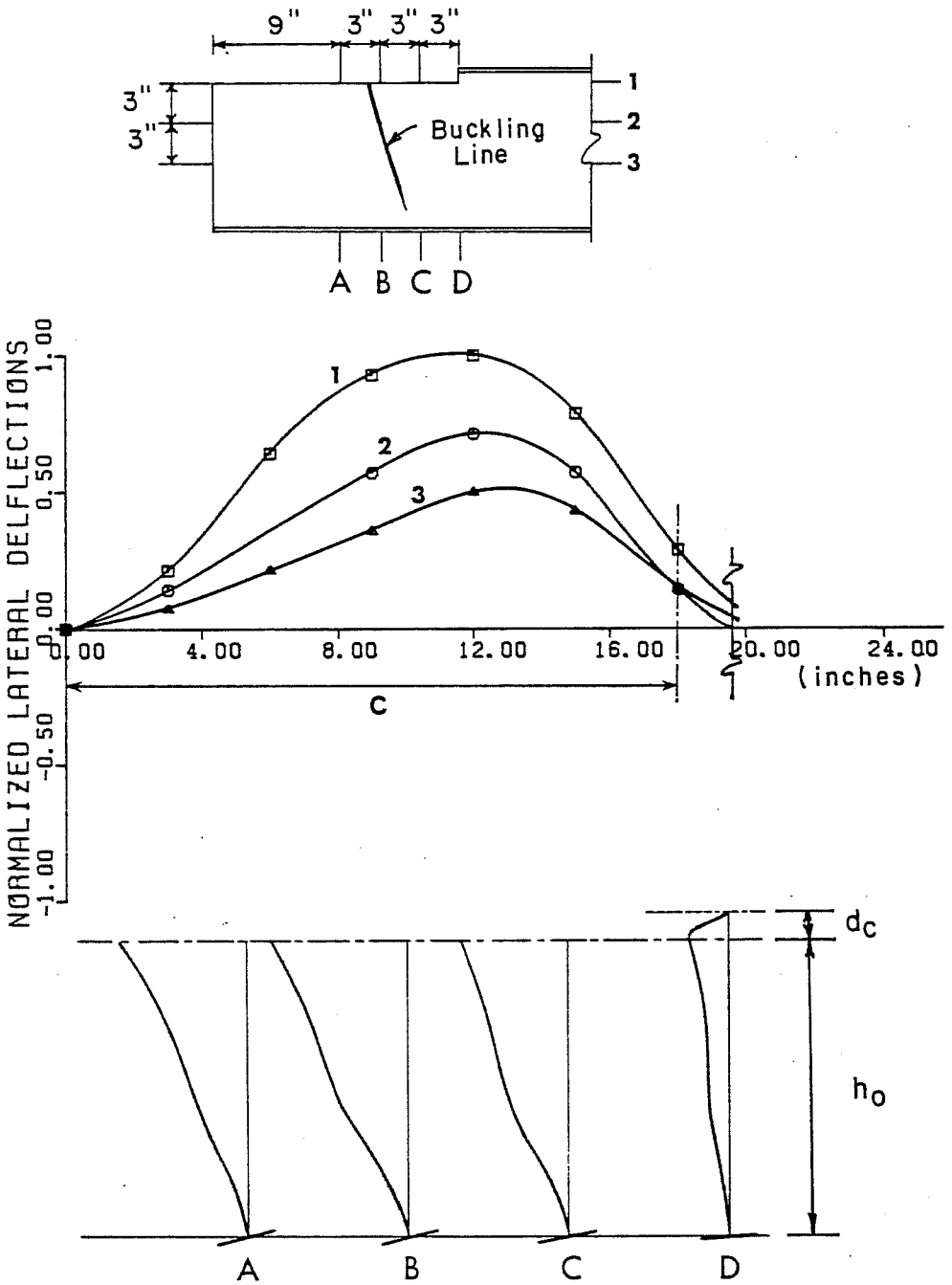

(b) Test RB 12C

Fig. 10.18 (Cont'd)

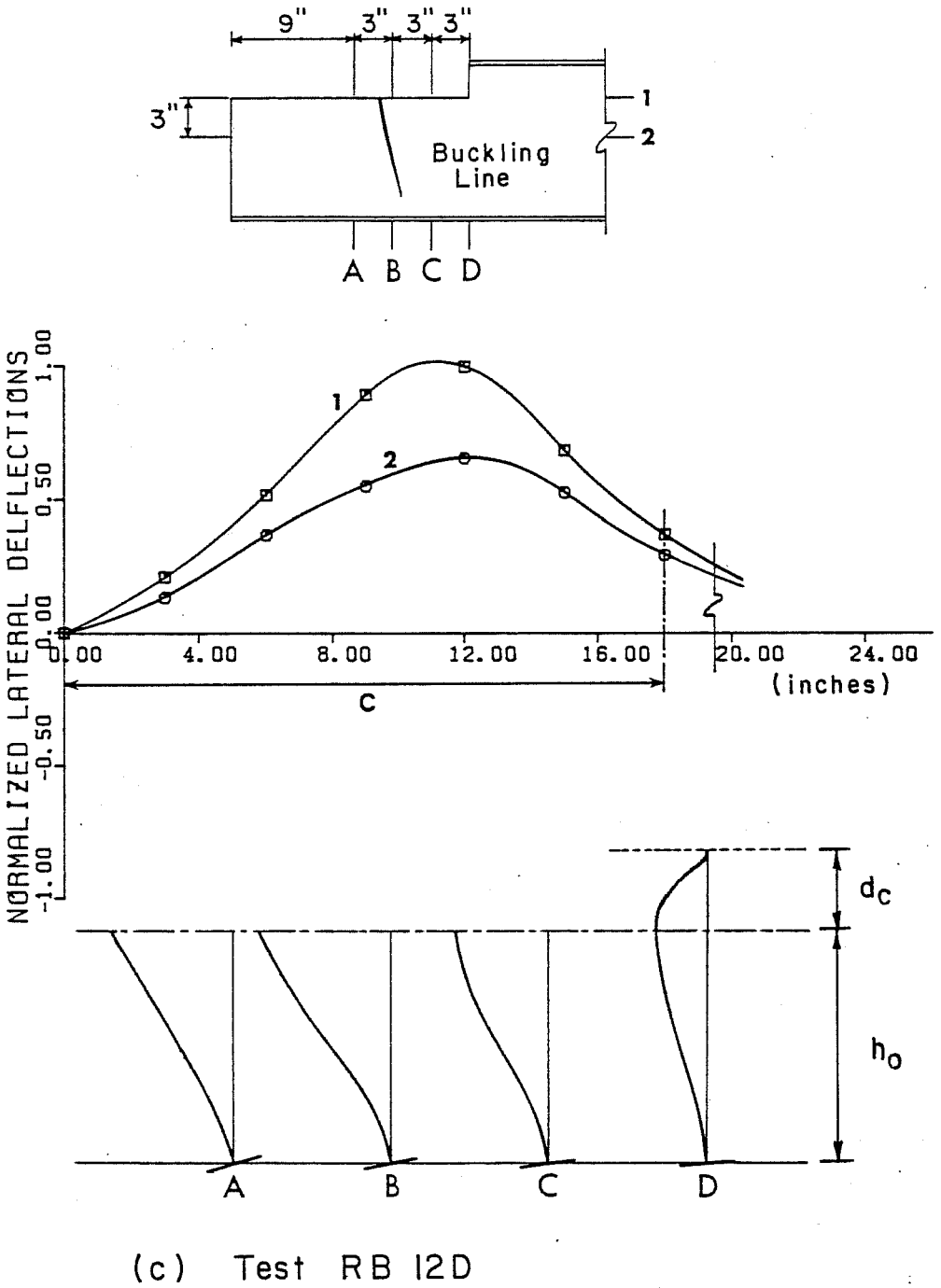

(c) Test RB 12D

Fig. 10.18 (Cont'd)

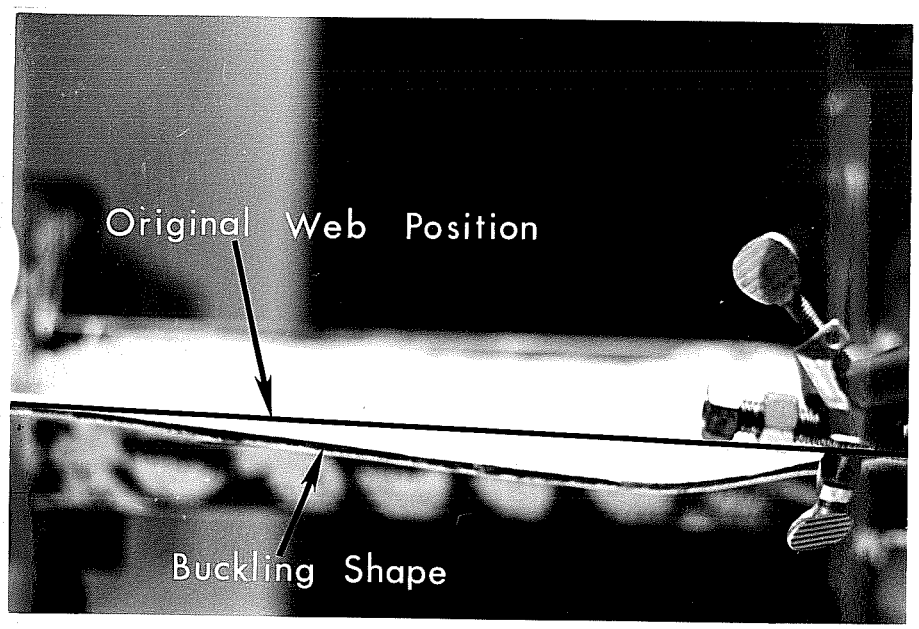

Fig. 10.19 Elastic Local Web Buckling - Rolled Sections

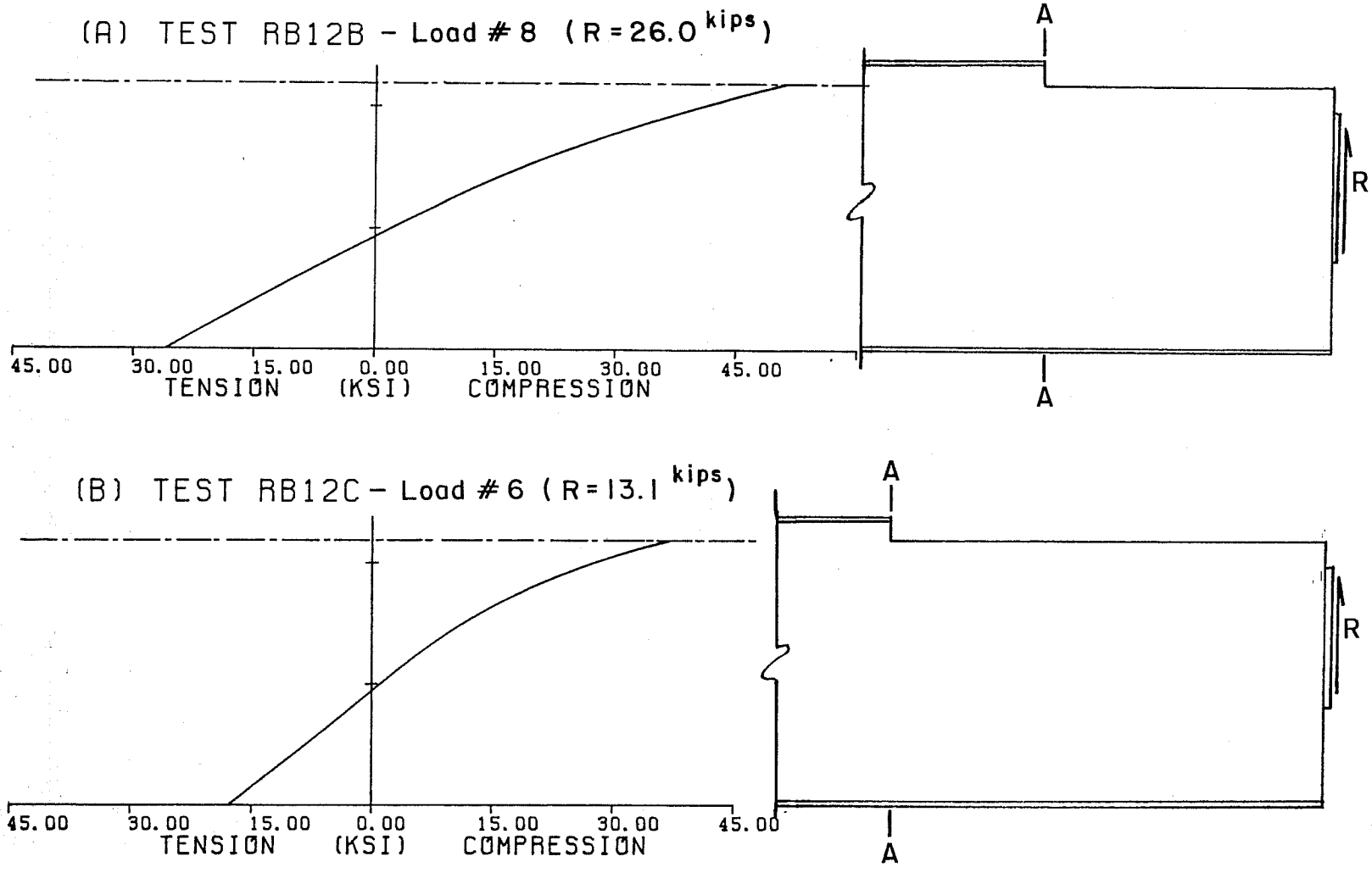

Fig. 10.20 Bending Stress Distributions of Tests RB12B and RB12C

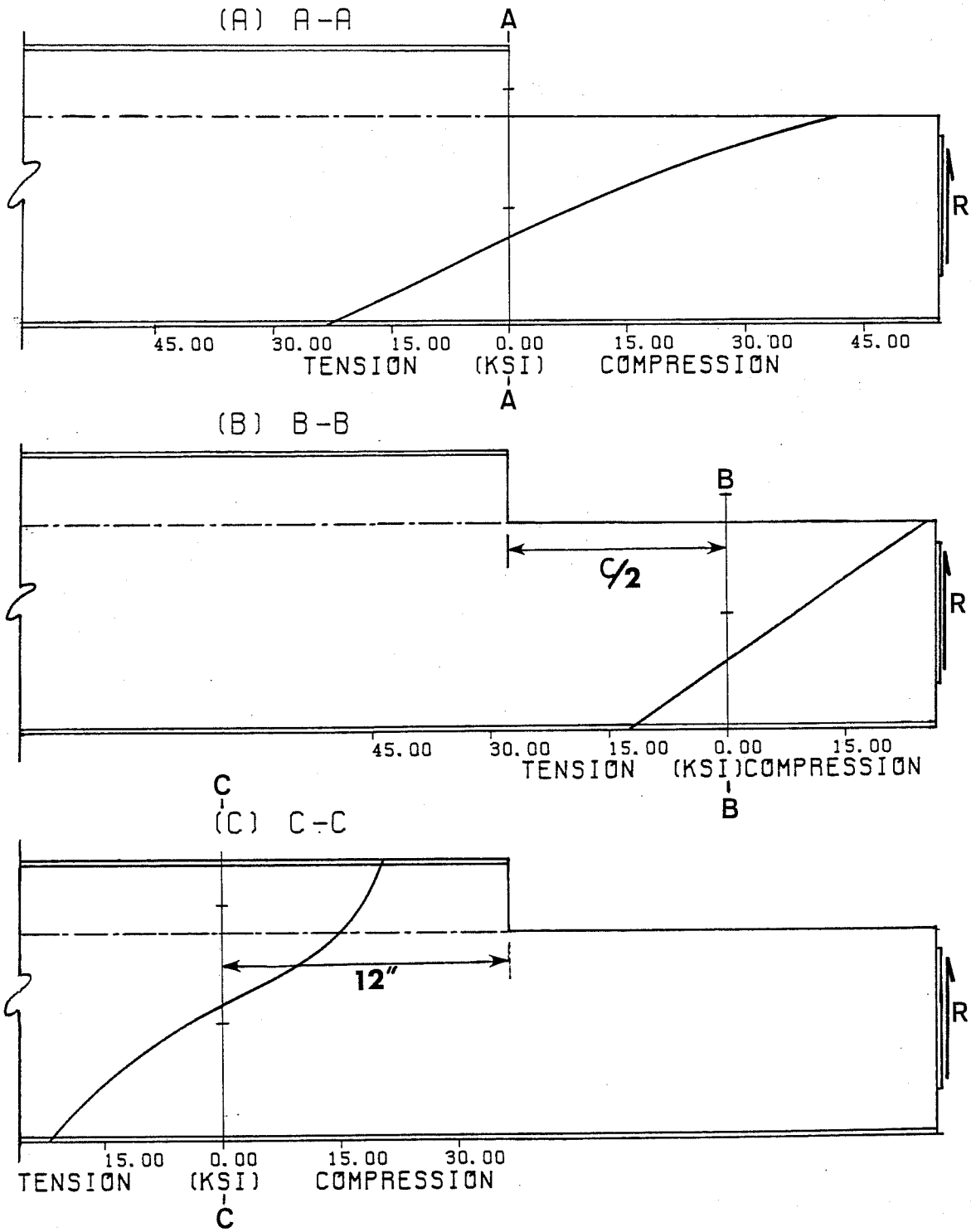

Fig. 10.21 Bending Stress Distributions of Test RB12D - Load#11 (R=12.1kips)

From Fig. 10.18 it is easy to see the effects of shear and cope depth. For short cope lengths which give the highest reaction, the inclination of the buckling line is almost 45 degrees whereas the line is vertical in Fig. 10.18(c) for the longest cope. The buckled shapes are very similar to the BASP solutions as discussed in Chapter 8 and will be further compared in the next section. Due to the similarity of the buckled shapes, only one photograph taken from Test RB12C is shown in Fig. 10.19.

Figure 10.20 shows that the stress distributions at line A are similar to typical elastic bending stress distributions as shown in Fig. 1.2. In order to provide further information, two extra sets of strain gages were placed at lines B and C for Test RB12D. The results in Fig. 10.21 show that the stress distributions at lines B and C are almost linear. In other words, the stress distribution away from the coped region follows the Mc/I distribution which confirms the theoretical study.

10.5.4 Elastic Local Web Buckling--Plate Girders (Tests PB26A and 26B). Due to the depth/thickness limitation of rolled sections, two tests were performed on thin web plate girders which allowed the beams to fail in elastic local web buckling for $c \leq d/2$. Test PB26A with $c = d/2$ was used to check Eq. (8.2). Test PB26B was designed to fail in elastic shear web buckling away from the copes instead of failing in local web buckling. The purpose of this test is to study the influence of elastic shear web buckling on local web

buckling capacity. The test results are shown in Fig. 10.22 through 10.25.

Figure 10.22 shows that Eq. (8.2) and the shear buckling formula give very conservative solutions for both tests. There are two major reasons. One is the conservative approach of Eq. (8.2) which has already been discussed. The other is the actual stress distribution as shown in Fig. 10.25. In order to reduce the effects of end restraint, a very thin and small end plate was used in the connections. Since the ratio of the cope length to the beam depth is small in these two tests, the bending stress distribution at line A (Fig. 10.25) was drastically changed from the typical bending stress distribution (Fig. 1.2). One extra set of strain gages was used in Test PB26B (Fig. 10.25) to provide further information on stresses in the coped region. Figure 10.25 indicates that the neutral axis for the actual stress distributions is very close to the top of the cope which reduces the compression area of the coped region and increases the buckling loads significantly. Test results show that Test PB26A failed by elastic local web buckling as expected. The non-linear reaction versus deflection curve of Test PB26A in Fig. 10.22 is due to a thin web with large initial out-of-flatness that caused one side of extreme fiber of web to reach yield at early load stages. Nevertheless, the localized yielding did not affect the maximum buckling capacity.

The buckled shapes of Test PB26B (Fig. 10.23) show that the failure mode is a combination of shear and local web buckling. When

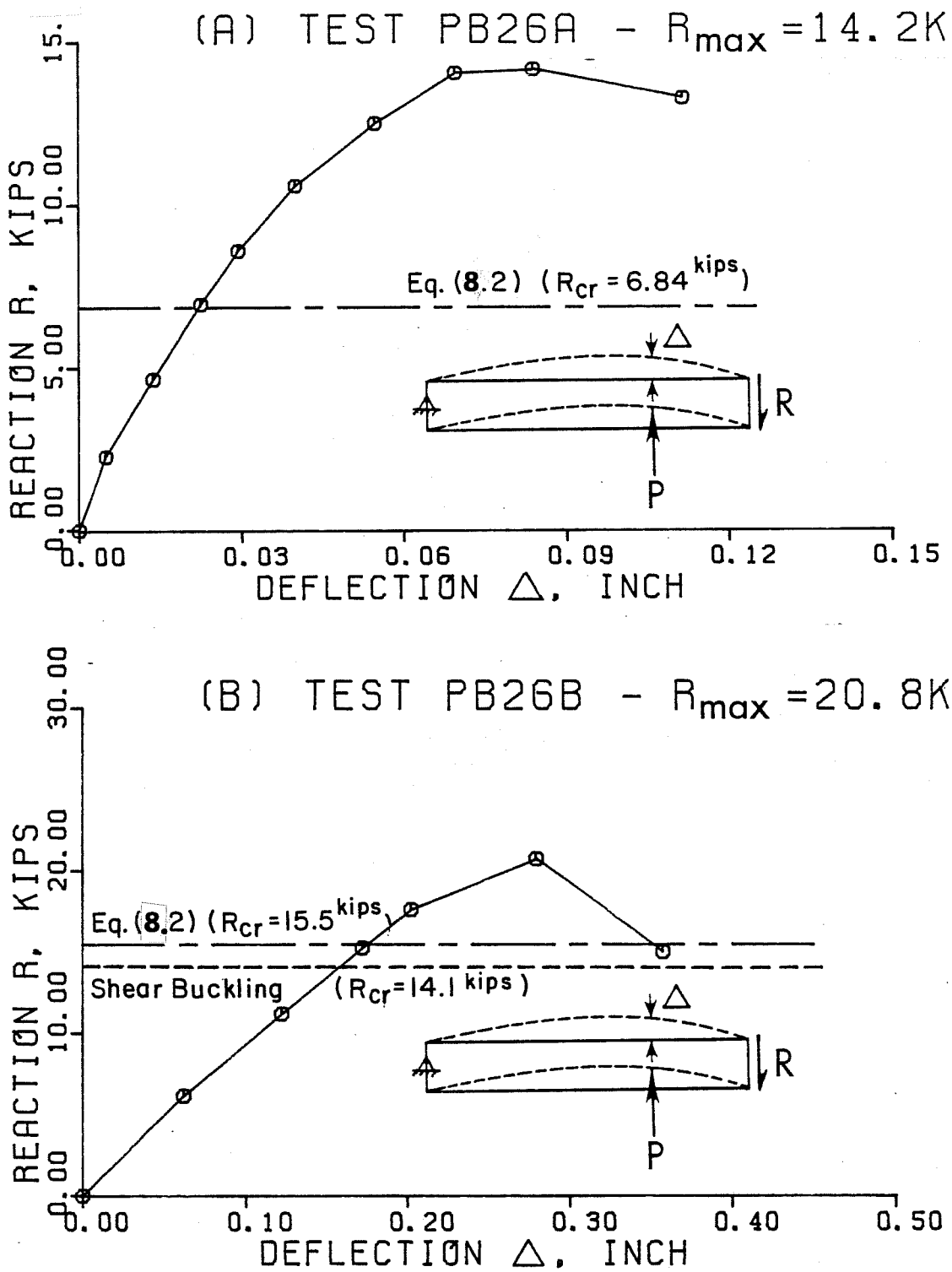

Fig. 10.22 Reaction vs Deflection Curves of Elastic Local Web Buckling - Plate Girders

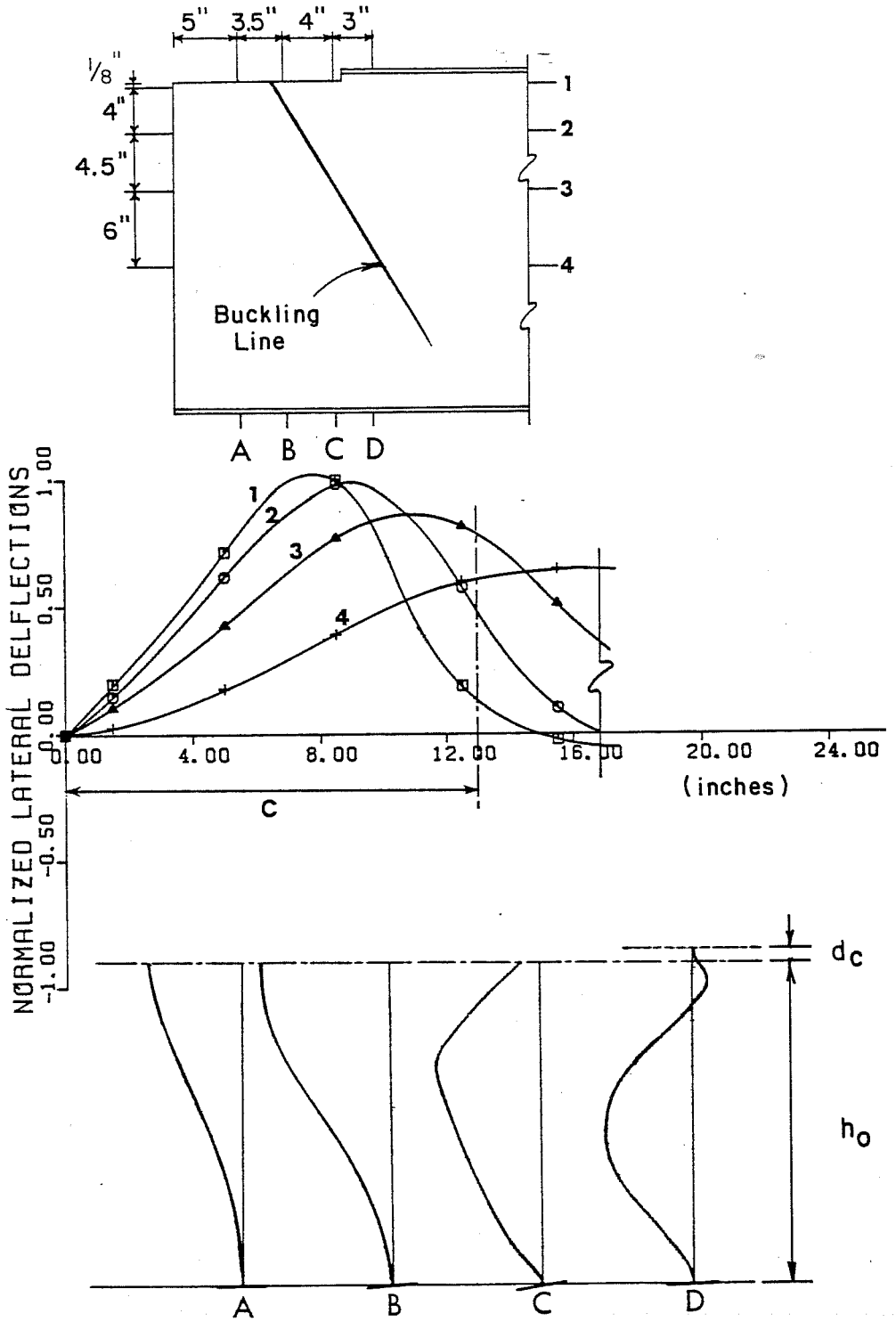

(a) Test PB26A

Fig. 10.23 Elastic Local Web Buckling Shapes - Plate Girders

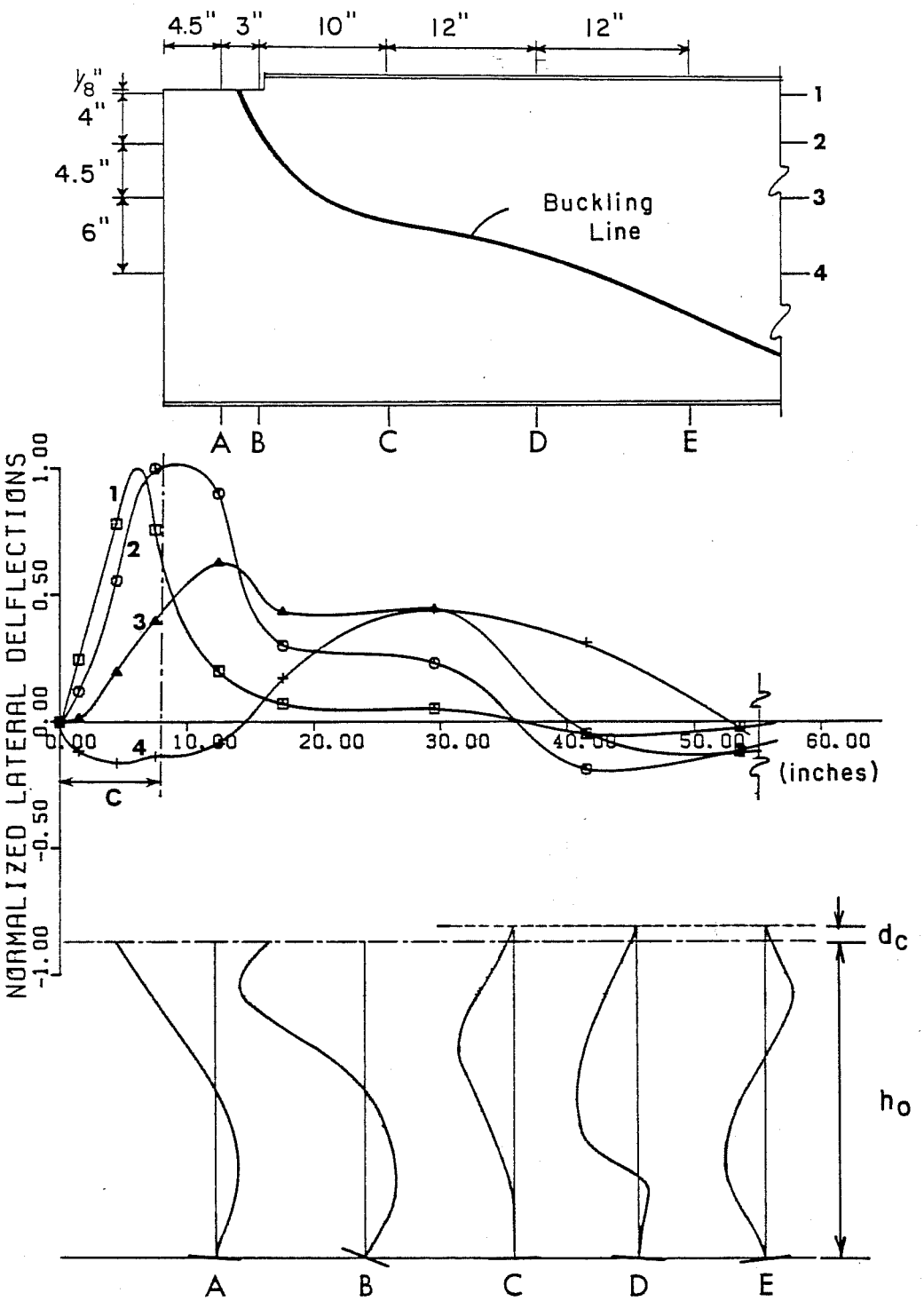

(b) Test PB26B

Fig. 10.23 (Cont'd)

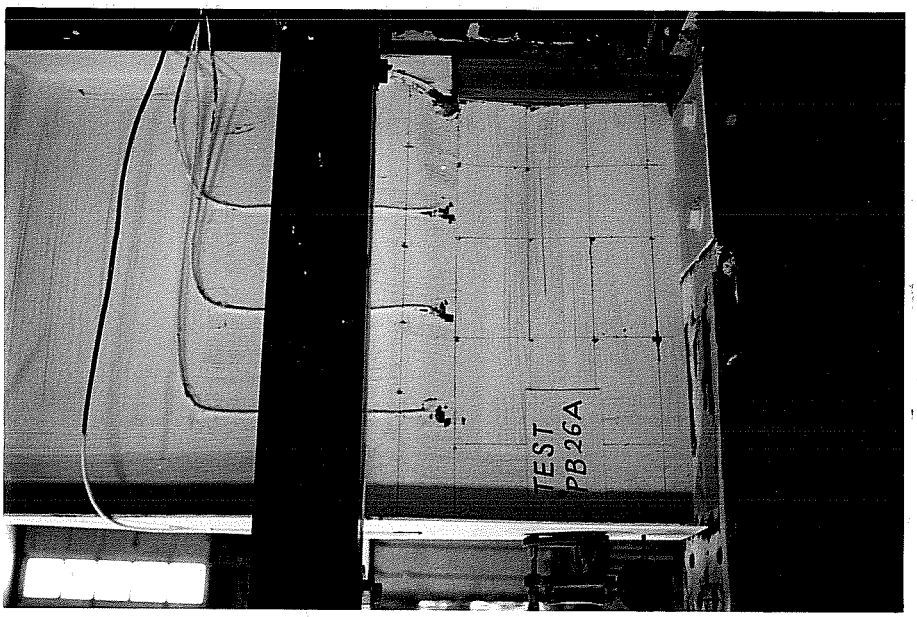

East Side

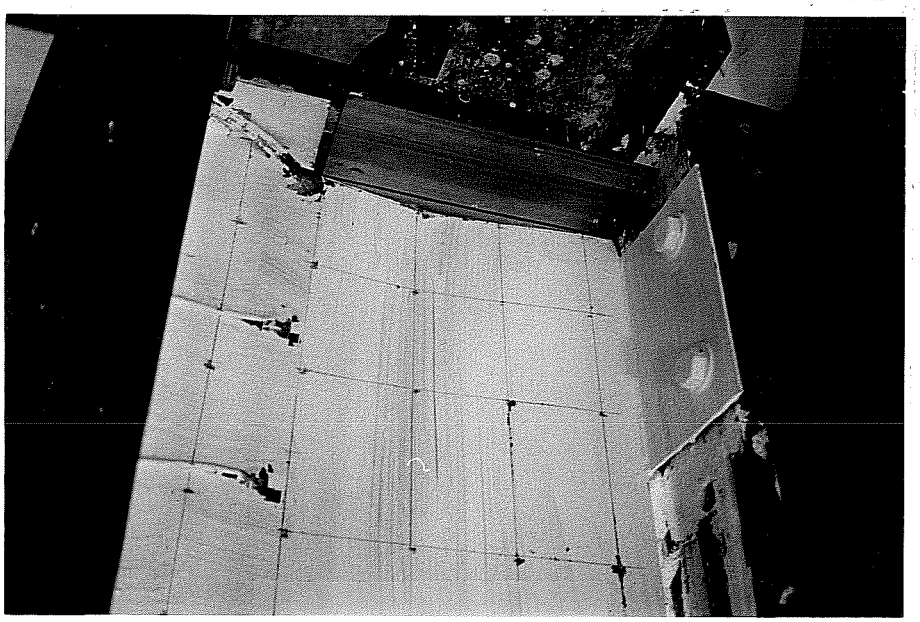

Close View of East Side

(a) Test PB26A

Fig. 10.24 Elastic Local Web Buckling - Plate Girders

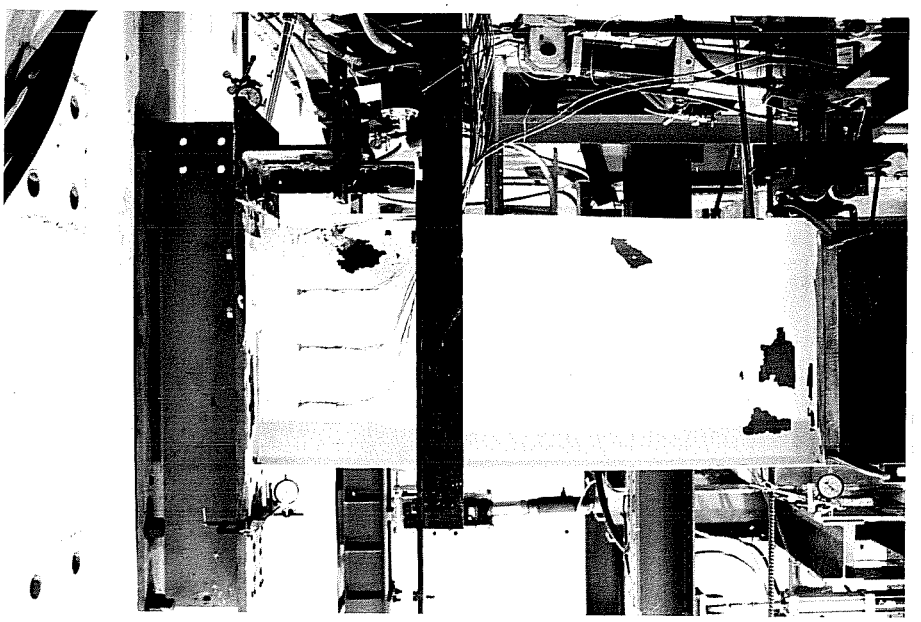

West Side

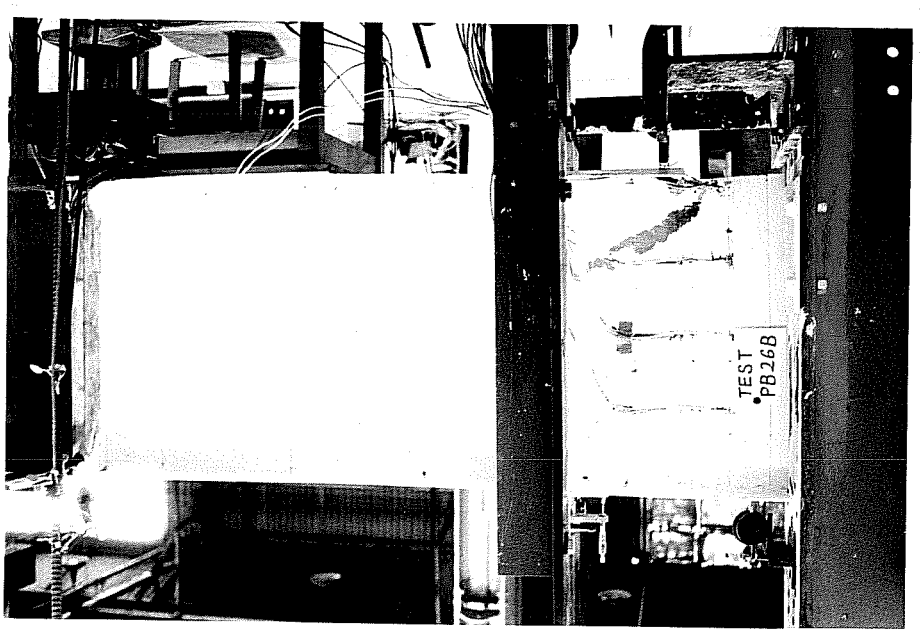

East Side

(b) Test PB26B

Fig. 10.24 (Cont'd)

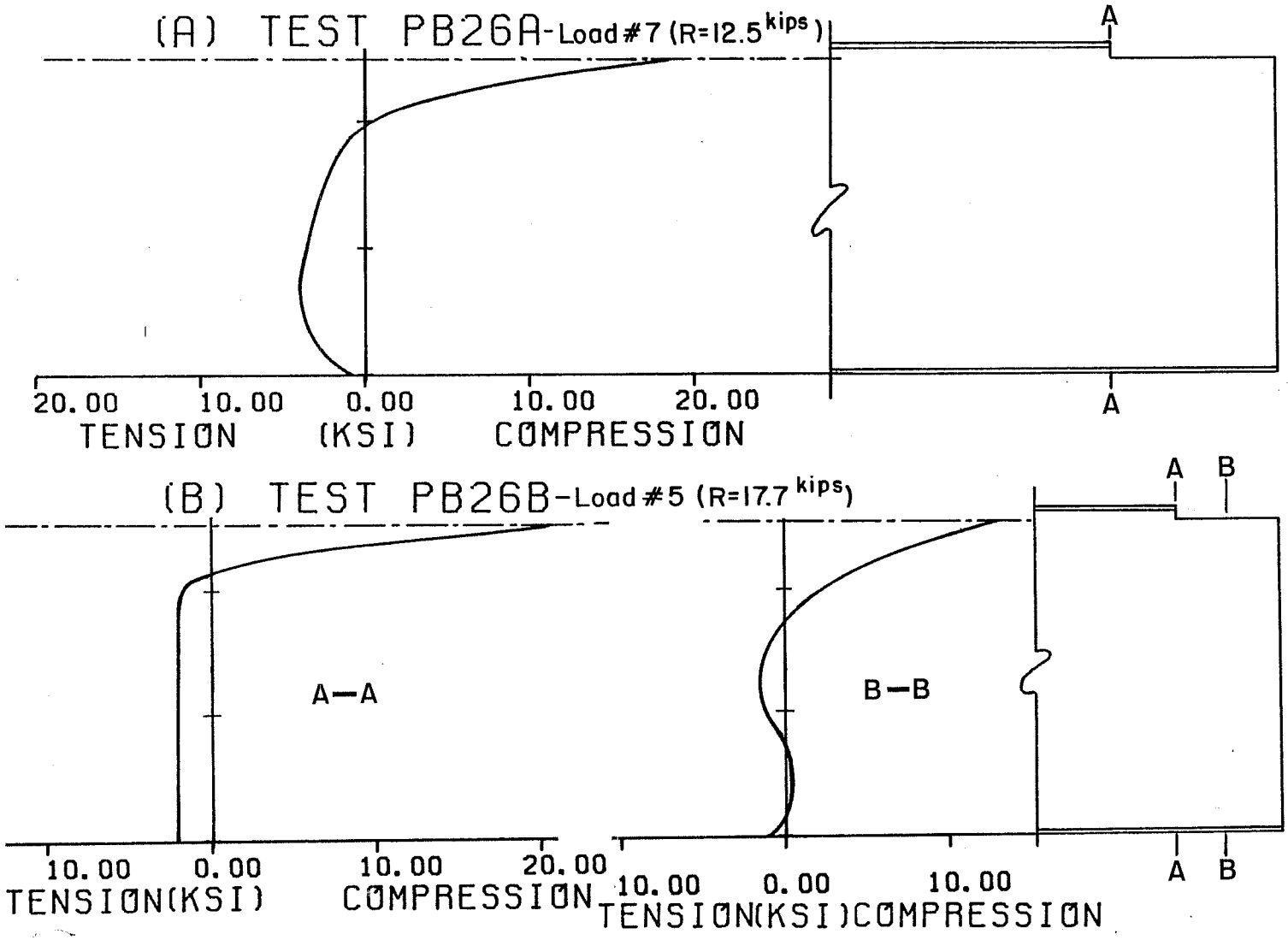

Fig. 10.25 Bending Stress Distributions of Elastic Local Web Buckling - Plate Girders

the reaction reached the shear buckling capacity, the shear panel developed tension field action which provide post-buckling strength. Finally, the reaction reached the buckling capacity of the coped region and failed in combination of shear and local web buckling modes. The flaking whitewash on the web gives a very good indication of the final failure mode (Fig. 10.24).

10.6 Discussion of Test Results

The summary of the inelastic and elastic local web buckling test results are shown in Tables 10.2 and 10.3 respectively. The results from four more tests labeled 10-4, 10-7, 18-14, and 18-15 which failed by inelastic local web buckling that were taken from another research project are also given in Table 10.2. The connection details and load-deflection curves of these later four tests are summarized in Appendix B. Web yielding strength and actual measured coping details of each test are listed in the tables. The highest measured test reactions, R_{max}, discussed in Section 10.5 are used for primary comparison.

The reactions which cause theoretical first yield in bending, R_y, and shear, R_{vy}, are listed in Table 10.2, and the design recommendation, R_{Design}, which is underlined, is the lower value of these two reactions. In order to further check the reliability of the analysis programs and the design recommendation, R_{Design}, two computer analyses were done on models from each of the specimens that failed by flexural yielding. One analysis used the design model

TABLE 10.2 Summary and Comparison of Inelastic Local Web Buckling Test Results

Test No.	Section	F_y (Web) (ksi)	Coping Details	R_{max} (kips)	R_y (kips)	R_{vy} (kips)	$\frac{R_{max}}{R_{Design}}$*	$\frac{R_{max}}{(R_{Design})_{ABAQUS}}$	$\frac{R_{max}}{R_{ABAQUS}}$	$\frac{R_{max}}{App.\ C}$**
W-1	W18x35	39.4	c = 3.5" d_c = 1.25"	115.2	229.6	<u>110.3</u>	1.04	---	---	1.28
W-2	W18x35	39.4	c = 6.5" d_c = 1.25"	111.5	123.6	<u>110.3</u>	1.01	---	---	2.30
W-3	W18x35	39.4	c = 10.0" d_c = 1.25"	99.0	<u>80.4</u>	110.3	1.23	---	---	3.15
RB18A	W18x35	39.4	c = 18.0" d_c = 3.06"	46.5	<u>36.3</u>	102.2	1.28	1.21	1.01 (e=5.1")	2.69
RB12A	W12x14	55.3	c = 8.9" d_c = 1.25"	37.9	<u>35.4</u>	71.9	1.07	1.10	1.10 (e=0.1")	3.05
10-4	W10x22	50.3	c = 8.0" d_c = 1.17"	47.0	<u>31.8</u>	63.3	1.48	1.39	0.99 (e=3.2")	2.37
10-7	W10x22	50.3	c = 5.0" d_c = 1.75"	59.0	<u>44.7</u>	60.1	1.32	----	----	1.90
18-14	W18x60	36.5	c = 8.0" d_c = 1.5"	150.7	<u>137.7</u>	140.0	1.09	----	----	1.52
18-15	W18x60	36.5	c = 5.0" d_c = 1.5"	164.2	220.3	<u>140.0</u>	1.17	----	----	1.04

* R_{Design} = lower load of bending yield (R_y) and shear yield (R_{vy}), shown underlined.

** App. C = buckling load calculated by App. C design approach without F.S.

which assumes no end restraints in coped connections and the buckling load obtained is defined as $(R_{Design})_{ABAQUS}$. The other used the test model which included the in-plane (end moment) end retraint calculated from actual test results. The end moment taken from the load stage before buckling was converted to an eccentricity "e" by dividing it by the reaction at the connection. The eccentricity "e" of each test was used in the analysis and listed in Table 10.2. Out-of-plane restraint was not included in the analysis. However, a thicker web was used for bolted or welded connections in determining the critical reaction. The buckling reaction of the second model is defined as R_{ABAQUS}. Since the entire web cross section is assumed to reach yield when shear yielding controls, the analysis was not performed for tests that failed in shear yielding or where the maximum load was within 15 percent of the shear yielding reaction. The current design method, based on Appendix C of the AISC Specification, is also presented in Table 10.2 for comparison. It should be noted that the AISC Detailing Manual design approach which is not shown in Table 10.2 yields the same results as R_{Design} for inelastic local web buckling. The buckled shapes of the top coped line of the R_{ABAQUS} solutions along with test results for Test RB12A are plotted in Fig. 10.26. The results from both analyses and the test results yield very similar buckled shapes.

In Table 10.2, both the shear and bending yield criteria give conservative solutions compared to the test results. When shear yielding controls, the predictions are close to the maximum reaction

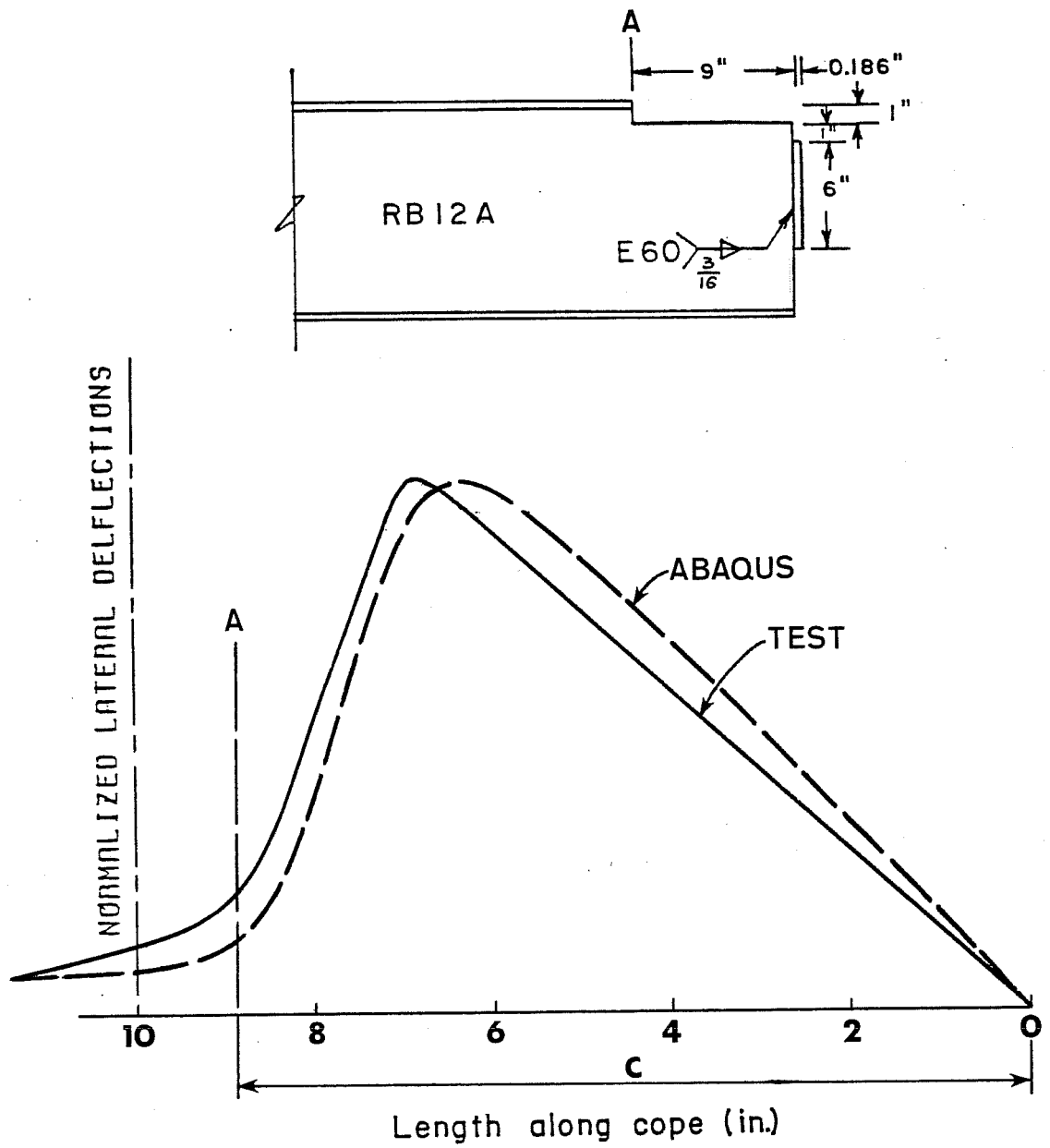

Fig. 10.26 Comparison of the Coped Line Buckled Shapes of Test RB12A with ABAQUS Results

recorded with an average ratio of test over design recommendation equal to 1.07. The good correlation is due to the fact that after the entire coped region reached shear yield, there was little post-buckling strength regardless of the types of connection. It also indicates that the localized yielding due to stress concentration will not reduce the inelastic local web buckling strength. The accuracy of the design recommendation for cases when bending yield controls depends on the magnitude of the end restraints. In-plane end restraint will reduce the bending stress at the copes and out-of-plane restraint will increase the buckling capacity of the coped region. In addition, the bending yield stresses are more localized, thus providing more opportunity for redistribution which can be seen from the stress distributions shown in Fig. 10.16. Thus, the bending yield criterion always yielded conservative results with an average R_{max}/R_{Design} = 1.245 and a range of 1.07 - 1.48. However, R_{Design} agrees fairly well with $(R_{Design})_{ABAQUS}$ which also has no end restraints. R_{ABAQUS}, which included eccentricity, shows good correlation with the test results R_{max}. As expected, Appendix C's design approach gives very conservative results, especially when the cope length is long.

Table 10.3 summarizes the results of tests where failure occurred by elastic local web buckling. The same definitions given in Table 10.2 are used in Table 10.3 except $(R_{Design})_{BASP}$ and R_{BASP} are both determined by the elastic buckling program BASP and R_{Design}

TABLE 10.3 Summary and Comparison of Elastic Local Web Buckling Test Results

Test No.	Section	F_y (web) (ksi)	Coping Details	R_{max} (kips)	$\frac{R_{max}}{R_{Design}}$	$\frac{R_{max}}{(R_{Design})_{BASP}}$	$\frac{R_{max}}{R_{BASP}}$	$\frac{R_{max}}{\text{Detail Manual}^{**}}$	$\frac{R_{max}}{\text{App. C}^{**}}$
RB12B	W12x14	54.9	c = 12" d_c = 1.13"	27.8	1.33	1.02	0.96 (e=0.4")	1.01	2.80
RB12C	W12x14	54.9	c = 18.1" d_c = 1.0"	16.8	1.44	1.24	0.98 (e=2.1")	0.90	2.56
RB12D	W12x14	55.3	c = 17.9" d_c = 3.13"	12.9	1.40	1.16	1.15 (e=0.1")	1.00	1.95
PB26A	h/t_w = 26/0.132 = 197.0	59.4	c = 13.1" d_c = 1.13"	14.1	2.06	1.60	1.58 (e=0.1")	0.16	4.51
PB26B	h/t_w = 197.0	59.4	c = 8.16" d_c = 0.91"	20.8	1.48*	1.32*	1.32* (e=0.1")	0.15	4.17

* Critical load controlled by elastic web shear buckling away from copes.

** Buckling loads calculated by Detail Manual and App. C design approaches without F.S.

is calculated by Eq. (8.2). The coped line buckled shapes of Test RB12C are compared with R_{BASP} results in Fig. 10.27, which shows very similar buckled shapes.

Due to the conservative nature of Eq. (8.2), R_{Design}, the web buckling model as shown in Fig. 8.1 was analyzed using the BASP program to obtain exact solutions for comparison. For the rolled section tests, $(R_{Design})_{BASP}$ gives reasonable and conservative solutions. The conservative results can be contributed to the end restraints of the connections. R_{BASP}, which included eccentricity, shows better agreement with the test results. As discussed in Section 10.5, the BASP solutions yield very conservative results for the two plate girder tests. The major reason is due to the fact that the short end plate connections cause the neutral axis for the actual stress distributions to be close to the top of the cope, not the bottom flange, which increases the post-buckling strength of the test beams significantly. However, the BASP solutions always give conservative results. The AISC Detailing Manual design approach gives very good results for the rolled section tests because the buckling loads of all three tests are very close to the yield loads. For thin web plate girders, the AISC Detailing Manual approach gives very unconservative solutions. Again, Appendix C's design method underestimates the ultimate capacity of the coped beams. It should be noted that for coped beams with the same cope length, Appendix C's approach yields higher buckling loads as the cope gets deeper as shown for Tests RB12C and RB12D.

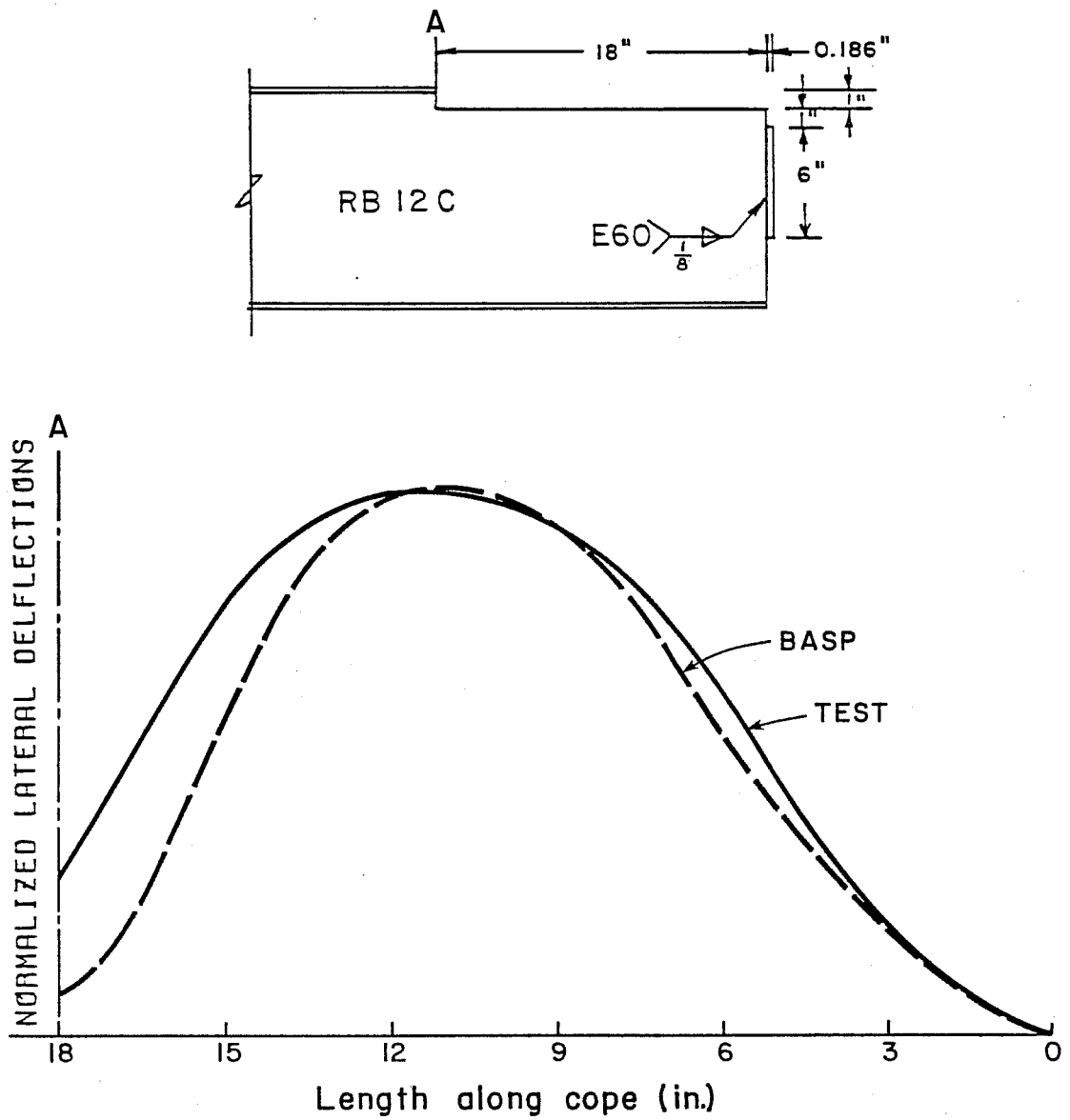

Fig. 10.27 Comparison of the Coped Line Buckled Shapes of Test RB12C with BASP Results

CHAPTER 11

REINFORCEMENT AND OTHER DETAILS

11.1 Reinforcement

Coping can cause local web buckling and decrease the capacity of beams significantly especially for the long and deep copes and the thin web plate girders. The capacity can be increased by using a thicker web. In some instances this may be expensive, so it may be more practical to reinforce the web to increase the capacity at the cope. The purpose of this section is to develop recommendations for various types of reinforcing details that can control web buckling. Because the behavior of the reinforced top and double flange coped beams are similar, only the top flange coped beam results will be shown and discussed.

Three types of reinforcement as shown in Fig. 11.1 were chosen in this study. Type A uses a horizontal stiffener at the top of the cope, Type B is similar to Type A but has a vertical stiffener at the end of the cope and Type C uses doubler plates. The BASP program was used to determine the buckling loads. A W16x26 section with maximum top flange copes ($c = 2d$, $d_c = d/2$) is used to illustrate the behavior of Type A reinforcement. Cope line buckling shapes for three different length stiffeners (Fig. 11.2) show that the concentrated load in the stiffeners cause a web crippling type failure and the reinforcing stiffeners deflect in a rigid-body

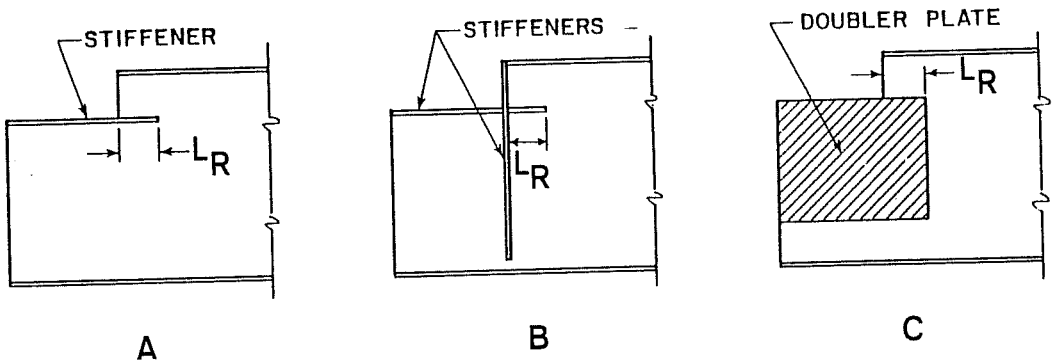

Fig. 11.1 Types of Web Reinforcement

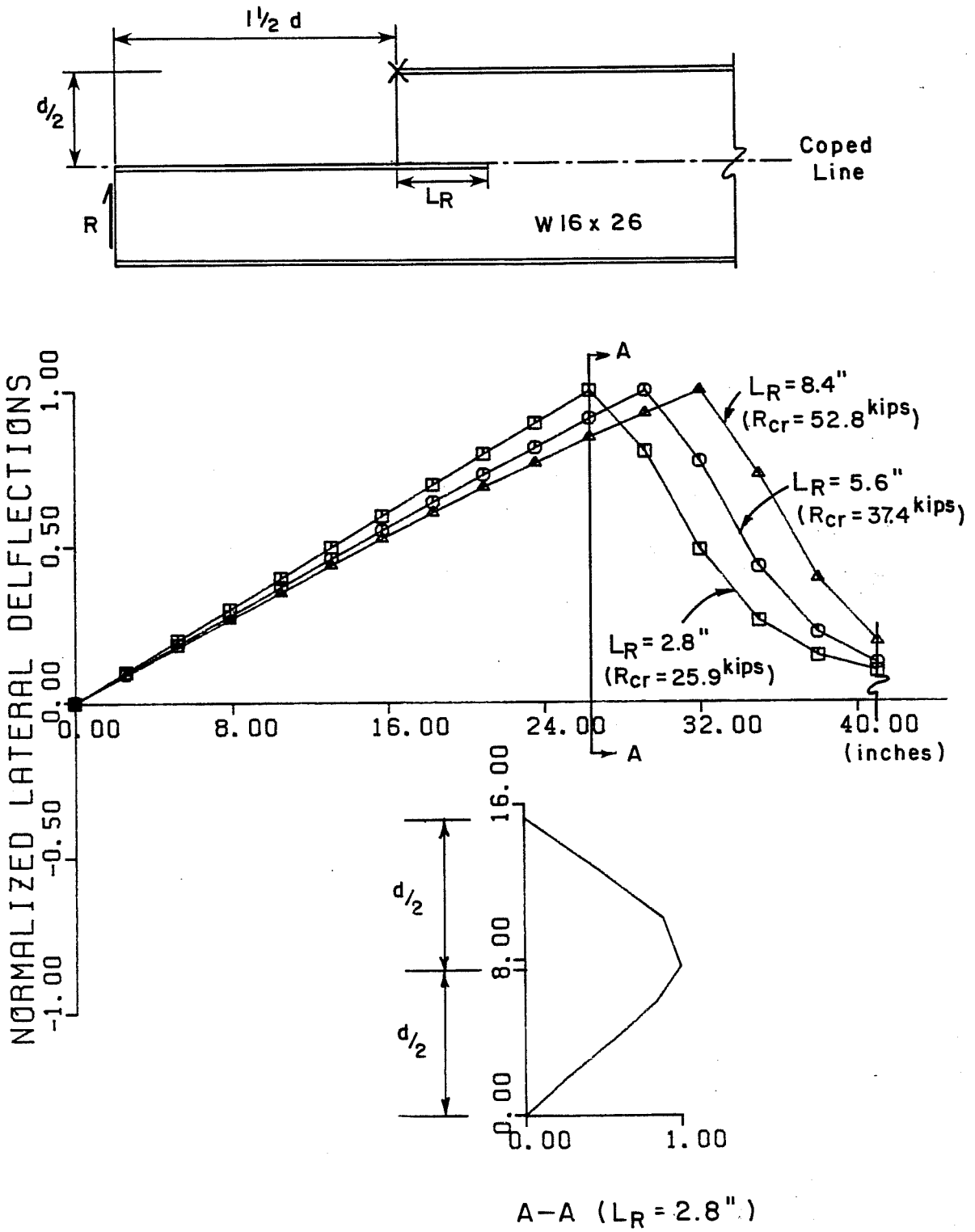

Fig. 11.2 Buckled Shapes of Type A Reinforcement

motion. However, the longer the stiffener is, the higher the buckling load. If the $L_R > d_c$ (see Fig. 11.1), the web crippling load of a W16x26 section are higher than the yielding load of the reinforced section R with Gr. 50 material as shown in Fig. 11.3. In other words, for rolled sections, it is safe to use type A reinforcement with $L_R \geq d_c$ since yielding will control the capacity of beams. However, for thin web plate girders, type A reinforcement will yield very low web crippling loads. Thus, for thin web plate girders ($d/t_w > 60$), type B reinforcement is recommended.

In Type B reinforcement, a vertical stiffener is added to prevent rigid body motion of the horizontal stiffener. If $L_R = 0$ for type B reinforcement, even though the rigid body motion is prevented by the vertical stiffener (assuming that the horizontal stiffener is welded to the vertical stiffener), the concentrated load in the horizontal stiffener may cause web crippling as shown in Fig. 11.4 since the horizontal stiffener acts like a flange which will develop buckling stress. Thus, it is necessary to check the web for crippling using standard AISC formulas. The stress in the stiffener can be calculated using Mc/I where M is the maximum moment at the stiffener at line A-A, the end of the cope. The bending force would be the stiffener stress times the area of the flange. When stiffeners are required, $L_R \geq c/3$ in type B reinforcement will be sufficient as discussed in Chapter 6.

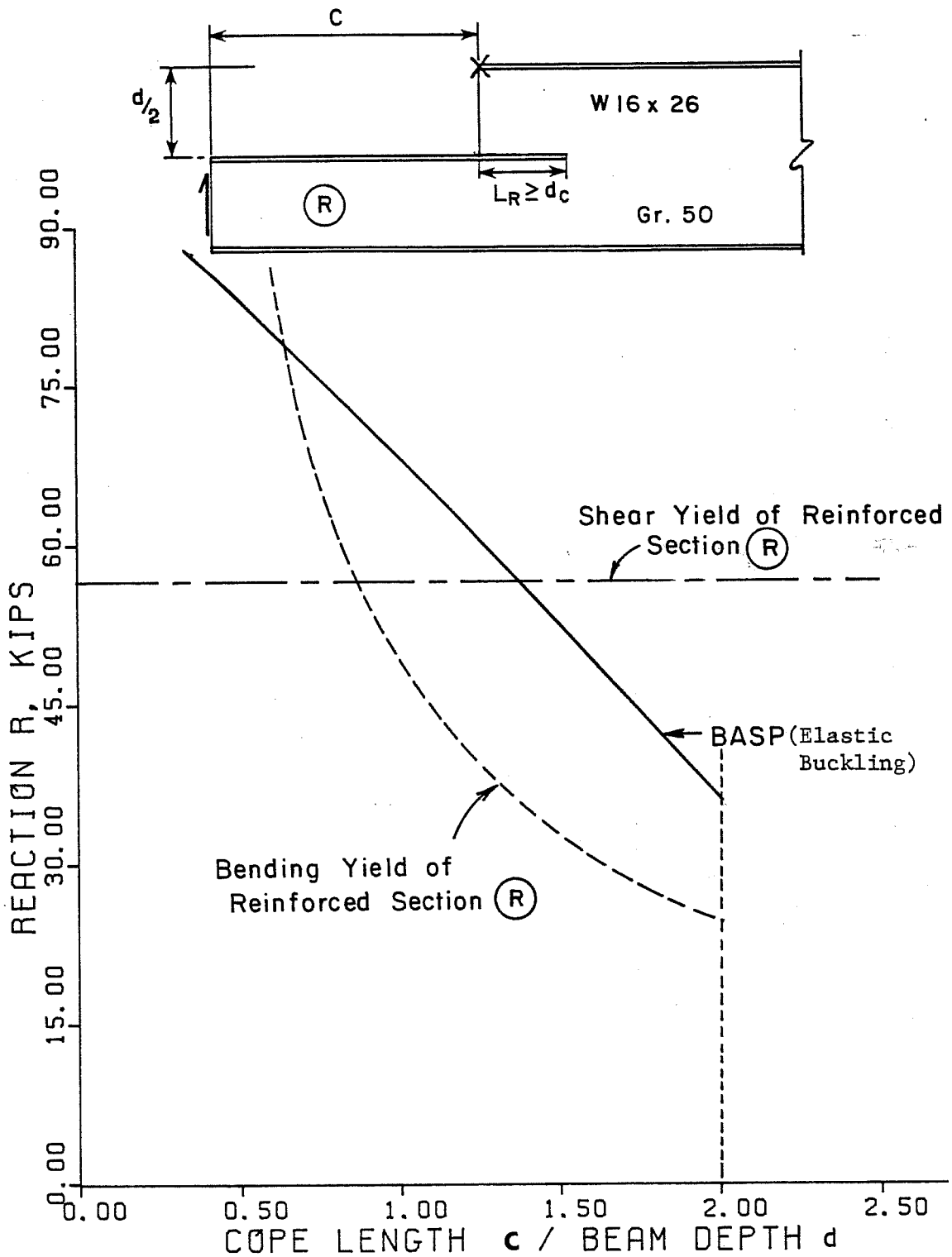

Fig, 11.3 Buckling Loads of Type A Reinforcement

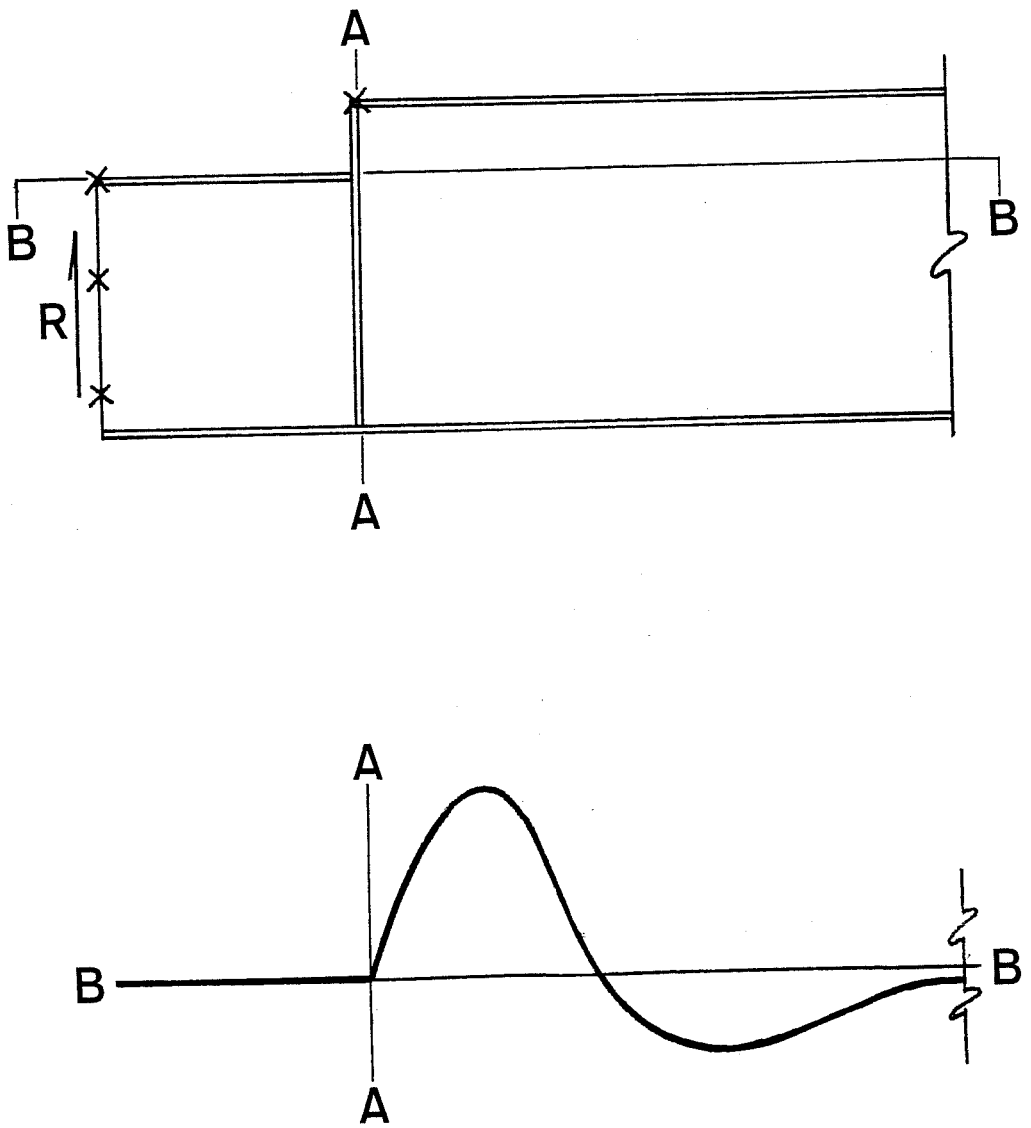

Fig. 11.4 Buckled Shape of Type B Reinforcement with $L_R=0$

The behavior of type C reinforcement is similar to type A reinforcement but the web crippling load is higher since the concentrated load of type A reinforcement is distributed vertically along the thicker web at the termination of the doubler plate. Thus, it is safe to use type C reinforcement for rolled sections as long as $L_R \geq d_c$. In order to reach the yielding load of the coped section, the required doubler plate thickness, t_d, is equal to t_w obtained from Eq. (8.2) (Eq. (9.4) for double copes) by using $F_{cr} = F_y - F_{cr}(t_w)$ where $F_{cr}(t_w)$ is calculated by Eq. (8.2) or Eq. (9.4) using t_w = web thickness.

In summary, type A and C reinforcing details with $L_R \geq d_c$ are recommended for rolled sections and type B reinforcement with $L_R \geq c/3$ is recommended for thin web members ($d/t_w > 60.0$). If $L_R = 0$ in type B reinforcement it is necessary to check web crippling using standard AISC formulas. In addition, for all three types of reinforcement, it is necessary to check the material yielding of the reinforced section.

11.2 Effects of End Restraint

A top flange coped W16x26 beam with d_c = 1.5 in. and various cope lengths was used to study the effects of end restraint. The results of both in-plane and out-of-plane end restraint are shown in Figs. 11.5 and 11.6, respectively.

The results show that the in-plane restraint will increase the buckling load significantly because the end moment will decrease

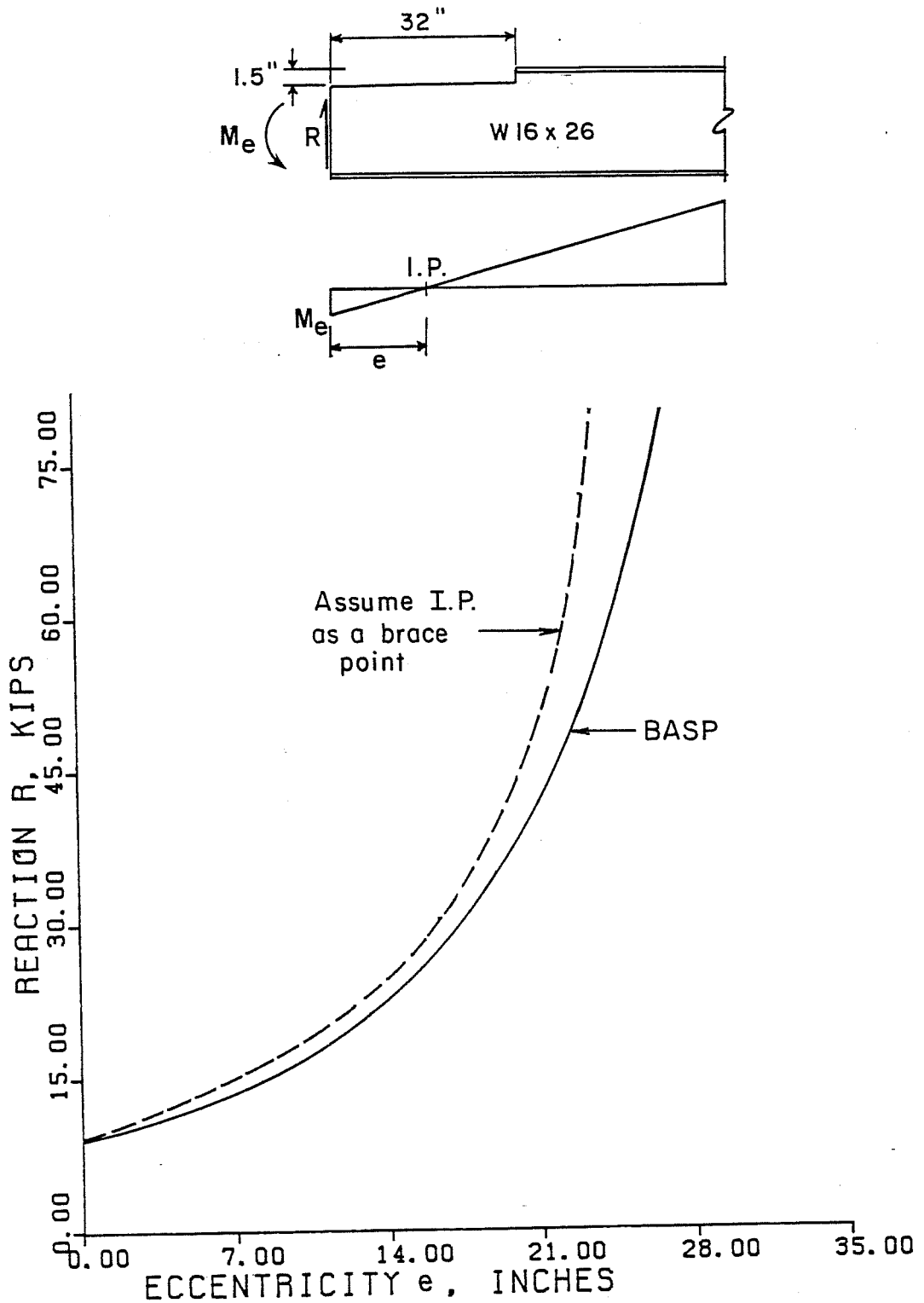

Fig. 11.5 Effects of In-plane End Restraint

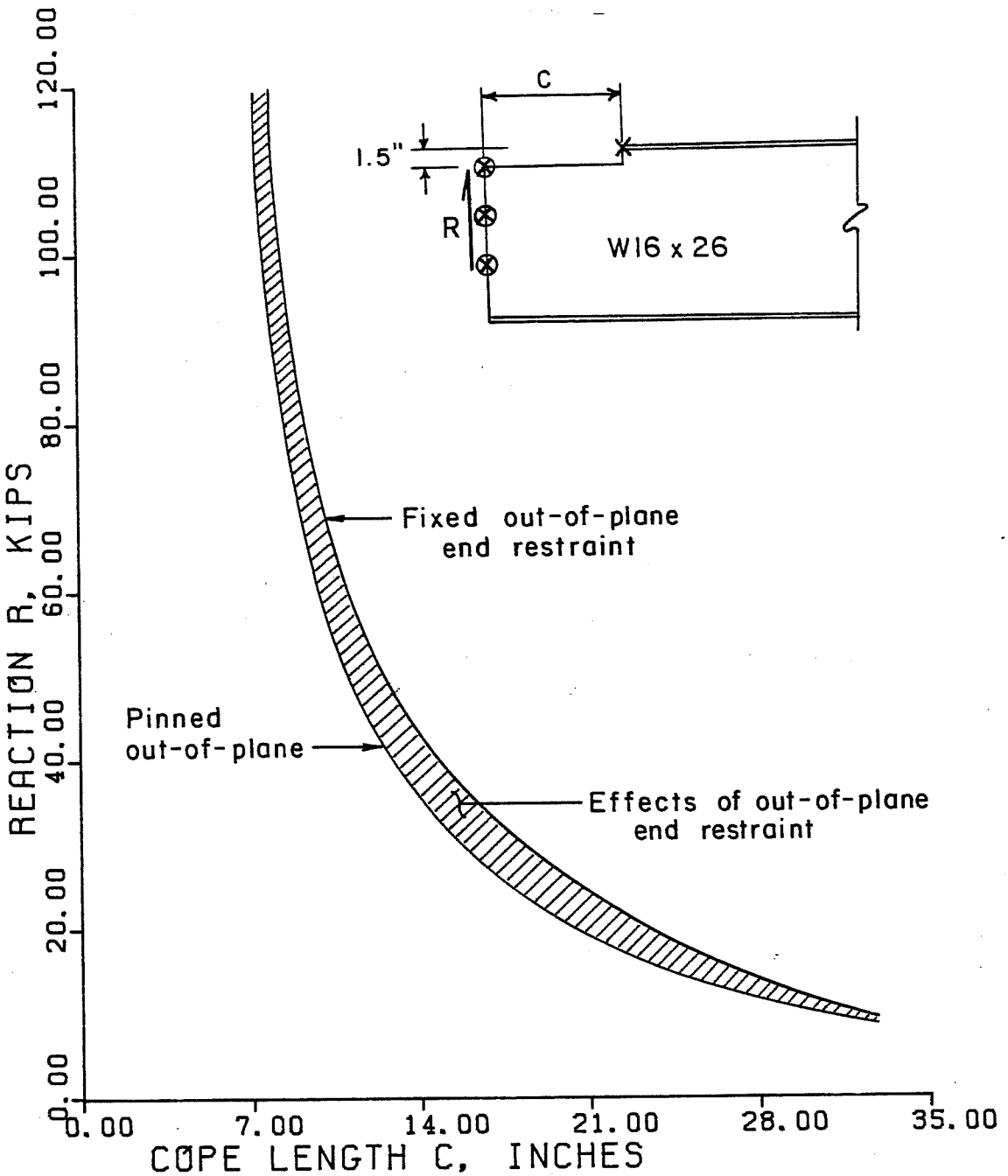

Fig. 11.6 Effects of Out-of-plane End Restraint

the maximum bending stress at the end of copes. If the end moment produces an eccentricity of d/4 (4 in. for the W16x26 section) the buckling load will increase about 10%. Since the inflection point is not truly a brace point, the buckling load is lower than that assuming the inflection point as a brace point as shown in Fig. 11.5. As expected, the effects of out-of-plane end restraint are not as significant as in-plane end restraint. The reason is that the out-of-plane end restraint is at the end where the web bending stresses are zero. Thus, for longer coped length, where the maximum bending stress in the web plate is far removed from the fixed boundary, the effects of out-of-plane end restraint are decreased.

In double coped beams, end moments will produce compression in the bottom and the top of the web. Since the bottom compression will also tend to twist the web, the end moment will not improve the buckling load as significantly as in top flange coped beams.

11.3 Other Bracing Situations

The proposed design recommendations are derived based on the assumption that the compression flange is laterally braced at the end of the cope. In many practical applications, such as that shown in Fig. 11.7, there is no lateral support at this location. The purpose of this section is to investigate this bracing situation and check the validity of the design recommendations.

A W16x26 section with c = 8 in. and d_c = 1.5 in. and the approximate web-buckling model as shown in Fig. 11.7 was used in this

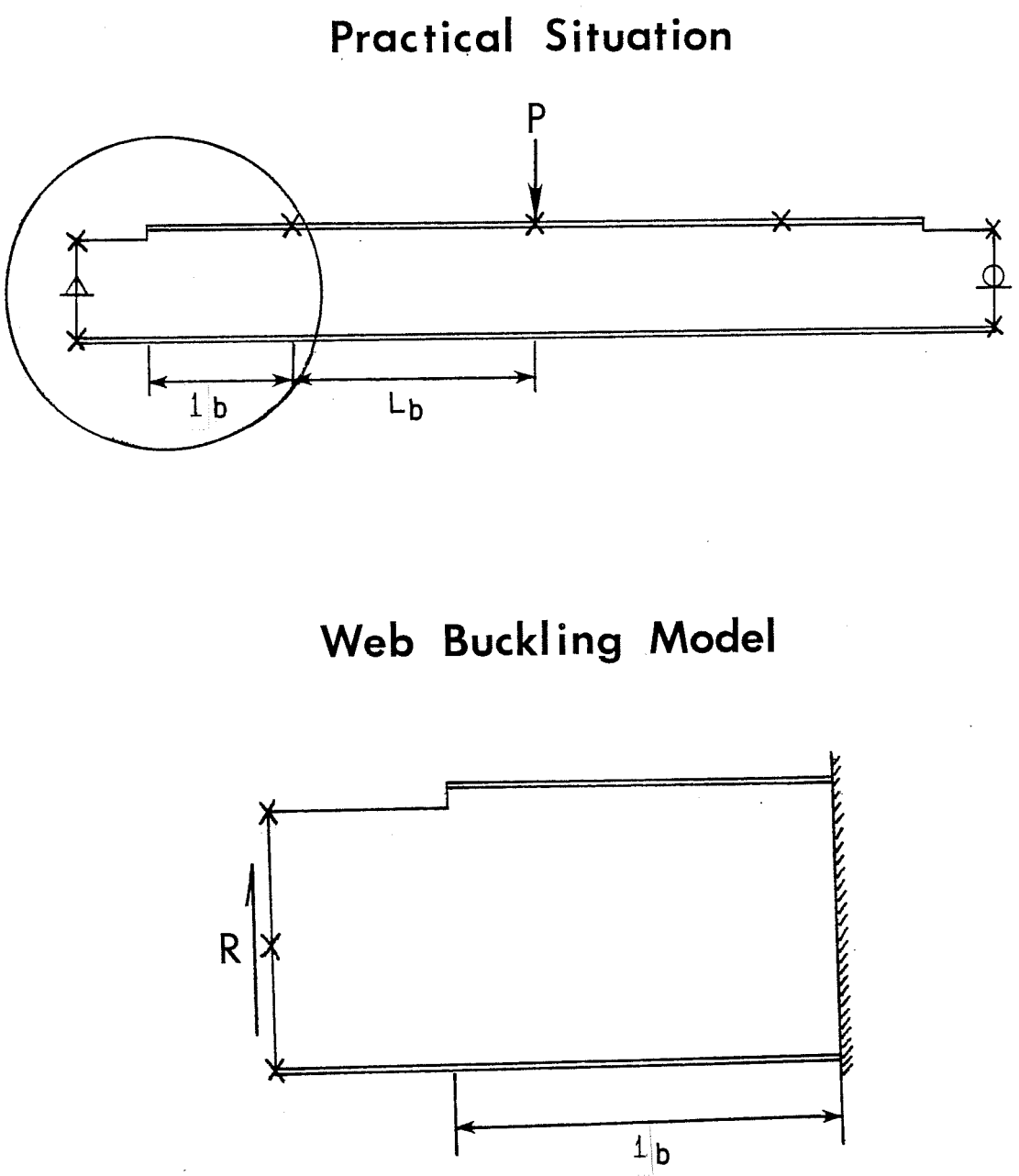

Fig. 11.7 Other Bracing Situations

study. If the right end of the web-buckling model is free to warp (torsionally pinned out-of-plane) which is equivalent to $L_b >> l_b$, (Fig. 11.7) the actual buckling load is 18.9 kips and the buckled shape is shown in Fig. 11.8. When the flange was braced at the cope, the critical load was 90.2 kips as given in Fig. 8.3. The buckled shape in Fig. 11.8 shows that the coped region behaves like the lateral-torsional buckling case as discussed in Chapter 2 and the buckling load calculated by the design recommendations in Chapter 2 is 18.6 kips which is 1.6 percent less than BASP solution. If warping is prevented at the fixed end of the web-buckling model which represents an adjacent unbraced span L_b that is very small, the results in Fig. 11.9 show that the reduction in capacity is proportional to l_b (distance from end of cope to bracing point). However, if l_b is relatively small (say 24 in. in this case), the reduction due to the unbraced length l_b is negligible. Besides, the study shows the reduction of capacity is not only a function of l_b but also the function of local web buckling capacity. In other words, the smaller the local web buckling capacity is as calculated by Eq. (8.2), the smaller the reduction in buckling capacity caused by unbraced length l_b.

Therefore, if the adjacent unbraced span is very long, the lateral-torsional buckling approach as discussed in Part I is recommended. If the distance between bracing points is small and the length l_b is relatively small, say < 2d, or the buckling load of span

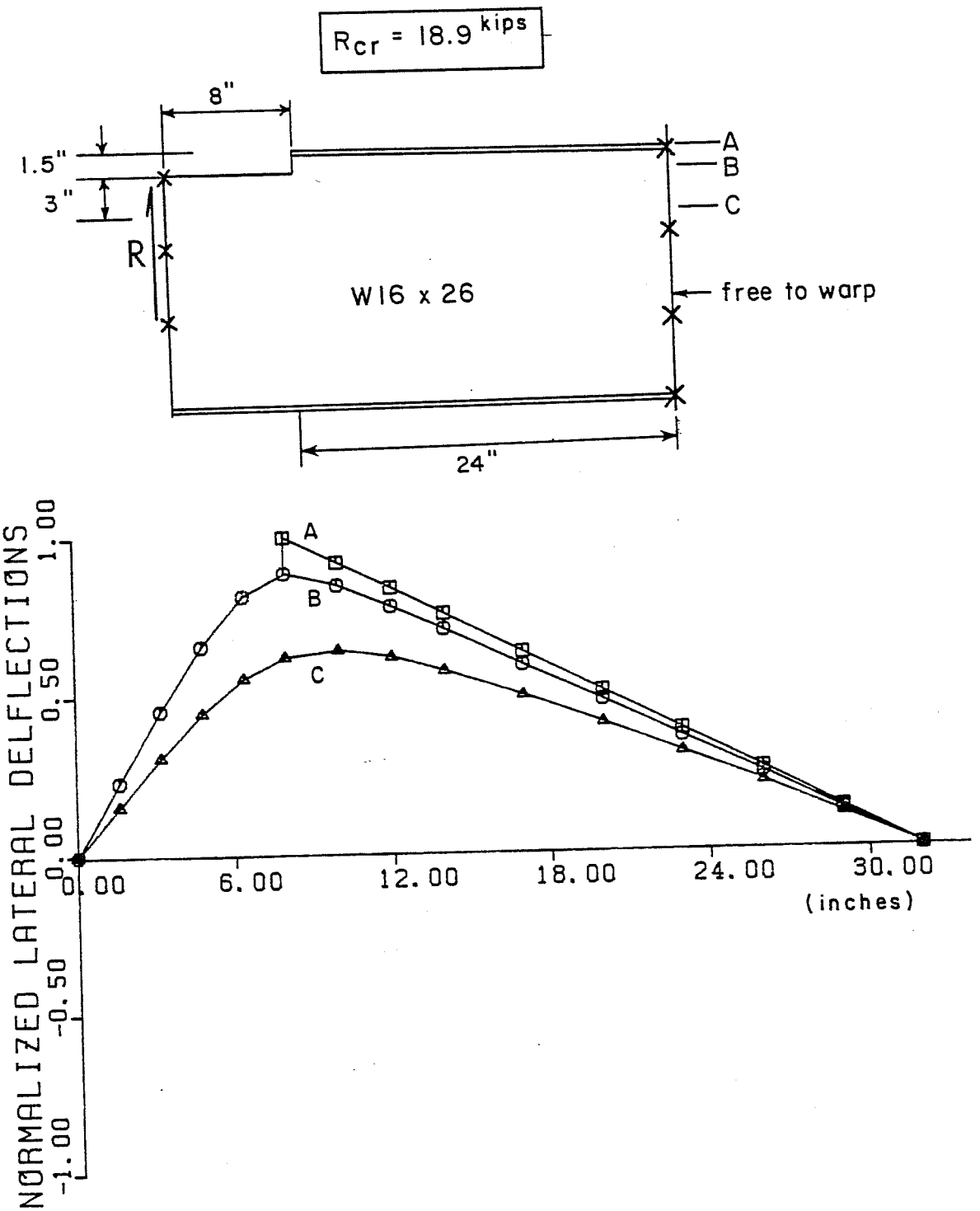

Fig. 11.8 Buckled Shape of Web Buckling Model with Free to Warp End Conditions

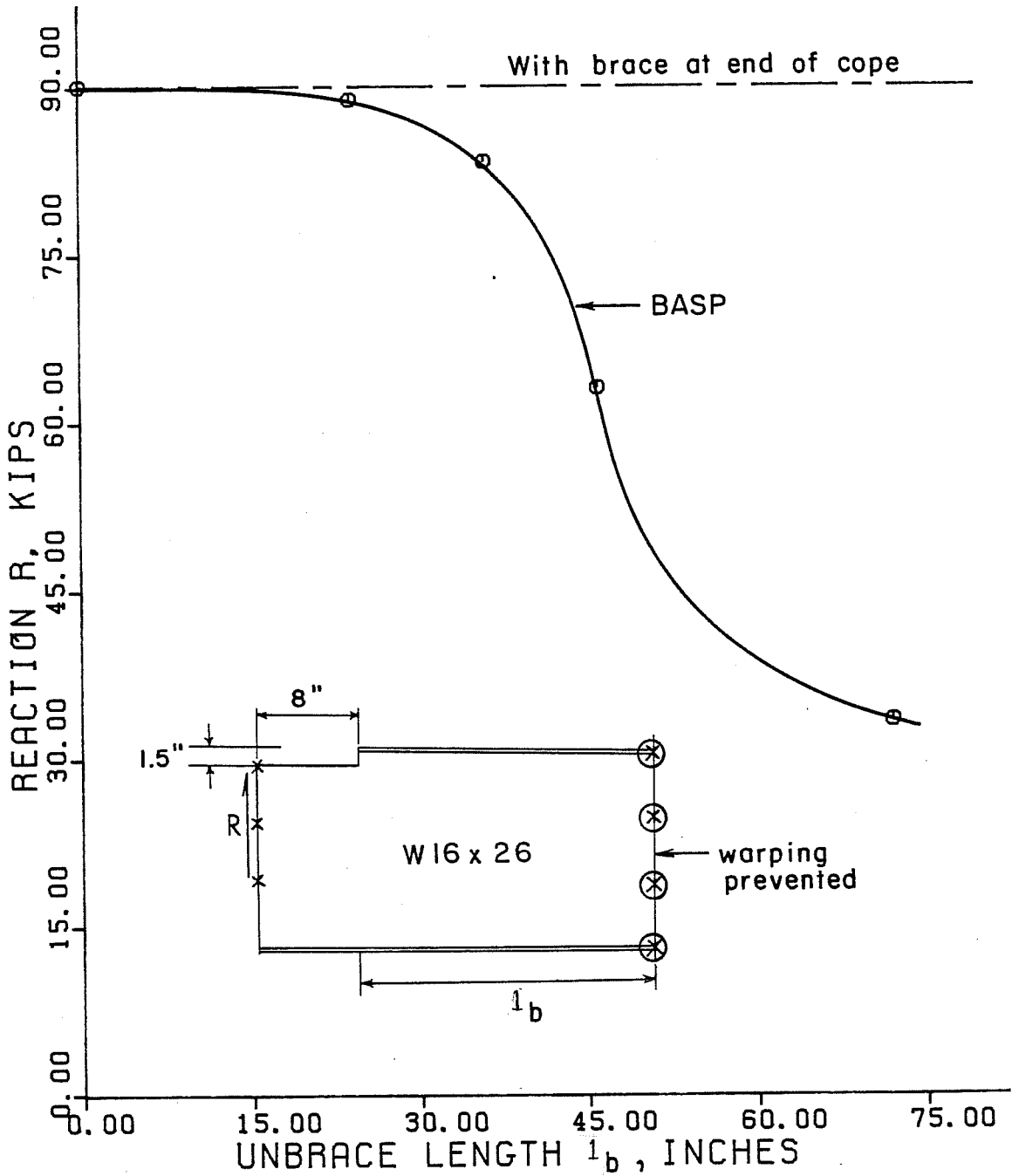

Fig. 11.9 Effect of Unbraced Length l_b with Warping Prevented End Conditions

length l_b is much higher than local web buckling capacity (Eq. (8.2)), the local web buckling approach is recommended.

CHAPTER 12

SUMMARY, RECOMMENDATIONS AND DESIGN EXAMPLES

12.1 Summary

The theoretical study of local web buckling of coped beams was discussed in Chapters 8 and 9 and the design recommendations were proposed accordingly. Ten tests with various cross sections and coping details were used to check the reliability of the theoretical results. Four other tests from another research project were also used for comparison. In summary, the research showed that:

1. Bottom (tension) flange coped beams will not fail in local web buckling. Thus, only top (compression) flange coped or double coped beams require consideration of local web buckling failure.
2. Localized yielding due to stress concentration will not significantly affect the buckling capacity of coped beams. Conventional Mc/I, $V/h_o t_w$ calculations against bending and shear yielding of coped region provide a conservative approach for checking inelastic local web buckling for both top and double flange coped beams.
3. For elastic local web buckling, the behavior of top and double flange coped beams can be predicted by plate and lateral buckling models, respectively. However, due to the stress and restraint complexities in the coped region, an

adjustment factor is needed to correlate the theoretical buckling loads to approximate models.

4. The magnitude of the SCF depends upon the coping details. The longer the cope length, the lower the SCF. Top flange coped beams have much higher SCF than double flange coped beams. Since the stress concentration effect is limited to a small length at the end of the cope, the effect of stress concentration decreases if the cope length increases.
5. Local web buckling of coped beams can be prevented by reinforcing the coped region. However, some caution is needed against web crippling and for reinforcing against local web buckling for thin web members.
6. End restraints of connections can increase the local web buckling capacity of coped beams.
7. The theoretical results give conservative but reasonable results compared with the test results. The conservative results can be contributed to the end restraints and post-buckling strength of coped beams.

12.2 Design Recommendations

The recommendations for local web buckling of coped beams are applicable to copes with a length less than twice the beam depth ($c \leq 2d$) and with a depth less than one half the beam depth ($d_c \leq d/2$) ($d_c \leq 0.2d$ in each flange for double copes). The

recommendations are summarized below; a factor of safety must be applied to these formulas when used in design.

1. Top (Compression) Flange Coped Beams:

$$F_{cr} = \frac{\pi^2 E}{12(1-\nu^2)} (t_w/h_o)^2 \, kf \leq F_y$$

where $k = 2.2 \, (h_o/c)^{1.65}$ for $c/h_o \leq 1.0$

$k = 2.2 \, (h_o/c)$ for $c/h_o \geq 1.0$

and $f = 2 \, c/d$ for $c/d \leq 1.0$

$f = 1 + c/d$ for $c/d \geq 1.0$

$$F_v = R/h_o t_w \leq 0.577 \, F_y = F_{vy}$$

2. Double Flange Coped Beams:

$$F_{cr} = 0.62 \, \pi E (t_w^2/ch_o) f_d \leq F_y$$

where

$$f_d = 3.5 - 7.5 \, (d_c/d)$$

$$F_v = R/h_o t_w \leq 0.577 \, F_y$$

3. Reinforcements:

Types of reinforcement

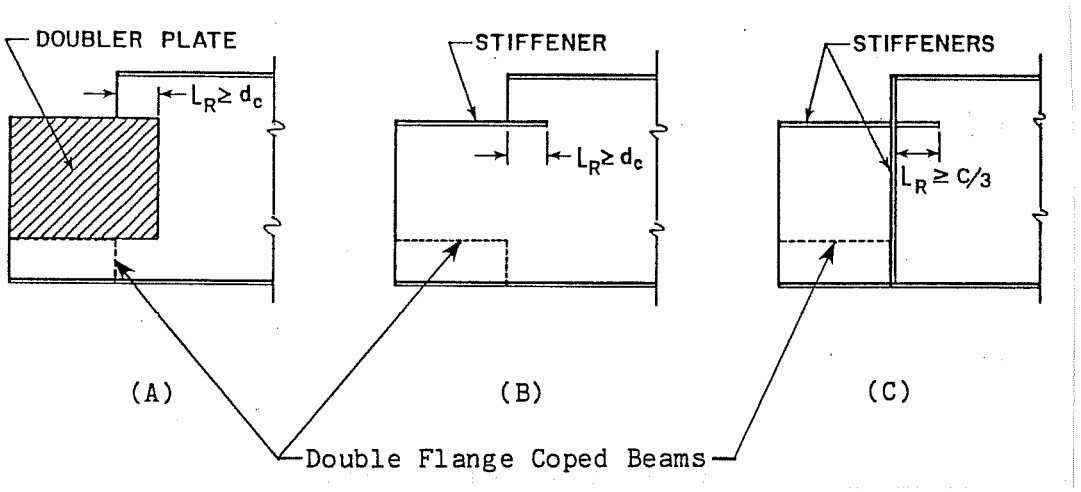

Type (A) and (B) reinforcing details with $L_R \geq d_c$ are recommended for all rolled sections ($h/t_w \leq 60.0$).

Type (C) reinforcing detail with $L_R \geq c/3$ is recommended for thin web plate girders ($h/t_w \geq 60.0$).

No reduction is needed for reinforced members. However, it is necessary to check the yielding and buckling capacity of reinforced sections. The design recommendations as summarized above can be used to check the local web buckling capacity of reinforced sections of type (A) reinforcement.

12.3 Design Examples

The cope details given for Tests W3, RB12C, and PB26B are used to illustrate the design procedure of coped beams. Examples are

also shown for double flange coped beams which have the same detail top and bottom.

In the following example problem, it is assumed that P is a factored ultimate load. For allowable stress design where P is a service load, a factor of safety of 1.67 is recommended so that $F_{allow} = F_{cr}/1.67$. For yielding $F_b = 0.6\ F_y$ and $(F_{allow})_v = 0.35\ F_y$.

Illustrative Example 1

Inelastic Local Web Buckling--Test W-3

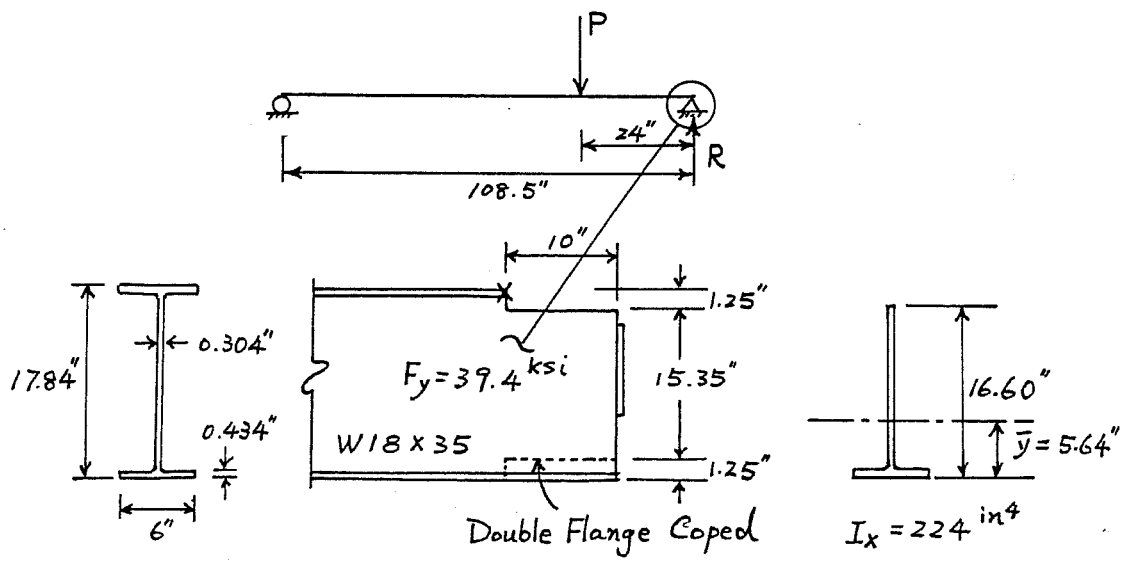

a) Top (Compression) Flange Coped:

Local Web Buckling

$c/h_o = 0.6 \leq 1.0$ $\qquad k = 2.2\ (h_o/C)^{1.65} = 5.08$

$c/d = 0.56 \leq 1.0$ $\qquad f = 2\ c/d = 1.12$

$$F_{cr} = \frac{\pi^2 E}{12(1-\nu^2)} \left(\frac{t_w}{h_o}\right)^2 kf = 50^{ksi} > F_y = 39.4^{ksi}$$

$\therefore$ Yielding Controls

$$M_{cr} = \frac{F_y \cdot I_x}{(h_o - \bar{y})} = 805^{k\text{-}''}$$

$$\therefore R_{cr} = \frac{805}{c} = \boxed{80.5^{kips}}$$

Shear Yielding

$$F_v = \frac{R_{cr}}{h_o t_w} = 16.0^{ksi} \leq 0.577\ F_y = 22.7^{ksi}$$

b) Double Flange Coped:

Local Web Buckling

$$f_d = 3.5\text{-}7.5\ (d_c/d) = 2.97$$

$$F_{cr} = 0.62\ \pi\ E\ \frac{t_w^2}{ch_o}\ f_d = 101^{ksi} > F_y = 39.4^{ksi}$$

$\therefore$ Bending Yielding Controls

$$M_{cr} = \frac{F_y\ \frac{1}{12}\ t_w h_o^3}{h_o/2} = \boxed{470^{k\text{-}''}}$$

$$\therefore R_{cr} = \frac{470}{c} = 47^{kips}$$

Shear Yielding

$$F_v = \frac{R_{cr}}{h_o t_w} = 10^{ksi} \leq 0.577\ F_y = 22.7^{ksi} \quad OK$$

Illustrative Example 2

Elastic Local Web Buckling (Rolled Sections)--Test RB12C

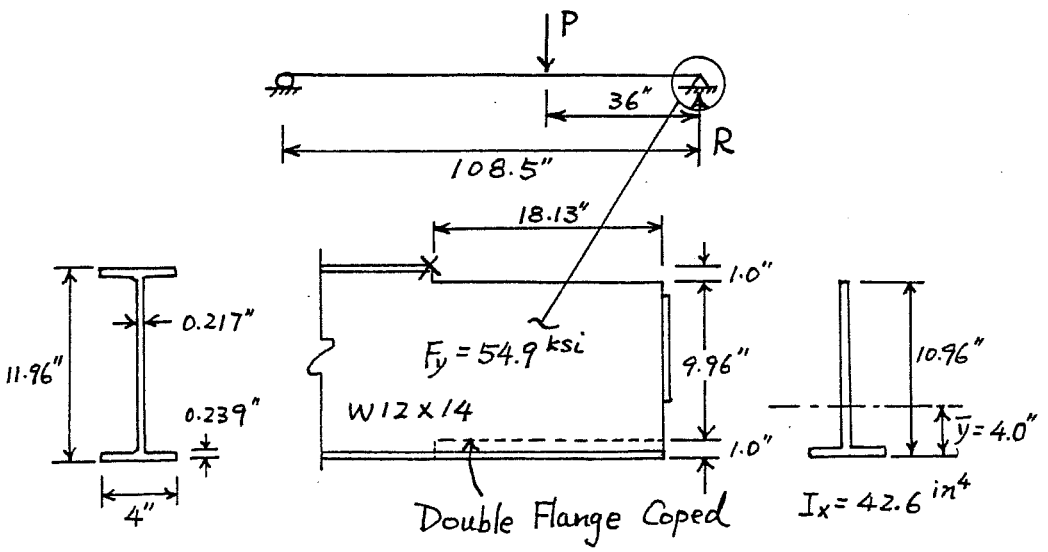

a) Top (Compression) Flange Coped:

Local Web Buckling

$c/h_o = 1.65 \geq 1.0$ $\qquad k = 2.2\ (h_o/c) = 1.33$

$c/d = 1.57 \geq 1.0$ $\qquad f = 1 + c/d = 2.52$

$$F_{cr} = \frac{\pi^2 E}{12(1-\nu^2)} \left(\frac{t_w}{h_o}\right)^2 kf = 34.4^{ksi} < F_y = 54.9^{ksi}$$

$\therefore$ Elastic Local Web Buckling Control:

$$M_{cr} = \frac{F_{cr} I_x}{(h_o - \bar{y})} = 210.6^{k-''}$$

$$\therefore R_{cr} = \frac{M_{cr}}{c} = \boxed{11.6^{kips}}$$

Shear Yielding

$$F_v = \frac{R_{cr}}{h_o t_w} = 4.88^{ksi} \leq 0.577\ F_y = 31.7^{ksi}$$

b) Double Flange Coped:

Local Web Buckling

$$F_d = 3.5 - 7.5\,(^{dc}/d) = 2.87$$

$$F_{cr} = 0.62\,\pi\,E\,\frac{t_w^2}{ch_o}\,f_d = 42.3^{ksi} < F_y = 54.9^{ksi}$$

$\therefore$ Elastic Local Web Buckling Control

$$M_{cr} = \frac{F_{cr}\,\frac{1}{12}\,t_w h_o^3}{h_o/2} = 152^{k\text{-}''}$$

$$\therefore R_{cr} = \frac{M_{cr}}{c} = \boxed{8.37^{kips}}$$

Shear Yielding

$$F_v = \frac{R_{cr}}{h_o t_w} = 3.87^{ksi} \leq 0.577\,F_y = 31.7^{ksi} \quad \text{OK}$$

Illustrative Example 3

Elastic Local Web Buckling (Plate Girders)--Test PB26B

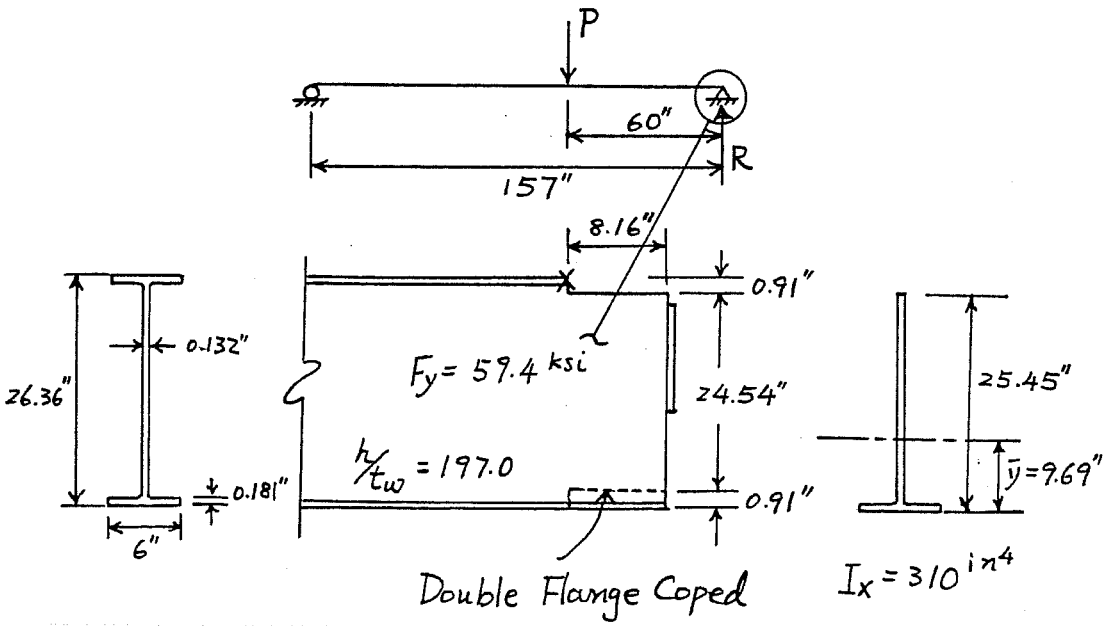

a) Top (Compression) Flange Coped:

Local Web Buckling

$c/h_o = 0.32 \leq 1.0$ $\qquad k = 2.2\,(h_o/c)^{1.65} = 14.37$

$c/d = 0.31 \leq 1.0$ $\qquad f = 2\ c/d = 0.62$

$$F_{cr} = \frac{\pi^2 E}{12(1-\upsilon^2)}\left(\frac{t_w}{h_o}\right)^2 kf = 6.28^{ksi} < F_y = 59.4^{ksi}\ \text{OK}$$

$$M_{cr} = \frac{F_{cr}\ I_x}{(h_o-\bar{y})} = 123.5^{k-''}$$

$$R_{cr} = 123.5/c = \boxed{15.13^{kips}}$$

Elastic Shear Buckling

$$F_v = \frac{\pi^2 E}{12(1-\upsilon^2)}\left(\frac{t_w}{h}\right)^2 k_v$$ ——— AISC (1.10-1) (Factor of Safety Removed)

$$k_v = 5.34 + 4.0\ (a/h)^2 = 5.34 + 4.0\ (60/26)^2 = 6.09$$

$\therefore F_v = 4.11^{ksi} < 0.577\ F_y = 34.3^{ksi}$

$R_v = F_v . t_w . h = \boxed{14.1^{kips}} < R_{cr}$

$\therefore$ Elastic Shear Buckling Control with $\underline{R_v = 14.1^{kips}}$

b) Double Flange Coped:

Local Web Buckling

$$f_d = 3.5 - 7.5\ (d_c/d) = 3.24$$

$$F_{cr} = 0.62\ \pi E \frac{t_w^2}{ch_o} f_d = 15.92^{ksi}$$

$$M_{cr} = \frac{F_{cr} \frac{1}{12} t_w h_o^3}{h_o/2} = 210.9^{k-''}$$

$$R_{cr} = 210.9/c = \boxed{25.8^{kips}} > R_v = 14.1^{kips}$$

$\therefore$ Elastic Shear Buckling Control with $\underline{R_v = 14.1^{kips}}$

12.4 Future Research

Special attention should be placed on the local web buckling of coped beams in the following areas:

1. Effect of cope depth to reduce the differences between design recommendations and theoretical BASP solutions (see Fig. 8.18).
2. Effects of end restraint of various types of connections on the local web buckling capacity of coped beams.
3. Post-buckling capacity of coped beams, especially for thin web plate girders.
4. More experimental studies on different coping details and reinforcements to control local web buckling of coped beams are necessary, especially for double flange coped beams and thin web plate girders.

A P P E N D I X A

DESIGN EXAMPLES OF CURRENT DESIGN METHODS FOR LOCAL WEB BUCKLING

The same design example as used in the Illustrative Example 2 of Chapter 12 is used to illustrate the current design methods for the local web buckling of coped beams.

It should be noted that the Appendix C design approach yields a higher buckling load of double flange coped beams than the buckling load of top flange coped beams.

Illustrative Example

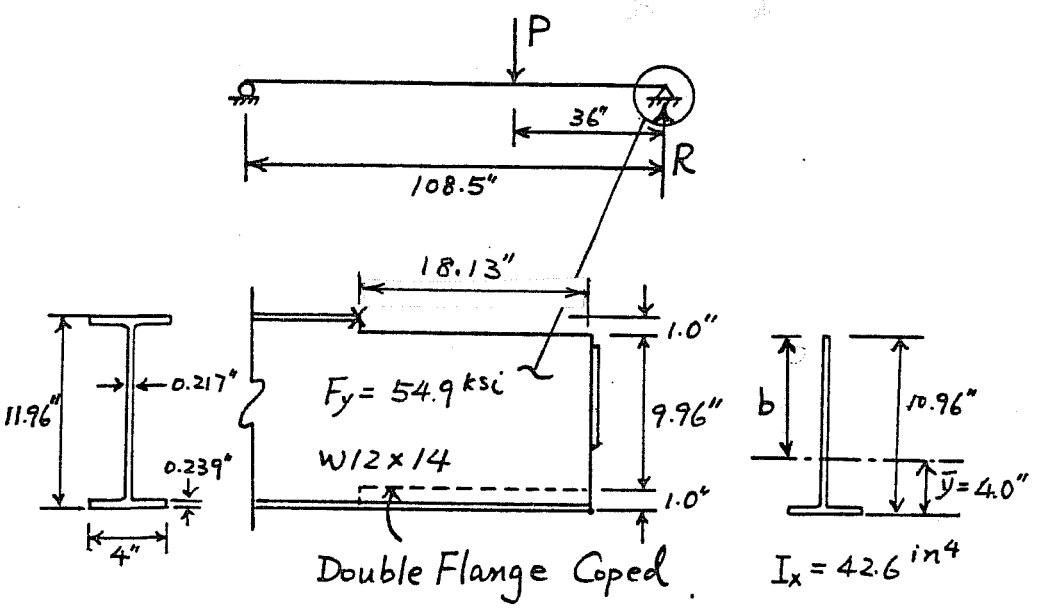

A) Top (Compression) Flange Coped

1) Detailing Manual

$$F_b = 0.6\ F_y = 32.94^{ksi}$$

$$Mallow = \frac{I_x\ F_b}{b} = \frac{42.6 \cdot 32.94}{(10.95-4)} = 201.6^{k-"}$$

$$\therefore Rallow = \frac{Mallow}{C} = \underline{11.12^{kips}}$$

$$f_v = \frac{Rallow}{h_o\ t_w} = 4.68^{ksi} < 0.4\ F_y = 21.96^{ksi}\ \text{OK}$$

$$\therefore R_{cr} = \text{F.S. X Rallow} = 1.67 \cdot 11.12^{kips}$$

$$= \boxed{18.75^{kips}}$$

2) Appendix C

$$b/t_w = 6.96/0.217 = 32.0 > \frac{176}{\sqrt{F_y}} = 23.8$$

$$Q_s = 2000/[F_y \times (b/t_w)^2] = 0.345$$

$$Rallow = \frac{0.6\ F_y\ Q_s\ I_x}{cb} = \underline{3.94^{kips}}$$

$$R_{cr} = F.S. \cdot Rallow = 6.58^{kips}$$

b) Double Flange Coped

1) Detailing Manual

$$F_b = 0.6\ F_y = 32.94^{ksi}$$

$$Mallow = \frac{I_x \cdot F_b}{h_o/2} = \frac{\frac{1}{12}\ (0.217)\ 9.96^3 (32.94)}{9.96/2} = 118.2^{k-''}$$

$$\therefore Rallow = \frac{Mallow}{C} = \underline{6.52^{kips}}$$

$$f_v = \frac{Rallow}{h_o t_w} = 3.02^{ksi} < 0.4\ F_y = 21.96^{ksi} \quad OK$$

$$\therefore R_{cr} = 1.67 \cdot Rallow = \boxed{10.89^{kips}}$$

2) Appendix C

$$\frac{h_o/2}{t_w} = 22.95 < 176/\sqrt{F_y} = 23.8$$

$$> 127/\sqrt{F_y} = 17.1$$

$$Q_s = 1.908 - 0.00715\ (22.95)\sqrt{F_y} = 0.692$$

$$Rallow = \frac{0.6\ F_y Q_s I_x}{C\ (h_o/2)} = \frac{0.6(54.9)\ (0.692)\ \frac{1}{12}\ (0.217) 9.96^3}{18.13\ \ (9.96/2)}$$

$$= \underline{4.51^{kips}}$$

$$R_{cr} = 1.67 \cdot Rallow = \boxed{7.53^{kips}}$$

A P P E N D I X B

CONNECTION DETAILS AND LOAD-DEFLECTION CURVES OF FOUR OTHER TESTS

Four unpublished tests failed in inelastic local web buckling were done by Ricles and Yura in an AISC research project, Web Shear Connection tests. The connection details can be seen in Fig. B.1. The first two connections, labeled 10-4 and 10-7, are clip angle bolted connections and the test beams are 10 ft long W10x22 sections with A36 material. Tests 18-14 and 18-15 are clip angle welded connections and the test beams are 10 ft long W18x60 sections also with A36 material. The summary of material and section properties of test beams are listed in Table B.1. The reaction vs. deflection at load point curves and maximum reactions are shown in Fig. B.2.

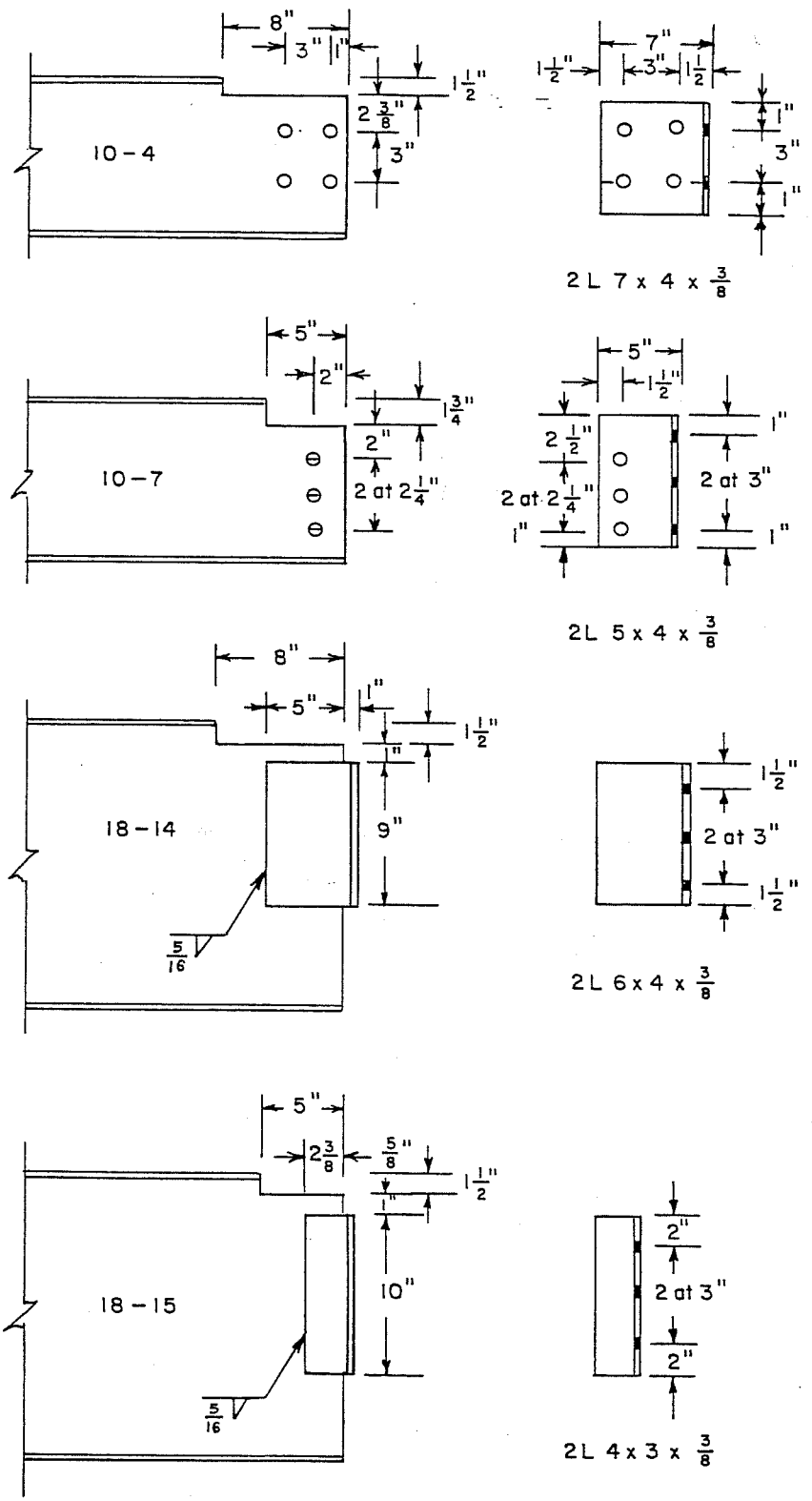

Fig. B.1 Detail of Coping Connections

TABLE B.1 Material and Section Properties

Tensile Coupon Test Results

Test Specimens	Flange Static Yield (ksi)	Flange Static Ultimate (ksi)	Web Static Yield (ksi)	Web Static Ultimate (ksi)
Tests 10-4 10-7	40.37	57.79	50.31	64.14
Tests 18-14 18-15	33.94	57.01	36.55	58.00

Measured Section Properties

Test Specimens	Beam Depth d (in.)	Flange Width b_f (in.)	Flange Thickness t_f (in.)	Web Thickness t_w (in.)
Tests 10-4 10-7	9.92	5.70	0.360	0.251
Tests 18-14 18-15	18.19	7.47	0.685	0.423

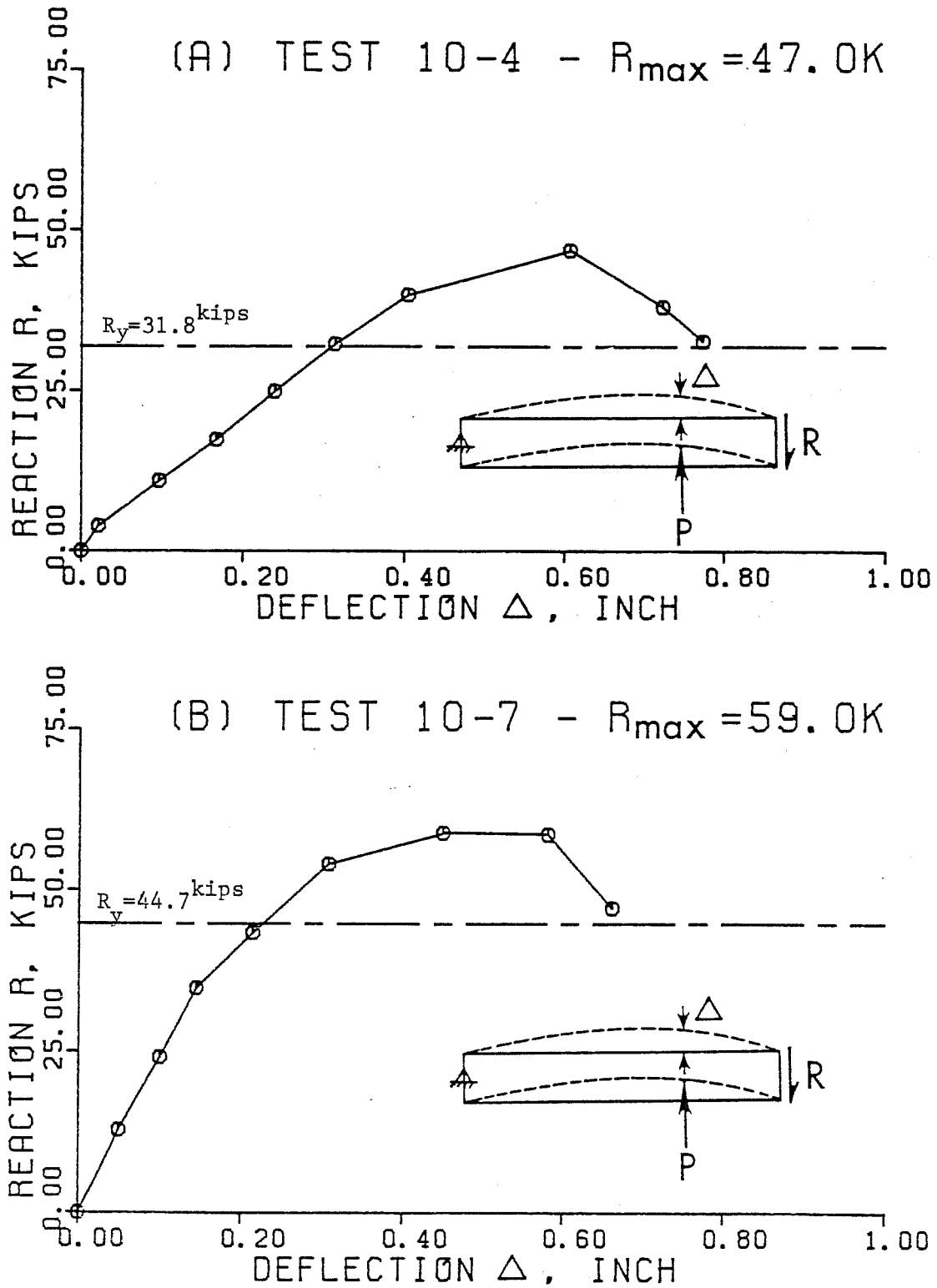

Fig. B.2 Reaction vs Deflection Curves

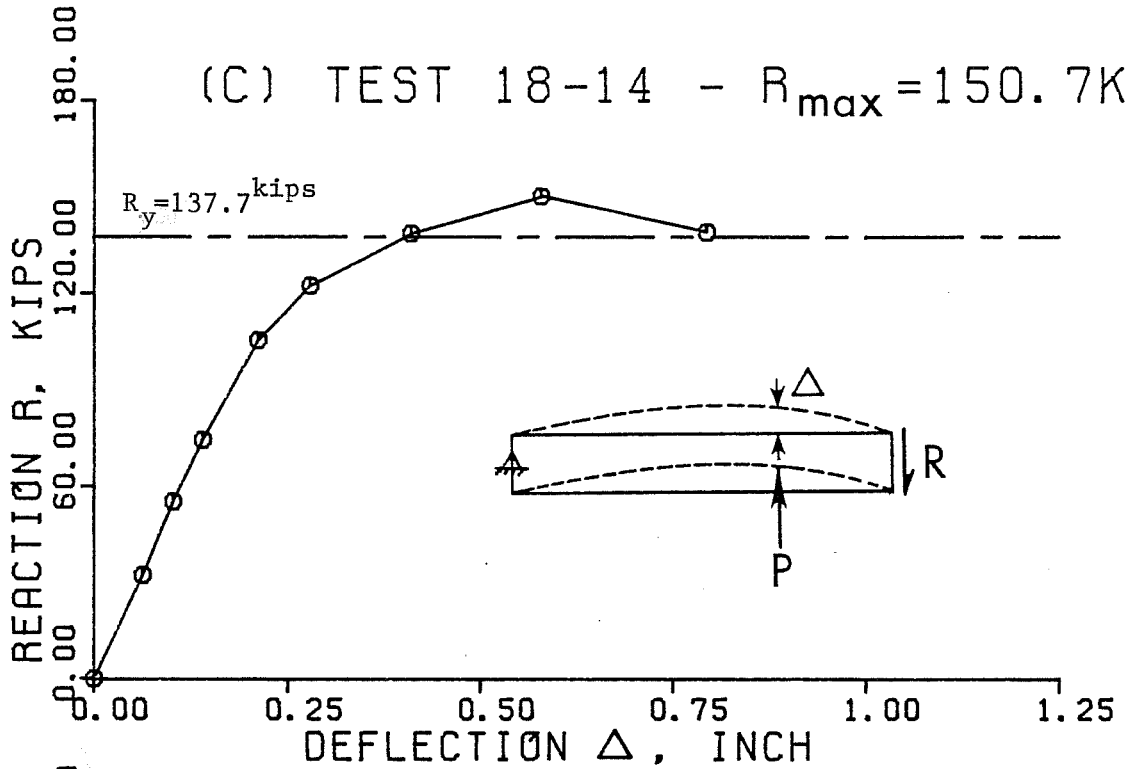
(C) TEST 18-14 - R_{max}=150.7K
R_y=137.7kips
REACTION R, KIPS
180.00
120.00
60.00
0.00
0.00
0.25
0.50
0.75
1.00
1.25
DEFLECTION Δ, INCH
Δ
R
P

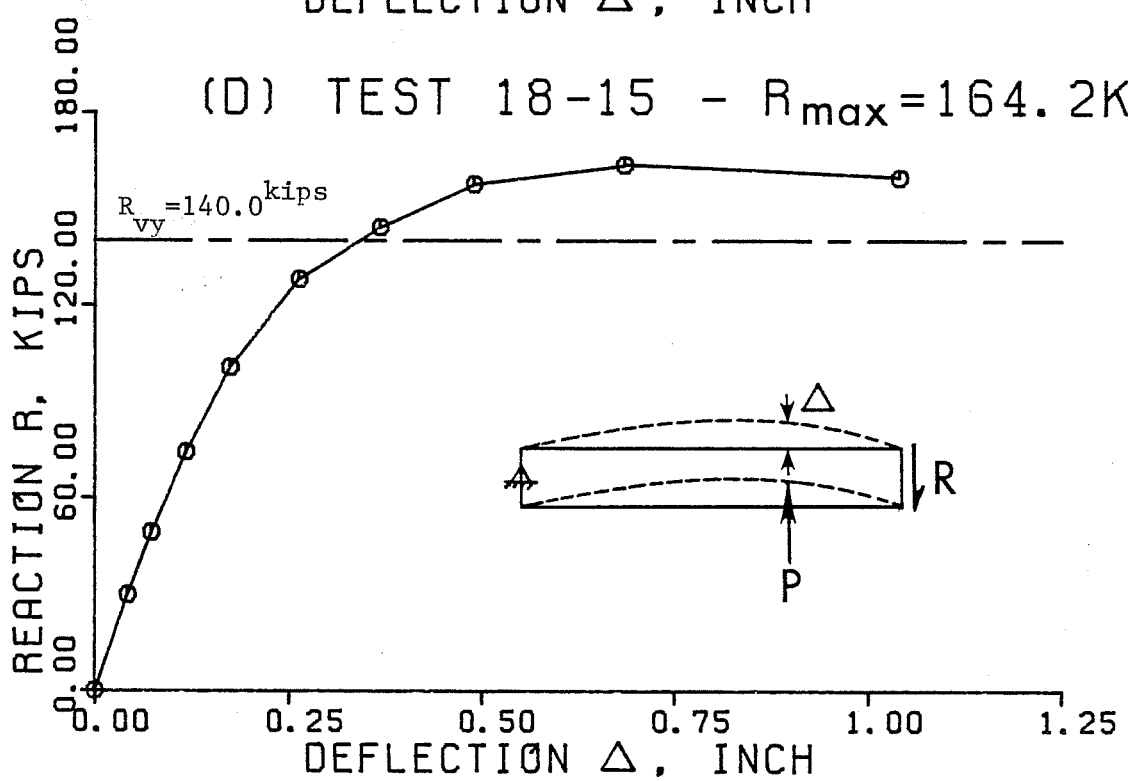
(D) TEST 18-15 - R_{max}=164.2K
R_{vy}=140.0kips
REACTION R, KIPS
180.00
120.00
60.00
0.00
0.00
0.25
0.50
0.75
1.00
1.25
DEFLECTION Δ, INCH
Δ
R
P

Fig. B.2 (Cont'd)

NOTATION

A	Cross-sectional area (in.^{2})
C_b	Bending coefficient depending upon loading conditions
C_w	Warping constant for a section (in.^{6})
E	Modulus of elasticity of steel (29,000 ksi)
E_{st}	Modulus of strain hardening of steel (ksi)
F_{allow}	Allowable stress permitted in a coped beam (ksi)
$(F_{allow})_v$	Allowable shear stress permitted in a coped beam (ksi)
F_{cr}	Critical bending stress in a coped beam (ksi)
F_v	Critical shear stress in a coped beam (ksi)
F_y	Yield stress of steel (ksi)
G	Shear modulus of elasticity of steel (11,200 ksi)
I	Moment of inertia of a section (in.^{4})
I_x	Moment of inertia of a section about the x-x axis (in.^{4})
I_y	Moment of inertia of a section about the y-y axis (in.^{4})
J	Torsional constant of a cross-section (in.^{4})
K_z	Lateral spring constant (kip/in.)
$K\phi$	Rotational spring constant (k-in./rad)
L	Span length (ft)
L_b	Unbraced length (ft)
L_R	Reinforcing length (ft)
LTB	Lateral torsional buckling of a beam
M	Moment (kip-in.)

NOTATION (continued)

M_{LTB}	Elastic lateral torsional buckling moment of an uncoped beam (kip-in.)
M'_{LTB}	Elastic lateral torsional buckling moment of an uncoped beam with brace 1 modified by the tipping effect (kip-in.)
M''_{LTB}	Elastic lateral-torsional buckling moment of an uncoped beam with brace 2 modified by the tipping effect (kip-in.)
M_{lg}	Larger moment at the end of an unbraced length (kip-in.)
M_{sm}	Smaller moment at the end of an unbraced length (kip-in.)
M_p	Plastic moment (kip-in.)
M_{Rec}	Elastic lateral torsional buckling moment of a rectangular section beam (kip-in.)
M_{Tee}	Elastic lateral torsional buckling moment of a tee section beam (kip-in.)
M'_{Tee}	Critical moment of the elastic lateral torsional buckling of a tee section beam modified by the tipping effect (kip-in.)
M_{Tip}	Critical moment due to tipping effect (kip-in.)
M_y	Yield moment (kip-in.)
P	Load (kip)
P_{BASP}	Critical load solved by BASP (kips)
P_{cr}	Critical load of a coped beam (kips)
$(P_{cr})_{uncope}$	Critical load of an uncoped beam (kips)
P_{Design}	Critical load calculated by design recommendations (kips)

$(P_{Design})_{BASP}$	Critical load solved by BASP without considering any restraint (kips)
P_{eq}	Equivalent axial force in column analogy model (kips)
P_{LTB}	Elastic lateral torsional buckling load of an uncoped beam (kips)
P'_{LTB}	Elastic lateral torsional buckling load of an uncoped beam with brace 1 modified by the tipping effect (kips)
P''_{LTB}	Elastic lateral-torsional buckling load of an uncoped beam with brace 2 modified by the tipping effect (kips)
P_{max}	Maximum experimental load (kips)
P_{Rec}	Elastic lateral torsional buckling load of a rectangular section beam (kips)
P_{Tee}	Elastic lateral torsional buckling load of a tee section beam modified by the tipping effect (kips)
P'_{Tee}	Elastic lateral torsional buckling load of a tee section beam modified by the tipping effect (kips)
P_{Tip}	Critical load due to tipping effect (kips)
P_y	Yield load (kips)
Q	Static moment of area ($in.^3$)
Q_s	Axial stress reduction factor where width-thickness ratio of unstiffened elements exceeds limiting value
R	Reaction (kips)
Ⓡ	Reinforced section
R_{ABAQUS}	Critical reaction solved by ABAQUS (kips)
R_{BASP}	Critical reaction solved by BASP (kips)
R_{cr}	Critical reaction (kips)
R_{Design}	Critical reaction calculated by design recommendations (kips)

NOTATION (continued)

$(R_{Design})_{ABAQUS}$	Critical reaction solved by ABAQUS without considering end restraints (kips)
$(R_{Design})_{BASP}$	Critical reaction solved by BASP without considering end restraints (kips)
R_{max}	Maximum experimental reaction (kips)
R_v	Critical reaction due to the elastic shear buckling (kips)
R_{vy}	Shear yield reaction (kips)
R_y	Yield reaction (kips)
SCF	Stress concentration factor
V	Shear force (kips)
V_{allow}	Allowable shear force (kips)
a	Clear distance between transverse stiffeners (in.)
b	Distance between neutral axis of reduced section and top coped line = $h_o - \overline{y}$ (in.)
b_f	Flange width of rolled beam or plate girder (in.)
c	Cope length (in.)
d	Depth of a beam (in.)
d_c	Cope depth (in.)
e	Eccentricity due to in-plane end moment (in.)
f	Adjustment factor of plate buckling model
f_b	Computed bending stress (ksi)
f_d	Adjustment factor of lateral buckling model
f_v	Computed shear stress (ksi)
h	Clear distance between flanges of a beam or girder (in.)

NOTATION (continued)

h_o Depth of a beam at coped region = d - d_c (in.)

k Plate buckling coefficient

k_d Effective length factor of lateral buckling model

k_v Coefficient relating elastic shear buckling strength of a plate

l Distance

l_b Unbraced length from end of cope to the adjacent brace point (in.)

n Ratio of flange stiffness (β_b) to lateral spring stiffness (β_e)

p Unit flange force due to moment (kip/in.)

γ_m Monosymmetric parameter of tee section lateral torsional buckling

t Thickness (in.)

t_d Doubler plate reinforcing thickness (in.)

t_f Flange thickness (in.)

t_s Stiffener thickness (in.)

t_w Web thickness (in.)

$\bar{y}$ Distance between the neutral axis of reduced section and extreme fiber of flange (in.)

β_x Defined in Eq. (2.2b) (in.)

β_b Flange stiffness (kip/in.)

β_e Lateral spring stiffness due to cope depth

σ_{cr} Critical buckling stress of a plate (ksi)

ϵ_y Yield strain of steel (in./in.)

ν Poisson's ratio of steel = 0.3

Δ Deflection (in.)

NOTATION (continued)

θ Out-of-plane rotation (rad)

ϕ In-plane rotation (rad)

x Lateral bracing

⊗ Lateral and torsional bracing

——— Free edge

═══ Simply supported edge

REFERENCES

1. Yura, J. A., Galambos, T. V., and Ravindra, M. K., "The Bending Resistance of Steel Beams," Journal of the Structural Division, ASCE, Vol. 104, ST9, September 1978, pp. 1355-1370.

2. Milek, W. A., "A Cautionary Note on Beam Copes," Engineering Journal, American Institute of Steel Construction, Vol. 17, No. 3, 1980, pp. 72-73.

3. Timoshenko, S. P., and Gere, J. M., Theory of Elastic Stability, 2nd ed., McGraw-Hill Book Company, Inc., New York, 1961.

4. du Plessis, D. P., "Lateral-Torsional Buckling of End-Notched Steel Beams," International Colloquium on Stability of Structures under Static and Dynamic Loads, Washington, D. C., May 1977, pp. 563-572.

5. Ricles, J. M., and Yura, J. A., "The Behavior and Analysis of Double-Row Bolted Shear Web Connections," Department of Civil Engineering, Phil M. Ferguson Structural Engineering Laboratory, The University of Texas at Austin, Thesis No. 80-1, September 1980.

6. Shelton, B. G., and Yura, J. A., "Tests of Bolted Shear Web Connections," Department of Civil Engineering, Phil M. Ferguson Structural Engineering Laboratory, The University of Texas at Austin, Report No. 80-1, February 1981.

7. Birkemoe, P. E., and Gilmer, M. I., "Behavior of Bearing Critical Double Angle Beam Connections," Engineering Journal, American Institute of Steel Construction, Vol. 15, No. 4, 1978, pp. 109-115.

8. Richards, J. A., and Mueller, R. A., "FCCU Structural Failure," Cities Service Company, Tulsa, Oklahoma, May 1982.

9. Steel Construction Manual, 8th Ed., American Institute of Steel Construction, New York, 1980.

10. "Specification for the Design, Fabrication and Erection of Structural Steel for Buildings," American Institute of Steel Construction, New York, 1978.

11. Johnston, B. G., ed., Structural Stability Research Council, Guide to Stability Design Criteria for Metal Structures, 3rd Ed., New York, John Wiley & Sons, Inc., 1976.

12. Structural Steel Detailing, 2nd Ed., American Institute of Steel Construction, New York, 1971.

13. Akay, H. U., Johnson, C. P., and Will, K. M., "Lateral and Local Buckling of Beams and Frames," Journal of the Structural Division, ASCE, Vol. 103, ST9, September 1977, pp. 1821-1832.

14. "ABAQUS User's Manual," Hibbit & Karlsson, Inc., Version 3, June 1979.

15. Hogan, T. J., and Thomas, I. R., "Design of Tee Section Members to ASI250," Steel Construction, Journal of the Australian Institute of Steel Construction, Vol. 14, No. 2, 1980.

16. Southwell, R. V., "On the Analysis of Experimental Observations in Problems of Elastic Stability," Proceedings of the Royal Society of London, Vol. 135, 1932, pp. 601-616.

17. Lundquist, E. E., "Generalized Analysis of Experimental Observations in Problems of Elastic Stability," National Advisory Committee for Aeronautics, Technical Note. 658, 1938.

18. Meck, H. R., "Experimental Evaluation of Lateral Buckling Loads," Journal of the Engineering Mechanics Division, ASCE, Vol. 103, EM2, April 1977, pp. 331-337.

19. Yura, J. A., Discussion of "Deformations of Geometrically Imperfect Beams," Journal of the Structural Division, ASCE, Vol. 96, ST1, January 1970, pp. 162-163.

20. Galambos, T. V., and Ravindra, M. K., "Properties of Steel for Use in LRFD," Journal of the Structural Division, ASCE, Vol. 104, ST9, September 1978, pp. 1459-1468.

21. Thurlimann, B., "New Aspects Concerning Inelastic Instability of Steel Structures," Transactions, ASCE, Vol. 127, 1962, Part II, pp. 448-470.

22. "Handbook of Structural Stability," Column Research Committee of Japan, Tokyo, 1971.

PHIL M. FERGUSON STRUCTURAL ENGINEERING LABORATORY
THE UNIVERSITY OF TEXAS AT AUSTIN

10100 Burnet Road • Austin, Texas 78758-4497 • (512) 471-3062 • Fax (512) 471-1944

Memorandum

To: Renee DeGroat
Kinko's

From: Regina Forward (471-5702) RF

Date: December 8, 2000

Re: copies of PMFSEL Report 84-1

Copies of PMFSEL Report 84-1

Warning – this is an old report and the paper quality varies from one page to the next. Some pages are actually thin tracing paper. Many pages have figures and/or photos taped to them. I hope that won't cause a problem for your machines.

1. Please make **10** copies, single-sided through intro material, duplex beginning with Chapter 1.
2. White cardstock covers, printed on front (included).
3. Tape bind with white tape.
4. Please deliver by Friday, December 15, 2000.

Thanks!

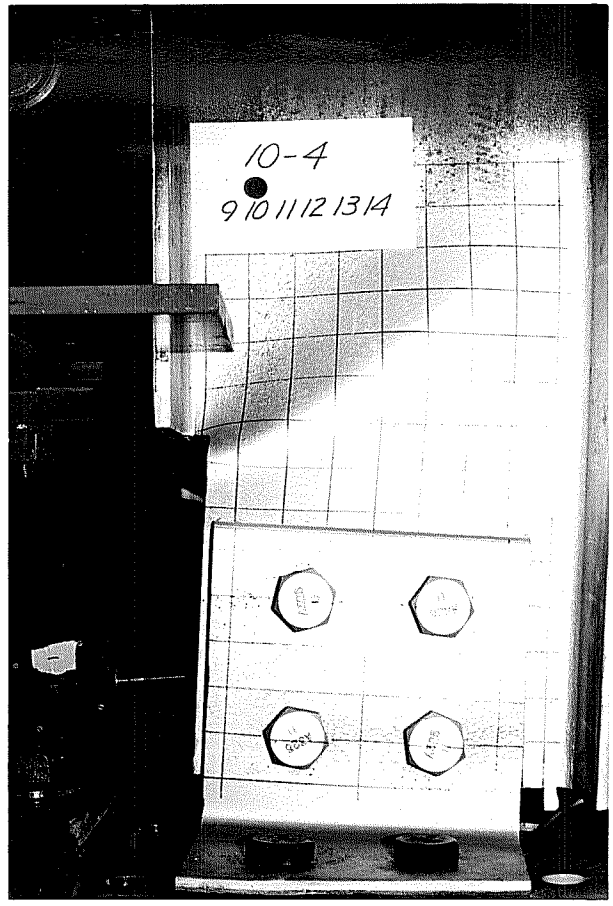
10-4
9 10 11 12 13 14

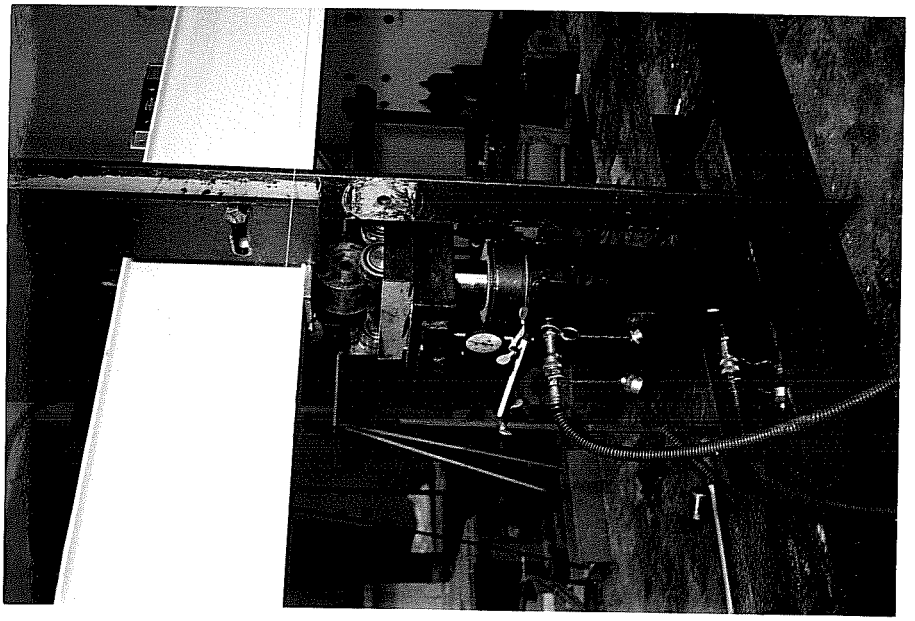

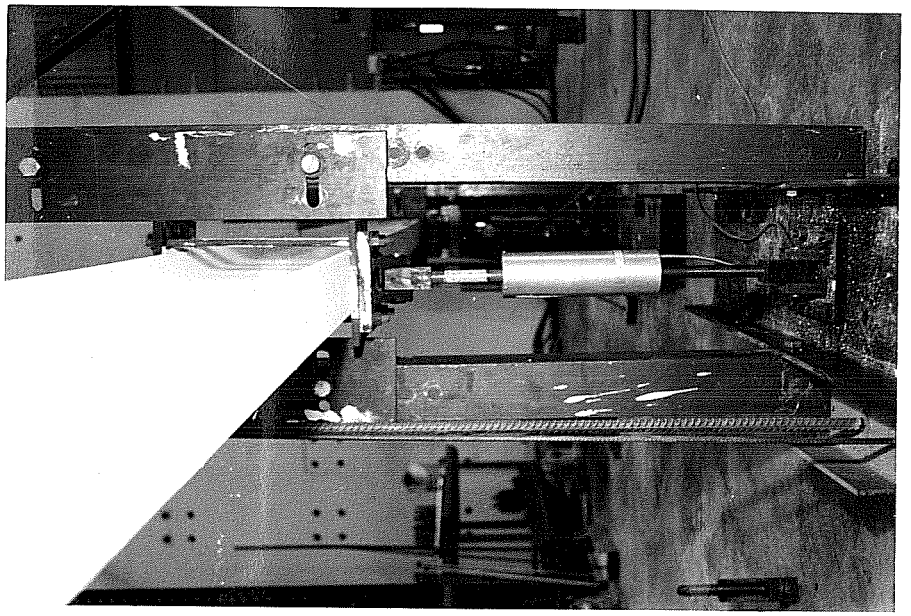

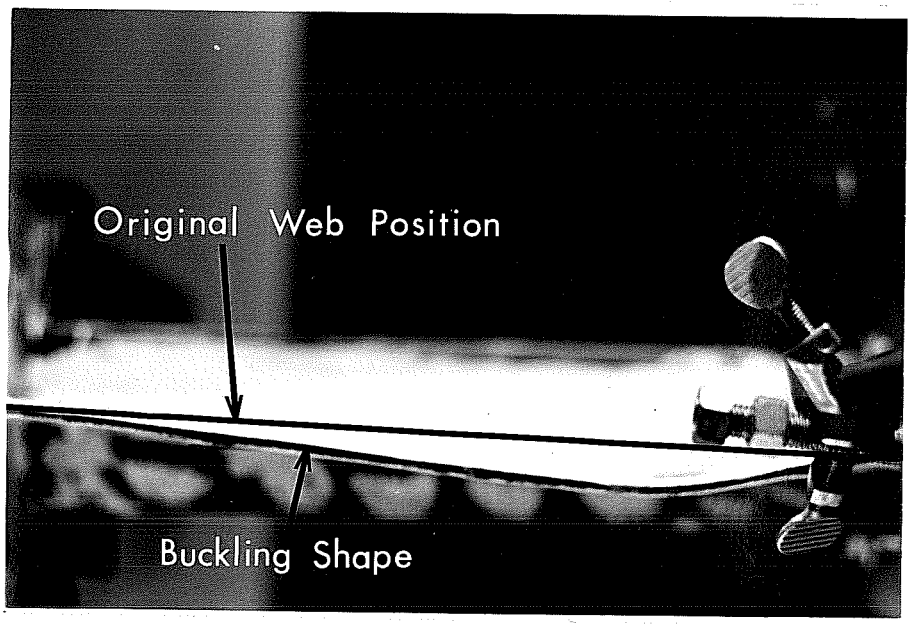
Original Web Position
Buckling Shape

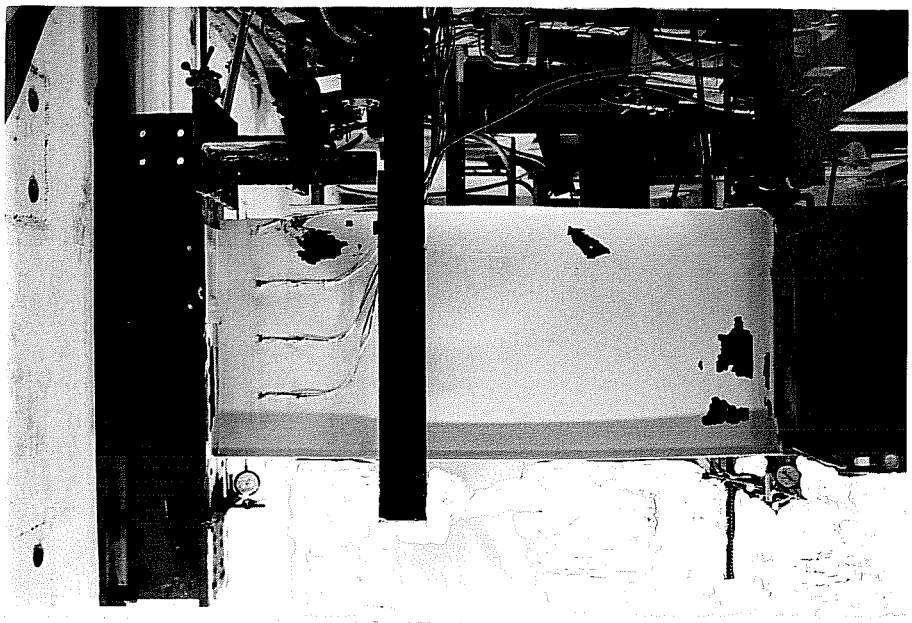

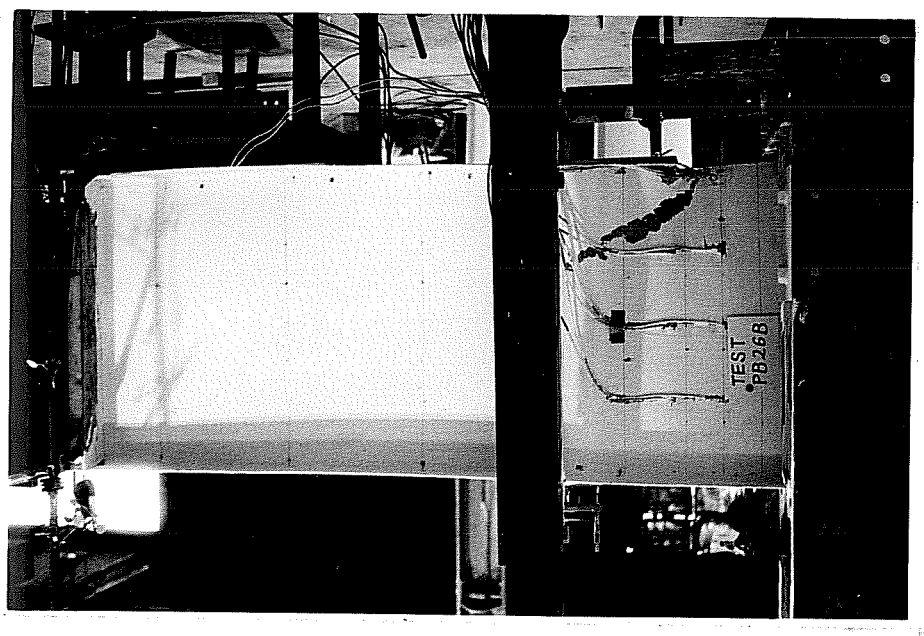
TEST
PB26B

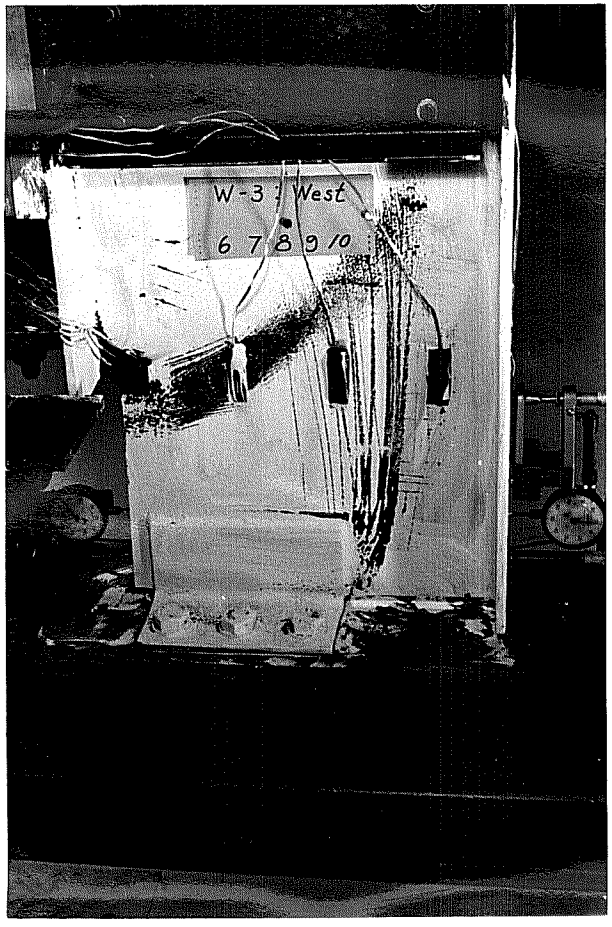
W-3 : West
6 7 8 9 10

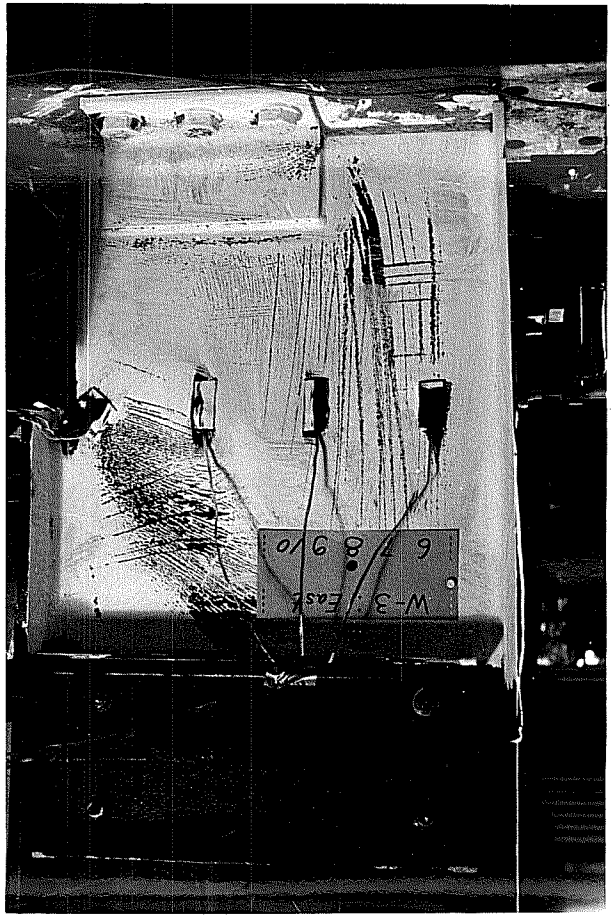
W-3 : East
6 7 8 9 10

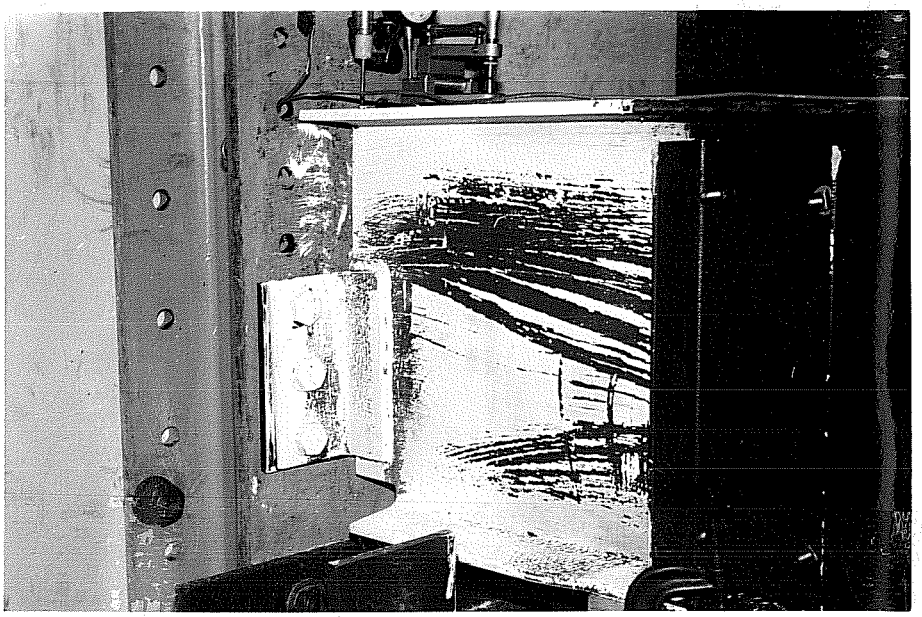

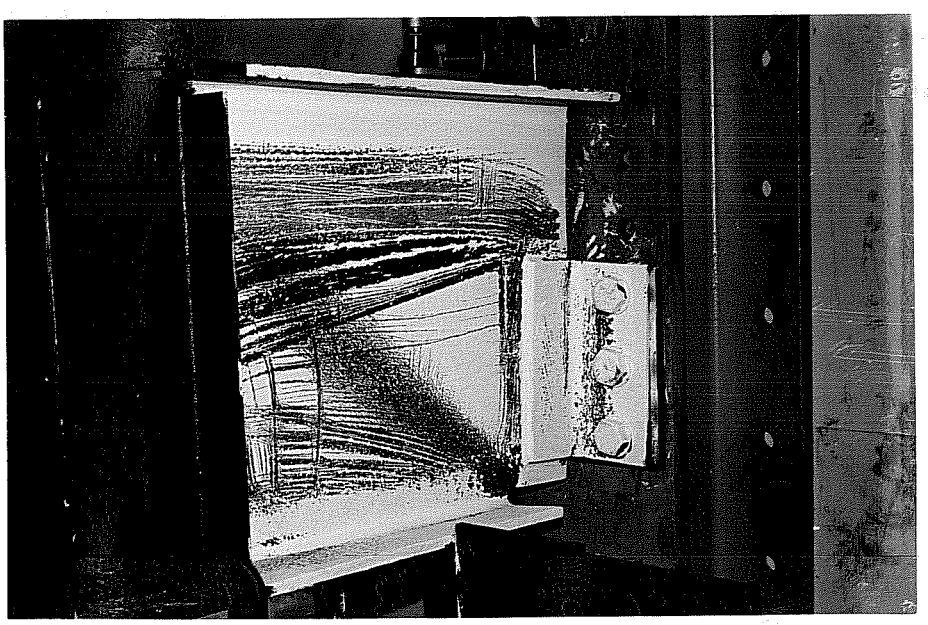


TEST
RB12A

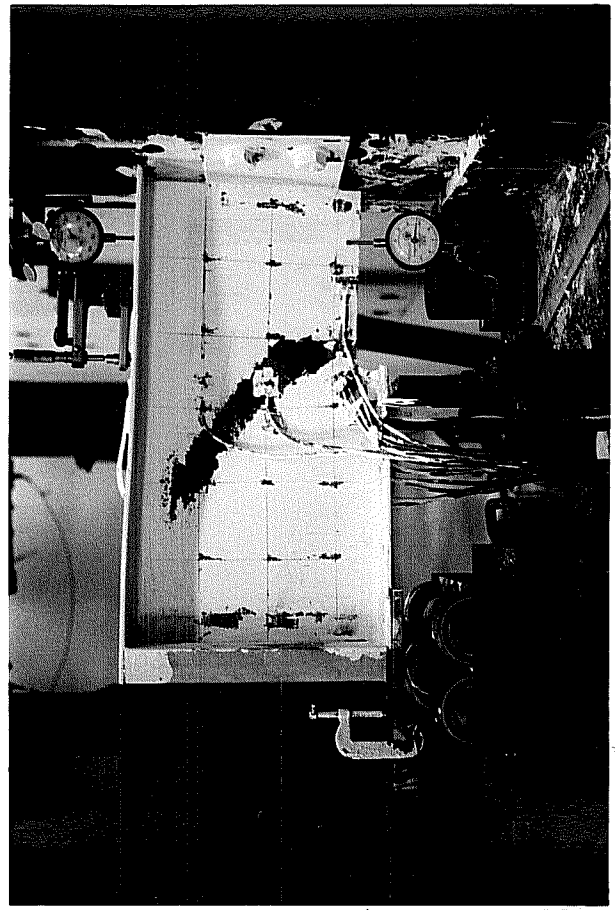

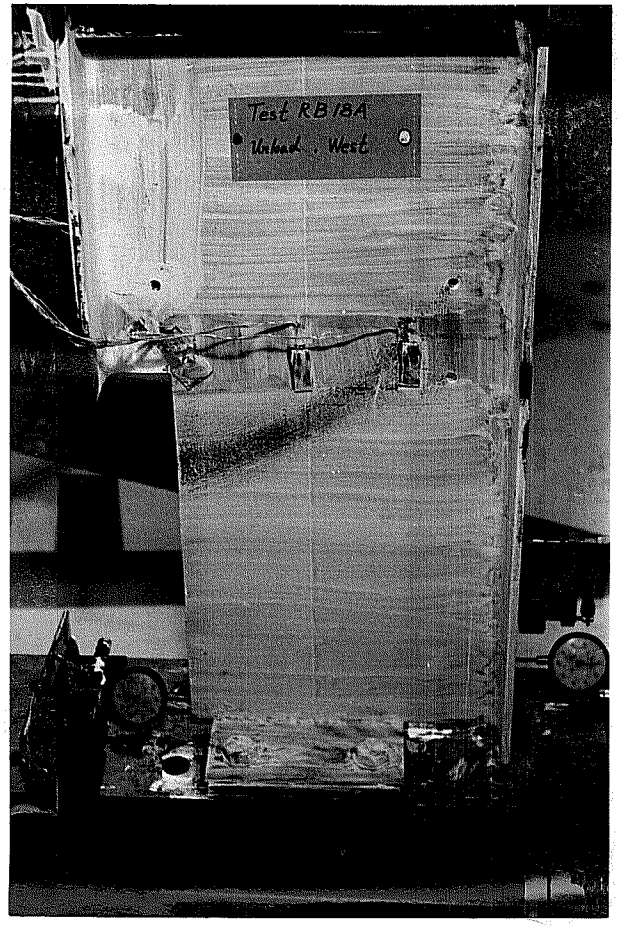
Test RB 18A
Unload . West

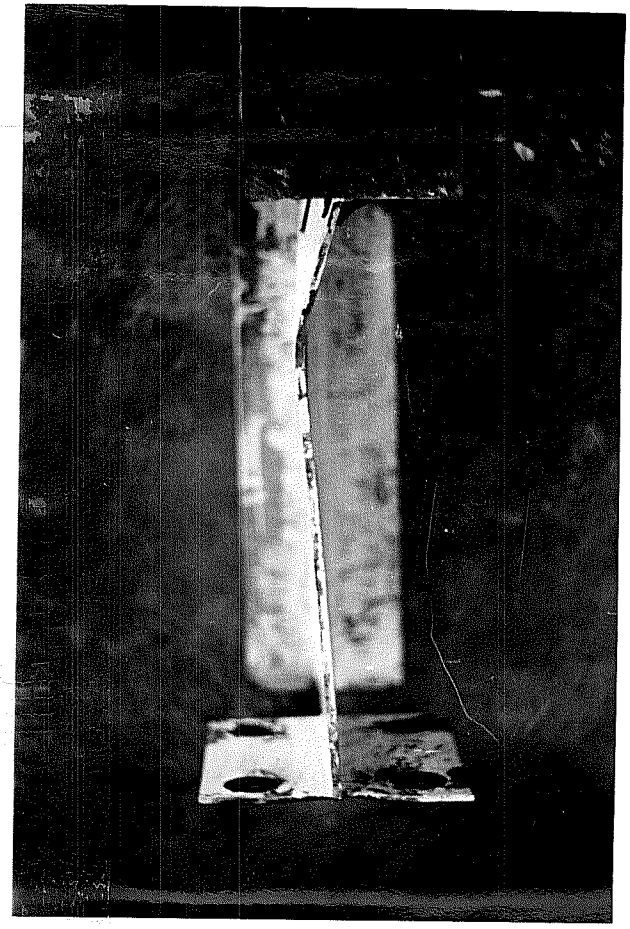

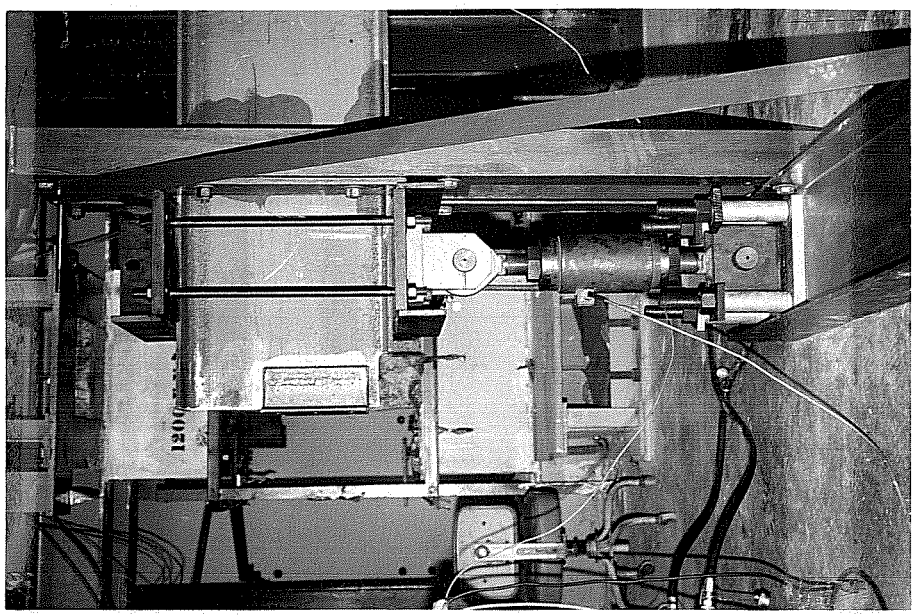

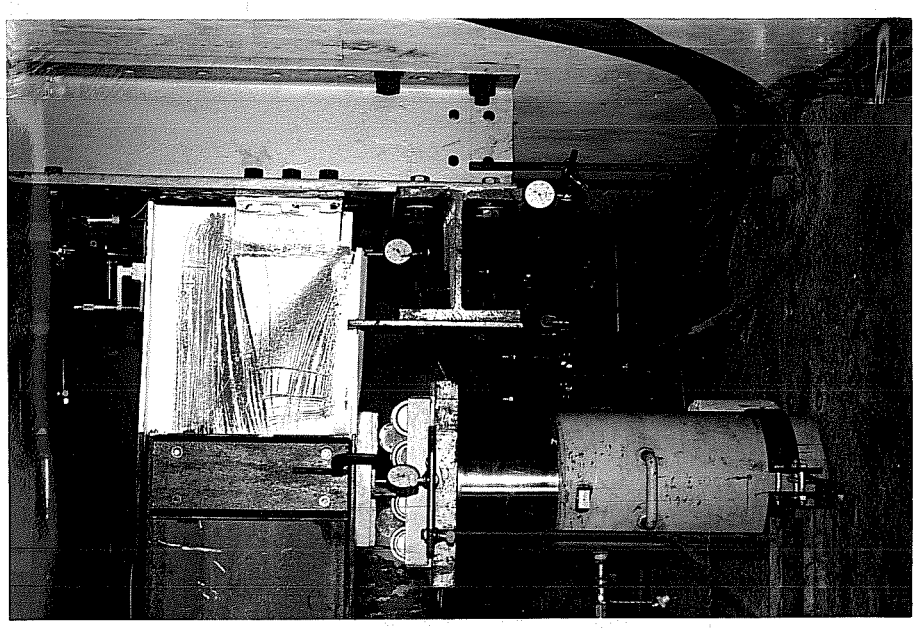

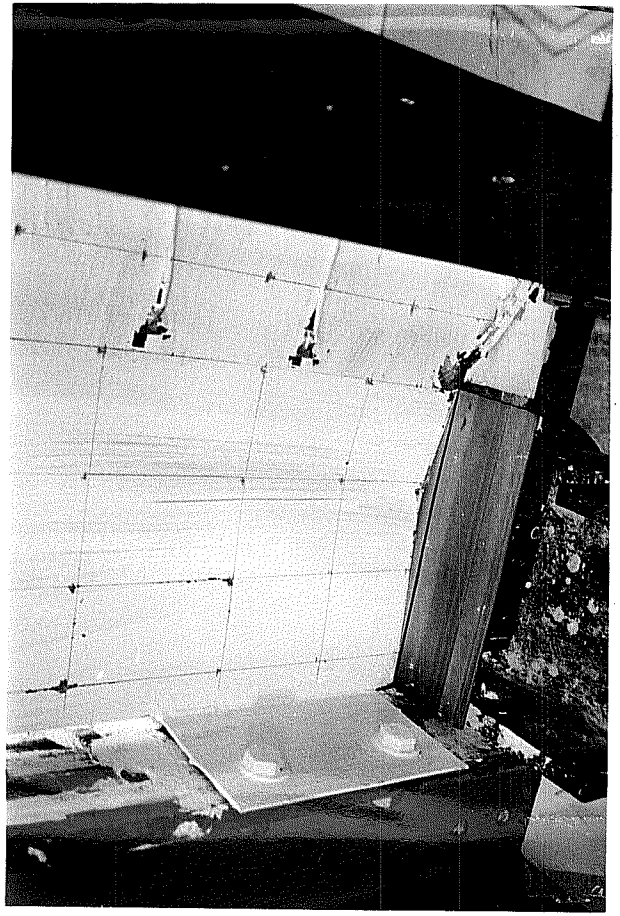

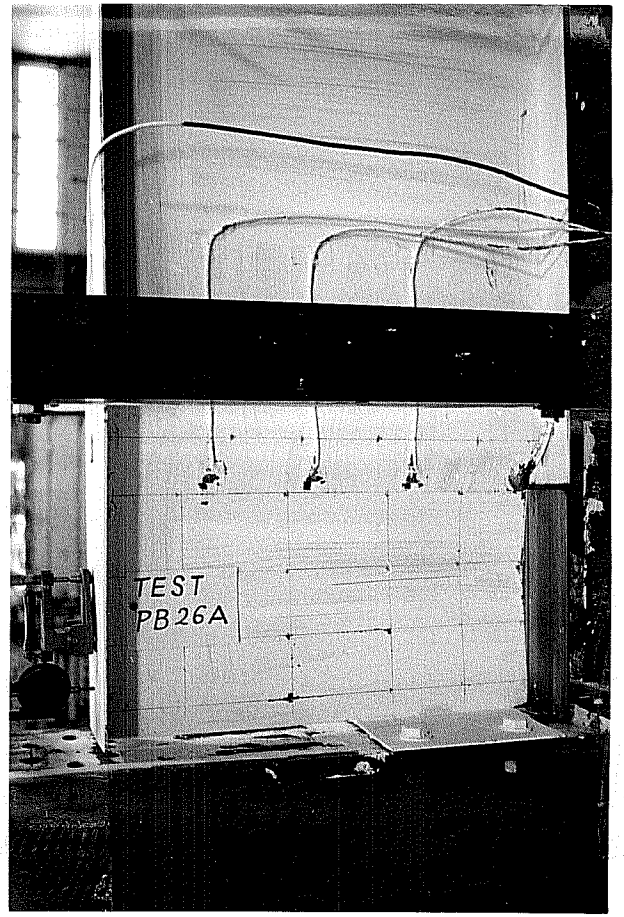
TEST
PB 26A

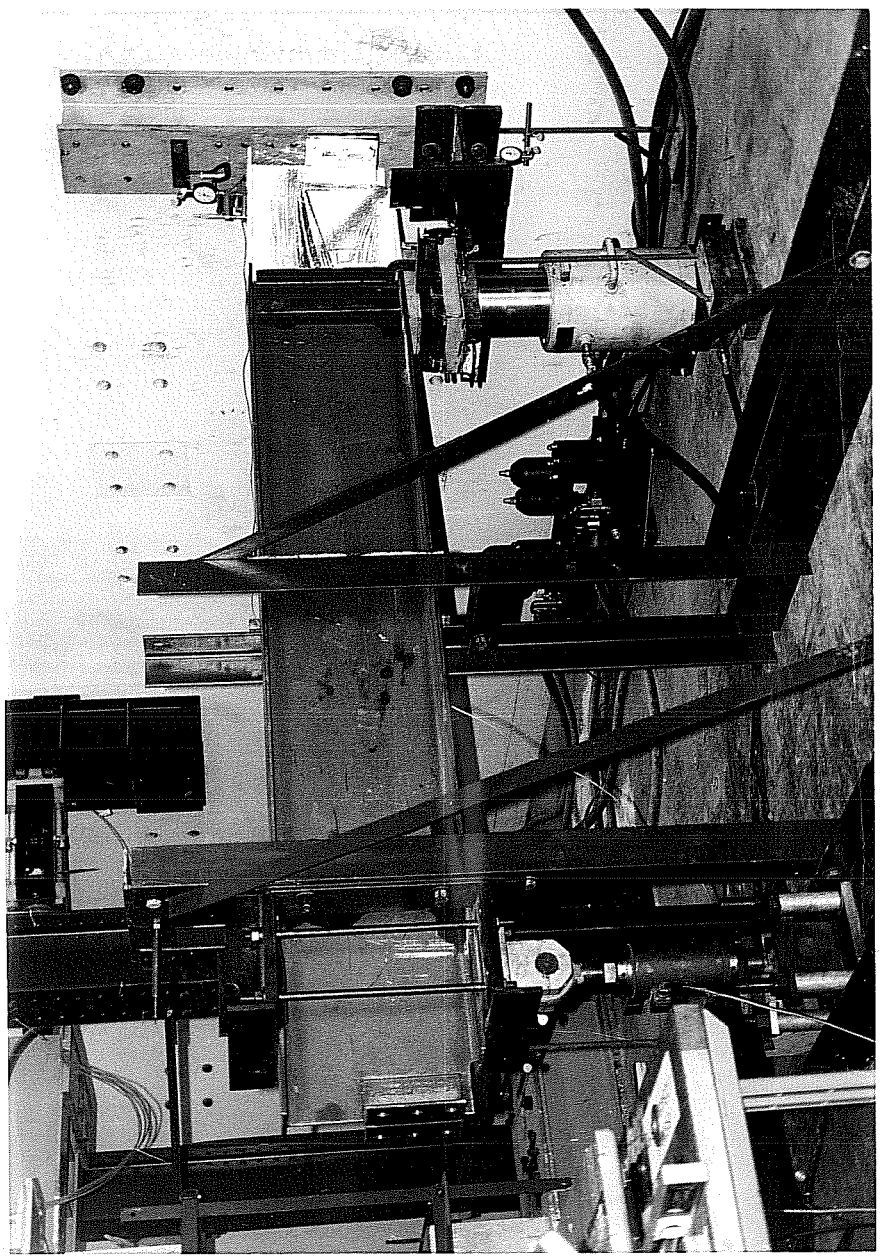

CB1-5

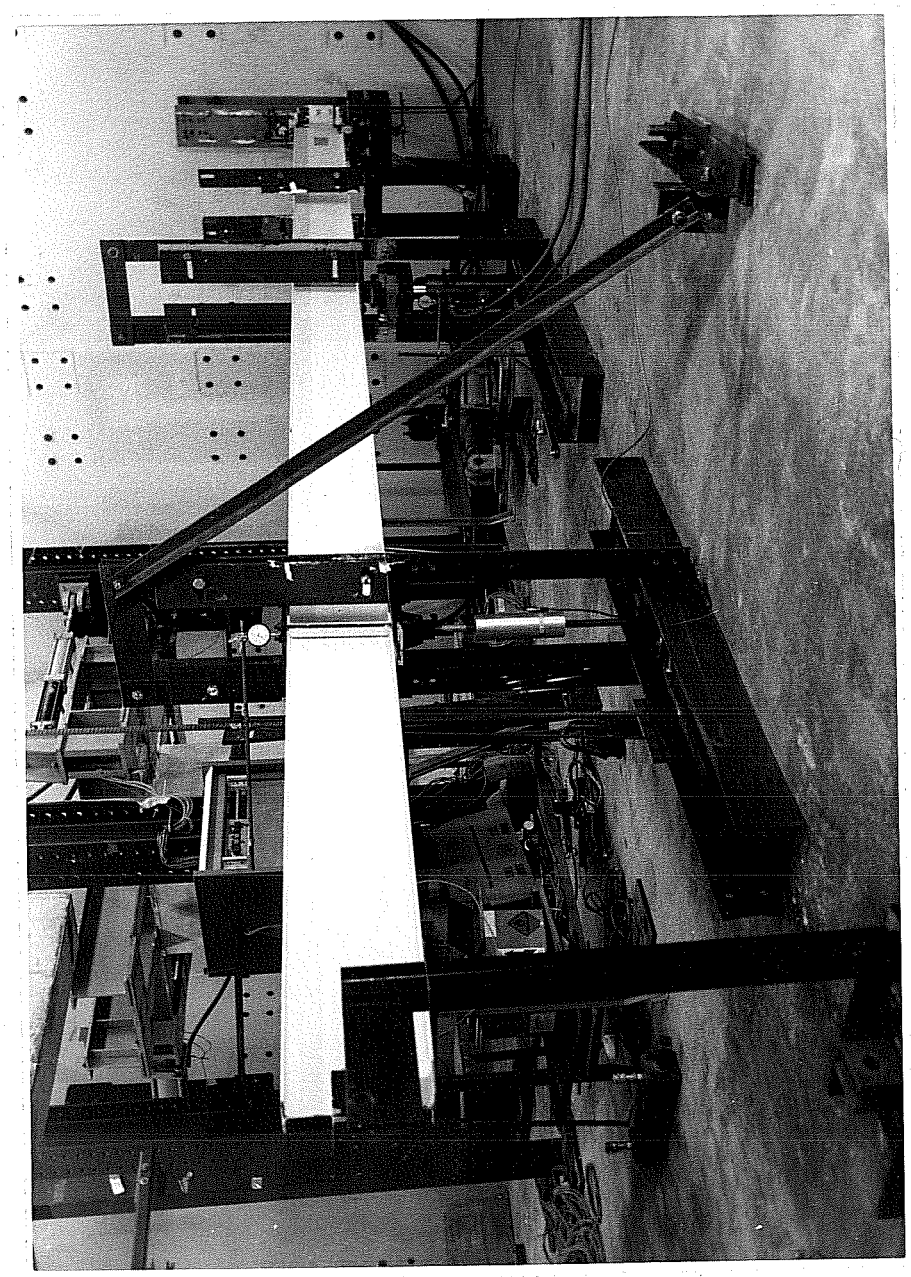

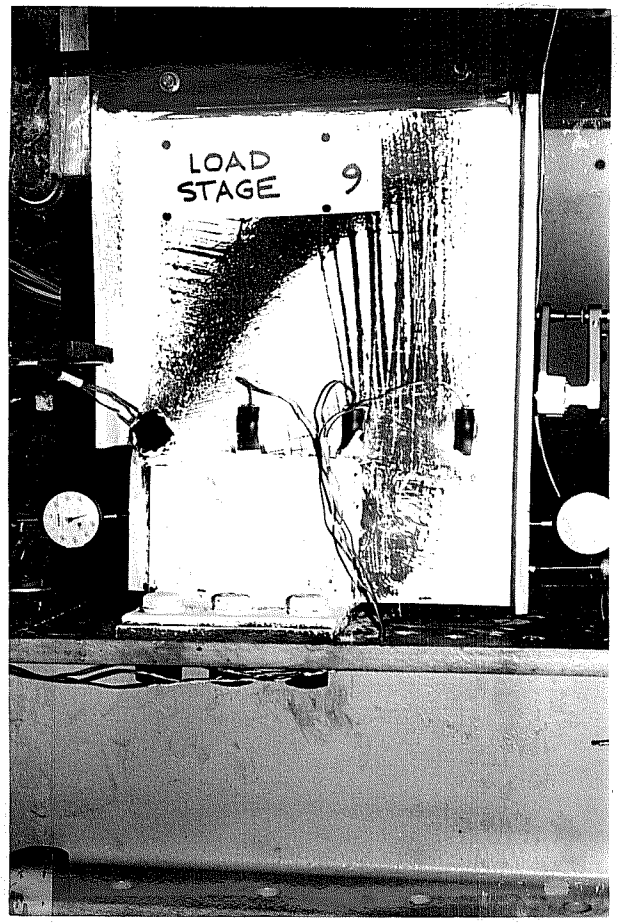
LOAD
STAGE 9

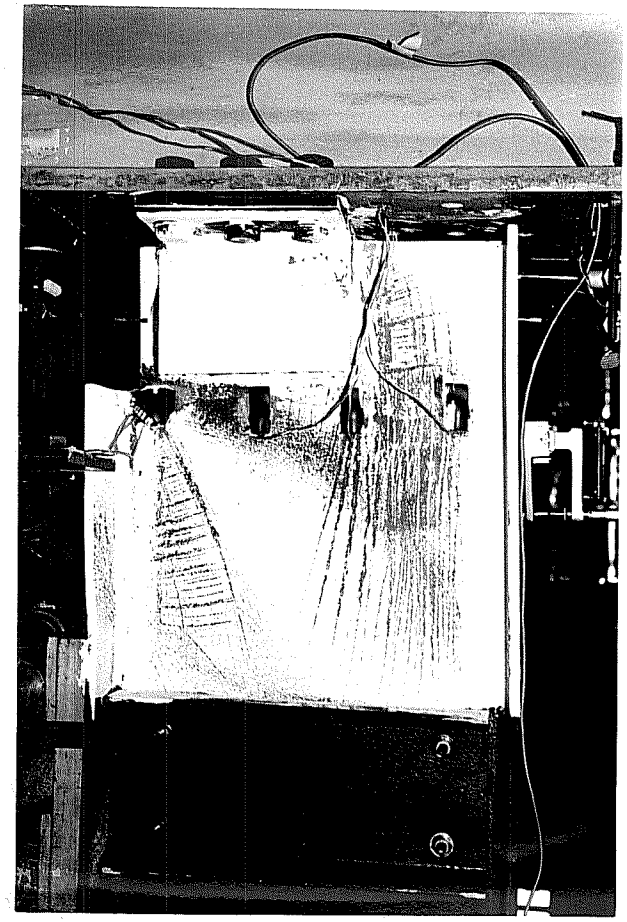

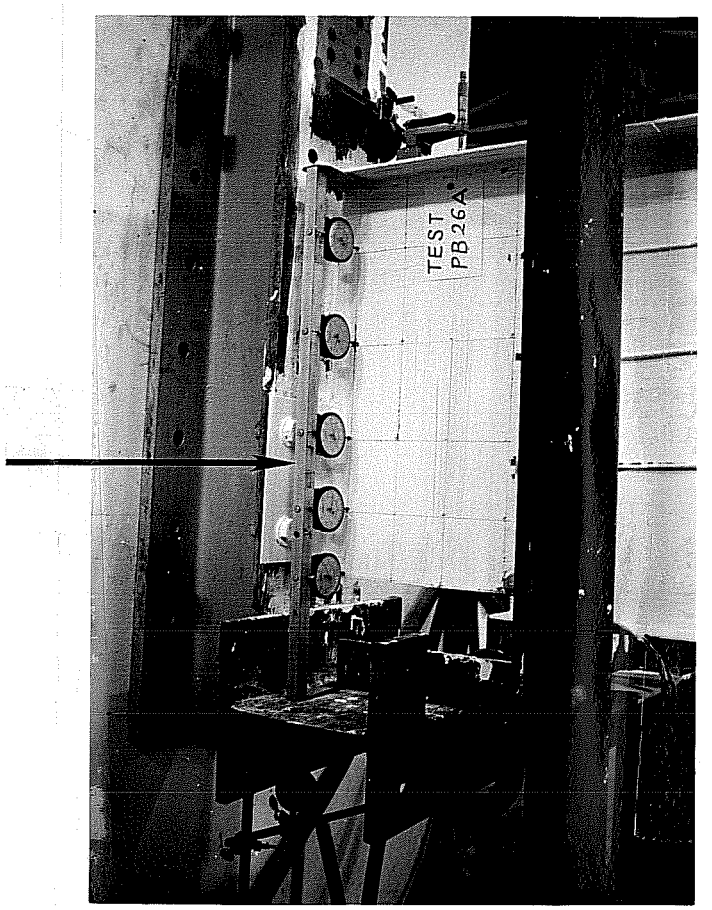
Measuring
Apparatus
TEST
PB26A